The University Of Sheffield.

Modeling and Control of De-weighting Upper-Limb Exoskeleton

A thesis submitted to the University of Sheffield for the degree of Doctor of Philosophy

by

Siti Khadijah Ali

Department of Automatic Control and Systems Engineering
The University of Sheffield
Mappin Street,
Sheffield, S1 3JD
United Kingdom

October 2017

Abstract

One of the common problems humans face when performing physical tasks is muscle/joint fatigue. Muscluskelatal disease is identified as one of the major health issues which result from fatigue. Fatigue could also cause performance degradation. Exoskeletons have been identified as means of overcoming such issues.

Although, the realisation of exoskeletons for use in rehabilitation, military and industry applications has been widely carried out, however, their realisation for tackling human fatigue is very limited, and those researched are based on biology-based signal input such as electromyography signals. In addition, issues such as the design of upper-limb exoskeleton and conrresponding control approach need to be addressed. Several approaches have been proposed to de-weight the exoskeleton by using mechanical elements such as springs and intelligent control approaches based on fuzzy logic theory.

The main aim of the research is to develop humanoid and exoskeleton models, within SimMechanics virtual environment, to perform an initial validation of proposed controller. The target users are people involved in prolonged and repetitive activity in domestic environments. The exoskeleton is aimed to assist and augment the upper-extremity in performing prolonged repetitive tasks by avoiding muscle/joint fatigue.

A de-weighting upper extremity exoskeleton mechanism is proposed in this thesis. The de-weighting exoskeleton consists of a fuzzy-based PD and an extended fuzzy controller. To represent the human fatigue condition in the virtual platform, the quasi-static joint-level fatigue model is included. The exoskeleton is activated based on the information received from the human fatigue model. The results achieved demonstrate the capability of the exoskeleton with the proposed control approach in assisting human to carry out prolonged repetitive tasks.

Acknowledgement

All praise be to Allah, the Most Merciful and Beneficent. There is no God but Allah and Prophet Muhammad (Peace be upon him) is the Messenger of Allah. With His wills and gracious, I have successfully completed my thesis.

First of all, I wish to express my gratitude to my supervisor Dr. Osman Tokhi for the trust, chance, support, guidance, patient, encouragement during my studies, as well as my friends'. Also to Dr HL Wei, thanks for your willingness to accept me to be one of your students.

I gratefully acknowledge the Malaysia of High Education, Universiti Putra Malaysia (UPM) and Automatic Control and System Engineering of University of Sheffield (ACSE-UoS) for sponsoring my studies.

I would like to express my deepest gratitude to my family especially to my father, Ali bin Alias, and my late-mother, Salnah binti Ali, to whom I am indebted for the devotion to our family wellness and education, my sister and brother-in-law, Nur Hafizah Ali and Mahmud Iskandar, for the warm hospitality, and also to my others sisters-brothers, and brothers-in-law. Also to both of my nieces, Izz Nurina and Izz Nurhan. Thanks for always making me happy.

I am thankful to all colleagues who supported me during my doctoral studies. Especially, to Da'Krutz member, sister Normaniha Ghani, sister Asnor, sister Daniella, sister Ghasaq, sister Norafizah, sister Lucyantie, sister Aini Azeqa, sister Faten Najwa, Dr Azmin, brother Omar, brother Hadi, brother Nafri, brother Hyreil, brother Ahmad, brother Abdolha, brother Abdullah and brother Bukhari.

And also to my future-husband, thanks for supporting me from far. I don't know you, but I know you are there.

Contents

Abstract i

Acknowledgement ii

List of figures ix

List of tables xi

Acronyms xii

1 Introduction 1

1.1 Introduction and Motivation 1
1.2 Exoskeleton as a Possible Solution to Human Upper-Extremity Fatigue . 2
1.3 Aim and Objectives of the Research 3
1.4 Thesis Outline 4
1.5 Contributions and Publications 4

2 Literature Review 6

2.1 Introduction 6
2.2 Musculuskeletal System 6
2.3 Muscle Fatigue 15
2.4 Collaborative Robot 20
2.4.1 Upper-Extremity Exoskeleton 22
2.5 Discussion: Issues in Developing an Exoskeleton 25
2.6 Summary 29

3 Human and Upper-Limb Exoskeleton Model 30

3.1 Introduction 30
3.2 Software Tools 30
3.2.1 SolidWorks 31
3.2.2 SimMechanics 31
3.3 Human Model 31

3.4 Upper-Limb Exoskeleton . . . 34
3.4.1 Kinematics of the Designed Exoskeleton . . . 35
3.4.1.1 Forward Kinematic . . . 35
3.4.1.2 Inverse Kinematic . . . 39
3.4.2 Dynamics of the Exoskeleton . . . 43
3.5 Summary . . . 48

4 Control Design of an Upper Limb Exoskeleton 50
4.1 Introduction . . . 50
4.2 Control of an Exoskeleton . . . 50
4.2.1 Control Mechanism of an Exoskeleton . . . 51
4.2.2 Proportional-Integral-Derivative Control . . . 53
4.2.3 Fuzzy Logic Control . . . 55
4.3 Implementation of Controllers . . . 59
4.3.1 PID-Control of the Exoskeleton . . . 60
4.3.2 Fuzzy-based PD Control of the Exoskeleton . . . 61
4.3.3 Extended-Fuzzy Control . . . 63
4.4 Results and Discussion . . . 65
4.4.1 PID Control of Exoskeleton without Disturbance . . . 66
4.4.1.1 Abrupt Movement . . . 66
4.4.1.2 Non-abrupt Movement . . . 69
4.4.2 Fuzzy-Based PD Control without Disturbance . . . 72
4.4.2.1 Abrupt Movement . . . 73
4.4.2.2 Non-abrupt Movement . . . 80
4.4.3 PID and Fuzzy-Based PD Control with Disturbances . . . 85
4.4.4 Extended Fuzzy Control Without and With Disturbances . . . 89
4.5 Summary . . . 93

5 Control of Upper-limb Exoskeleton with Human 94
5.1 Introduction . . . 94
5.2 Control of Human-Exoskeleton System . . . 94
5.2.1 PID Control of the Human-Exoskeleton System . . . 98
5.2.2 Extended-Fuzzy Control of the Human-Exoskeleton system . . . 99
5.3 Results and Discussion . . . 100
5.3.1 PID Control of Single Joint Movement . . . 100
5.3.2 Extended-Fuzzy Control of a Single Joint Movement . . . 103
5.3.3 PID Control of Multi-Joint Movement . . . 105
5.3.4 Extended-Fuzzy Control of Multi-Joint Movement . . . 110
5.4 Summary . . . 114

6 Control of Upper-Extremity Exoskeleton including Fatigue Human 116
6.1 Introduction . . . 116
6.2 Joint Fatigue Model . . . 116
6.2.1 Implementation of Joint-Level Fatigue Model . . . 120
6.3 Integration of Human with Fatigue Model with Upper-Extremity Exoskeleton 124
6.4 Results and Discussions . . . 127
6.4.1 Implementation of Fatigue Model . . . 128
6.4.2 Single-Joint Movement . . . 129
6.4.3 Multi-Joint Movement . . . 132
6.5 Summary . . . 137

7 Conclusions and Future Works 138
7.1 Summary and Conclusion . . . 138
7.2 Recommendation for Future Work . . . 139

References 141

Appendices 148

A Parts and functions of muscles for upper-extremity 149

B Dynamic representation of human upper-extremity 151

List of Figures

2.1 Stress-strain curve of collagen and elastic fibres (Chaffin, 1984). 7
2.2 Structure of upper-extremity. Source: Hudson Valley School of Personal, Retrived; www.hvcpt.com/upper-exremity.html (accessed on 21 November 2016). 8
2.3 Muscle contraction period: latent, contraction and relaxation. Source: OpenStax; cnx.org/contents/Adm7XcTb@3/Nervous-System-Control-of-Musc (accessed on 18 August 2017). 10
2.4 Planes and axed of human movement. 12
2.5 Shoulder movements: Initial position 1(a) Abduction 1(b) Adduction 2(a) Extension 2(b) Flexion 3(a) Internal Rotation 3(b) External Rotation. . . . 13
2.6 Elbow movements: Initial position (a) Extension (b) Flexion (c) Pronation (d) Supination. 13
2.7 Wrist movements: Initial position (a) Extension (b)Flexion (a) Ulnar deviation (b) Radial deviation. 14
2.8 Pull/push movements(a) Activity of muscle for push/pull (b) Activity of (a) with fatigue (Ma et al., 2013b). 19
2.9 Types of cobot: (a) Categorisation by Stienen et al. (2009) (b) Categorisation by Van Ninhuijs et al. (2013). 21
2.10 Low-level and high-level control (Ozkul and Barkana, 2011). 25
2.11 Example of high-level control (Ozkul and Barkana, 2011). 26
2.12 Summary of categorisation of exoskeletons. 26

3.1 Human: (a) Front-view (b) Side-view (c) Perspective-view (Carlos, 2012). 32
3.2 Mate in SolidWorks. The red square block presents the mates. 32
3.3 SimMechanics environment 33
3.4 Revolute Joint. 34
3.5 Exoskeleton in three views: (a) Front view (b) Right-side view (c) Perspective view. 35
3.6 Forward and Inverse Kinematics. 36
3.7 (a) Schematic Diagram (b) Denavit-Hartenberg Table. 36
3.8 Unit circle. 40
3.9 Specification for θ_3 and θ_4. 40
3.10 Position of θ_4. 42
3.11 SimMechanics and Simulink diagram to simulate the dynamical system. . 46
3.12 Angular position: (a) Static (b) Flexion/extension. 47
3.13 Angular velocity for static. 47
3.14 Torque for static. 48
3.15 Angular Velocity for flexion and extension. 49

3.16 Torque for flexion and extension. 49

4.1 Control design: (a) Control structure of an exoskeleton (b) The process of joints activation. 52
4.2 Control design: (a) Control structure of an exoskeleton (b) Controller. . . 52
4.3 PID Control System. 53
4.4 Configuration of fuzzy controller. 57
4.5 Fuzzy membership function. 58
4.6 Evaluation steps (a) First evaluation (b) Second evaluation. 60
4.7 Block diagram of the PID controller. 61
4.8 An exoskeleton with the PID controller. 61
4.9 Block diagram of the fuzzy-based PD controller. 62
4.10 Details of fuzzy-based PD control: (a) Fuzzy logic 3D surface (b) Membership functions for inputs and outputs for the exoskeleton joints motions. 63
4.11 Details of fuzzy-based de-weighting control: (a) Fuzzy logic 3D surface (b) Membership functions for inputs and outputs for de-weighting the exoskeleton joints. 64
4.12 Block diagram of the extended fuzzy controller. 65
4.13 Predefined trajectory. 66
4.14 Performance of PID controller for abrupt movement: (a) Trajectory tracking (b) Error (c) Torque. 67
4.15 P-term, I-term and D-term (Joint 1 and Joint 4). 68
4.16 Derivative definition. 69
4.17 Predefined trajectory. 69
4.18 Performance of PID controller for non-abrupt movement: (a) Trajectory tracking (b) Error (c) Torque. 70
4.19 Performance of PID controller with parameter gain 1 for non-abrupt movement (Joint 1): (a) Trajectory tracking (b) Error (c) Torque. 71
4.20 Performance of PID controller with parameter gain 2 for non-abrupt movement (Joint 1): (a) Trajectory tracking (b) Error (c) Torque. 72
4.21 Performance of fuzzy-based PD controller for abrupt movement: (a) Trajectory tracking (b) Error (c) Torque. 73
4.22 Trajectory tracking performance of (Joint 1):(a) PID (b) Fuzzy-based PD controller 74
4.23 The torque required by Joint 1: (a) PID (b) Fuzzy-based PD controller. . . 75
4.24 Trajectory tracking performance at Joint 4: (a) PID (b) Fuzzy-based PD controller 75
4.25 The torque required for Joint 4: (a) PID (b) Fuzzy-based PD controller. . . 76
4.26 Trajectory tracking performance at Joint 2: (a) PID (b) Fuzzy-based PD controller 77
4.27 The torque required by Joint 2: (a) PID (b) PD-Fuzzy Controller. 78
4.28 Trajectory tracking performance at Joint 3: (a)PID (b)Fuzzy-based PD controller. 79
4.29 The torque required by Joint 3: (a) PID (b) Fuzzy-PD controller. 79
4.30 Performance of fuzzy-based PD controller for non-abrupt movement: (a) Trajectory tracking (b) Error (c) Torque. 80
4.31 Trajectory tracking performance of (Joint 1): (a) PID (b) Fuzzy-based PD controller. 81

4.32 The torque required by (Joint 1): (a) PID (b) Fuzzy-based PD controller. . 82
4.33 Trajectory tracking performance at Joint 2: (a) PID (b) Fuzzy-based PD controller. 82
4.34 The torque required by Joint 2: (a) PID (b) Fuzzy-based PD controller. . . 83
4.35 Trajectory tracking performance at Joint 3: (a) PID (b) Fuzzy-based PD controller. 83
4.36 The torque required by (Joint 3): (a) PID (b) Fuzzy-based PD controller. . 84
4.37 Trajectory trajectory performance at Joint 4: (a) PID (b) Fuzzy-based PD controller. 84
4.38 The torque required by (Joint 4): (a) PID (b) PD-Fuzzy Controller. 85
4.39 Exoskeleton: (a) Exoskeleton movement (b) External disturbance. 85
4.40 Performance of PID controller with external forces (1000 Nm) in first condition. 87
4.41 Performance of fuzzy-based PD controller with external forces (1000 Nm) in first condition. 87
4.42 Performance of PID controller with external forces (1000 Nm) in second condition. 88
4.43 Performance of fuzzy-based PD controller with external forces (1000 Nm) in second condition. 88
4.44 Performance for extended-fuzzy controller (Without disturbance). 90
4.45 Performance for PID controller (Without disturbance). 90
4.46 Performance for extended-fuzzy controller with external force (1000 Nm). 91
4.47 Performance for PID controller with external force (1000 Nm). 92
4.48 Comparison in tracking performance, error and torque required of Joint 4 with external force: (a) Extended-fuzzy (b) PID controller 92

5.1 Structure of human-exoskeleton system. 95
5.2 Control structure. 95
5.3 Human exoskeleton model. 96
5.4 User control system. 97
5.5 Simulink control diagram of shoulder and elbow joints of human and exoskeleton. 98
5.6 Implementation of PID control system. 98
5.7 Implementation of extended-fuzzy controller. 99
5.8 PID controller for a single joint (shoulder). 100
5.9 Desired trajectory: Single joint. 101
5.10 Graphical issue of signal builder. 101
5.11 Results of PID controller of single joint movements for: (a) Trajectory tracking (b) Error (c) Torque. 102
5.12 Results of extended fuzzy controller of single-joint movements for: (a) Trajectory tracking (b) Error (c) Torque. 103
5.13 Desired trajectory: Multi joint. 106
5.14 Results of PID controller of multi joint movement for shoulder abduction: (a) Trajectory tracking (b) Error (c) Torque. 106
5.15 Results of PID controller of multi joint movement for elbow flexion: (a) Trajectory tracking (b) Error (c) Torque. 108
5.16 Results of extended fuzzy controller of multi joint movement for shoulder abduction: (a) Trajectory tracking (b) Error (c) Torque. 111

5.17 Results of extended-fuzzy controller of multi-joint movements for elbow flexion:(a) Trajectory tracking (b) Error (c) Torque. 112

6.1 (a)Schematic diagram of human upper-limb (b) Denavit-Hartenberg (DH) table. 121
6.2 Integration of joint-level model to a human. 122
6.3 Initial position of human upper-extremity. 123
6.4 Control scheme with human and fatigue model, and the exoskeleton. . . . 124
6.5 The integration of an exoskeleton and fatigue and recovery model. 125
6.6 Block diagram of human joint with fatigue model and the exoskeleton. . . 127
6.7 Desired displacement, velocity and acceleration of a shoulder joint. 128
6.8 Identification of fatigue risk: (a) Torque demand by task (τ_{task}) (b) Human reduction strength (τ_{cem}) (c) Zoom in of τ_{max} (d) Fatigue risk. 129
6.9 Desired trajectory for the shoulder joint. 130
6.10 Results of extended-based controller of an exoskeleton for a single-joint movement: (a) Trajectory tracking (b) Conditions of human and exoskeleton joint (c) Maximum Voluntary Contraction of shoulder joint (τ_{mvc}). . . 131
6.11 Results of extended-based controller of an exoskeleton for a single-joint movement ($k = 0.17min^{-1}$): (a) Trajectory tracking (b) Conditions of human and exoskeleton joint. 132
6.12 Desired trajectory: (a) Shoulder joint (b) Elbow joint. 133
6.13 Result of extended-based controller of an exoskeleton for a multi-joint movement: (a) Trajectory tracking (b) Conditions of human and exoskeleton joint (c) Maximum voluntary contraction of shoulder joint. 134
6.14 Result of extended-based controller of an exoskeleton for a multi-joint movement: (a) Trajectory tracking (b) Conditions of human and exoskeleton joint (c) Maximum voluntary contraction of elbow joint. 134
6.15 Result of extended-based controller of an exoskeleton for a multi-joint movement (shoulder joint): (a) τ_{cem} for heuristic approach (b) τ_{cem} for IWO algorithm. 136
6.16 Result of extended-based controller of an exoskeleton for a multi-joint movement (elbow joint): (a) τ_{cem} for heuristic approach (b) τ_{cem} for IWO algorithm. 136

List of Tables

2.1 Characteristics of the contractile properties 11
2.2 Movements of human upper-limb exoskeleton 13
2.3 Range of motion and torques for human upper-extremity 14

3.1 Physical model parameters (Male) (Głowiński et al., 2015) 33
3.2 The end-effector positions given different values of θ_2 39

4.1 Construction of fuzzy rules 62
4.2 Construction of fuzzy rules: Fuzzy-based de-weighting controller 64
4.3 Torque limits of human arm (Głowiński et al., 2015; Carignan et al., 2007; Gupta and Malley, 2006) 65
4.4 Controller gains for abrupt movements 67
4.5 Controller gains for non-abrupt movements 70
4.6 Option for parameter gains for Joint 1 71
4.7 Controller Gains for abrupt movements (Fuzzy-based PD controller) . . . 73
4.8 RMSE and MAE for conventional PID and Fuzzy-based PD controller . . 74
4.9 Parameter gains for non-abrupt movements (Fuzzy-based PD Control) . . 80
4.10 RMSE, MAE and MAT for PID and fuzzy-based PD controller (Non-abrupt movement) 81
4.11 Controller gains for PID and fuzzy-based PD control (first condition) . . . 86
4.12 Controller gains for PID and fuzzy-based PD control (second condition) . 86
4.13 Controller gains for extended-fuzzy and PID controller 89
4.14 RMS Error of Joints with an existense of external force 91
4.15 Maximum torque of joints with an existense of external force 93

5.1 Three conditions: Single Joints 99
5.2 Controller gains for single joint movement: PID controller 102
5.3 Controller gains for single joint movement: Hybrid-based fuzzy controller 103
5.4 RMSE and MAE for PID and extended-based fuzzy controllers 104
5.5 MAT for PID and extended-based fuzzy controllers 105
5.6 Three conditions: Multi-joints movements 106
5.7 Controller gains for multi-joint movement: PID controller 107
5.8 Error and torque analysis (PID controller): Shoulder 108
5.9 Error and torque analysis (PID controller): Elbow joint 109
5.10 Controller gains for multi-joints movements: Extended fuzzy controller . 110
5.11 Error and torque analysis (Extended Fuzzy): Shoulder 112
5.12 Error and torque analysis (Extended Fuzzy): Elbow 113
5.13 RMSE, MAE and MAT for PID and Extended-fuzzy controllers: Shoulder 113
5.14 RMSE, MAE and MAT for PID and Extended-fuzzy controllers: Elbow . 114

6.1 Parameters in muscle fatigue model 117
6.2 Replacement parameters in joint fatigue model 119
6.3 Maximum joint capacity (τ_{mvc}) for static movement proposed by Chaffin et. al (1999) 120
6.4 The joints and the description 120
6.5 Controller gains for single joint movement: Hybrid-based fuzzy controller 130
6.6 Controller gains for multi-joint movements: Hybrid-based fuzzy controller 133
6.7 Controller gains for multi-joint movements (MIWO): Hybrid-based fuzzy controller 136

A.1 Superficial anterior muscles of the body 149
A.2 Superficial posterior muscles of the body 150

Acronyms

MSD Musculuskeletal Disease

EMG Electromyography

CDT Cumulative Trauma Disorder

MVC Maximum Voluntary Contraction

TVA Torque–Velocity–Angle

MET Maximum Endurance Time

COBOT Collaborative-Robot

ADL activities of daily living

EEG Electroencephalography

FES Functional Electrical Stimulation

MCRs Muscle Circumference Sensor

DOF Degree-of-freedom

CoM Centre of Mass

DH Denavit-Hartenberg

CAD Computer Aided Design

PID Proportional-Integral-Derivative

PD Proportional-Derivative

FLC Fuzzy Logic Control

SISO Single Input Single Output

MISO Multi Input Single Output

MIMO Multi Input Multi Output

RMSE Root Mean Square Error

MAE Maximum Absolute Error

MAT Maximum Absolute Torque

MIWO Modified Invasive Weed Optimization

MVC Maximum Voluntary Contraction

N Newton

Nm Newton-meter

Chapter 1

Introduction

1.1 Introduction and Motivation

Muscle fatigue is a common problem in humans. Fatigue is defined as the condition when the motion strength capacity is lower than the strength needed to perform a task (Carmichael et al., 2010; Ma et al., 2010). Several factors have been identified that lead to muscle fatigue. These include manual handling of objects, heavy physical activities, repetitive work, improper body posture and duration of exposure to working environment (Coffin, 2012). Muscle fatigue could affect the quality of human life and there is a high chance or risk of getting musculuskeletal disease (MSD) and performance degradation.

Work-related musculuskeletal disease (WMSD) or MSD is a destruction of body structure. The impairment of body structure could happen to muscles, joints, tendons, nerves and ligaments. MSD is the most common disease that is experienced by industrial workers in Europe and United States (US) (Martinez et al., 2008; Ma et al., 2009). Martinez et al. (2008) reported that in Europe 25% of workers suffer from backache and 23% having muscular pain. This shows that fatigue affects industrial workers.

The causes for WMSD or MSD are categorised into three groups (Nunes and Bush, 2011). These are physical, psychosocial and individual. Physical factors describe the work conditions such as type of posture during work. Psychosocial factors are the subjective perceptions of workers toward organization such as task required and social support. The individual factors relate to the worker such as maximum voluntary capability, age and gender (Nunes and Bush, 2011).

Besides of industrial working environment, rehabilitation procedure could also lead to muscle fatigue. Ambrosini et al. (2014) and Lalitharatne et al. (2012) have reported that therapists or patients have high probability to get fatigued during the rehabilitation process. Domestic activities such as painting and fixing a bulb might trigger the muscles to fatigue, similar to activities in industry and during rehabilitation process (Nunes and Bush, 2011).

The above situations have motivated the development of robotic exoskeleton as a solution for reducing the tendency of getting muscle fatigue or MSD (Carmichael et al., 2010). Hence, the main goal of this work is to develop powered assistive upper-extremity exoskeleton to reduce the possibility of muscle fatigue for people carrying repetitive tasks. Investigations are carried out in a virtual environment. The upper-limb exoskeleton is able to identify the condition of the muscle and is activated when needed. In addition, the developed exoskeleton is targeted for use in domestic environments.

1.2 Exoskeleton as a Possible Solution to Human Upper-Extremity Fatigue

An exoskeleton is defined as an external wearable mechanism that is worn and move parallel to human body. In general, exoskeletons could be categorised into upper-extremity, lower-extremity and whole body types (De Looze et al., 2015; Anam and Al-Jumaily, 2012). The functions of the exoskeleton are varied. An exoskeleton may be used for augmentation or supplementation, for rehabilitation or assistance (Anam and Al-Jumaily, 2012).

Issues of significant importance that need to be considered in research and development of an exoskeleton include the following:

- Design challenges

  It is essential to ensure that the exoskeleton is safe, ergonomic and portable. Safety considerations are important from the user's perspective. In most developed exoskeletons and robotic mechanisms, a stop button is included for emergency situations. An ergonomic design is needed to ensure the exoskeleton is able to mimic

the movement of human upper-limb motion. In addition, the motion range of the exoskeleton is to follow the range of motion of human hand. Since in this work, the exoskeleton is intended for use in domestic applications, hence a portable type of exoskeleton is needed. In most cases an upper-limb exoskeleton is bulky or is attached to the wall, ground or wheelchair and it is set-up in hospitals or rehab center and a specialist is needed to monitor the patient.

- Control challenges

  The control approach is another important element in the development of an exoskeleton. The controller is used to ensure the exoskeleton is able to move in a smooth manner with the human limb. In addition, the control approach should be able to interact and respond to movements generated by human. In this work, the proposed control mechanism needs to identify human's strength. The assistice by the exoskeleton will be provided when the strength is reduced.

The work presented in this thesis investigates the above.

1.3 Aim and Objectives of the Research

The main aim of the research is to investigate the development and evaluation of an assistive upper-limb exoskeleton with hybrid control approach to provide support to people at postures involving prolonged activities in domestic environments. The exoskeleton is aimed to support the upper-extremity to avoid muscle fatigue. The joint fatigue model is included and is used as a detector to activate the exoskeleton.

The objectives of the research are thus as follows:

(i) Design the human model and upper-limb exoskeleton.
  (i) Investigate and validate the dynamics of the exoskeleton.
  (ii) Develop and implement the human upper-limb fatigue model.

(ii) Develop the control system that enhanced human capability
  (i) Investigate and develop a de-weighting control approach of the upper-limb exoskeleton.

(ii) Implement the de-weighting control approach of the upper-limb exoskeleton with human upper-limb fatigue model.

1.4 Thesis Outline

The thesis consists of seven chapters in total, including the current Introduction chapter.

Chapter 2 presents a human upper-limb system and muscle fatigue model. The chapter further presents a review of literature on development of upper-limb exoskeleton systems.

Chapter 3 presents modeling of an exoskeleton and human. The exoskeleton and human are modelled using Solidworks and integrated with Simmechanics. The kinematics and dynamics of the exoskeleton are described and validated.

The investigation through simulation for the control of an exoskeleton is shown in Chapter 4. The proposed control technique is introduced in this chapter. The proposed control consists of fuzzy-based motion and fuzzy-based compensator. The results, comparison, discussions and associated conclusions are presented.

In Chapter 5, the controller proposed in Chapter 4 is evaluated with human. Three conditions of human are evaluated and the performances of the exoskeleton with the proposed controller are presented in this chapter. PID control is used for purpose of performance comparison.

In Chapter 6, the quasi-static joint-level model is included in human. Then, the exoskeleton with the proposed controller is evaluated to augment the human strength during the occurence of fatigue.

The conclusion of the whole thesis and recommendations for future works are presented in Chapter 7.

1.5 Contributions and Publications

1. Ali, S.K, and Mo Tokhi. ”Upper-Limb Exoskeleton For Human Muscle Fatigue.” Human-centric Robotics-Proceedings Of The 20th International Conference Clawar 2017. World Scientific, 2017.

2. Ali, S. K., Firdaus, A. R., Tokhi, M. O., and Al-Rezage, G. (2016). Tracking human upper-limb movements with sliding mode control type-ii fuzzy logic. In Methods and Models in Automation and Robotics (MMAR), 2016 21st International Conference on, pages 426–431. IEEE.
3. Sitikhadijahali, M. T., Ishak, A. J., and AL, G. (2015). PID and adaptive spiral dynamic algorithm in controlling human arm movements. In Assistive Robotics: Proceedings of the 18th International Conference on CLAWAR 2015, page 87. World Scientific.

Chapter 2

Literature Review

2.1 Introduction

In this chapter, a brief overview of musculuskeletal system of human upper-extremity is presented. It is essential to understand and have an insight of upper-extremity in developing an exoskeleton. Then, an exoskeleton is intoduced to deal with limitations of upper-extremity.

In this chapter, the structure of human upper limb is presented. Then, types of exoskeleton and control approaches are presented. Control approaches are highlighted and recent advances in exoskeleton are described.

2.2 Musculuskeletal System

Musculuskeletal system is one that provides stability, support, movement and protection of the human body. It consists of connective tissue, muscles and joints. The connective tissue consists of bones, ligaments, tendons, fascia and cartilage. The task of the connective tissue in the musculuskeletal system is to provide support, transmit forces and to maintain the whole structure of the human body. The connective tissue is made up of both cells and extracellular matrix. The extracellular matrix is composed of fibres and ground substance. Fibres could be grouped in two types: collagen fibres and elastic fibres. These two types of fibres play an important role in the mechanical properties of the tissue. To differentiate these two types of fibres, the capability of high and low tensile is observed. The collagen

fibres have high tensile strength, hence they are not easy to deform. On the other hand, elastic fibres, have low tensile properties and are easy to deform.

Ligaments, tendons and fascia are dense-type connective tissue. Ligaments are the connective tissue that connect bone to bone while tendons are the connective tissue that connect muscles to bone. Tendons are also involved in transmitting forces from muscles. Meanwhile, fascia, is a connective tissue, which covers organs or parts of organs and separates them from each other. The distribution and arrangement of the fibres determine the mechanical properties of the different tissues.

Figure 2.1 shows the different attributes in collagen and elastic fibres.

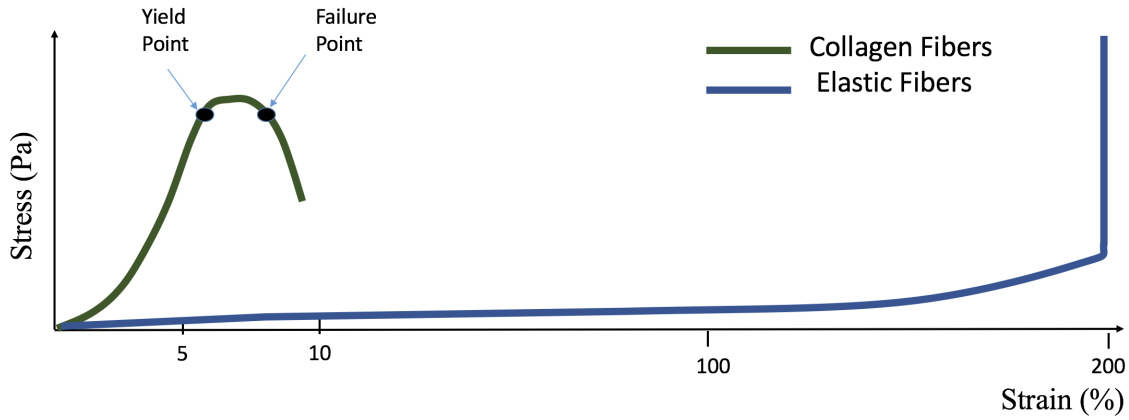

Figure 2.1: Stress-strain curve of collagen and elastic fibres (Chaffin, 1984).

Figure 2.1 shows that, after tension is applied onto an elastic fibre, it will deform and the length is increased by more than 100%. Once it reaches to the maximum strain, the elastic fibre becomes stiff and fails to continue to deform. It is different from collagen fibres when tension is applied. The collagen fibres are strengtening and stiff when they reach the yield point. The range of yield and failure point is called plastic region, where the fibre experiences a destructive change and an irreversible change occurs in the tissue (Chaffin, 1984).

Bones (skeleton) could be considered as composite structure and as one of the connective tissue. It could be defined generally, as a hard and rigid structure that form human. The bones could be categorised into two categories: axial and appendicular skeleton. The upper and lower limb can be categorised as appendicular bone. The word 'appendicular'

originally from Latin, *appendere*, means 'to hang from'. In general, an upper-extremity could be divided into three main group: arm, forearm and hand. An arm consists of clavicle, scapula and humerus. Forearm comprises of radius and ulna. Hand consists of carpals, metacarpals and Phalanges (Chaffin, 1984).

Figure 2.2 shows the structure of the upper-extremity.

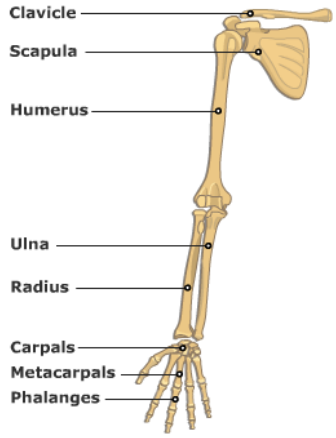

Figure 2.2: Structure of upper-extremity. Source: Hudson Valley School of Personal, Retrived; www.hvcpt.com/upper-exremity.html (accessed on 21 November 2016).

Clavicle bone is a horizontal bone which is located anteriorly at the root of the neck. It is connected to and supported with the interrosseous skeleton by sternoclavicular joint and muscles. Sternoclavicular joint connects the upper-limb to the axial skeleton. The acromioclavicular joint connects the clavicle to the acromion of the scapula. The scapula connects to the head of humerus at the glenoid cavity of the scapula.The glenoid cavity is assumed to be a socket, and the head of the humerus is assumed to be a ball. The intersection occurs at glenoid cavity,which is also known as glenohumeral joint (ball and socket articulation). The humeral bone is connected to forearm (Chaffin, 1984).

The forearm consists of two bones: ulna and radius. Ulna and radius are located lateral to each other, and radius is positioned at the same side of thumb (see Figure 2.2). The forearm is connected to the hand at radiocarpal joint (wrist joint).The hand can be divided into three divisions: carpus (wrist), metacarpal and phalanges bones. The wrist or carpus is composed of 8 short bones and these bones are connected by ligaments. The primary mobility of these bones is for gliding movement (Chaffin, 1984).

Muscles are another important element in musculoskeletal system. The importance of

the muscles is in providing power or moment about the joint to enable movement for joints and bones. Muscles are attached to the bones by tendons and cross one or more joints. Muscles could be categorised into three groups: smooth, cardiac and skeletal muscles. Smooth- and cardiac-type muscles are needed for survival and the contraction of these two types of muscles occurs in unconcious thought. The examples of location for the smooth muscles are at the walls of stomach intestines and uterus, and the cardiac muscle only found in the heart. The skeletal muscles are controlled by voluntary nervous system, known as somatic nervous system. The skeletal muscles are found at the arm and leg. Since the skeletal muscles are located at the arm, the skeletal-type muscles will be the focus in this work (Chaffin, 1984).

The skeletal muscles works in pairs. When one muscle is contracting, the other is relaxing. It is important to know that, muscles always pull (contract) and never push. There are several ways of muscle contraction. These are isometric (static), isotoic (concentric, miometric or shortening), eccentric (pliometric or lengthening), isokinetic and isoinertial contractions. An isometric contraction is a phenomenon where no change occurs in external muscles length. When no change occurs in muscles length, it means that the muscles are not moving in a gross motion, thus, no work is done and power could not be measured. This is the reason for representing an isometric as a static situation. An isotonic contraction occurs when a constant internal force is produced and the muscle shortens. The isotonic contraction also called as a dynamic activity with a constant resistance. Contrary to isometric contraction, the power and work could be measured for the isotonic contraction (Chaffin, 1984).

The eccentric contraction happens when the external force of the muscle is greater than the internal force. This makes the muscle lengthen while continuing to maitain tension. For this type of contraction, the muscles act to control the movement, instead of initiating the movement. However, the muscles with this contraction are vulnerable to break suddenly compared to other contractions. Isokinetic contraction is a contraction that occurs with a constant velocity. Due to the controlled velocity, the isokinetic contraction does not exist in a typical movement of human. Isoinertial contraction is a type of contraction that occurs

when muscles contract against a constant load. If the torque generated by muscles is larger than the load, the muscle length will change and the additional torque will accelerate the body segment (Chaffin, 1984).

Twitch is a contraction phenomenon that occurs when a muscle is stimulated by a single nerve action potential. There are three periods that represent the twitch: latent, contraction and relaxation period (Figure 2.3). The latent period is a short period that occurs between the stimulation and the onset of the actual contraction. The contraction period is a short time period that occurs from an actual contraction to the maximum contraction. The relaxation period is the time of lengthening (Chaffin, 1984).

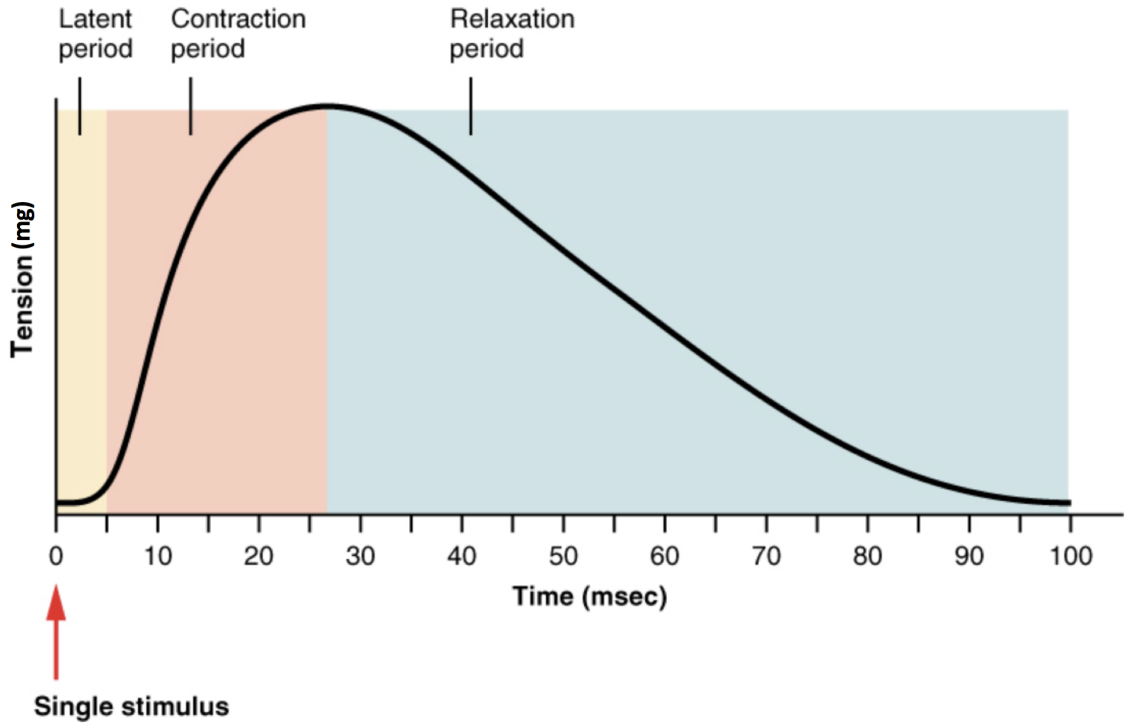

Figure 2.3: Muscle contraction period: latent, contraction and relaxation. Source: OpenStax; cnx.org/contents/Adm7XcTb@3/Nervous-System-Control-of-Musc (accessed on 18 August 2017).

There are primary factors that contribute to the response of the muscle twitch. The factors are the frequency and size of the stimulus, the fibre composition of the muscle and the length and velocity of the muscle and the velocity of the muscle contraction. The first factor occurs when the fibres are stimulated while a previous contraction is still contracting, then the magnitude of the second contraction will be greater. This phenomenon is called as temporal or wave summation. It is possible for the relaxation period or phase to dissapear

when incomplete tetanus phenomenon occurs. Tetanus is a maximal sustained tension or force. This phenomenon occurs due to increase frequency of motor neuron signal (Chaffin, 1984).

The next factor is the composition of the muscle fibre. The muscle fibre could be categorised into three categories according to their contractile properties. Generally, there are three types of contractile properties, namely type-I, type-IIa and type-IIb. These properties could be distinguished in three characteristics: twitch speed, force generation capability and level of fatigue resistence. Table 2.1 represents the charateristics of each type (Chaffin, 1984).

Table 2.1: Characteristics of the contractile properties (Chaffin, 1984)

Contractile properties	Twitch speed	Force generation	Level of fatigue resistance
Type-I	Slow	Small	High
Type-IIa	Moderate	Moderate	Moderate
Type-IIb	Fast	High	Low

The superficial anterior and posterior of the skeletal muscle and functions are in Appendix A.

Joint, is another part in the musculuskeletal system. A joint could be defined as a union of two or more bones. Joints are important for human's movement. Joints could be classified into three types: synovial, fibrous and cartilaginous joints. However, for human upper-extremity, the main joints are fibrous and synovial joints. All human upper-extremity movements involve synovial joint except pronation and supination actions. Pronation and supination movements involve syndesmosis joint which is categorised under fibrous joint. The human movement could be identified by anatomical planes and anatomical axes. The anatomical planes are sagittal, coronal (frontal), and transverse (axial) planes. The anatom-

ical axes are medial or lateral, posterior or anterior,and superior or inferior. The planes and axes of human is shown in Figure 2.4.

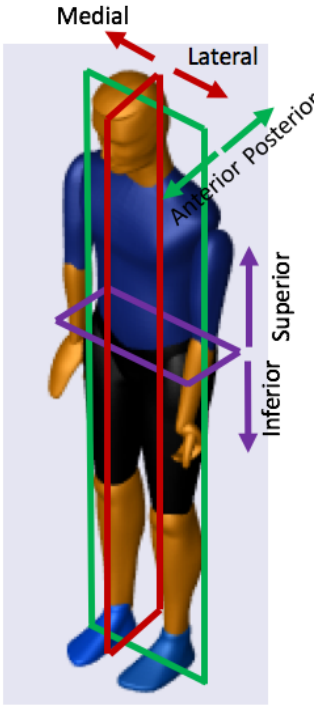

Figure 2.4: Planes and axed of human movement.

For human to move, a reference point is needed. The movement or motion could be defined generally, as an action or body segment change with respect to a reference point. For human upper-limb extremity, there are three reference points or joints. The three joints are shoulder, elbow and wrist joints. The movements also could be described in terms of degrees of freedom. In the case of human upper-extremity, there are several number of Degree-of-freedom (DOF). Different numbers of DOF have been highlighted by the researchers. The basic of DOFs reported are seven, eight and nine (Lo, 2014; Gopura et al., 2010). With the high number of DOF, more workspace could be reached by human with high maneuverability. However, the DOF of hand are excluded in this work. The human upper-extremity movements are summarised in Table 2.2.

Figures 2.5-2.7 show some of the major basic movements of human upper-extremity. The daily upper-extremity activities are the combinations of these basic movements. In addition, it is essential to identify the maximum angles of the basic movements and the torques. The information is shown in Table 2.3. The maximum ranges of movements

Table 2.2: Movements of human upper-limb exoskeleton

Joints	—Rotation					Translation	
	Flex / Ext	Abd / Abb	Int / Ext	Pro / Sup	Rad / Ulnar	Up / Down	Fward / Bward
Shoulder	✓	✓	✓			✓	✓
Elbow	✓						
Wrist	✓			✓	✓		

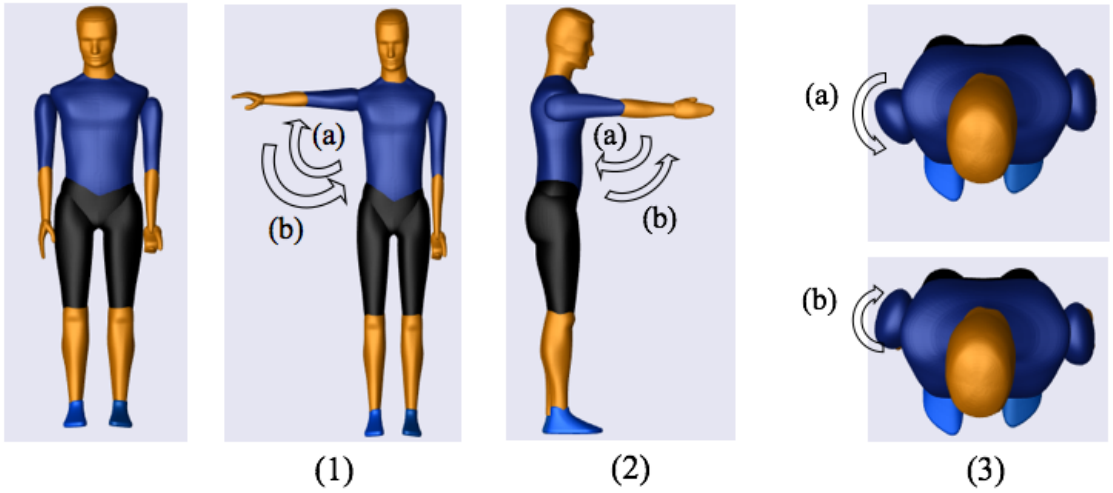

Figure 2.5: Shoulder movements: Initial position 1(a) Abduction 1(b) Adduction 2(a) Extension 2(b) Flexion 3(a) Internal Rotation 3(b) External Rotation.

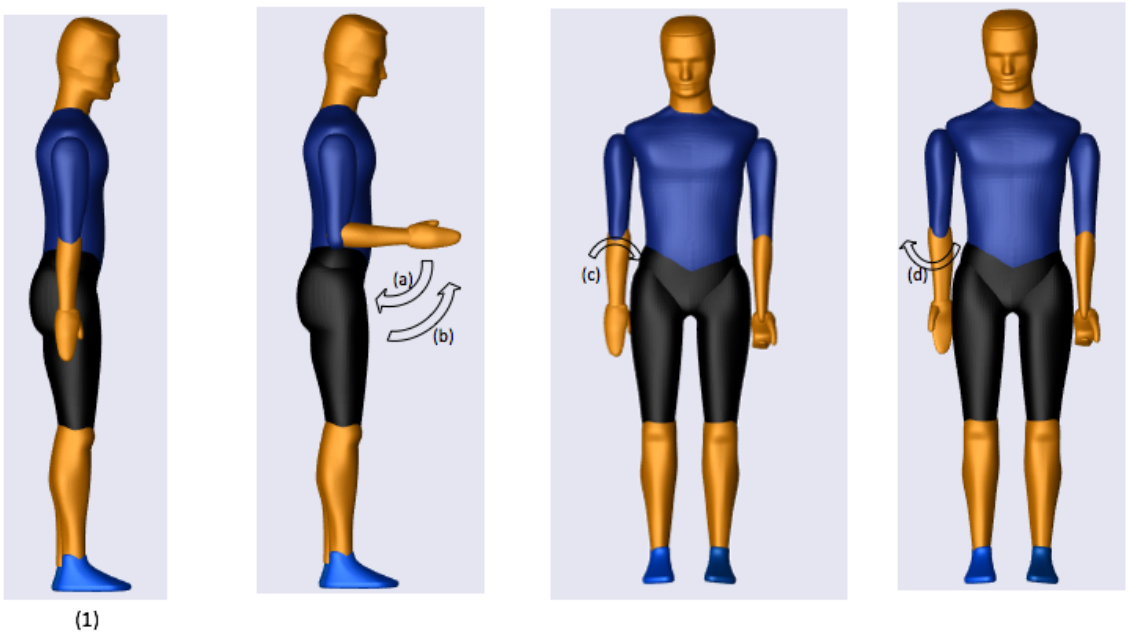

Figure 2.6: Elbow movements: Initial position (a) Extension (b) Flexion (c) Pronation (d) Supination.

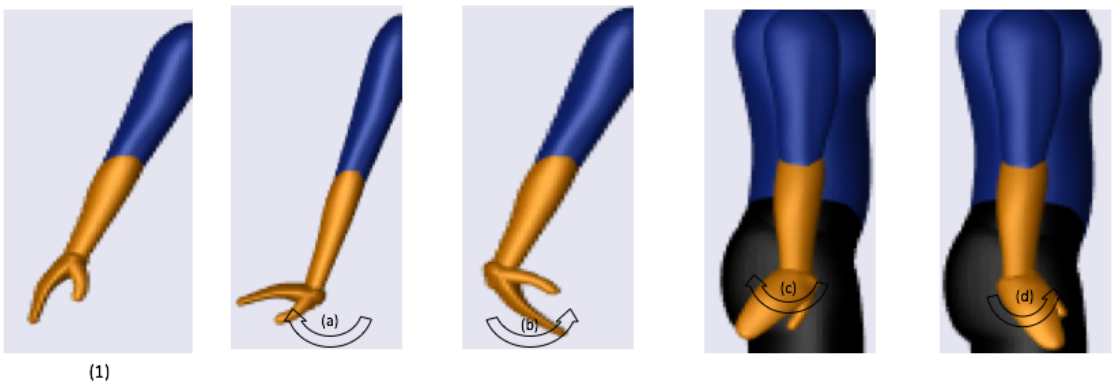

Figure 2.7: Wrist movements: Initial position (a) Extension (b)Flexion (a) Ulnar deviation (b) Radial deviation.

and moments are obtained from Głowiński et al. (2015), Gupta and Malley (2006) and Carignan et al. (2007).

Table 2.3: Range of motion and torques for human upper-extremity (Głowiński et al., 2015; Gupta and Malley, 2006; Carignan et al., 2007)

Joints	Range of Motion (θ)	Torque, τ (Nm)
Shoulder flexion	0 - 130°/180°	115
Shoulder extension	0 - 30°/80°	110
Shoulder abduction	0 - 180°	134
Shoulder adduction	0 - 50°	94
Shoulder medial (Internal)	0 - 60°/90°	39.2
Shoulder lateral (External)	0 - 90°	39.2
Elbow flexion	0 - 160°	72
Elbow extension	0 - 140°/146°	42
Forearm pronation	0 - 80°	9
Forearm supination	0 - 85°	7
Wrist flexion	0 - 90°	-
Wrist extension	0 - 80°	-
Wrist abduction	0 - 30°/40°	-
Wrist adduction	0 - 15o°	-

In the next section, the impairment that usually occurs in human due to muscle fatigue will be described. The tools to measure the level of muscle fatigue are presented. Moreover, solution to the fatigue is also described.

2.3 Muscle Fatigue

Muscle fatigue is a natural phenomenon that occurs due to inability of muscle to exert force in response to a voluntary effort (Enoka and Duchateau, 2008; Chaffin, 1984). The level of muscle fatigue and the basic mechanism of the muscle fatigue development depends on the type of muscle exercise or activity. There are activities that require the muscle to contract high and low, and there are exercises that need the muscle to perform sustained or intermittent actions. There are also exercises or activities that require the muscle to stay either static or dynamic.

There are two factors that are identified as causes to muscle fatigue. These are metabolic changes within the muscle and an impaired activation in muscle fatigue. The metabolic changes that occur in the fibre cytoplasm contributes to a decline in force. In addition, the content of an oxygen and energy substrate could contribute to a decline in force. These two agents are carried by the blood flow. The type of exercise and level of muscle contraction could cause the ischemia or the lack of oxygen in the muscle. However, the ischemia could be avoided periodic rest is included during the activities.

The impairment of muscle activation is also be one of the causes of muscle fatigue. There are two types of impairment: central and peripheral fatigue. The central fatigue is associated with human motivation, sense of effort and the integrity of the motor command mediated by descending pathways. These three factors could affect the production of the force by muscles. Motivation and sense of error are related to each other. A motivational command could momentarily compensate for the central fatigue by inducing the 'sense of the extra effort'. The mechanism that causes the central fatigue, would actually affect the peripheral fatigue due to a reduction of the motorneuron firing rate. The peripheral fatigue occurs when the muscle fails to excite. This condition could be observed by using Electromyography (EMG). The EMG signals would show the changes during sustained exertions.

As mentioned earlier, muscle fatigue could cause the reduction of power, lead to discomfort and pain. In addition, muscle fatigue could lead to Musculuskeletal Disease (MSD) and Cumulative Trauma Disorder (CDT) (Seth et al., 2016; Sakka et al., 2015; Ma

et al., 2013b, 2009, 2008). Two parameters are frequently used to predict the occurence of fatigue. The parameters are the endurance time and the muscle contraction levels. Several techniques have been designed to directly assess the occurence of fatigue. The example of a direct approach for estimating the fatigue is by observing or measuring the reduction of Maximum Voluntary Contraction (MVC) or force output. The measurement is done after the activity. The indirect approaches are by examining or observing the endurance time, the EMG signals or muscle fibre twitch interpolation (Zhang et al., 2014).

In occupational context, several types of fatigue model have been developed to evaluate the fatigue level and time-to-happen of fatigue. This is important because the aim of the developements of these models is to avoid the associated health problems in the working population. In addition, uncontrolled muscle fatigue, which possibly lead to MSD, could cause heavy economic costs to companies. The example of heavy economic costs are loss of productivity and required training for new workers. Muscle fatigue has also been reported in some rehabilitation processes (Xu et al., 2014; Lu et al., 2014; van Diemen et al., 2016). This could limit the number of training sessions (van Diemen et al., 2016).

Giat et al. (1993) developed a fatigue model based on the relationship between force and the intracelluar-pH (pH) by using musculotendon model. This relationship is fitted with exponential function. Although this approach is useful at the single muscle level, the relations presented are complicated. They include many parameters that need to be considered and determined. This will pose difficulty in implementing and applying the approach to the multiple muscle level (Ma et al., 2013a; Xia and Law, 2008; Liu et al., 2002). Liu et al. (2002) developed a mathematical model of fatigue and recovery in macroscoposy level, which is based on muscles as a group of motor units. The macroscopic level represents the position of the skeletal muscle. In this level, the origin of the muscles is at a point of attachment to a tendon and terminate at the end of another tendon of an adjoining bone. The pattern of the motor units is used in this model. The model also includes the muscle activation and represents the relationship of muscle activation, fatigue and the recovery. Contrary to Giat et al. (1993), in this model, the brain effort is included. This model can estimate the maximal static exertions, and not submaximal or dynamic conditions.

Rodriguez et al. (2002) proposed a new fatigue model, which is also, based on mechanical properties of muscle groups. Rodriguez et al. (2002) and Santiago (2003) have categorised the fatigue assessment at joint and muscle level. As mentioned above, joint is a union of two or more bones, and muscles are used to generate the force. Hence, the fatigue evaluation that occurs at joint level, is the fatigue that is produced by a group of muscles acting on a joint. On the other hand, accessing fatigue in muscle level could be more challenging because the number of human muscle is large. In addition, one muscle can be involved in several motions. Furthermore, the amount of force exerted by a muscle due to the different motions could be different as in one action, it may act as a main source of force, and in others it may be needed as an assistant muscle.

Rodriguez et al. (2002) and Santiago (2003) chose to develop the fatigue model precisely with a fatigue index. Fatigue index is defined as the evaluation or measurement of the fatigue feeling of human (Ma et al., 2008). The fatigue model in their work is presented at the joint-level. The concept that Rodriguez et al. (2002) and Santiago (2003) applied in their work is called half-joint fatigue concept. In this concept, they split each single DOF into two coordinated half-joints. For instance, given a flexion and extension for a single DOF motion. The first half-joint presents the flexion motion, and the second half-joint presents the extension movement. The fatigue level described in this work is based on the actual holding time normalized by maximum holding time of the half-joint. The limitation of this model is that it is able to predict the fatigue occurence at the static posture only. This is due to the maximum holding time that is presented in this model is determined in a static position. In addition, the model is not be able to predict a single muscle fatigue, due to the half-joint concept. This is because one motion may be activated by several muscles (Ma et al., 2008, 2009).

Xia and Law (2008) extended the approach presented by Liu et al. (2002) by inclusion of the compartment theory and task-related muscle fatigue factors. With such enhancement, this model could define the general model behaviour with only two constant parameters, which are fatigue and recovery by modelling the sub-maximal and relaxation contraction. In this model, they identified the muscle force or tension in the joint-level,

instead of muscle-level. This is due to the muscle redundancy and complexity of the force moment arm-joint angle relationship. To overcome these problems, they have used 3D Torque–Velocity–Angle (TVA) surface representations to gather the joint strength. However, the validation and the analysis of the different fatigability of different muscle groups are not presented in this work (Ma et al., 2011). Instead, they present both of these issues in Frey-Law et al. (2012). However, the model is tested and validated using an isometric contraction only and possibly may and may not be suitable to use for non-isometric contraction tasks (Frey-Law et al., 2012).

Ma et al. (2008) proposed a new muscle fatigue and fatigue index model. They also developed a new framework which includes the fatigue model. The function of this framework is to identify the potential for human to get MSD and to evaluate human work. The fatigue model is developed in the muscle-level. There are four important factors in this framework: postures and motion, force, and individual factors. In the development of the muscle fatigue, external load, workload history, and individual differences are the three important factors. Since the parameters used to measure the fatigue index and the muscle fatigue model are not many, the mathematics calculation is considered simple, and easy to implement in real time calculation. The validation of the proposed framework and muscle fatigue model are presented by Ma et al. (2009). Ma et al. (2008) has used Maximum Endurance Time (MET) to validate the muscle fatigue model. 24 static models and three dynamic models have been used to validate this model. However, this model still needs to be validated experimentally for more dynamic motions (Ma et al., 2009).

Ma et al. (2010) extended the muscle fatigue model developed by Ma et al. (2008) to the joint-level fatigue model. This model has been extended to the joint-level due to limitations in acquiring the actual load of the muscle. Hence, an alternative to obtain an accurate load, is to use inverse dynamics and calculate the torque of each joint. In addition, joint level is common for analysts to evaluate the physical exposure in ergonomics applications. The model, however, is validated with static drilling posture only. Another limitation of this model is that the co-contraction of paired muscles factor is not included.

Ma et al. (2012) extended the model developed by Ma et al. (2010) to the dynamic

working conditions. The push-and-pull activities of elbow joint are used to validate this model. The observation shows that this model is able to be used for evaluating and measuring fatigue for dynamic condition. However, more experimental validations are still needed (Ma et al., 2012). Ma et al. (2013b) extended the application of fatigue model proposed by Ma et al. (2009) to the pull-push activities of shoulder and elbow joints. An observation shows that there is a potential in the model developed by Ma et al. (2009) to provide information to predict the fatigue occurence and the safe working periods for pushing and pulling activities. This could be done by combining the activities into one system. Figure 2.8 shows the alternating muscle activity of push and pull for shoulder and elbow joints.

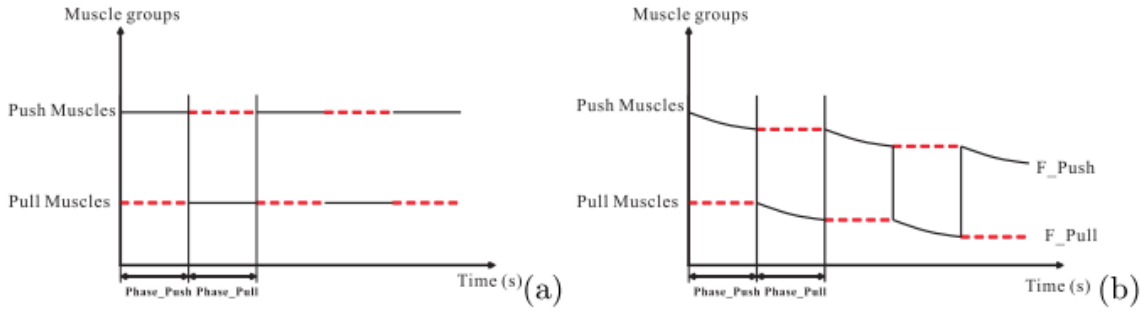

Figure 2.8: Pull/push movements(a) Activity of muscle for push/pull (b) Activity of (a) with fatigue (Ma et al., 2013b).

Sakka et al. (2015) extended the idea of Ma et al. (2010) to a more general movement in simulation environment and applied it in the joint-level. They did not claim in their work that the movement is a dynamic movement because in a dynamic situation, joint configuration and joint motion are needed. Hence, in their work, the movement is a quasi-static movement where, only the joint motion is included. The flexion and extension movement of the shoulder and elbow joints are used to observe the capability of fatigue model of Ma et al. (2010) in the joint-level. These movements are chosen in their work because these could be considered as major movements in daily life activities. Examples of flexion and extension motions are drilling and left and right shifting objects. The observation shows that during pushing, the elbow joint fatigues earlier than shoulder joint, while during pulling, the elbow is lower than shoulder joint. Hence, from the results, this model could be used to predict the occurence of fatigue, hence, it is possible to identify the safe

working environment and reduce the potential of MSDs.

The research evolving around fatigue has not only been in developing new model, but also in applying the model to real environments. For instance, Zhang et al. (2014) adopted the theoretical model in predicting the muscular strength and Maximum Endurance Time (MET) of Ma et al. (2009) and made a comparison between males and females. The observations show that for pushing action, females are more resistant than males, and the prediction model of Ma et al. (2009) is acceptable. Moreover, the predicted MET highly corresponded to the empiral models used in this work.

In general, most of the developments of fatigue model, are used to identify the occurence of fatigue and to reduce the MSDs by identifying suitable postures during work. These models are used in ergonomics research for indutrial applications. Another technique to reduce the fatigue, is by supporting human with Collaborative-Robot (COBOT), specifically an exoskeleton. Several works have been done to investigate the capability of the exoskeletons in supporting and helping human in performing tasks. In the next section, the current state of research on exoskeletons is presented.

2.4 Collaborative Robot

A collaborative robot, referred to as cobot, is a robot that is working with human. Cobot could be categorised based on the application, human-interaction, mechanical design, control approach or techniques. In terms of application, cobot has been developed to provide support to patients during rehabilitation (Głowiński et al., 2015; Huang et al., 2015a; Ochoa Luna et al., 2015; Jung et al., 2014; Huang et al., 2014; Rahman et al., 2015; Song et al., 2015; Chen et al., 2013; Xu et al., 2011; Chang, 2010; Tsai et al., 2010). Cobot has also been developed for assisting people with a limited range of arm movements during activities of daily living (ADL) (Chen et al., 2013; Kiguchi, 2007; Kiguchi and Hayashi, 2012a; Lalitharatne et al., 2012; Khan et al., 2014; Carmichael and Liu, 2015; Herder et al., 2006). Furthermore, cobot has been developed to augment healthy people while carrying physical tasks (De Looze et al., 2015; Rashedi et al., 2014; Sylla et al., 2014; de Gea and

Kirchner, 2008).

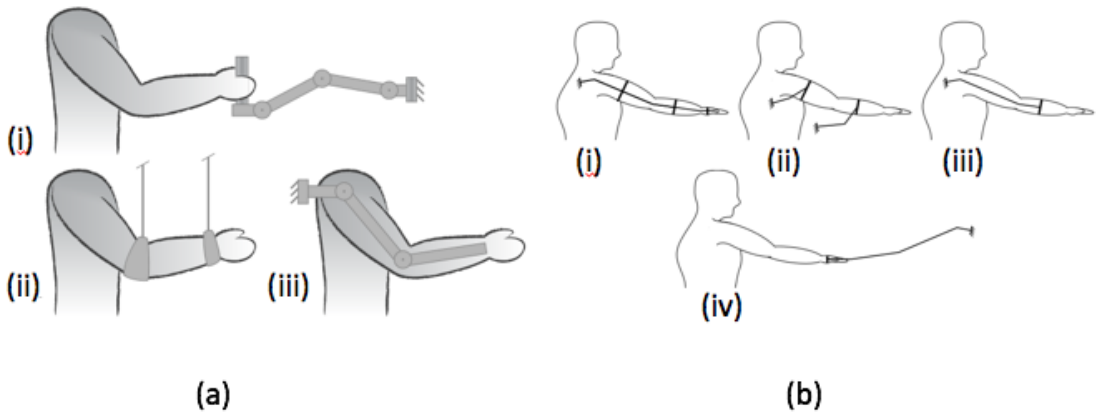

Figure 2.9: Types of cobot: (a) Categorisation by Stienen et al. (2009) (b) Categorisation by Van Ninhuijs et al. (2013).

In general, the cobot could be categorised into two: exoskeleton, and end-effector (end-point) manipulators (Gopura et al., 2011; Maciejasz et al., 2014; Van Ninhuijs et al., 2013; Lo and Xie, 2012; Stienen et al., 2009). Figure 2.9 shows the categoriesation of the cobot. As shown, the exoskeleton is attached parallel to the human upper-arm (Figure 2.9(a)(iii) and Figure 2.9(b)(i)). Meanwhile, the end-effector manipulator is shown to be attached to human in non-parallel manner as shown in Figure 2.9(a)(i) and Figure 2.9(b)(ii,iii and iv). The end-effector manipulator usually is attached to the human in single or multiple points. As shown in Figure 2.9(a) and Figure 2.9(b), the end-effector is attached at the forearm and hand.

Each type of cobot has its advantages and disadvantages. For instance, an exoskeleton is able to control the limb independently. The limitation of an exoskeleton is a complex control system for controlling the movements of each joint. In the case of end-effector, since this type of cobot is attached non-parallel to the limb, the structure of end-effector is simpler and the control algorithm is less complicated. In addition, there is no need to ensure the kinematic of end-effector to be exactly the same as the human upper-limb. However, since the attachment of the manipulator to the human is at one or several positions, there is a possibility of combination of movements of shoulder and elbow to occur. Moreover, an end-effector manipulator needs more workspace to operate (Li et al., 2015;

Maciejasz et al., 2014; Van Ninhuijs et al., 2013).

By observing the advantages and limitations of the exoskeleton and end-effector manipulator, and the main aim of this work, an exoskeleton is chosen. This is because, an exoskeleton is working parallel with human upper-arm. Hence, it is possible for the exoskeleton to assist human by providing an assistive torque to enable human with less strength to continue do the tasks. In the next section, assisting upper-extremity exoskeletons are presented.

2.4.1 Upper-Extremity Exoskeleton

In general, an exoskeleton can be described as an 'external robotic cloth' for human. It is designed according to human's part. There are upper-extremity, lower-extremity and whole-body exoskeletons. As mentioned earlier, the focus of this work is to investigate the possibility of human upper-extremity exoskeleton in providing assistance to not-so-strong human. Hence, the upper-limb exoskeleton is investigated in this section.

Research on an exoskeletons has started in early 1960's with the development of "Man-Amplifier", later known as "Hardiman", by the US army for defense purpose. Since the development of the exoskeletons are extended to others applications such as for rehabilitation, augmentation of lost physical strength , and supplementation of human strength (Carmichael et al., 2010; Yang et al., 2008). There are several ways to categorise the exoskeletons such as by application/environment, target group (user), actuation and control method (Gopura et al., 2016; De Looze et al., 2015; Gopura et al., 2011; Maciejasz et al., 2014; Van Ninhuijs et al., 2013; Anam and Al-Jumaily, 2012; Stienen et al., 2009; Yang et al., 2008).

In terms of application (environment), exoskeletons are developed for teleoperation, augmenting human (Yang et al., 2008), and military and medical (rehabilitation)(De Looze et al., 2015). For the target user category, the users of an exoskeleton could be patients due to stroke or an accident, leading to limitation in mobility, or elderly people needing helper for completing their ADL (van Diemen et al., 2016; Xu et al., 2014). In addition, an exoskeleton is also used by healthy people as an assistive device to reduce fatigue (Park

and Cho, 2017; Sylla et al., 2014; Carmichael et al., 2010).

For the actuation classification, in general, an exoskeleton could be classified into two categories: passive and active actuation (Looze et al., 2017; Anam and Al-Jumaily, 2012; Lo and Xie, 2012). This categorisation is made according to energy source of an exoskeleton. An active exoskeleton uses an actuator to produce an external energy to augment the human's power and help in actuating the human joints. Examples of actuators used for active exoskeleton are electric motors, hydraulic and pneumatic muscles. Examples of such exoskeletons are reported by Gopura et al. (2009) and Nef et al. (2009). Passive exoskeletons are not able to produce an external energy, instead it is able to absorb the potential or pre-stored energy. Due to this property, passive exoskeletons do not require an actuator. Examples of material used in passive exoskeleton to absorb or pre-store the energy are springs and dampers. For instance, Altenburger et al. (2016) and Stienen et al. (2009) have used spring in the development of their exoskeletons.

In terms of control system of an exoskeleton, there are two important elements that work parallel to each other: human brain or actions and robot controller. It is essential to note that, the controller for exoskeleton-based assistive device must be able to control the exoskeleton based on the human intention. The control method could be divided into three parts: controller input (input signal), control strategy and output of the controller (Gopura et al., 2016; Maciejasz et al., 2014; Anam and Al-Jumaily, 2012; Gopura and Kiguhi, 2009). Amongst these, controller input is important as this could influence the control strategy. In addition,this would identify the human motion. The controller input could be identified in three groups: biology based, non-biology based and independent platform based (Gopura et al., 2016; Gopura and Kiguhi, 2009).

The biology-based control input, basically, uses direct information from human such as surface Electromyography (EMG) signal and Electroencephalography (EEG) (Kiguchi and Hayashi, 2012b; Laliratne, 2014). The main issue that evolve in biology-based signal is muscle fatigue. Muscle fatigue could affect the estimation of human intention as it could influence the variations of the sEMG signal. Due to this reason, it is important to consider the fatigue elements in developing an exoskeleton especially with the biology-

based control input. The advantags of the biology-based contol input is that the information is obtained directly from human. However, more tasks need to be done such as placing the electrodes to the skin and filtering to ensure only the needed information is obtained, and this needs time to complete.

Non-invasive sensing tools such as force/torque sensors and dynamic limb model, are used to detect the human desired movements as presented by Kim et al. (2014), Xu et al. (2014) and Lu et al. (2014). Xu et al. (2014) implemented the muscle model with inclusion of fatigue element in developing the exoskeleton. In this work, the fatigue is triggered by implementation of Functional Electrical Stimulation (FES) of the muscle. Kim et al. (2014) proposed a Muscle Circumference Sensor (MCRs) as a non-biology-based control input. However, they did not include fatigue element in the model. Lu et al. (2014) have not included the muscle model in the development of their control method, instead they modelled the dynamics of human and exoskeleton and included the fatigue as one of the unknown bounded disturbances. However, Lu et al. (2014) implemented this technique in lower-limb exoskeleton. Other examples are those reported by Yu and Rosen (2010) and Huang et al. (2015b) where models in both works do not include fatigue element.

In terms of control strategy, Maciejasz et al. (2014) classified this into two levels: high-level and low-level control (Figure 2.10). Meanwhile, Anam and Al-Jumaily (2012) classified the control strategy into three categories: task (usage)-level, high-level and low-level. However, the task(usage)-level described by Anam and Al-Jumaily (2012) shows no difference with the high-level control. Hence, it could be summarised that, the control strategies could be classified into two categories: high-level and low-level control.

For a better understanding, the high-level controller is used to recognise the intention of human motion, environment and device. This could be done either in a single of direct voluntary and activity mode recognition, or in a combination of both. One of the high level controller categorised by Maciejasz et al. (2014) is assistive control. There are four types of assistive control: impedance-based, counterbalance-based, EMG-based and performance-based adaptive control.

During the beginning of the impedance-based control, the exoskeleton is passive and

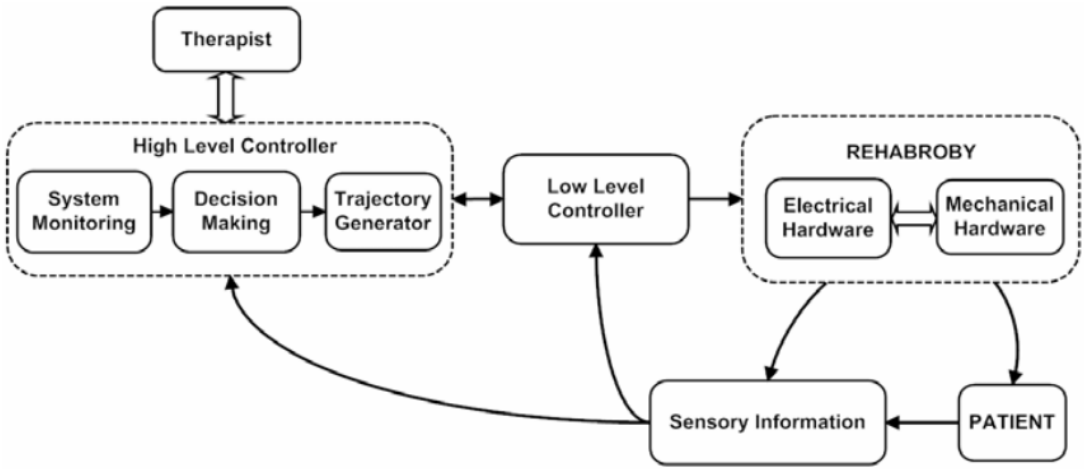

Figure 2.10: Low-level and high-level control (Ozkul and Barkana, 2011).

human is active, until the exoskeleton 'is told' that patient is moving away from the desired trajectory. The exoskeleton will produce force to retract patient to the desired position. For some exercises or movements such as shoulder flexion is influenced by the gravity force (Perry et al., 2009). For such movement, a counterbalance-based controller is applied to provide the partial, passive or active weight counterbalance so that the amount of force needed to move the limb is reduced. Currently, information from human or patient is obtained using the sEMG either to trigger the exoskeleton or proportionally control the assistance.

Low-level control is used to provide necessary motion to an exoskeleton to complete the task in desired manner. In general, the low-level control achitecture or strategy contains feedback loop that calculates the deviation (error) for each specific joint of an exoskeleton. Examples of low-level control are impedance approach and admittance approach. Basically, high-level control will received an input from human, and activate the suitable low-level control, as shown in the example in Figure 2.11.

Figure 2.12 shows an overall summary of categorisation exoskeletons.

2.5 Discussion: Issues in Developing an Exoskeleton

As mentioned in the beginning of this section, an exoskeleton could be considered as an external robotic clothe for a human. One of an issues that exists in patients and healthy

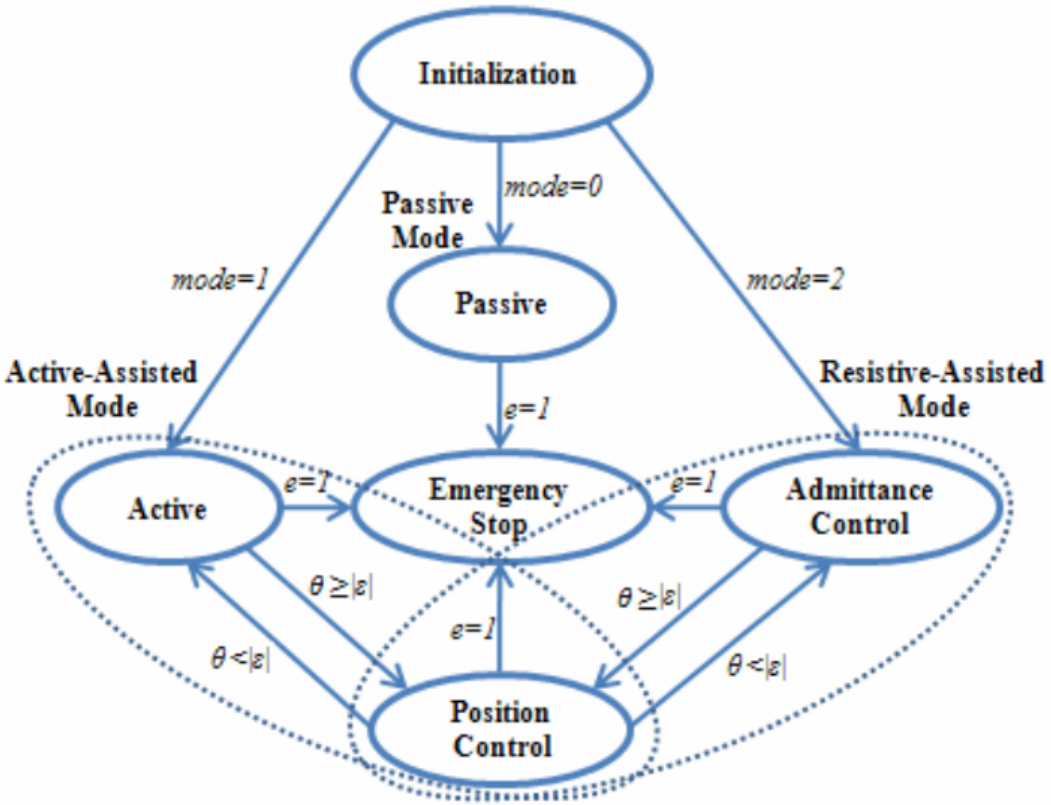

Figure 2.11: Example of high-level control (Ozkul and Barkana, 2011).

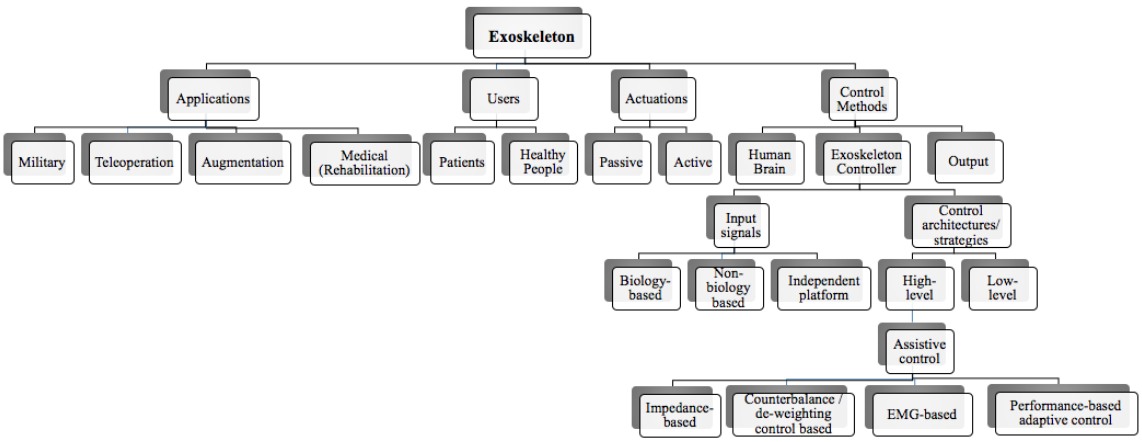

Figure 2.12: Summary of categorisation of exoskeletons.

people is fatigue. Fatigue as explained in Section 2.3 occurs due to chemical reaction in muscles during physical activities. In addition to helping to support a patient or elderly person, exoskeletons are used to reduce fatigue in humans, Although realisation of use of exoskeletons in rehabilitation, military and industry applications has been widely carried out, their realisation for tacking human fatigue is very limited, and those researched are based on use of biology-based signal input such as EMG-signals and EEG-signals (Lali-

ratne, 2014; Kiguchi and Hayashi, 2012b).

An advantage of implementing biology-based input signals in development of an exoskeleton is, the information is obtained directly from human. However, the information will be too large and difficult to process and thus, it is time consuming. The EMG-signals are also easily influenced by the environment such as the location of the electrodes and types of electrodes (Huang et al., 2015b). Moreover, some of the exoskeletons with the EMG-based signal are not suitable foe use outside rehabilitation centres (Kiguchi and Hayashi, 2012b). Hence, it is beneficial to include non-biological based input signals such as dynamic model with the fatigue model to represent the condition of upper-extremity muscles and to trigger the exoskeleton to act when needed.

There is a possibility that the exoskeleton could be a burden to the human while human wears the exoskeleton due to gravity torque, in the dynamics of the human upper-limb. It is known that the gravity torque is dominated than inertia, coriolis and centrifugal torques, in human's upper-limb movements during normal daily activities (Perry et al., 2009). For this reason, some researchers have considered fatigue as part of physical disturbance (Lu et al., 2014). Hence, it is important to consider a de-weighting upper-limb exoskeleton so that the human does not feel the weight of exoskeleton and of upper-limb (Huang et al., 2017; Moubarak et al., 2010). The term de-weighting approach is used interchangeably with gravity compensator approach. There are two approaches to compensate or de-weight the gravity forces: by using mechanical components (mechanical schemes) or actuators. Both approaches (mechanical and actuators) have their own advantages and disadvantages.

The de-weighting based mechanical approach uses mechanical element or suitable design for an exoskeleton, with for example springs or counterweights, that store potential energy, to compensate for or eliminate the gravitational joint torques. The mechanical approaches could be divided into two categories; active mechanical de-weighting and passive mechanical de-weighting. The active mechanical compensation approach involves mechanical modification or adjustment in time and could be controlled by user. In contrast, passive mechanical compensation approach involves a fixed modification or adjustment mechanical approach (Machorro-Fernández et al., 2009). The de-weight based passive

component suits for a single payload in a small workspace, whereas, the de-weight based active component suits to a vice-versa condition.

Since no external power (actuator) is required for compensating the gravity forces in the mechanical approach, this could avoid a bulky design (Miller, 2006). However, this approach need a resetting procedure for each person, and this procedure is time consuming and this approach also is difficult to present an accurate cancellation reading (Hsu et al., 2012; Miller, 2006). Examples of exoskeletons developed with mechanical or design-based gravity compensator included those reported by Altenburger et al. (2016), Spagnuolo et al. (2015), Otten et al. (2015) and Dubey and Agrawal (2011).

Contrary to mechanical components actuators are used to produce an equal and opposite torque in each joint to the gravity forces (Machorro-Fernández et al., 2009; Miller, 2006). The advantage of this approach is that it could be applied for a large class of manipulators and the disadvantage is, it consumes high power. A challenge in this approach is to estimate the gravitational load that needs to be compensated. Several ways are identified to estimate the gravitational term/load. Integral or iterative method is identified as one of the ways to estimate the gravity term in the robot dynamic system (Sutton et al., 1997; De Luca and Panzieri, 1994; Luca and Panzieri, 1993). The correction or compensation activity is done at the motor joint torque level. The limitation of this approach is the possibility of occurence of integrator wind up (De Luca and Panzieri, 1994).

Another method that could enhance the former approach is the prediction approach. In this approach, a prediction of the torque required is made in every position of motor joint. This is done experimentally and look-up tables used as predictor. However, due to large memory storage requirements, this approach is suitable for very small degree of freedom robotic systems. It is essential to assume that the mass and centre of mass (Centre of Mass (CoM)) are known. However, due to limitation in obtaining the exact mass and CoM, hence, it is difficult to predict the exact gravity load (Miller, 2006).

Moubarak et al. (2010) proposed a technique for estimating the gravity compensation based on the geometric model and accurate measurement of torque from chosen position of the robot. This technique does not require mass in estimating the gravity torques. How-

ever, the control strategy is not presented in their work. Another way to develop the gravity model is by using vector projection (Luo et al., 2011). However, the gravity torques obtained from this approach still need to predict the exact mass and CoM. This approach could be implemented with a non-complex design because it is not difficult to estimate the mass and the CoM.

Researches have found it beneficial to employ an intelligent approach such as fuzzy logic theory to tackle issues such as predicting the uncertainties and disturbances (Abane et al., 2017; Proietti et al., 2016; Xiao et al., 2010). By implementing a fuzzy logic approach, the mathematical representations or details of the exoskeleton or system are not needed to be known. Xiao et al. (2010) identified that the robot configurations and task conditions could affect the gravity on each joint of robot. Although, their research was conducted for wall-climbing microbots, this information suits the gravity terms that exist in the dynamic equation. In addition, there is no need to estimate the values of mass and CoM.

2.6 Summary

In the next chapter, the modeling of the exoskeleton and human is presented. This chapter has presented a background on muscle fatigue and detailed review of the exoskeleton such as controller and sensor, along with the main challenges. Next chapter presents the development of the exoskeleton and the human model.

Chapter 3

Human and Upper-Limb Exoskeleton Model

3.1 Introduction

This chapter presents development of humanoid with upper-limb exoskeleton models using SolidWorks and SimMechanics. It is important to choose the suitable design for the plant in order to ensure the simulated system is operated accurately. SolidWorks is chosen to re-model the humanoid and to re-design the exoskeleton. SolidWorks allows realistic design of complex 3D models. The model can be exported to SimMechanics First Generation. SimMechanics is a simulation environment for 3D mechanical systems provided by MathWorks further provides an environment for development of control mechanisms for the designed plant.

This chapter also presents mathematical model for the exoskeleton. The kinematics of an upper-limb exoskeleton are developed using Denavit-Hartenberg (DH) notation. The Lagrange formulation technique is used to present the dynamics of the exoskeleton. Then, the dynamic model for the exoskeleton is validated using SimMechanics.

3.2 Software Tools

This section presents the set of the software tools used in this work.

3.2.1 SolidWorks

Solidworks is a Computer Aided Design (CAD) software that allows designers/ users/ engineers to create 2D and complex 3D sketches and is used in this work to develop the exoskeleton and humanoid models. As mentioned earlier, SolidWorks allows to design complex 3D realistic models. In addition, the designs can easily be imported to other software/applications such as VisualNastran and SimMechanics. The parameters for human model and an upper-limb exoskeleton are referred to Głowiński et al. (2015). The upper-limb exoskeleton will be attached parallel to the human upper-limb to support the movement. The human-exoskeleton design, is then imported to SimMechanics for control system evaluation purpose.

3.2.2 SimMechanics

SimMechanics is a part of Simulink Toolbox provided by MATLAB. It is chosen due to its ability to allow users to model mechanical systems. Furthermore, SimMechanics allows the user to evaluate the response when different inputs are applied. SimMechanics is used for animation or simulation purposes. With the help of SimMechanics, the performance of developed control mechanisms can be evaluated.

3.3 Human Model

The human model used in this work was taken from GrabCad, designed by Carlos (2012). The model is created by using the SolidWorks (Figure 3.1). The measurements for the length and mass of human model are taken from Głowiński et al. (2015). These measurements are presented in Table 3.1. Each part of the humanoid, is assembled in SolidWorks. The function 'mate' in SolidWorks helps in putting the parts together. Mate function creates relationship between assembly components. The coincident mate is added to assemble the human shoulder to the trunk, the elbow shoulder to the upper arm, and the wrist to the lower arm. The coincident mate is also applied to the other parts.

The complete human model, is then exported to the SimMechanics environment. In

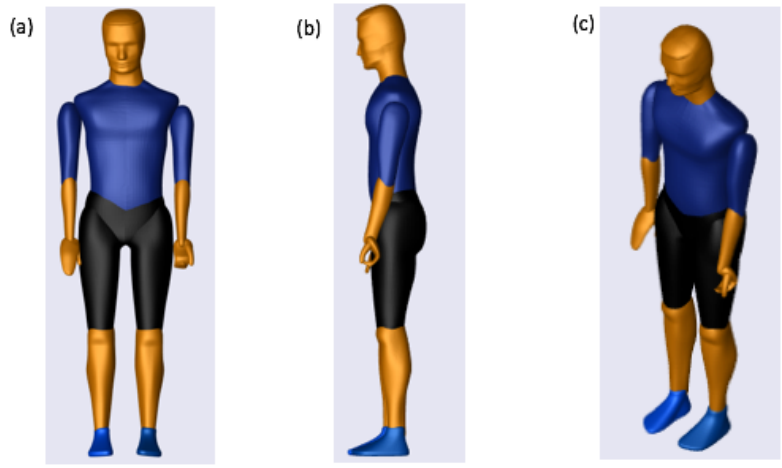

Figure 3.1: Human: (a) Front-view (b) Side-view (c) Perspective-view (Carlos, 2012).

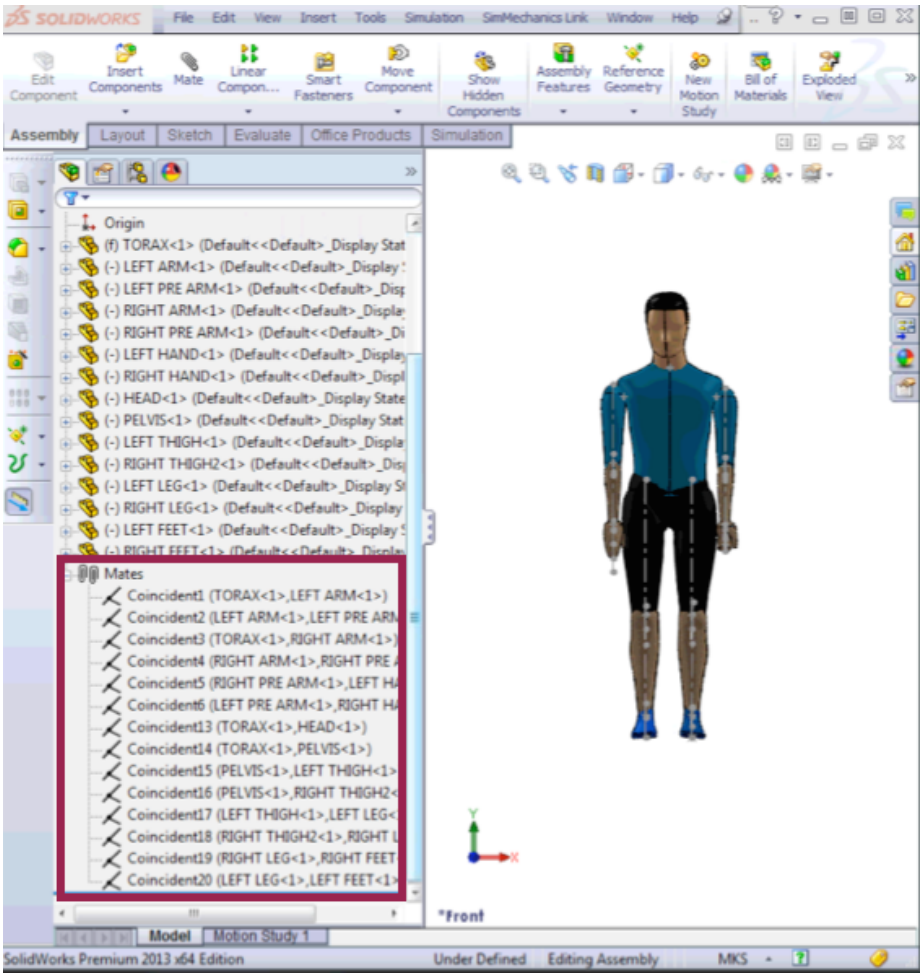

Figure 3.2: Mate in SolidWorks. The red square block presents the mates.

Table 3.1: Physical model parameters (Male) (Głowiński et al., 2015)

Segment	Length (cm)	Weight (kg)
Head	22	3
Neck	8.8	1.085
Trunk	49	34
Pelvis	5	4.686
Upper Arm	31.32	2.17
Lower Arm	28.08	1.30
Hand	19.42	0.49
Thigh	41.6	7
Calf	41.8	3.26
Foot	25.8	1.015

SimMechanics environment, the coincident mate (Figure 3.2) is changed to Joint (Figure 3.3). Basically, there are 15 Joints in SimMechanics First Generation (1G). If there is an error during the export process, the Mate will be exported to Weld Joint. The Weld Joint represents a zero degree of freedom (rigid joint). The Revolute Joint is chosen automatically by SimMechanics to represent the shoulder, elbow and wrist joints. For simplicity purposes, the rest of the joints are exported to Weld Joint.

The Revolute Joint (Figure 3.4) shows three axes of action (x, y and z). This is suitable to identify rotation for the shoulder joint. Human shoulder joint is identified to have three movements (internal/external, abduction/adduction and extension/flexion). Hence, with these three axes, it is easy to choose which movement to move.

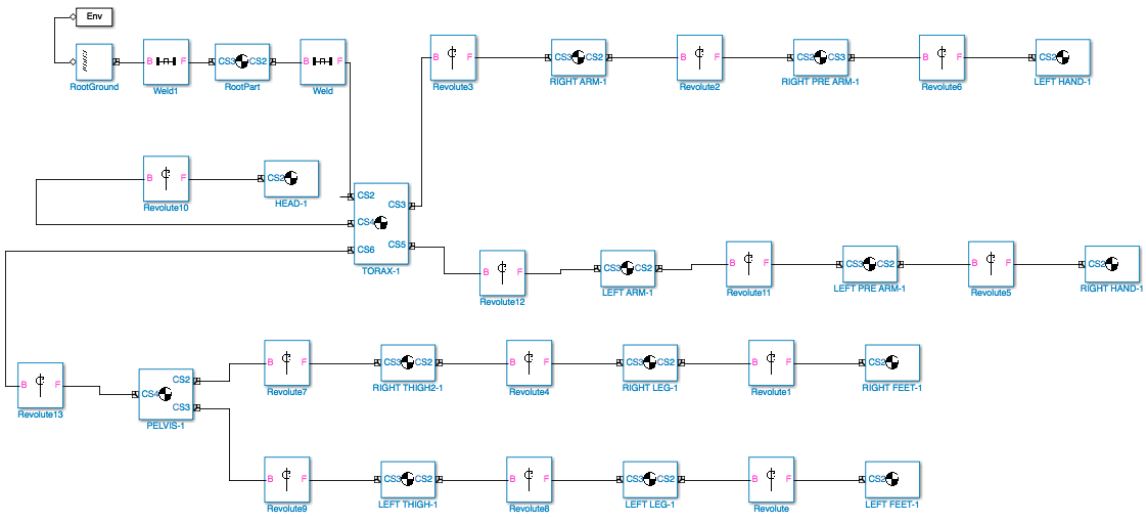

Figure 3.3: SimMechanics environment

The x-axis presents the flexion/extension motion, the y-axis shows the internal/external movement, and z-axis describes the abduction/adduction movement. To identify the (-) and (+) sign for each axis, the right hand thumb rule is applied for each axis. The next section will presents the development of the exoskeleton.

3.4 Upper-Limb Exoskeleton

Similar to as human model, the upper-limb exoskeleton is modelled using SolidWorks. The design used in this work is inspired by TitanArm (Beattie et al., 2012). This design is chosen because it is simple, capable of powered use and data transmission in a mobile fashion.

The entire upper-limb exoskeleton is shown in Figure 3.5. The exoskeleton was designed with aluminum to provide the exoskeleton structure with a relatively light weight, since aluminum is a low density material and has reasonable strength characteristics. The

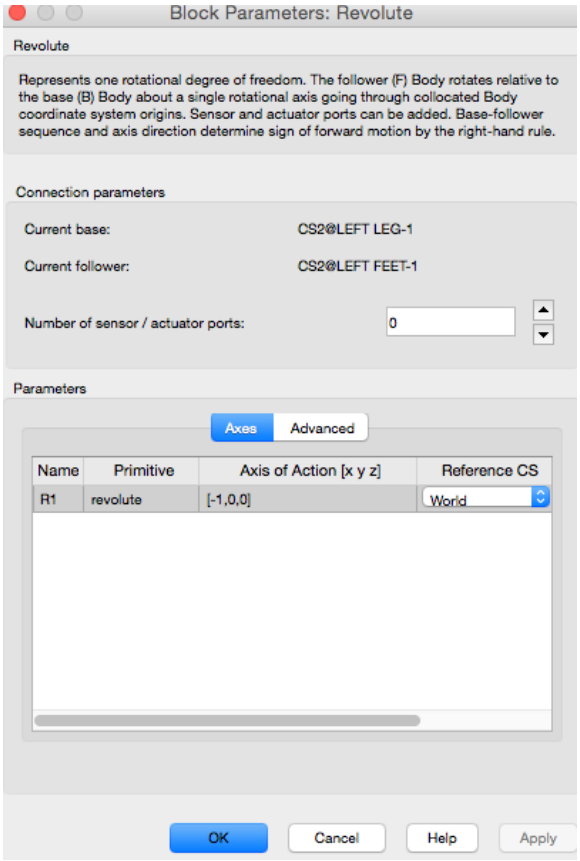

Figure 3.4: Revolute Joint.

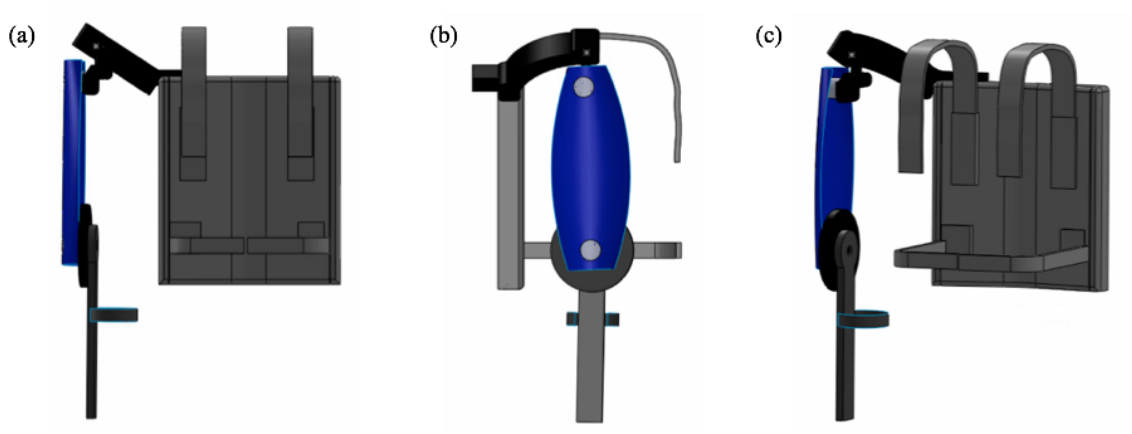

Figure 3.5: Exoskeleton in three views: (a) Front view (b) Right-side view (c) Perspective view.

exoskeleton is designed to be worn on the lateral side of the upper limb in order to provide naturalistic movements of the shoulder, elbow and wrist joint. The designed exoskeleton has four revolute joints. The revolute joints represent shoulder abduction/adduction , shoulder internal/external , shoulder extension/flexion and elbow extension/flexion . The parameters used to design the exoskeleton are based on the anthropometry measurement which taken from Głowiński et al. (2015).

3.4.1 Kinematics of the Designed Exoskeleton

Kinematics and dynamics are the two terms mostly used in robotic research. Kinematics is defined as the study of motion without considering the force, torque and moment. Two groups of kinematics are, forward kinematics and inverse kinematics. Forward kinematics is a process of obtaining the end-effector position when the angles of the joints are given. Inverse kinematics is a process of calculating the angles of the joints when the end-effector position is given. This may be described as shown in Figure 3.6.

3.4.1.1 Forward Kinematic

The Denavit-Hartenberg (DH) convention is used to obtain forward kinematics. The DH notation is chosen because it allows to compose coordinate transformation into one homogenous transformation matrix. The homogenous transformation matrix provides the

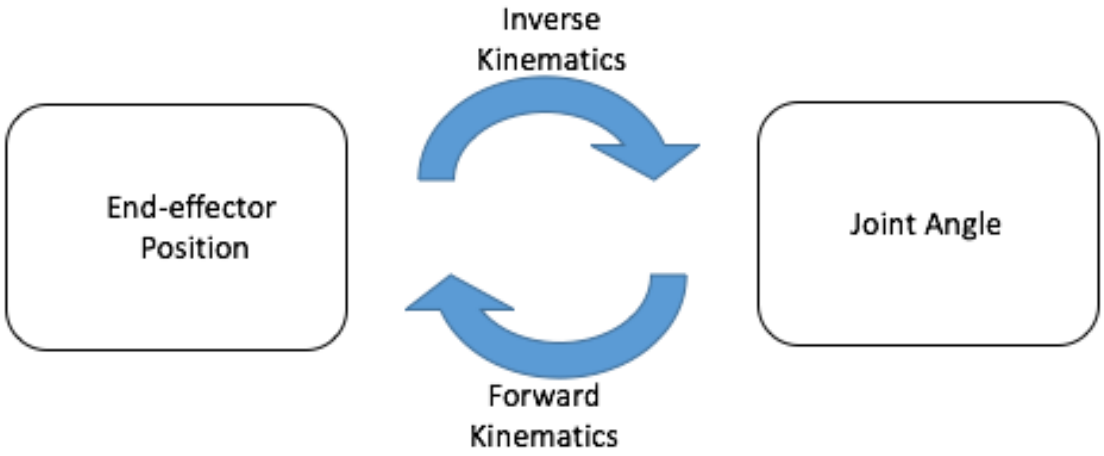

Figure 3.6: Forward and Inverse Kinematics.

relative position and orientation of two consecutive frames. This information is used to connect two consecutive frames. The two consecutive frames could be described as $i-1$ and i. As shown in Figure 3.7 (a), the base frame for the exoskeleton is denoted as O_0. The O_0 also represents the shoulder adduction/abduction motion. The O_1, O_2 and O_3 represent shoulder internal/external motion, shoulder extension/flexion and elbow extension/flexion respectively. O_4 represents the end-point of the exoskeleton.

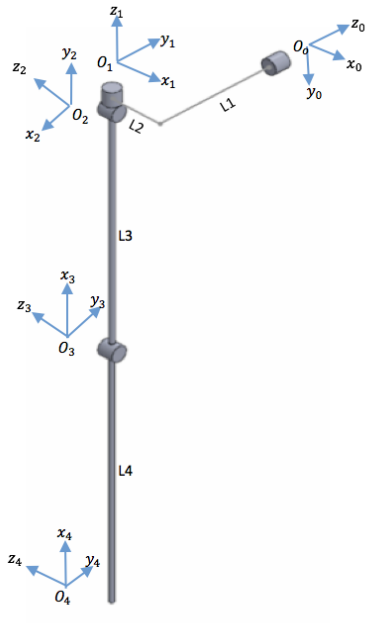

(a)

Frame	θ_i	α_i	d_i	a_i
1	θ_1	$\frac{\pi}{2}$	L_1	L_2
2	$\theta_2 - \frac{\pi}{2}$	$\frac{\pi}{2}$	0	0
3	$\theta_3 + \frac{\pi}{2}$	0	0	L_3
4	θ_4	0	0	L_4

(b)

Figure 3.7: (a) Schematic Diagram (b) Denavit-Hartenberg Table.

In Figure 3.7 (b), the DH table consists of four parameters : θ_i, α_i, a_i and d_i where

1. θ_i represents the angle between X_{i-1} and x_i measured around Z_{i-1}
2. α_i represents the angle between Z_{i-1} and Z_i measured around X_i
3. a_i is the distance along X_i from O_i to the intersection of the axis X_i and Z_{i-1}
4. d_i is the distance along Z_{i-1} from O_{i-1} to the intersection of X_i and Z_{i-1} axes

There are steps to determine the frame for each joint. The first step is to determine the origin of the axes, denoted by O_i. The z-axis designates the direction of motion for each joint. The O_1, O_2, O_3 and the z-axes for the designed exoskeleton are shown as in Figure 3.7. The following step is to determine the x-axes for the joints. There are three rules to choose the direction of the x-axis. The rules are based on the position of the Z_{i-1} and Z_i, and are given as follows:

(i) If the Z_{i-1} and Z_i are not co-planar, there exists a unique line segment perpendicular to both Z_{i-1} and Z_i. This line defines x-axis for frame i.

(ii) If the Z_{i-1} and Z_i are parallel, there exists an infinite line segments perpendicular to Z_{i-1} and Z_i, and the x-axis for frame i can be chosen from one of these lines. There are two options for choosing the direction of the x_i-axis ; could be pointing to Z_{i-1} and not pointing to Z_{i-1}. For this category, the d_i and a_i, both will be equal to 0.

(iii) If the Z_{i-1} and Z_i are intersecting, the X_i is chosen normal to the plane formed by Z_{i-1} and Z_i. For this case, the a_i would be equal to 0. The final step is the assignment of the y-axes. The y-axis is gathered using the right-hand rule.

The homogenous transformation can be obtained by:

$$
\begin{aligned}
T_i^{i-1} &= Rot(Z,\theta_i)Trans(Z,d_i)Trans(X,a_i)Rot(X,\alpha_i) \\
&= \begin{pmatrix}
\cos(\theta_i) & -\sin(\theta_i)cos(\alpha_i) & \sin(\theta_i)sin(\alpha_i) & a_i\cos(\theta_i) \\
\sin(\theta_i) & \cos(\theta_i)\cos(\alpha_i) & -\cos(\theta_i)\sin(\alpha_i) & a_i\sin(\theta_i) \\
0 & \sin(\alpha_i) & \cos(\alpha_i) & d_i \\
0 & 0 & 0 & 1
\end{pmatrix}
\end{aligned} \tag{3.1}
$$

Using equation (3.1), the individual homogenous transfer matrix that relate two successive frames can be obtained. After substituting the DH parameter into equation (3.1), the homogenous transformation matrix for frame 1, frame 2, frame 3 and frame 4 can be

obtained as:

$$T_1^0 = \begin{pmatrix} \cos(\theta_1) & 0 & \sin(\theta_1) & L_2\cos(\theta_1) \\ \sin(\theta_1) & 0 & -\cos(\theta_1) & L_2\sin(\theta_1) \\ 0 & 1 & 0 & L_1 \\ 0 & 0 & 0 & 1 \end{pmatrix} \tag{3.2}$$

$$T_2^1 = \begin{pmatrix} \cos(\pi/2-\theta_2) & 0 & -\sin(\pi/2-\theta_2) & 0 \\ -\sin(\pi/2-\theta_2) & 0 & -\cos(\pi/2-\theta_2) & 0 \\ 0 & 1 & 0 & 0 \\ 0 & 0 & 0 & 1 \end{pmatrix} \tag{3.3}$$

$$T_3^2 = \begin{pmatrix} \cos(\pi/2+\theta_3) & -\sin(\pi/2+\theta_3) & 0 & L_3\cos(\pi/2+\theta_3) \\ \sin(\pi/2+\theta_3) & \cos(\pi/2+\theta_3) & 0 & L_3\sin(\pi/2+\theta_3) \\ 0 & 0 & 1 & 0 \\ 0 & 0 & 0 & 1 \end{pmatrix} \tag{3.4}$$

$$T_4^3 = \begin{pmatrix} \cos(\theta_4) & -\sin(\theta_4) & 0 & L_4\cos(\theta_4) \\ \sin(\theta_4) & \cos(\theta_4) & 0 & L_4\sin(\theta_4) \\ 0 & 0 & 1 & 0 \\ 0 & 0 & 0 & 1 \end{pmatrix} \tag{3.5}$$

The homogenous transformation matrix that relates frame 4 to frame 0 can be obtained as:

$$T_4^0 = \left[T_1^0.T_2^1.T_3^2.T_4^3\right] \tag{3.6}$$

This represents the position and orientation of the end-effector (frame 4 / axis-4) with respect to the fixed reference frame (frame 0 / axis-0). The homogenous transformation matrix in equation (3.6) can be presented in a simplified form as :

$$T_4^0 = \begin{bmatrix} R_4^0 & P_4^0 \\ 0 & 1 \end{bmatrix} \tag{3.7}$$

where R_4^0 represents the orientation and P_4^0 the position of the end-effector. The position information that is gathered from the homogenous transformation matrix in equation (3.7) will be used in inverse kinematics to derive the dynamics of the designed exoskeleton.

3.4.1.2 Inverse Kinematic

The inverse kinematics may be obtained with two ways: closed form and numerical solution. Numerical method is used if the closed form solution fails or is too difficult to obtain. Closed-form solution, on the other hand, could give indifinite solutions. Hence, a specification is needed to ensure the right solution. Since the structure of the exoskeleton is not complex, closed form solution is considered. Specifically, the algebraic method of closed form solution is used to obtain the inverse kinematics in this work.

As shown in Figure 3.7, the exoskeleton has four joints and are described with θ_1, θ_2, θ_3 and θ_4. The θ_1, θ_2, θ_3 and θ_4 represent the angle of shoulder abduction/adduction, shoulder internal/external, shoulder extension/flexion and elbow extension/flexion respsectively. In this work, θ_2, makes no different in terms of the position of the end-effector as shown in Table 3.2. Therefore, in this work, there is no need to obtain the inverse kinematic for θ_2. θ_2 is also restricted to rotate between -60 to 60.

Table 3.2: The end-effector positions given different values of θ_2

θ_2(rad)	x_4	y_4	z_4
0	0.1777	-0.7023	0.1354
0.1754	0.1777	-0.7023	0.1354
-0.1754	0.1777	-0.7023	0.1354

Since θ_2 is known, by using a position information from forward kinematics, θ_3 could be obtained. A position information from z at joint 3 is used. The position z_3 is given as follows:

$$z_3 = L_1 - L_3\cos(\frac{\pi}{2}+\theta_3)\sin(\frac{\pi}{2}-\theta_2) \tag{3.8}$$

This can be simplified as:

$$z_3 = L_1 + L_3(\sin(\theta_3))\cos(\theta_2) \tag{3.9}$$

Rearranging the above results:

$$\theta_3 = \arcsin(M); M = \frac{z_3 - L_1}{L_3\cos(\theta_2)} \tag{3.10}$$

As mentioned earlier, closed-form approach could gives more than one solution. There

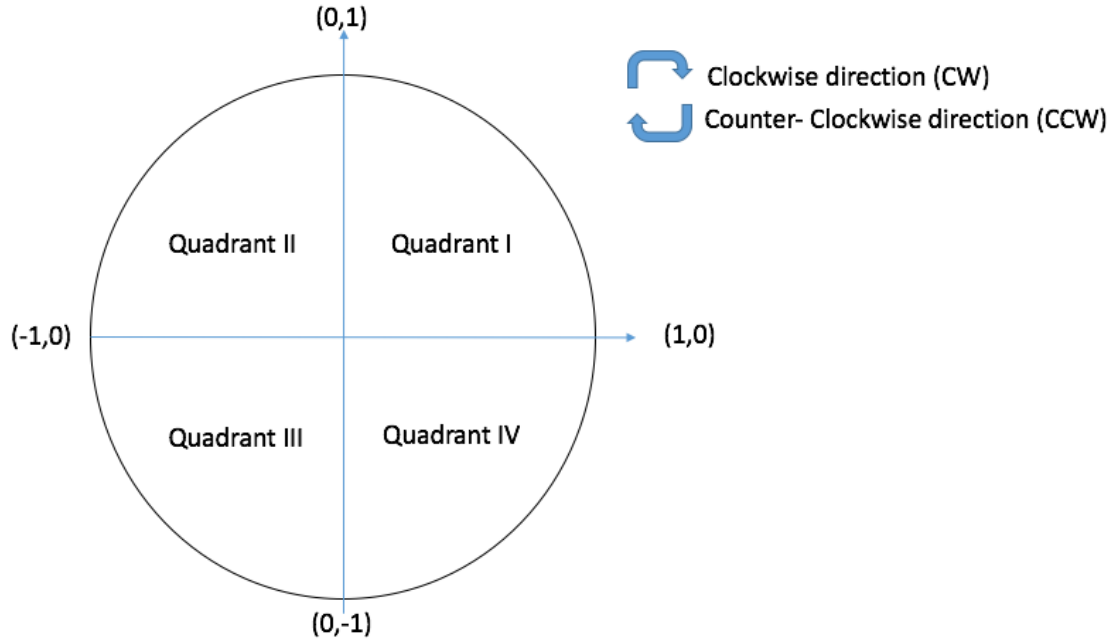

Figure 3.8: Unit circle.

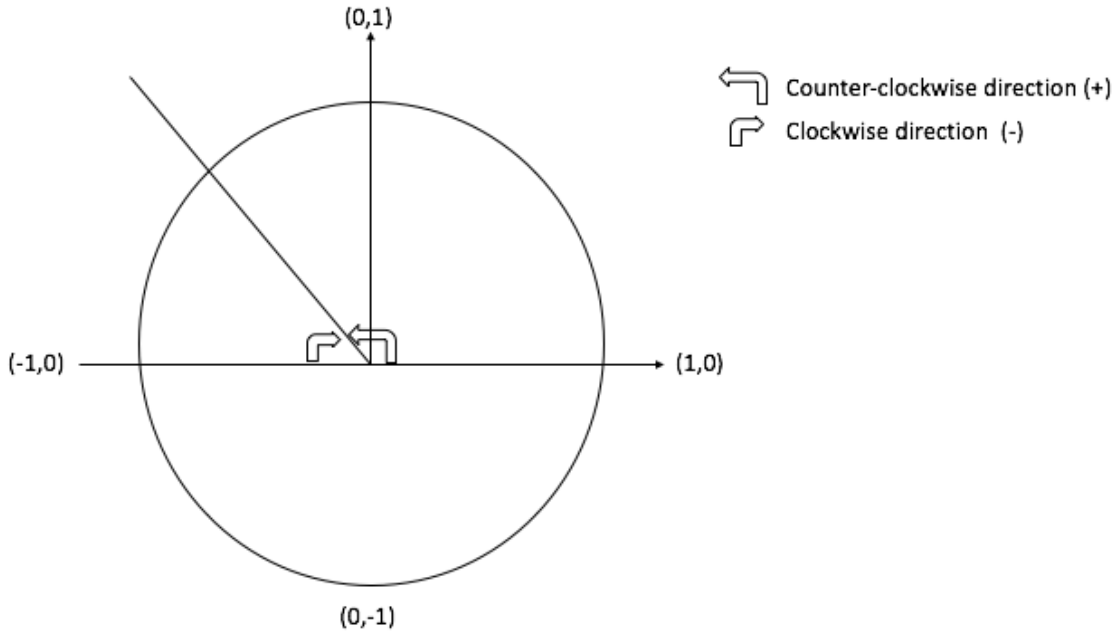

Figure 3.9: Specification for θ_3 and θ_4.

is a possibility for one angle to obtain two signs (+ and -). Hence, by using unit circle as shown in Figure 3.8, a unique solution could be obtained. The unit circle consists of length with radius 1. As seen in Figure 3.8, the unit circle is divided into four quadrants: Quadrant I, Quadrant II, Quadrant III and Quadrant IV. In this work, the range for θ_3 is restricted to be between 0 to π. Therefore, θ_3 exists in Quadrant I or II.

A tricky part in determining the unique solution for θ_3 is, to decide the sign. To determine the (+) and (-) signs, one condition as illustrated in Algorithm 1 is applied. This condition is applied according to the direction of unit circle (Figure 3.9). After the direction for θ_3 is known, it is important to determine the position of the θ_3 (Quadrant I or Quadrant II). Algorithm 2 shows the approach used to determined the Quadrant for the θ_3 for the case following CCW direction. The value obtained for the θ_3 in equation (3.10) is compared with the input. If the θ_3 is greater or equal to input, the final θ_3 is equal to θ_3 (Equation 3.10). Else, if θ_3 is less than input, then the final θ_3 is equal to the substraction of θ_3 from π. For the case CW, if the θ_3 is equal to the input, the final θ_3 is equal to equation (3.10). Else, the final θ_3 is equal to the substraction of θ_3 from π (Algorithm 3). The complete algorithm that is used to obtain the final θ_3 is presented in Algorithm 4.

Algorithm 1 Conditional statement for (+) and (-) sign

1: If input $>= 0$
2: The sign is following the CCW (+)
3: else
4: The sign is following the CW (-)

Algorithm 2 Conditional statement for determining Quadrants for the case CCW

1: If θ_3 $>=$ input
2: θ_3 = θ_3
3: Else
4: θ_3 =π - θ_3

Algorithm 3 Conditional statement for determining Quadrants for the case CW

1: If θ_3 $==$ input
2: θ_3 = θ_3
3: Else
4: θ_3 = $-(\pi + \theta_3)$

To obtain θ_4, cosine law is used. This law is used to obtain θ_a (Figure 3.10). θ_4 can be identified as an angle between the initial position of the elbow joint to some specific position as shown in Figure 3.10. The initial position is shown in dot lines (Figure 3.10). The length, L, can be calculated by taking the distance between position of shoulder joint, S, and wrist joint, W. The positions of shoulder and wrist joints can be defined as (x_1, y_1, z_1)

Algorithm 4 Complete algorithm for final θ_3

```
If input >= 0
    If θ3 >= input
        θ3 = θ3
    Else
        θ3 =π - θ3
Else
    If θ3 == input
        θ3 = θ3
    Else
        θ3 = −(π + θ3)
```

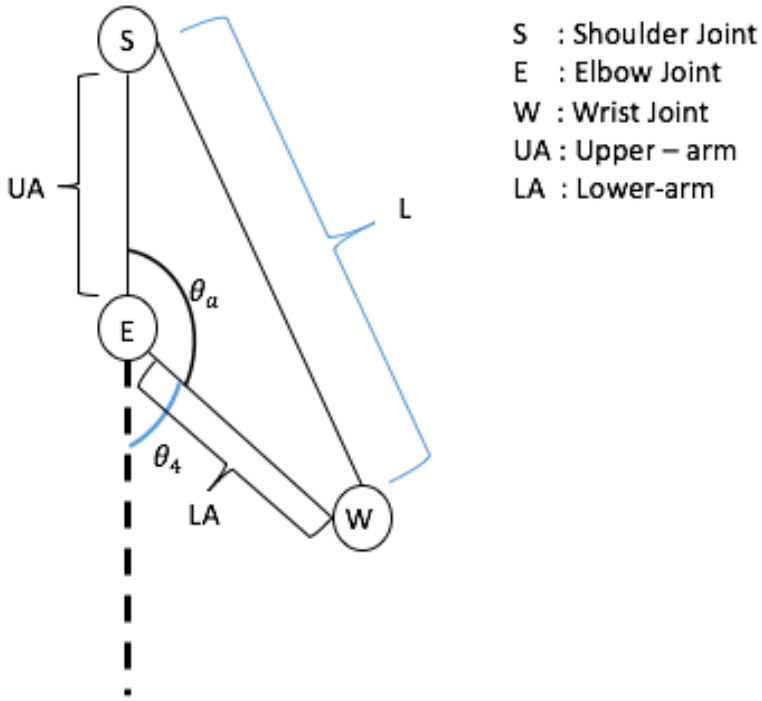

Figure 3.10: Position of θ_4.

and (x_4, y_4, z_4). Thus, the distance between these two points is:

$$L = \sqrt{(x_1 - y_1)^2 + (x_2 - y_2)^2 + (x_3 - y_3)^2} \tag{3.11}$$

To implement cosine law, the lengths of exoskeleton upper-arm (UA) and lower-arm (LA). The formula of cosine law gives :

$$L^2 = UA^2 + LA^2 - 2 * UA * LA * \cos(\theta_a) \tag{3.12}$$

Thus, θ_a, is given as:

$$\theta_a = \arccos(\frac{UA^2 + LA^2 - L^2}{2 * UA * LA}) \tag{3.13}$$

By letting $M = \frac{UA^2+LA^2-L^2}{2*UA*LA}$, equation (3.13) can be written as:

$$\theta_a = \arccos(M) \tag{3.14}$$

θ_4 is calculated as:

$$\theta_4 = \pi - \theta_a \tag{3.15}$$

Note that, θ_4 is restricted to [0, π].

Since θ_4 is restricted to between 0 and π, therefore, θ_4, could be in Quadrant I and Quadrant II. An algorithm is developed to determine the Quadrant for θ_4 and is described as in Algorithm 5.

Algorithm 5 Conditional statement for (+) and (-) sign

1: If input $>= 0$
2: $\theta_4 = \theta_4$
3: Else
4: $\theta_4 = -\theta_4$

To obtain θ_1 for the inverse kinematics, a position of x at Joint$_1$, is used. This position is obtained from the DH convention presented in forward kinematics and given as:

$$x_1 = L_2 \cos(\theta_1) \tag{3.16}$$

By rearranging equation (3.16), θ_1 is obtained as:

$$\theta_1 = \arccos(\frac{x_1}{L_2}) \tag{3.17}$$

Algorithm 5 is used to decide the sign for θ_1. To avoid confusion, algorithm 6 is presented for θ_1. Therefore, equation (3.17) with a combination of algorithm 6, will give a final θ_1.

Algorithm 6 Conditional statement for (+) and (-) sign

1: If input $>= 0$
2: $\theta_1 = \theta_1$
3: Else
4: $\theta_1 = -\theta_1$

3.4.2 Dynamics of the Exoskeleton

The dynamics of the system are defined as the study of the motion considering the moment, force or torque. In this work, the dynamic system of the designed exoskeleton is

developed by Euler-Lagrange approach because it is frequently used for modeling multi-rigid robotic systems. It contains the kinetic energy and potential energy. The Lagrangian can be described as $L = T - V$ where, T is the kinetic energy and V is the potential energy of the system. The Lagrangian is a function of generalized coordinates, q_j and generalized velocities, $\dot{q}_j$, which be represented as:

$$L = L(q_1, ..., q_j, ..., q_d, \dot{q}_1, ..., \dot{q}_j, ...\dot{q}_d) \tag{3.18}$$

where the d is the number of degree of freedom.

In this research, the d is four. Thus, the equation (3.18) become $L = L(q_1, q_2, q_3, q_4, \dot{q}_1, \dot{q}_2, \dot{q}_3, \dot{q}_4)$. The kinetic energy, T and the potential energy, V, for the designed exoskeleton are obtained by differentiating the vector position for each joint. The position vectors for the joints (θ_1, θ_2, θ_3 and θ_4) with respect to the fixed coordinate system are presented as:

$$\begin{pmatrix} x_1 \\ y_1 \\ z_1 \end{pmatrix} = \begin{pmatrix} L_2\cos(\theta_1) \\ L_2\sin(\theta_1) \\ L_1 \end{pmatrix} \tag{3.19}$$

$$\begin{pmatrix} x_2 \\ y_2 \\ z_2 \end{pmatrix} = \begin{pmatrix} L_2\cos(\theta_1) \\ L_2\sin(\theta_1) \\ L_1 \end{pmatrix} \tag{3.20}$$

$$\begin{pmatrix} x_3 \\ y_3 \\ z_3 \end{pmatrix} = \begin{pmatrix} L_2c_1 + L_3s_1c_3 - L_3c_1s_3s_2 \\ L_2s_1 - L_3c_1c_3 - L_3s_1s_2s_3 \\ L_1 + L_3s_3c_2 \end{pmatrix} \tag{3.21}$$

$$\begin{pmatrix} x_4 \\ y_4 \\ z_4 \end{pmatrix} = \begin{pmatrix} L_2c_1 + L_4c_4 * (s_1c_3 - c_1s_3s_2) + L_4s_4(-s_3s_1 - c_1c_3s_2) + \\ L_3s_1c_3 - L_3c_1s_3s_2 \\ L_2s_1 - L_4c_4(c_1c_3 + s_3s_1s_2) - L_4s_4(-c_1s_3 + s_1c_3s_2) - \\ L_3c_1c_3 - L_3s_3s_1s_2 \\ L_1 + L_3s_3c_2 + L_4c_4s_3c_2 + L_4s_4c_3c_2 \end{pmatrix} \tag{3.22}$$

where $c_1, c_2, c_3, c_4, s_1, s_2, s_3, s_4$ are $\cos(\theta_1), \cos(\theta_2), \cos(\theta_3), \cos(\theta_4), sin(\theta_1), \sin(\theta_2), \sin(\theta_3)$

and $\sin(\theta_4)$. The (x_i, y_i), in equations (3.19-3.22) are differentiated and shown below:

$$\begin{pmatrix} \dot{x}_1 \\ \dot{y}_1 \end{pmatrix} = \begin{pmatrix} -L_2 \sin(\theta_1)\dot{\theta}_1 \\ L_2 \cos(\theta_1)\dot{\theta}_1 \end{pmatrix} \tag{3.23}$$

$$\begin{pmatrix} \dot{x}_2 \\ \dot{y}_2 \end{pmatrix} = \begin{pmatrix} -L_2 \sin(\theta_1)\dot{\theta}_1 \\ L_2 \cos(\theta_1)\dot{\theta}_1 \end{pmatrix} \tag{3.24}$$

$$\begin{pmatrix} \dot{x}_3 \\ \\ \dot{y}_3 \end{pmatrix} = \begin{pmatrix} L_3c_1c_3\dot{\theta}_1 - L_2s_1\dot{\theta}_1 - L_3s_1s_3\dot{\theta}_3 - L_3c_1c_2s_3\dot{\theta}_2 - \\ L_3c_1c_3s_2\dot{\theta}_3 + L_3s_1s_2s_3\dot{\theta}_1 \\ L_2c_1\dot{\theta}_1 + L_3c_3s_1\dot{\theta}_1 + L_3c_1s_3\dot{\theta}_3 - L_3c_1s_2s_3\dot{\theta}_1 - \\ L_3c_2s_1s_3\dot{\theta}_2 - L_3c_3s_1s_2\dot{\theta}_3 \end{pmatrix} \tag{3.25}$$

$$\begin{pmatrix} \dot{x}_4 \\ \dot{y}_4 \end{pmatrix} = \begin{pmatrix} L_3c_1c_3\dot{\theta}_1 - L_2s_1\dot{\theta}_1 - L_3s_1s_3\dot{\theta}_3 + L_4c_1c_3c_4\dot{\theta}_1 \\ -L_3c_1c_2s_3\dot{\theta}_2 - L_3c_1c_3s_2\dot{\theta}_3 - L_4c_1s_3s_4\dot{\theta}_1 - L_4c_3s_1s_4\dot{\theta}_3 - \\ L_4c_4s_1s_3\dot{\theta}_3 - L_4c_3s_1s_4\dot{\theta}_4 - L_4c_4s_1s_3\dot{\theta}_4 + L_3s_1s_2s_3\dot{\theta}_1 - \\ L_4c_1c_2c_3s_4\dot{\theta}_2 - L_4c_1c_2c_4s_3\dot{\theta}_2 - L_4c_1c_3c_4s_2\dot{\theta}_3 - \\ L_4c_1c_3c_4s_2\dot{\theta}_4 + L_4c_3s_1s_2s_4\dot{\theta}_1 + L_4c_4s_1s_2s_3\dot{\theta}_1 + \\ L_4c_1s_2s_3s_4\dot{\theta}_3 + L_4c_1s_2s_3s_4\dot{\theta}_4 \\ L_2c_1\dot{\theta}_1 + L_3c_3s_1\dot{\theta}_1 + L_3c_1s_3\dot{\theta}_3 + L_4c_3c_4s_1\dot{\theta}_1 + \\ L_4c_1c_3s_4\dot{\theta}_3 + L_4c_1c_4s_3\dot{\theta}_3 + L_4c_1c_3s_4\dot{\theta}_4 + L_4c_1c_4s_3\dot{\theta}_4 - \\ L_3c_1s_2s_3\dot{\theta}_1 - L_3c_2s_1s_3\dot{\theta}_2 - L_3c_3s_1s_2\dot{\theta}_3 - L_4s_1s_3s_4\dot{\theta}_1 - \\ L_4c_1c_3s_2s_4\dot{\theta}_1 - L_4c_1c_4s_2s_3\dot{\theta}_1 - L_4c_2c_3s_1s_4\dot{\theta}_2 - \\ L_4c_2c_4s_1s_3\dot{\theta}_2 - L_4c_3c_4s_1s_2\dot{\theta}_3 - L_4c_3c_4s_1s_2\dot{\theta}_4 + \\ L_4s_1s_2s_3s_4\dot{\theta}_3 + L_4s_1s_2s_3s_4\dot{\theta}_4 \end{pmatrix} \tag{3.26}$$

The total kinetic energy, T of the whole system is given by:

$$\begin{aligned} T(q,\dot{q}) =& \frac{1}{2}(m_1(\dot{x}_1^2 + \dot{y}_1^2) + m_2(\dot{x}_2^2 + \dot{y}_2^2) + m_3(\dot{x}_3^2 + \dot{y}_3^2) + m_4(\dot{x}_4^2 + \dot{y}_4^2)) \\ &+ \frac{1}{2}(I_1\dot{\theta}_1^2 + I_2(\dot{\theta}_1 + \dot{\theta}_2)^2 + I_3(\dot{\theta}_1 + \dot{\theta}_2 + \dot{\theta}_3)^2 + I_4(\dot{\theta}_1 + \dot{\theta}_2 + \dot{\theta}_3 + \dot{\theta}_4)^2) \end{aligned} \tag{3.27}$$

The total potential energy of the four degree-of-freedom exoskeleton is presented as:

$$V(q) = m_1gy_1 + m_2gy_2 + m_3gy_3 + m_4gy_4 \tag{3.28}$$

Thus, equations (3.27) and (3.28) give the Lagrangians as:

$$L = T(q,\dot{q}) - V(q) \tag{3.29}$$

The dynamic equation can be obtained by applying partial derivatives to equation (3.29).

$$\frac{d}{dt}\left(\frac{\partial L}{\partial \dot{q}}\right) - \frac{\partial L}{\partial q} = \Gamma \tag{3.30}$$

A dynamic model of the exoskeleton (equation (3.30)) can be rewritten as:

$$M(q)\ddot{q} + C(q,\dot{q})\dot{q} + G(q) = \Gamma \tag{3.31}$$

in which $M(q)$ is the exoskeleton inertia matrix, $C(q,\dot{q})$ is a matrix containing the Coriolis and centrifugal terms, $G(q)$ is a vector containing the gravity torques, Γ is vector of external torques acting on the actuated degree-of-freedoms (DOF) and q, $\dot{q}$ and $\ddot{q}$ are positions, angular velocities and angular accelerations of the revolute joints.

The full presentation of the Lagrange equation are in Appendix B. The dynamic equation (Equation (3.31)) was validated using SimMechanics modul of Matlab (Figure 3.11). The validation process was done by applying angular position onto shoulder and elbow joints.

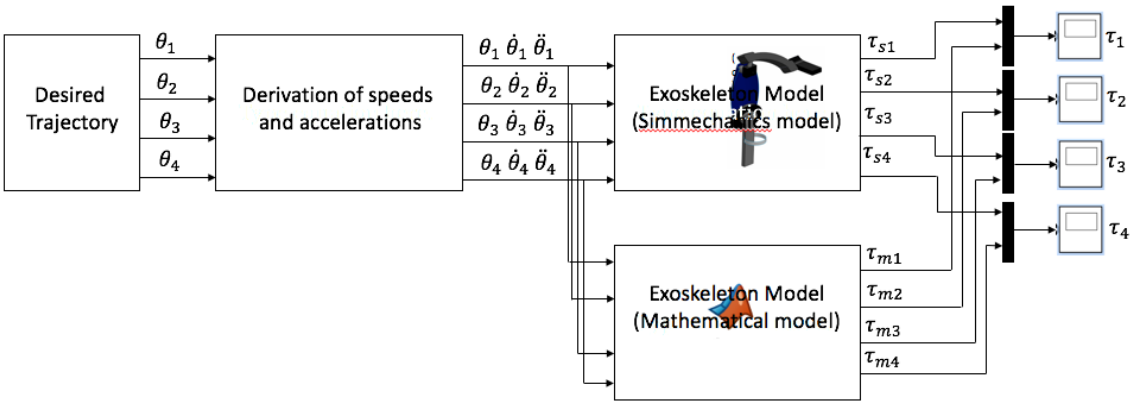

Figure 3.11: SimMechanics and Simulink diagram to simulate the dynamical system.

Two different motions states used (Figure 3.12): static and flexion/extension for shoulder and elbow joints.

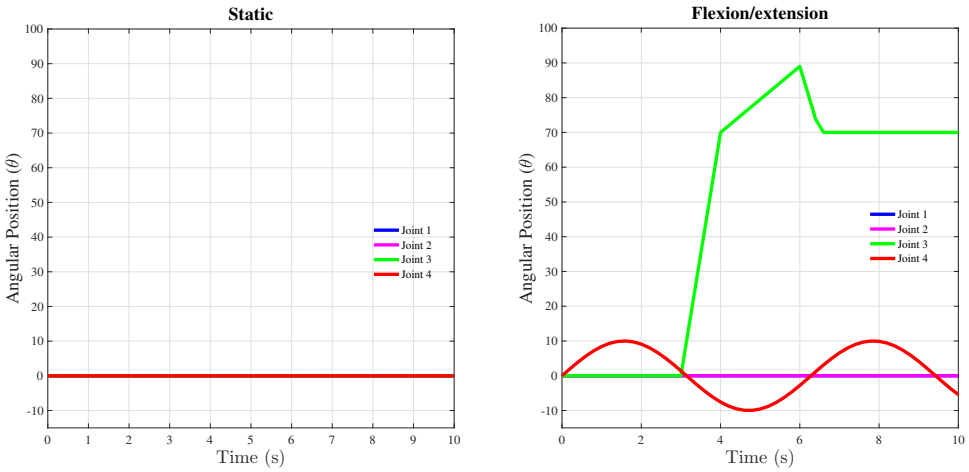

Figure 3.12: Angular position: (a) Static (b) Flexion/extension.

Figure 3.13 and Figure 3.14 show the angular velocity and torque measured from the static movement. It is obvious that these two measurements are 0 because there was no excitation applied to these joints.

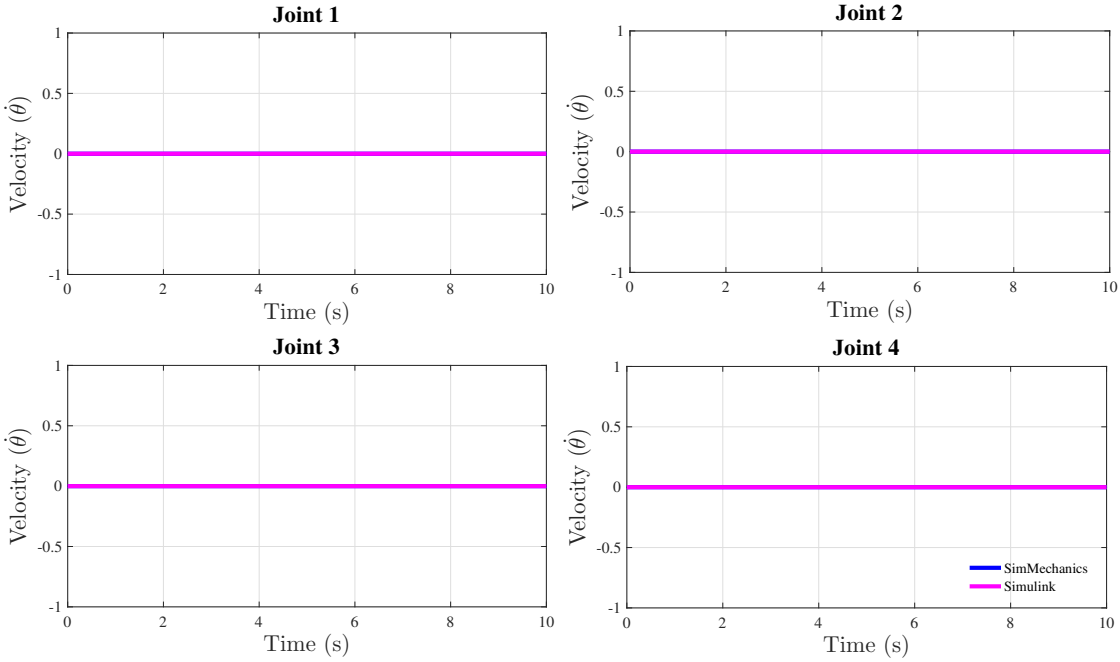

Figure 3.13: Angular velocity for static.

Meanwhile, Figure 3.15 and Figure 3.16 show changes for both joints. Although, excitation was applied for flexion to shoulder joint and flexion-extension to elbow joint,

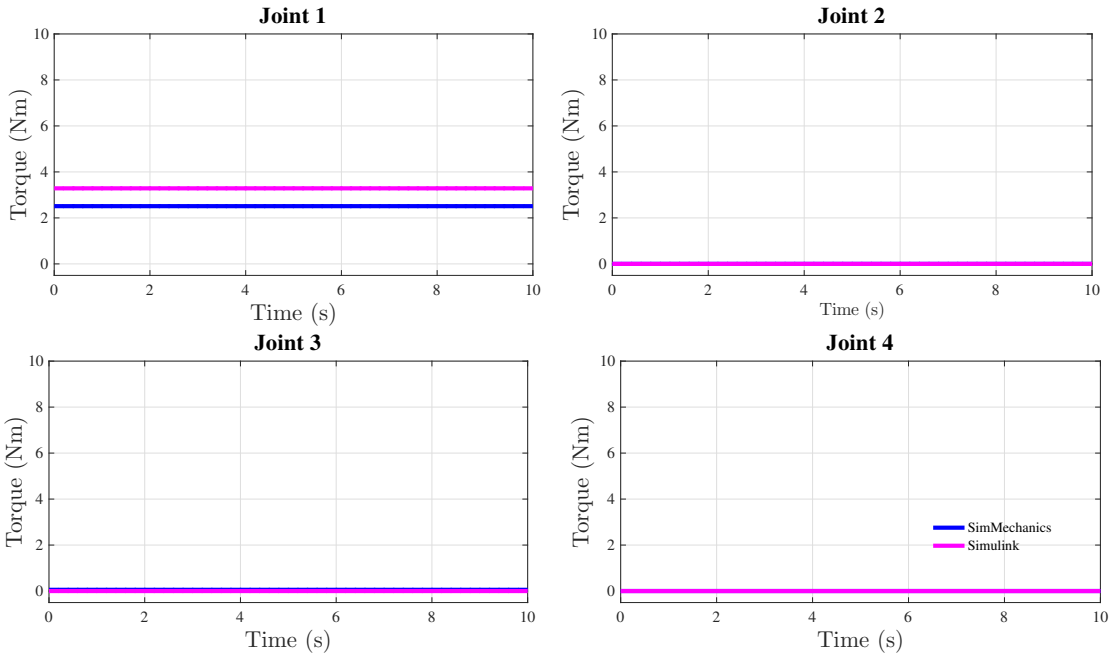

Figure 3.14: Torque for static.

the movements affected the torques of shoulder internal/external and shoulder abduction/adduction (Figure 3.16). This is due to the coupling effect of the exoskeleton. However, the effects were small.

The pattern of the τ_1, τ_3 and τ_4 of the SimMechanics and the mathematical representation of the dynamic system of the exoskeleton were similar in shape, although were different in values (Figure 3.16). The torque generated from the mathematical representation (Simulink) was slightly higher than that from SimMechanics. This could be due to minor differences in the geometrical model built in SimMechanics and parameters described in the mathematical equation (Biesiacki et al., 2015). However, for Joint_2, the pattern was different between SimMechanics and Simulink. However, since the discrepacies are less than 0.5 and, this can be considered insignificant.

3.5 Summary

This chapter has described an upper-limb exoskeleton developed in SimMechanics software as the system model. The exoskeleton and human model based on SolidWorks has

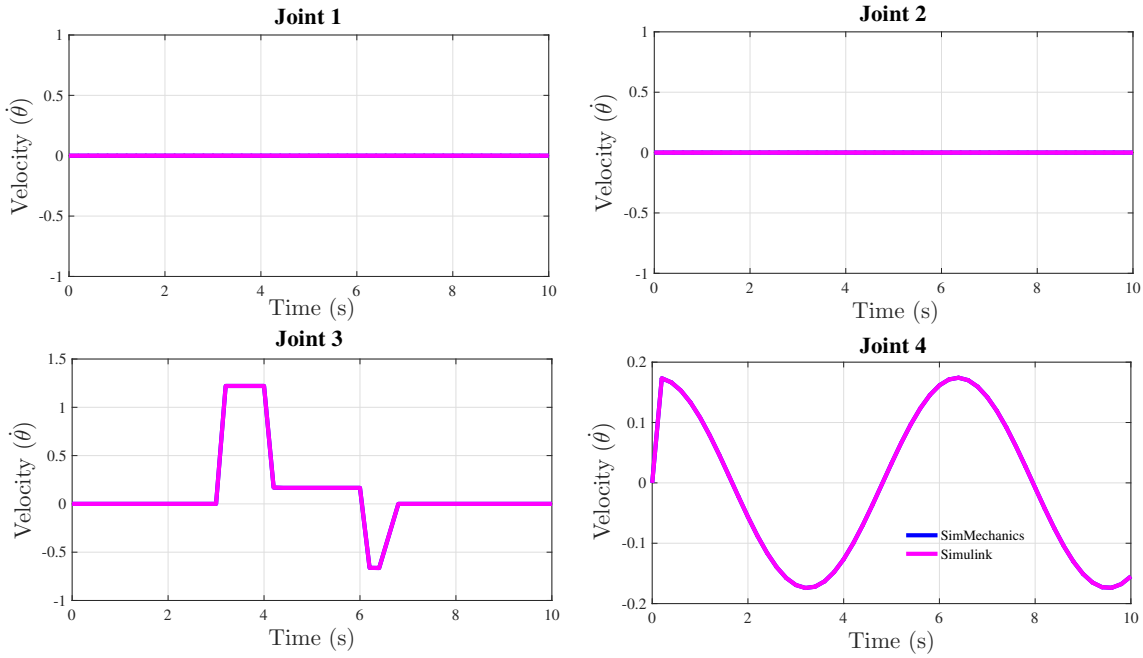

Figure 3.15: Angular Velocity for flexion and extension.

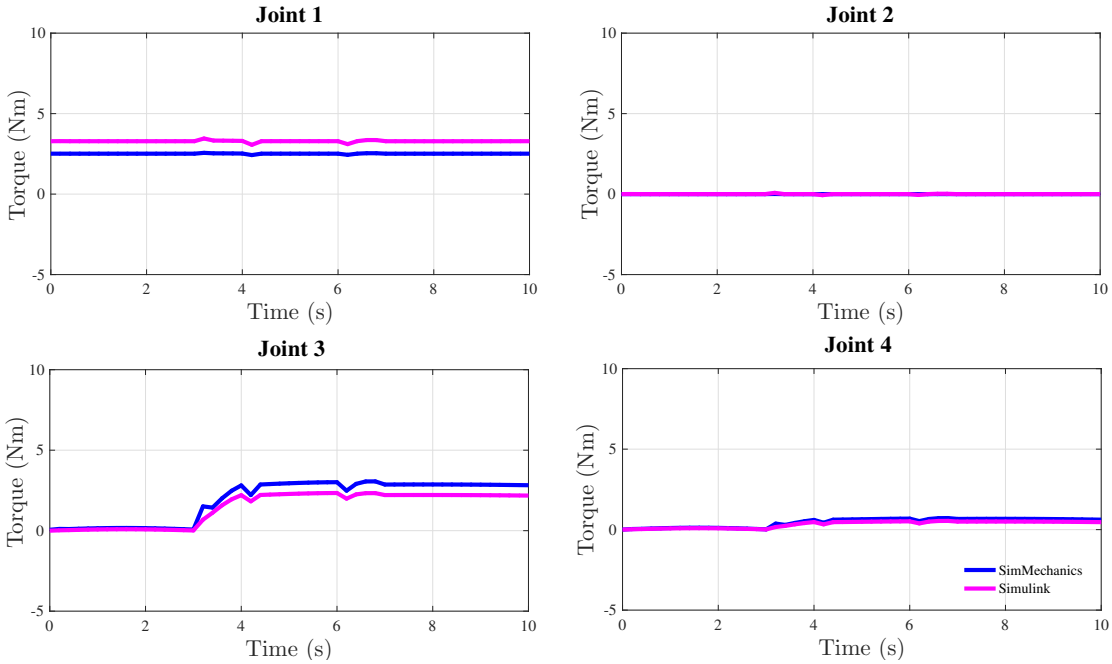

Figure 3.16: Torque for flexion and extension.

been integrated with SimMechanics to produce more realistic model. The exoskeleton and humanoid models thus developed in this study for purpose of control design and evaluation.

Chapter 4

Control Design of an Upper Limb Exoskeleton

4.1 Introduction

In this chapter, an investigation through simulation of control of an exoskeleton is presented. The Simmechanics and Simulink were used as a platform to present the simulation. The exoskeleton is used to track the desired trajectory by using a control torque. Two types of references are used to examine the tracking performance, deviation or error and torque required to move the joint of an exoskeleton. The two types of references are abrupt and non-abrupt movements. The observations begin by observing the performances of Proportional-Integral-Derivative (PID) control and fuzzy-based Proportional-Derivative (PD) control. According to the performances of both controllers, extended-fuzzy controller is proposed. The extended-fuzzy controller consists of the fuzzy-based PD and fuzzy gravity compensator controller. In the next section, the background to PID and fuzzy-based PD control are presented.

4.2 Control of an Exoskeleton

In this section, the control structure of an exoskeleton is presented. The controller is used to supply an assistive torque to human when human strength is decreasing. However, in this section, no human is integrated to the exoskeleton. The exoskeleton is controlled by the controller to achieve the desired trajectory. Two types of controller are investigated to track

the desired trajectory. The two controllers are PID and fuzzy-based PD controllers. The performances of the control system with these two controllers are compared and presented. In the next sections, the idea of the control approach is presented.

4.2.1 Control Mechanism of an Exoskeleton

The control strategy of the exoskeleton is shown in Figure 4.1. The controller starts with the identification of the source of reference trajectory. The reference or the desired trajectory could be obtained in two ways; from a predefined trajectory or gathered from a human. In this chapter, the reference is identified by a predefined trajectory and it is obtained from Ma et al. (2012). The details of obtaining the references from human will be presented in Chapter 5.

Next, is the joint activation. The exoskeleton consists of four joints which represent the shoulder abduction/adduction (J1), shoulder internal/external (J2), shoulder flexion/extension (J3) and elbow flexion/extension (J4). Joint activation will identify which joint is moving at one time. The joint activation is needed to ensure that the movement of the joint exoskeleton is parallel to human progress. To activate the joint movement, three pieces of information are needed. These are the current desired trajectory, the previous desired trajectory and the reference selection. Three important questions need to be asked before applying conditions to activate the joints. The questions are:

1. How the reference is obtained?
2. How to identify that the joint is moving?
3. What is the direction of the movement?

The first question is answered by the selection of the reference. As mentioned earlier, the predefined trajectory is used in this chapter. Hence the 'Ref' is equal to '0' (Figure 4.1 (b)). For the second question, to identify that the joint is moving, a condition is applied. The current desired trajectory (θ_{di}) is tested. If $\theta_{di} \neq 0$, where $i = 1,2,3,4$, then, the joint is moving. For the third question, two types of direction are identified. The joint could move approaching or move away from the initial position of the exoskeleton. To identify this, the current desired trajectory (θ_{di}) and previous desired trajectory (θ_{ddi}) are compared. The

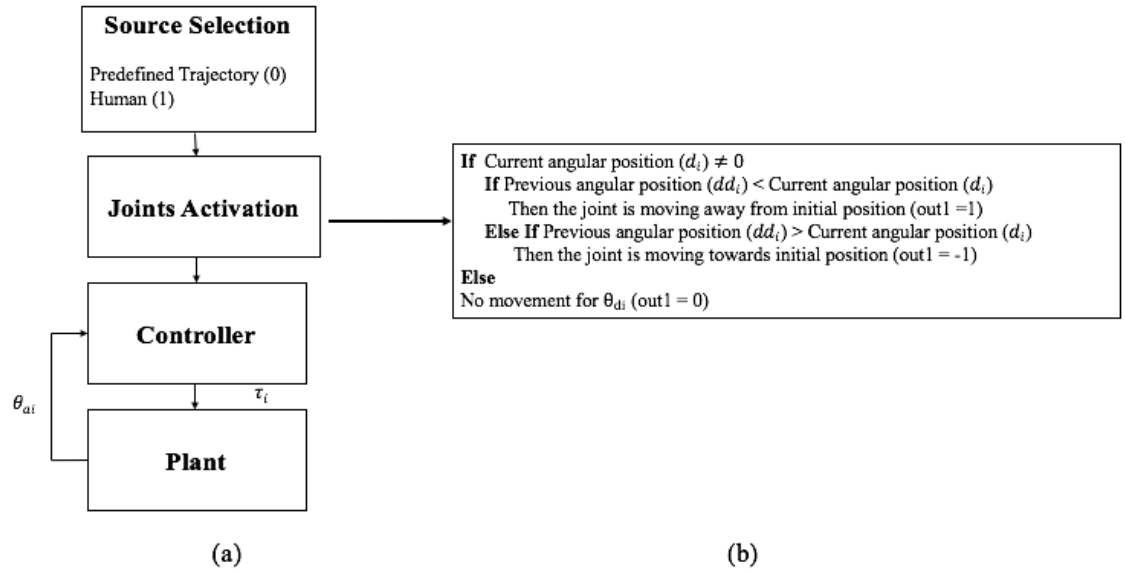

Figure 4.1: Control design: (a) Control structure of an exoskeleton (b) The process of joints activation.

joint is moving away from the neutral position if $\theta_{ddi} < \theta_{di}$ and the joint is approaching the neutral position if $\theta_{ddi} > \theta_{di}$.

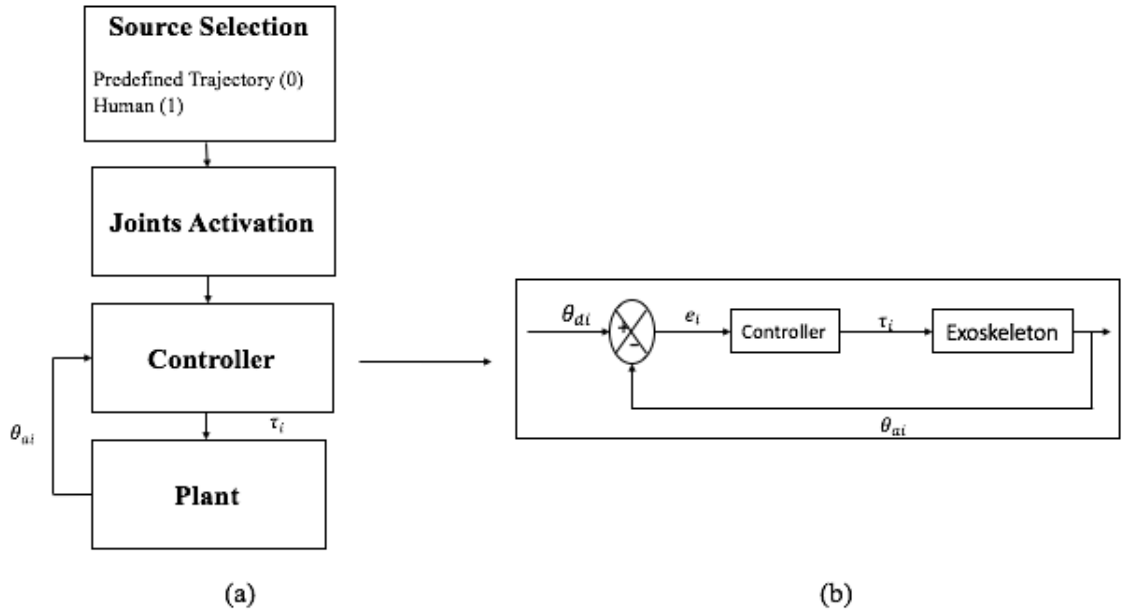

Figure 4.2: Control design: (a) Control structure of an exoskeleton (b) Controller.

There are three possible outcomes (out_i) from these conditions, and they are identified as 0, -1 or 1. The $out_i = 0$ means that, no movement for the joint. If the $out_i = 1$, the joint is moving away from the neutral position of the exoskeleton. If the $out_i = -1$, the joint is approaching the neutral position of the exoskeleton. If the $out_i = 1$ or $out_i = -1$, then,

the current desired trajectory (θ_{di}), is sent as the desired trajectory of the exoskeleton. The process in 'Joints Activation' has been summarised in Figure 4.1 (b).

The out_i will let the system know which joint needs to be moved. Then, the error is measured between the current desired trajectory (θ_{di}) and the actual trajectory, and then the error is sent to the controller. Based on the error information, the controller generates an appropriate amount of torque to produce the desired position of the joint. Figure 4.2 (b) shows the feedback control system of the exoskeleton.

In this scheme, three controllers are implemented and the performances are compared. The controllers are PID, fuzzy-based PD, and extended-fuzzy control.

4.2.2 Proportional-Integral-Derivative Control

PID controller is a well-known. It has been used widely in industry due to the simplicity in implementation and reliability. In addition, it is easy to tune to provide robust performance in any application and it does not need a mathematical model of the plant. Figure 4.3 shows the structure of PID control system.

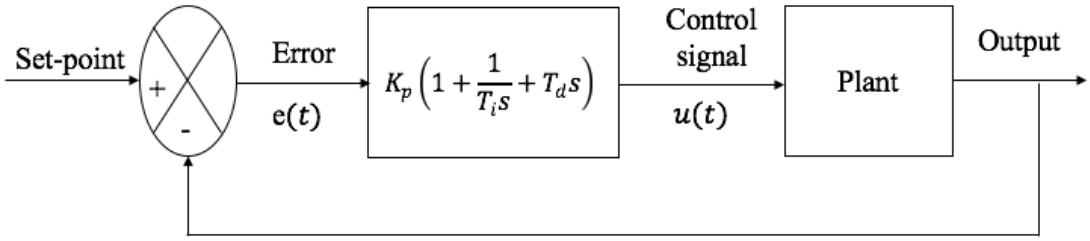

Figure 4.3: PID Control System.

The $e(t)$ represents the tracking error. The tracking error is obtained by subtracting the set-point from the output of the plant. Then, the tracking error is used as an input to the controller, and the controller generates the control signal. The control signal is fed to the plant. The output from the plant is fed back and compared to the reference/set-point. This process will continously occur until the set-point is achieved.

Each component (P, I, D) of the PID controller could be used as a controller, and each has its advantages and disadvantages. Thus, a combination of the P, I and D could balance the advantages and disadvantages of the components.

The proportional variable or term is a multiplication of a tracking error $e(t)$ with a proportional gain, known as K_p

$$Proportional = K_p \times e(t) \tag{4.1}$$

The proportional gain (K_p) needs to be tuned depending on the tracking error ($e(t)$). The high tracking error ($e(t)$) could cause an overshoot, thus the proportional gain (K_p) needs to be increased, and vice-versa if the tracking error ($e(t)$) is low. However, too high or too low proportional error could lead to oscillatory output. Hence, to ensure the stability of the system, the tuning process of the proportional gain needs to be continuously done until the the system is stable. Advantages of P controller are that, it could reduce the rise time and steady-state error. However, the steady state error could not be eliminated.

To eliminate the steady-state error, Integral (I) term is applied. The output of I term is an integration of tracking error, $\int e(t)dt$, multiplied with an integral gain, K_i

$$Integral = K_i \times \int e(t)dt \tag{4.2}$$

However, the I term could cause transient response to oscillate in a decreasing or increasing amplitude. Therefore, it is advisable to choose the smallest value of K_i at the beginning of the process.

The Derivative (D) variable is a differentiation of a tracking error, $\frac{de}{dt}$, multiplied with derivative gain, K_d

$$Derivative = K_d \times \frac{de(t)}{dt} \tag{4.3}$$

The D variable could be used to inhibit more rapid changes of the measurement than P and I controllers. Thus, D controller could anticipate the error and initialize an early corrective action, and tends to increase the stability of the system. The system could be stable by adding D variable, due to its capability to improve the transient response and reduce the overshoot/undershoot.

By considering the advantages and disadvantages of each variable, it is beneficial to put all the P, I and D terms together and present them as PID controller. Thus, the complete PID controller is presented as

$$u(t) = K_p e(t) + K_i \int e(t)dt + K_d \frac{de(t)}{dt} \tag{4.4}$$

This is alternatively represented as

$$u(t) = K_p(e(t) + \frac{1}{T_i} \int e(t)dt + T_d \frac{de(t)}{dt}) \tag{4.5}$$

where T_i and T_d are integral time and derivative time respectively.

A heuristic approach is mostly used in obtaining the P, I and D gains. It is essential to understand the effect of each variable on dynamic behaviour of the system. The effects after a step change in set-point are as follows:

- Too high oscillation at the plant output is caused by too large proportional gain (K_p).
- An overdamped response or a slow action, obtained at the plant output is caused by too small proportional gain (K_p).
- For a positive reference change, when the process output oscillates and stays above the reference longer than below, it means that the integral control action is too strong (integral time, T_i is too small)
- For a positive reference change, when the process output oscillates and stays under the reference longer than above the set-point, it means that the integral control action is too weak (integral time, T_i is too big)
- If the process output shows a high-frequency oscillation from the start to the steady state, then the derivative time T_d is too large. This is due to the amplification of a high frequency signal by the overly strong derivative term.

4.2.3 Fuzzy Logic Control

Fuzzy Logic Control (FLC) system is based on fuzzy logic theory. The fuzzy logic theory was proposed by Lotfi A. Zadeh (Zadeh, 1973). This theory is based on the idea that in this

world, there is no system, behaviour or decision making, that is entirely white or black, but it is white, black and in between. The category in between the white and black, is known as grey. The grey or shade area is categorised to be more or less white and more or less black. The degree of the categorisation depends on the previous experience of the black or white colour.

The implementation of the fuzzy logic in control has widely used in many systems that contain non-linearities and uncertainties. Fuzzy control is chosen for implementation in such applications due to its ability to execute rational decision making (Xiao et al., 2004). In addition, as part of computational intelligent approach, fuzzy logic has an advantage because the technique is close to human reasoning and decision making process. Moreover, the implementation of fuzzy logic in identifying the environment behaviour and real system is not difficult. Besides, in terms of theory and practicality, fuzzy logic control shows superiority compared to conventional methods (Wang, 1993). However, since the mathematical model of the plant is not needed in fuzzy control, formal stability analysis could not be performed (Wang, 1993).

Although the mathematical model was presented and validated in Chapter 3, the mass and center of mass were assumed to be known. Due to the reason of assuming that no mathematical equation is needed, and the advantages mentioned earier, the fuzzy logic control is chosen to be implemented in this work.

The following characteristics of fuzzy logic system strongly motivate the adoption of a fuzzy logic approach in this work.

- It is known that fuzzy logic control is suitable for a system that is difficult to model and obtain the mathematical representation (model-free approach). In this work, due to a complexity of the model, it will be difficult to obtain an accurate mathematical representation. Hence, by adopting fuzzy logic control, this problem could be avoided.
- In addition, each human has their own strength. With the capability of fuzzy logic control in dealing with uncertainties and nonlinearity, hence, this controller could deal with the variety of human's strength. This could be modelled in linguistic de-

scription from human expert.

- Moreover, with the capability in dealing with uncertainty of the system, fuzzy logic control also capable in dealing with the variation of the human size.

Figure 4.4 shows the configuration of fuzzy logic controller. There are three important elements in the fuzzy controller. The elements are fuzzification, inferens mechanism and defuzzification. It is essential in designing a fuzzy controller to identify variables of the plant such as input, output or state. Then, the universe of discourse is partitioned into a number of fuzzy sets. Next, the fuzzy set is assigned to linguistic labels such as slow, medium and fast, to each partition.

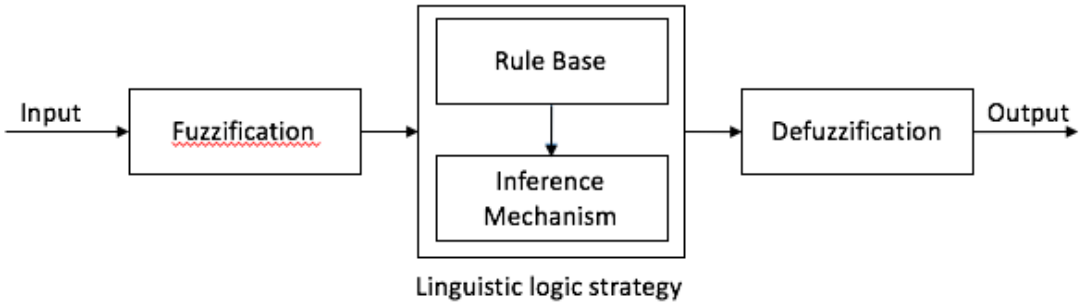

Figure 4.4: Configuration of fuzzy controller.

After the variables and the fuzzy set are identified, fuzzification is applied. This process involves transformation of crisp/numeric set into a fuzzy set. The crisp set is the exact measured input from sensors. It is determined by a bivalent truth function. It only considers the values 0 and 1, which means the element exists (1) in the set or does not exist (0) in the set. The fuzzy set is determined by a membership function (MF), which includes the intermediate values between 0 and 1. It also can be defined as a set of ordered pairs of an element, x, where x is a subset of universe of discourse set, U ($x \varepsilon U$), and its membership function $\mu_A(x)$. Hence, the fuzzy set A in U could be written as $\{(x_i, \mu_A(x_i))\}$.

Figure 4.5 shows the fuzzy membership, in a triangular shape, with an example of α-cut point at $\mu_A(x) = 0.8$. The membership function describes to what degree the element belongs to a fuzzy set in terms of certainty (degree of truth). The range for the membership function could be in the form of normalization, i.e [0, 1] or [-1, 1] or in the form of similar to the crisp range. There are various shapes to present the degree of truth or membership

function such as Trapezoidal, Gaussian and Triangle shapes. To ensure that the input and output variables could exist in the normalised range, scaling factors must be assigned to both variables.

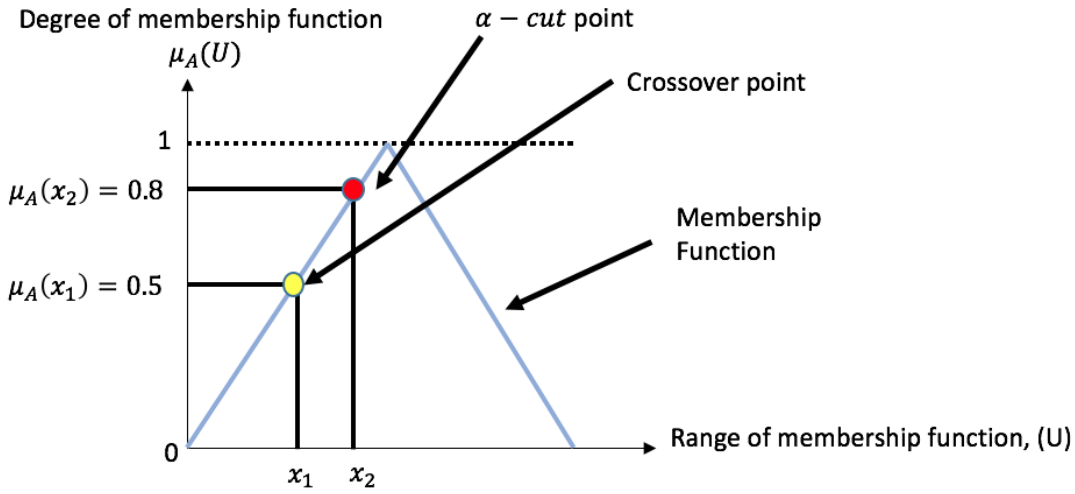

Figure 4.5: Fuzzy membership function.

The second step is an inference mechanism. By definition, inference is a process of gathering or obtaining new knowledge based on existing knowledge. In fuzzy logic, this process is essential because through this process, the relation between input and output could be developed by using deductive approach. This relation is formed by if-then rules. For an example:

if x is A, then y is B

where A and B are the linguistic labels/variables, and x and y are sets of a universal set. The 'if-then' rule is called a fuzzy implication, the 'if x is A' is known as antecedent or premise and the 'then y is B' is called as consequence or conclusion. There are two approaches to represent the deductive inference: Mamdani and Sugeno. The Mamdani approach presents the linguistic variables in input and output variables.

In Mamdani approach, there are two factors that are used to determine the number of rules: the number of input, b, and the number of linguistic variable, m. In general, the rules of the fuzzy logic control are determined using m^b. In addition, there is no limit for the linguistic variables to be involved in the 'if-then' rule. With this advantage, fuzzy logic

control is suitable to be applied to various types of system such as Single Input Single Output (SISO), Multi Input Multi Output (MIMO) and Multi Input Single Output (MISO) system. For the case of more than one input, the rule is linked by using the linguistic connectives such as 'and' and 'or'. For instance, the rule for MISO could be presented as:

if x is A and y is B, then z is C

where A, B and C are the linguistic variables, and x and y are the input and z is the output.

Compared to Mamdani, the Sugeno approach is more systematic in creating the fuzzy rules. Instead of using the linguistic variable for output, the Sugeno approach uses information of a crisp function of the input. However, extensive information is needed to use this approach. An example of the Sugeno inference approach is as follows:

if x is A and y is B, then z is z = f(x,y)

The third step in the FLC is defuzzier. Defuzzification is a process of translating the linguistic variable value to the crisp value. Then, the crisp value is sent to the plant. There are several approaches of defuzzification such as Centroid of Gravity, Max-Membership and Middle-of-Maxima (MoM) approach. All of these approaches are application dependent.

In the next section, the implementation of the controllers is presented.

4.3 Implementation of Controllers

In this section, the implementation of all controllers on an exoskeleton are presented. The implementations are divided into two sections. The first section will present the implementation of PID controller, fuzzy-based PD and the next section will present the implementation of extended-fuzzy controller. Two types of movement were used to observe the performances of PID and fuzzy-based PD controllers. The movements used were abrupt and non-abrupt movements. Based on the observation of PID and fuzzy-based PD controllers, the non-abrupt movement is chosen to access the performance of extended-fuzzy controller.

4.3.1 PID-Control of the Exoskeleton

In this section, the implementation of the PID controller on the exoskeleton is presented. The torque control is sent to the exoskeleton depending on the deviation of the actual and the desired position. The simulation is divided into two categories as shown in Figure 4.6. The first category is the evaluation without incorporation of the human model. With this category, the exoskeleton is evaluated with two conditions: with disturbance and without disturbance. The second category is the evaluation with the human model and the human is assumed to be in two conditions: non-fatigue and fatigue. The second category will be presented in Chapter 5 (See Figure 4.6(b)).

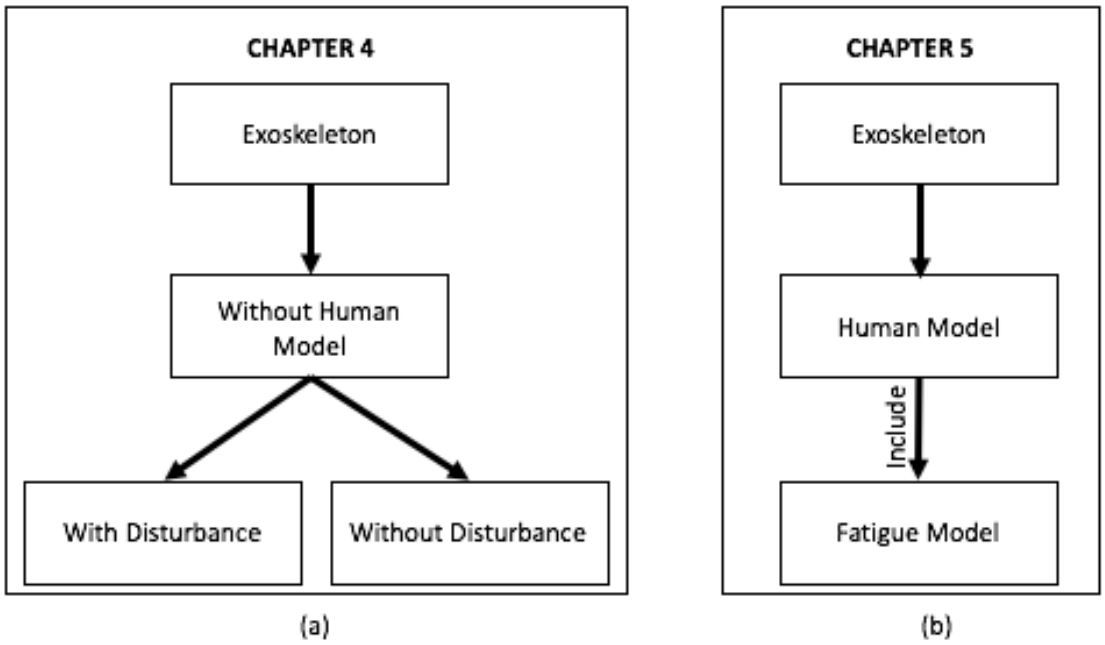

Figure 4.6: Evaluation steps (a) First evaluation (b) Second evaluation.

As shown in Figure 4.6(a), the first category will be presented and discussed in this chapter. The PID controller is chosen as a baseline for comparison purpose, due to the advantages mentioned in Section 4.2.2. The PID controller is used to supply the necessary torque to the exoskeleton in order for the exoskeleton to move or achieve the desired position or trajectory. Figure 4.7 shows the implementation of the PID controller on the exoskeleton for each joint in a joint-space environment. Figure 4.8 shows the overall system of the exoskeleton with the PID controller. In this chapter, the parameter gains are obtained by using a heuristic approach.

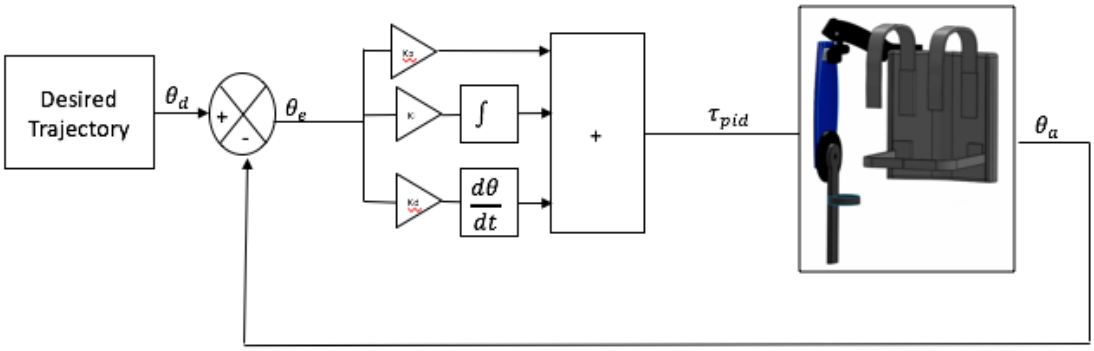

Figure 4.7: Block diagram of the PID controller.

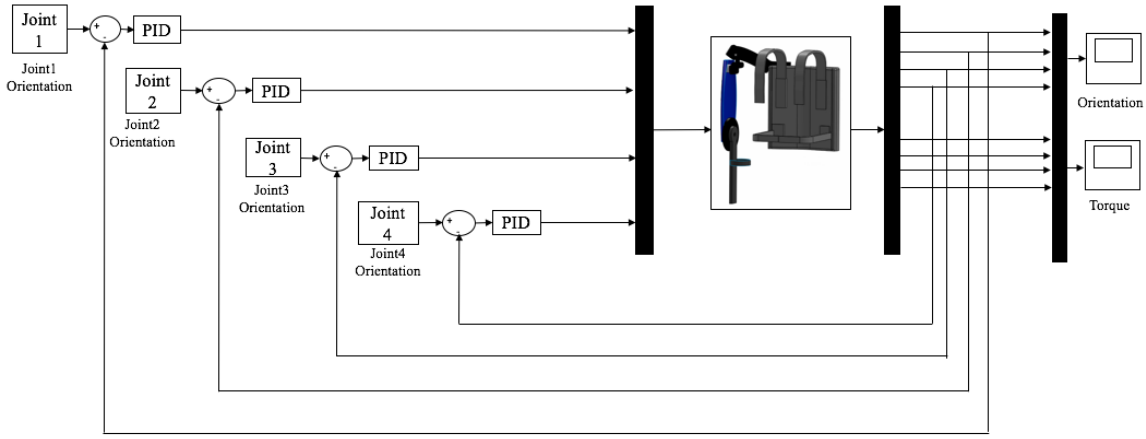

Figure 4.8: An exoskeleton with the PID controller.

4.3.2 Fuzzy-based PD Control of the Exoskeleton

Due to advantages mentioned in Section 4.2.3, the fuzzy-based PD Mamdani type controller is chosen for controlling the human-exoskeleton movement. However, in this section, only the movement of the exoskeleton is involved in the investigation. The combination of fuzzy-based PD is chosen due to the ability of PD in minimizing the steady-state error and the rise time, so that the power consumption is less.

Similar to that in Section 4.3.1, two conditions were applied. First, the system without external disturbance and the second condition is, the system with the external disturbance. Figure 4.9 shows the implementation of fuzzy-PD controller on exoskeleton system. The overall system of the exoskeleton for fuzzy-PD controller is similar to that in Figure 4.8.

As mentioned in Section 4.2.3, it is essential to identify the input and output of controller. The fuzzy-based PD controller consists of two inputs: the position error (e) and

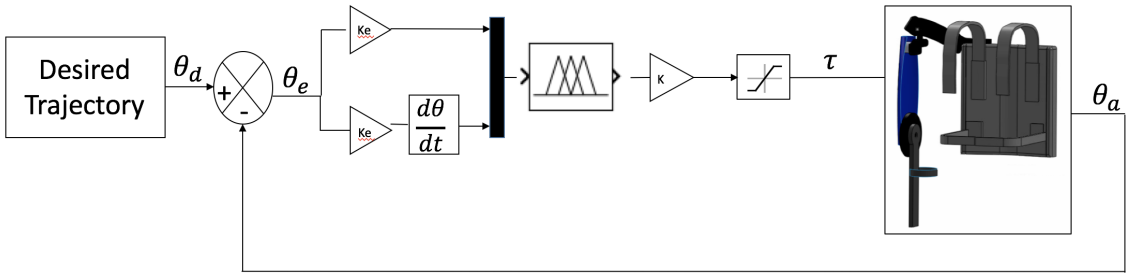

Figure 4.9: Block diagram of the fuzzy-based PD controller.

the rate of change of error ($\dot{e}$). The error is measured between the plant and the reference trajectory, and the rate of change of the errror is the derivative of the measured error. The output of the controller is the torque required to generate motion of each joint.

The controller also consists of five Gaussian type membership functions (MFs) to ensure that the system response is smooth. The five MFs are Negative Big (NB), Negative Small (NS), Zero (Z), Positive Small (PS) and Positive Big (PB). These membership functions were normalised in the range of [-1, 1]. It is known that the inputs (b) are two and the membership functions(m) are five. Hence, using the formula m^b, the number of rules are $5^2 = 25$ for each fuzzy controller with 50 % overlap between MFs. The 25 rules are presented in Table 4.1 and the the details are presented in Figure 4.10.

Table 4.1: Construction of fuzzy rules

$e/\dot{e}$	NB	NS	Z	PS	PB
NB	PB	PB	PB	PS	Z
NS	PB	PB	PS	Z	NS
Z	PB	PS	Z	NS	NB
PS	PS	Z	NS	NB	NB
PB	Z	NS	NB	NB	NB

In general, if the both error and change of error are both positive big (PB), the control action will produce negative big (NB) signal to bring back the output to the desired trajectory. On contrary, if both error and change of error are both negative big (NB), the control action will supply the positive big (PB) signal to ensure the output trajectory go to the desired position. For the case of error is positive big (PB) and change of error is negative big (NB) or vice-versa, zero (Z) control signal is applied to the system because

the system is at a steady-state condition.

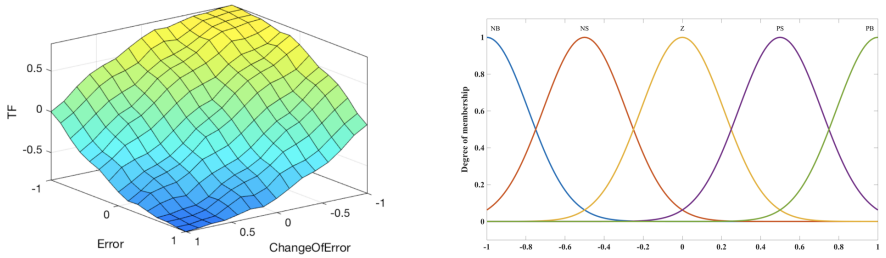

(a) (b)

Figure 4.10: Details of fuzzy-based PD control: (a) Fuzzy logic 3D surface (b) Membership functions for inputs and outputs for the exoskeleton joints motions.

These rules are developed based on the knowledge to minimize the position error of each joint of the exoskeleton and to ensure smoothness of the motion. In addition, the max-min inference is used to ensure that the exoskeleton could be moved fast. The centroid or centre of gravity is chosen to be used during the defuzzification process due to its fine and smooth transition output.

4.3.3 Extended-Fuzzy Control

The implementation of the extended-fuzzy controller is based on the observations of performance of the fuzzy-based PD. The extended-control consists of fuzzy-based motion and fuzzy-based de-weighting controller. The purpose of the extended-fuzzy control is to ensure that the exoskeleton is capable of moving to the desired trajectory accurately.

The fuzzy-based PD in Section 4.3.2 presents the fuzzy-based motion. According to the dynamic equation presented in Appendix B, the gravity torque depends on the robot position and orientation, and the movements' of the robot joints. Hence, the inputs to the fuzzy-based de-weighting are the joints deviation (e) and the current position of the joint (α). Whilst, the output of the fuzzy-based deweighting are the compensating torque of the gravitational force for each joint. Five membership functions are used: Negative Big (NB), Negative Small (NS), Zero (Z), Positive Small (PS) and Positive Big (PB). The fuzzy rules for the de-weighting controller are shown in Table 4.2 and the details of the membership is presented in Figure 4.11. The inference mechanism for the fuzzy-based de-weight is

max-min method and the defuzzification approach is the Centroid of Gravity.

Table 4.2: Construction of fuzzy rules: Fuzzy-based de-weighting controller

e/α	NB	NS	Z	PS	PB
NB	PB	PB	PB	PS	Z
NS	PB	PB	PS	Z	NS
Z	PB	PS	Z	NS	NB
PS	PS	Z	NS	NB	NB
PB	Z	NS	NB	NB	NB

Similar as in Section 4.3.2, if the both error and current position are both positive big (PB), the control action will produce negative big (NB) signal to bring back the output to the desired trajectory. On contrary, if both error and current position are both negative big (NB), the control action will supply the positive big (PB) signal to ensure the output trajectory go to the desired position. For the case of error is positive big (PB) and current position is negative big (NB) or vice-versa, zero (Z) control signal is applied to the system because the system is at a steady-state condition.

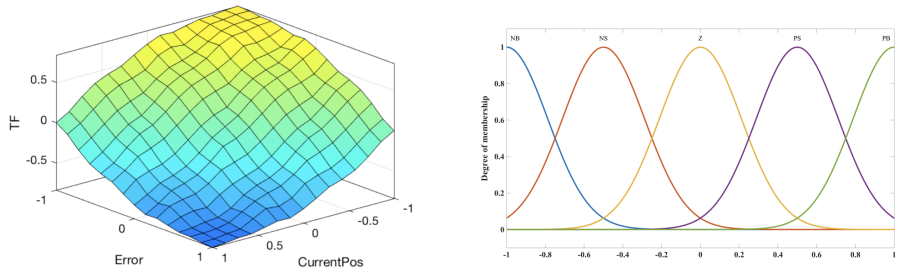

(a) (b)

Figure 4.11: Details of fuzzy-based de-weighting control: (a) Fuzzy logic 3D surface (b) Membership functions for inputs and outputs for de-weighting the exoskeleton joints.

Figure 4.12 shows implementation of the extended-fuzzy controller on the exoskeleton. The total torque (τ) is the summation of τ_m and τ_g. The τ_m is the torque due to motion, and τ_g presents the torque of gravity compensator. The saturation is included in the extended-fuzzy controller to ensure that the τ is not exceeding the human torque (Table 4.3).

The performance of tracking desired trajectory, deviation or error of trajectory and torque needed for moving the joints of both controllers are presented in the next section.

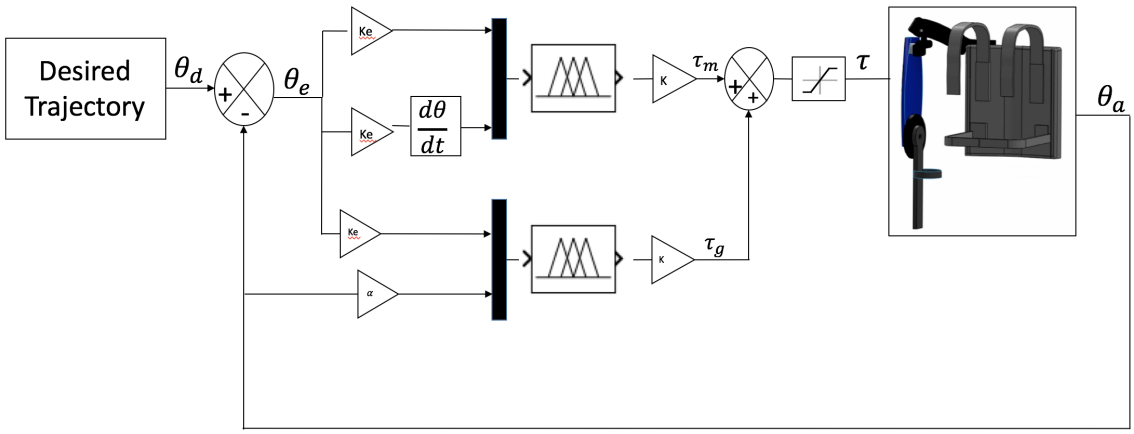

Figure 4.12: Block diagram of the extended fuzzy controller.

Table 4.3: Torque limits of human arm (Głowiński et al., 2015; Carignan et al., 2007; Gupta and Malley, 2006)

Joint	Human strength (Nm)
Shoulder flexion/extension	115/110
Shoulder abduction/adduction	134/94
Elbow flexion/extension	72.5/42
Forearm pronation/supination	9.1/7
Wrist palmer/dorsal flexion	19.8
Wrist abduction/adduction	20.8

4.4 Results and Discussion

In this section, the results and discussions on the performance of PID and fuzzy-based PD controller are presented. The next subsection presents the observation of PID controller in controlling the exoskeleton without disturbance. The next section presents the observation of fuzzy-based PD controller in controlling the exoskeleton with similar condition (without disturbance). In addition, the performances of the two controllers are compared in this section and associated conclusions drawn. Three measurements were used to evaluate the performance of the controllers. The measurements are Root Mean Square Error (RMSE), Maximum Absolute Error (MAE) and Maximum Absolute Torque (MAT). These measurements were measured as:

$$RMSE = \sqrt{\frac{\sum_1^n (\hat{\theta} - \theta)^2}{n}} \tag{4.6}$$

$$MAE = max(|\hat{\theta} - \theta|) \tag{4.7}$$

$$MAT = max(|\tau|) \tag{4.8}$$

$\hat{\theta}$ is the desired position and θ is the actual position; n is the number of data.

4.4.1 PID Control of Exoskeleton without Disturbance

In this section, the performance of the PID controller in controlling the movement of an exoskeleton is presented. The PID controller is evaluated in three aspects: tracking desired performance, error performance and the torque required. It is essential to provide the desired trajectory of the exoskeleton. In this section, a predefined trajectory is used. The space-task is sent to the exoskeleton and inverse kinematics is used to provide the desired trajectory in joint-space information. Two types of predefined trajectory were used to evaluate the PID controller. The trajectories were an abrupt and non-abrupt movement.

4.4.1.1 Abrupt Movement

Figure 4.13 shows the predefined trajectory used. Two joints were involved in the movement: Joint 1 and Joint 4. Joint 1 represents the shoulder abduction or adduction, and Joint 4 represents the elbow flexion or extension. Figure 4.13 shows that Joint 1 was abducted to 90° at 2 s and was adducted to the initial position at 4 s, and Joint 4 was flexed to 90° at 4.5 s until 10 s. There was no movement for Joint 2 and Joint 3. Joint 2 represents the shoulder internal and external movements, and Joint 3 represents the shoulder flexion and extension movements.

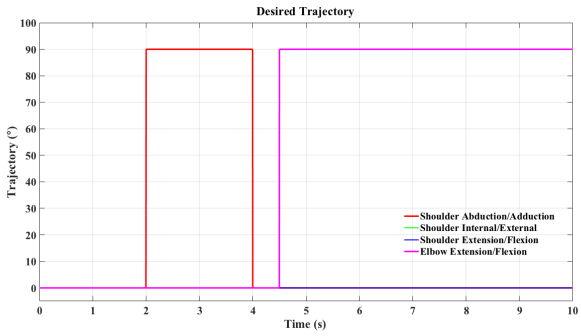

Figure 4.13: Predefined trajectory.

Table 4.4: Controller gains for abrupt movements

Gains	Joint 1	Joint 2	Joint 3	Joint 4
K_P	10	10	10	10
K_I	10	10	10	10
K_D	100	5	50	50

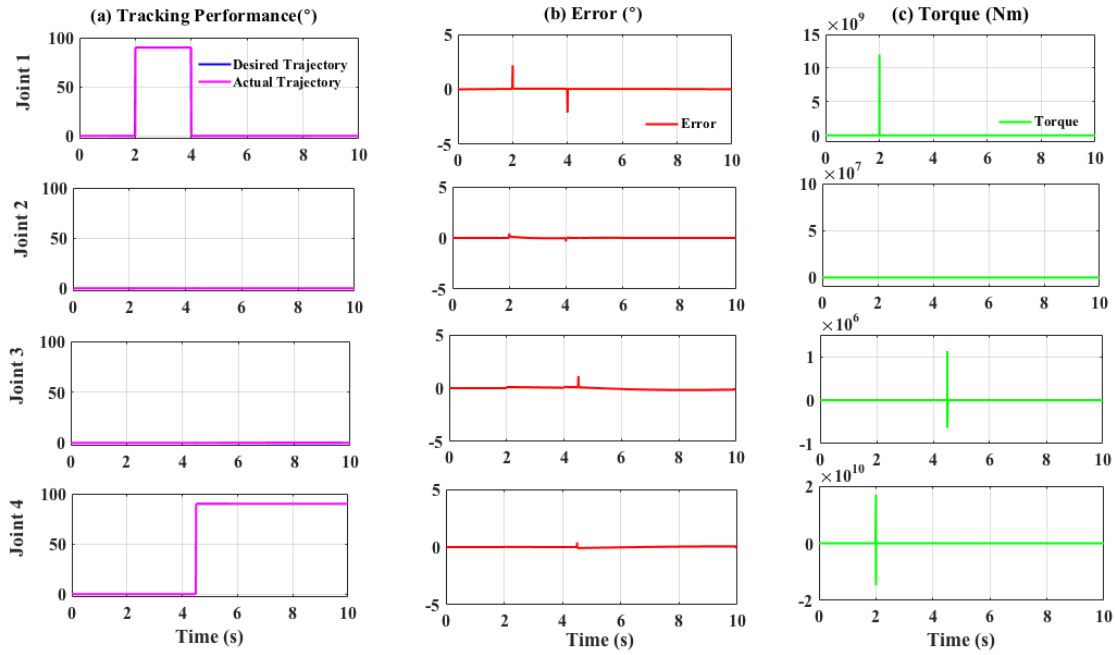

Figure 4.14: Performance of PID controller for abrupt movement: (a) Trajectory tracking (b) Error (c) Torque.

Table 4.4 presents the variable gains of P, I and D for an abrupt movement. These gains were obtained by a heuristic approach. Figure 4.14 shows the results of all joints for the tracking performance, error and torque required. In general, all joints were able to follow the desired trajectory. The variable gains for P-, I- and D-term for an abrupt movement were relatively big. These values were needed to ensure all joints were able to follow the desired trajectory as the desired trajectory has a sudden-change. As shown in Figure 4.14(b), the error for each joint was not more than 2.5°, and so is acceptable. Due to motion-coupling, Joint 2 and Joint 3 were affected when Joint 1 and Joint 4 were moving. This caused small deviation for Joint 2 and Joint 3 at the point where an abrupt movement occured.

Figure 4.14(c) shows that the torque needed to move the exoskeleton was extremely high. The high torque occurred at the abrupt change of motion. For Joint 1, the abrupt changes occurred at 2.0 s and 4.0 s. For Joint 4, the abrupt changes of motion occurred at 4.5 s. A close observation was made by identifying terms that contributed to the high torque values. The P-term, I-term and D-term were plotted as shown in Figure 4.15. It is noted that the high torques at Joint 1 and Joint 4 were contributed by the D-term. The value of P- and I-term could not be seen due to the high value of D-term. Mathematically, the derivative-term is used to measure the slope of a graph of a function at some particular time (Figure 4.16). In PID controller, the D-term is used to describe how fast the error is changing. As shown in Figure 4.16 , if the denominator part of slope formula, which is Δx is changed to time (Δt), then the slope formula will have 0 in the case of the abrupt movement. As a result, the joint torque becomes too large at the abrupt motion.

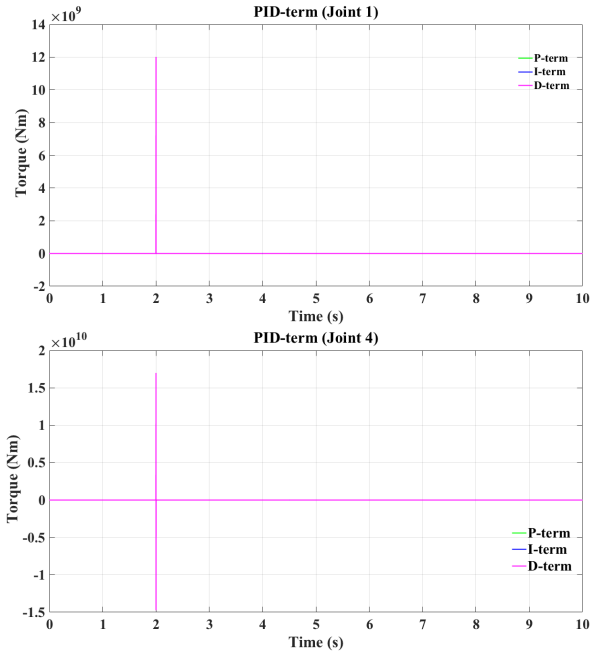

Figure 4.15: P-term, I-term and D-term (Joint 1 and Joint 4).

Although, the tracking performance was good and the deviation value was small, high torque was required to move the exoskeleton. This is not suitable for the exoskeleton. The high torque could damage the exoskeleton and potentially compromise safety of the user. In conclusion, PID controller is able to control an abrupt movement. However, it needs high torque to move the joint to follow the abrupt movement.

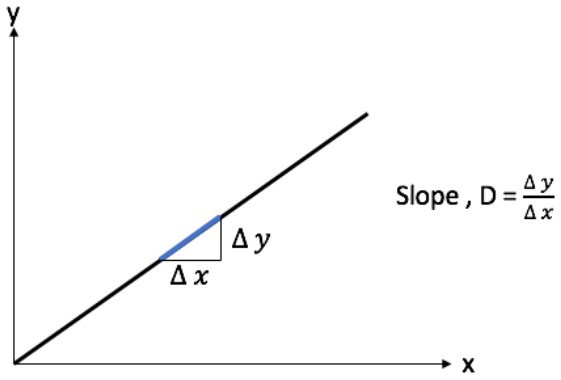

Figure 4.16: Derivative definition.

4.4.1.2 Non-abrupt Movement

In this section, the performance of the PID controller with non-abrupt movement is presented. Two joints were used: Joint 1 and Joint 4. The trajectory shown in Figure 4.17 was applied to both joints. The P, I and D gains were tuned by using heuristic approach and these are shown in Table 4.5.

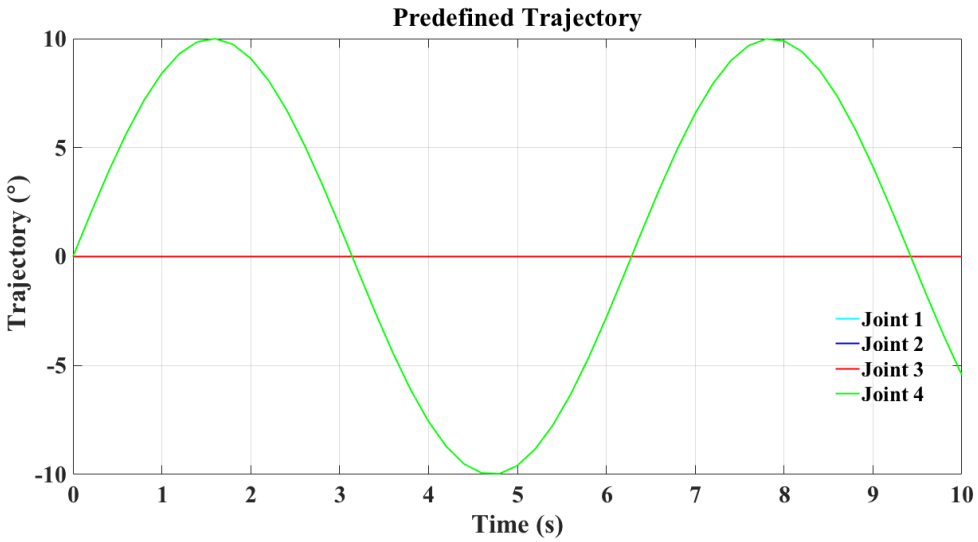

Figure 4.17: Predefined trajectory.

Figure 4.18 shows the results of trajectory tracking, deviation of the motion and torque required for all joints. In general, all joints were able to track the desired trajectory. As shown in Figure 4.18(a), Joint 1 was not able to achieve the desired trajectory at the first 3.0 s, and the maximum error for this joint during this period of time was approximately to 2°. Hence, an improvement was applied to improve the tracking performance. Since there

Table 4.5: Controller gains for non-abrupt movements

Gains	Joint 1	Joint 2	Joint 3	Joint 4
K_P	1.0	1.0	1.0	1.0
K_I	0.5	0.5	0.5	0.5
K_D	0.3	0.5	0.5	0.1

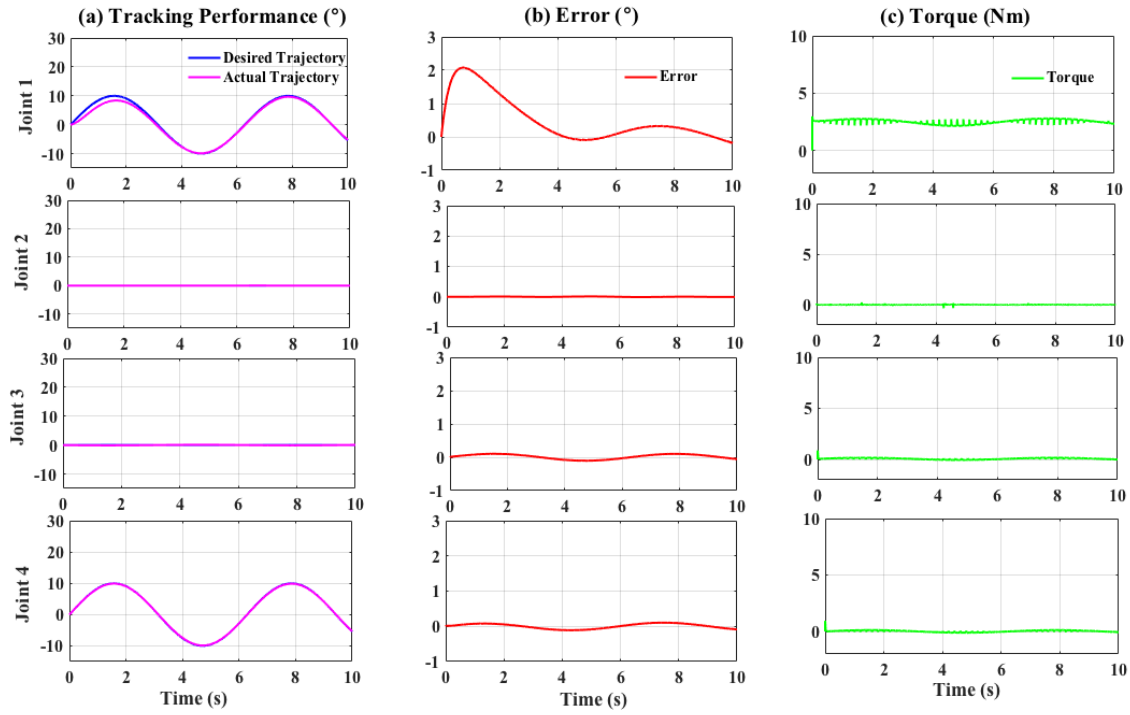

Figure 4.18: Performance of PID controller for non-abrupt movement: (a) Trajectory tracking (b) Error (c) Torque.

was no oscillation, the P- and I-term were increased.

Heuristic approach was used to choose the new P- and I-terms. A Root Mean Square Error (RMSE) and Maximum Absolute Error (MAE) were used to compare the chosen gains and to measure the accurate tracking trajectory.

Figure 4.19 and Figure 4.20 show the results of tracking performance, error and torque required for all joints with the new gains. Generally, improvement occurred during the period from 0 s to 3 s of Joint 1 for new gain 1 and new gain 2. As noted in Table 4.6, the MAE values for new gain 1 and new gain 2 were 0.4662° and 0.2455°. These values are smaller than 0.5°, and were smaller than the initial gain, which was 2.079°. The RMSE of new gain 1 was about 15% near to 0° and new gain 2 was about 8% near to 0°, compared

to initial gain. In light of the RMSE and MAE values and results in Figure 4.19 and Figure 4.20, it is noted that by increasing the P-term and I-term, the tracking performance was enhanced.

Table 4.6: Option for parameter gains for Joint 1

Parameter Gain	Initial Gain	New Gain 1	New Gain 2
K_P	1.0	5.0	10.0
K_I	0.5	3.5	5.5
K_D	0.3	0.3	0.3
RMSE	0.8318	0.1457	0.0814
MAE	2.079	0.4662	0.2455

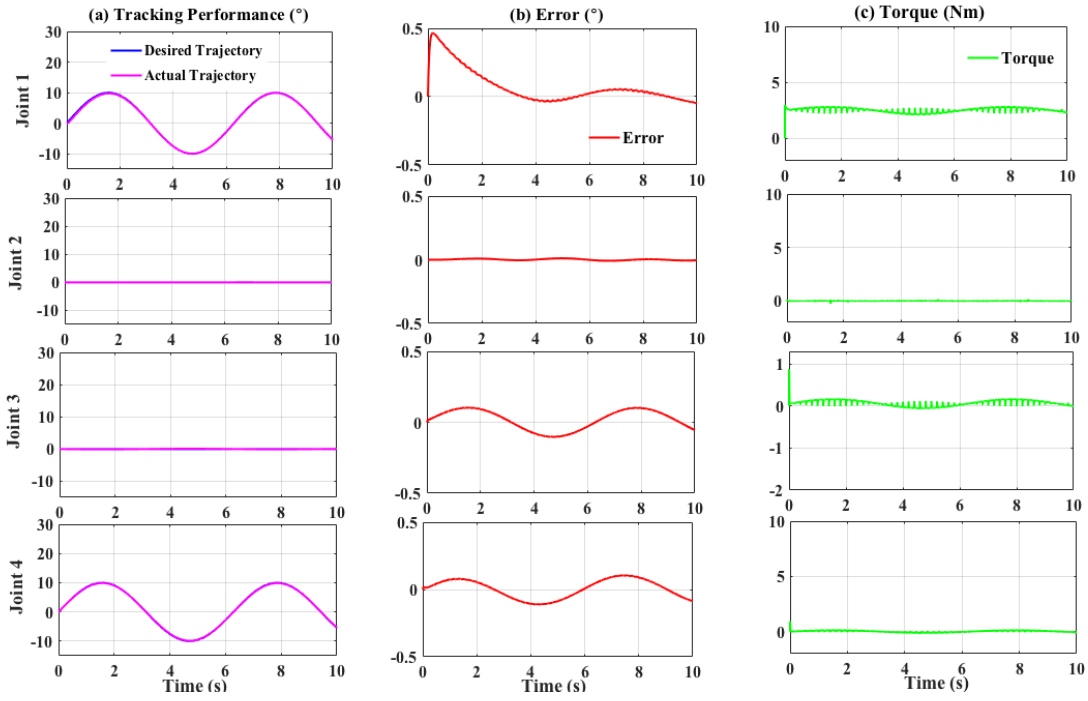

Figure 4.19: Performance of PID controller with parameter gain 1 for non-abrupt movement (Joint 1): (a) Trajectory tracking (b) Error (c) Torque.

Spikes occurred at $t = 0$, as shown in Figure 4.18(c), Figure 4.19(c) and Figure 4.20(c). These spikes were contributed by the D-term. At $t = 0$, the $\Delta y = 0$ and $\Delta t = 0$. Hence, the slope or derivative becomes large, causing spikes at the beginning of the movement. However, due to small values, the spikes could be considered as acceptable. Figure 4.18(c) also shows that the torques required by all joints for the non-abrupt movement were small;

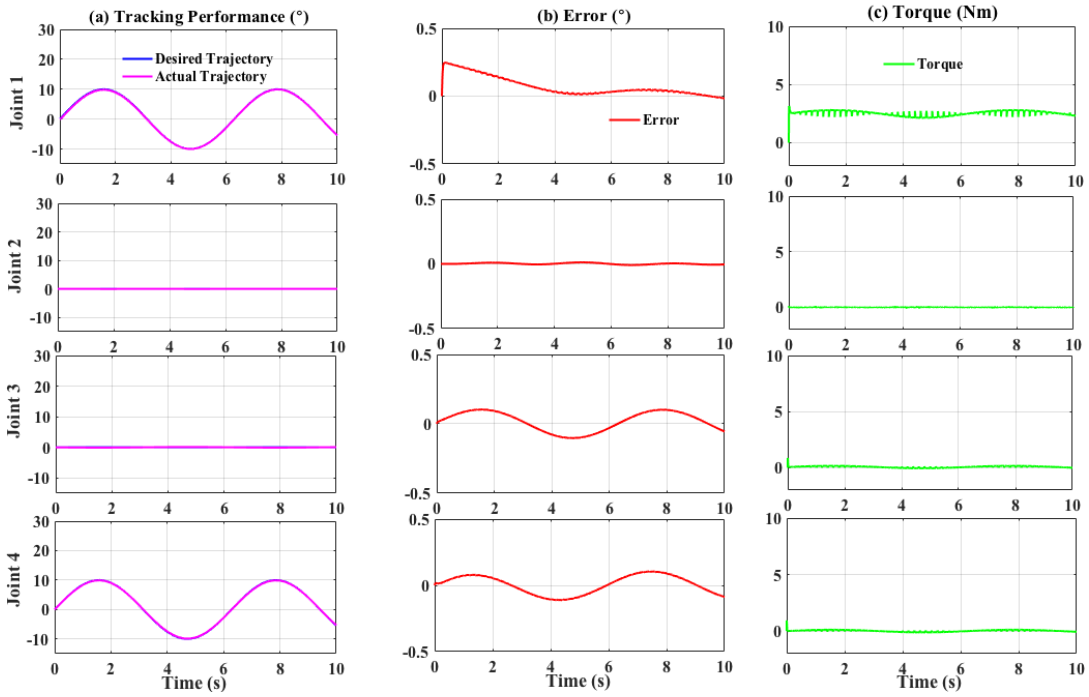

Figure 4.20: Performance of PID controller with parameter gain 2 for non-abrupt movement (Joint 1): (a) Trajectory tracking (b) Error (c) Torque.

not more than 5.0 Nm. In addition, the torque required with both new gains remained almost the same as with the initial gain.

From the observation, the non-abrupt movement is more suitable to be investigated in this work. Although PID was able to track the desired trajectory in the case of an abrupt movement, but due to D-term, the torque required was too large and unrelistic for the exoskeleton and human. Several ways could be considered to resolve this issue such as adding saturation to limit the maximum and minimum of torque for the actuator. Although, this is possible, in a real world, humans do not move in an abrupt motion. Hence, non-abrupt type of movement is used in this work.

4.4.2 Fuzzy-Based PD Control without Disturbance

In this section, the predefined trajectory is used. The predefined trajectory is sent to forward kinematics and is translated to space-task information. The space-task information is in Cartesian form and inverse kinematic is used to translate the Cartesian information to the joint-task information.

4.4.2.1 Abrupt Movement

This section presents the results and discussions of abrupt movements controlled by fuzzy-based PD controller. Similar abrupt movement as presented in Section 4.4.1.1, is applied. Then, performance comparison is made between PID controller and fuzzy-based PD. The parameter gains were tuned by using heuristic approach and these are presented in Table 4.7.

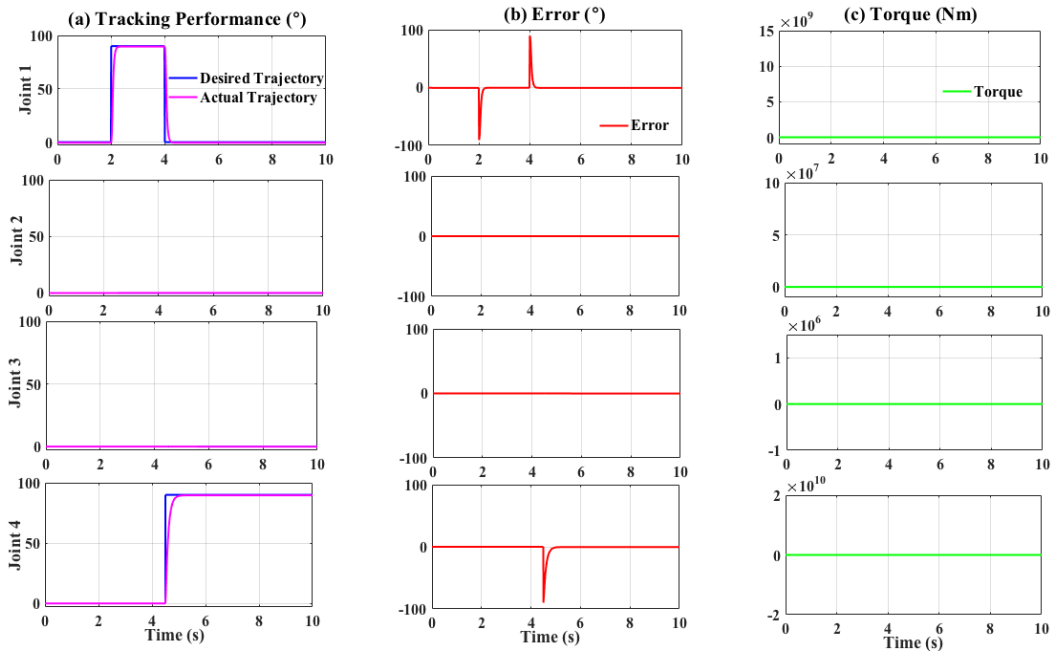

Figure 4.21: Performance of fuzzy-based PD controller for abrupt movement: (a) Trajectory tracking (b) Error (c) Torque.

Table 4.7: Controller Gains for abrupt movements (Fuzzy-based PD controller)

Gains	Joint 1	Joint 2	Joint 3	Joint 4
K_e	0.02	1.00E-05	50E-03	0.02
$K_{\dot{e}}$	1.00E-04	0.005	20E-04	2E-04
K	500	80	300	200

Figure 4.21 shows the results of tracking performance, deviation of the movement and torque required for the exoskeleton to achieve the target trajectory. The figure shows that the controller was able to track the desired trajectory for all joints. Joint 1 and Joint 4 showed smooth tracking movements. Figure 4.21(b) shows the error for each joint. Spikes

Table 4.8: RMSE and MAE for conventional PID and Fuzzy-based PD controller

Joint/Movement	RMSE		MAE	
	PID	PD-Fuzzy	PID	PD-Fuzzy
Joint 1	0.07040	22.62	2.191	90.55
Joint 2	0.03113	0.02105	0.431	0.05316
Joint 3	0.08613	0.03303	1.127	0.1091
Joint 4	0.02302	7.087	0.4074	90

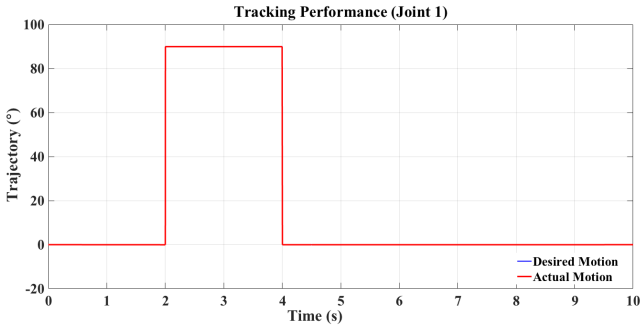

(a)

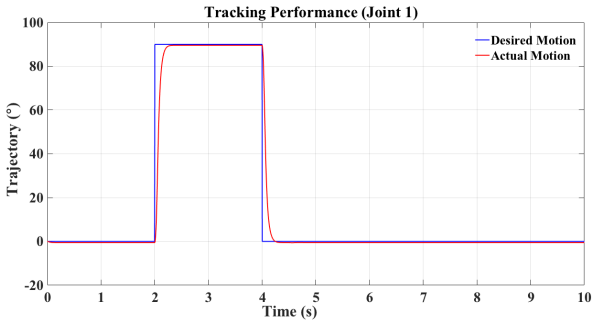

(b)

Figure 4.22: Trajectory tracking performance of (Joint 1):(a) PID (b) Fuzzy-based PD controller

appear in Figure 4.21(b) at the abrupt movement for Joint 1 and Joint 4. The errors generated by fuzzy-based PD controller for Joint 2 and Joint 3 were less than 0.15°. The errors for Joint 2 and Joint 3 were considered as small. Generally, the torque required by the exoskeleton to move Joint 1 and Joint 4, and to maintain Joint 2 and Joint 3 was less than 200 Nm. Generally, the torque required by fuzzy-based PD is close to the maximum human torque (Table 4.3). This shows that fuzzy-based PD is able to control an exokseleton in an abrupt motion with an acceptable range of human torque. As discussed in Section 4.4.1.1, the spikes were contributed by the D-term.

Figure 4.22 shows the tracking performance for PID and fuzzy-based PD controller for Joint 1. In general, as shown in this figure, both controllers were able to track the desired

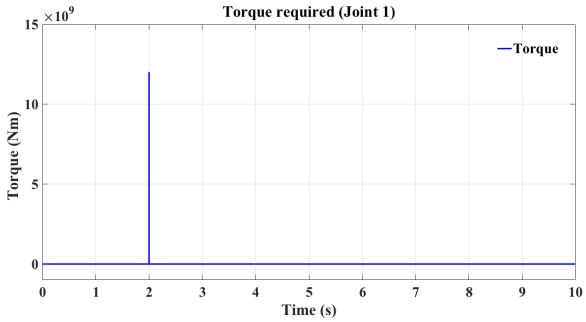

(a)

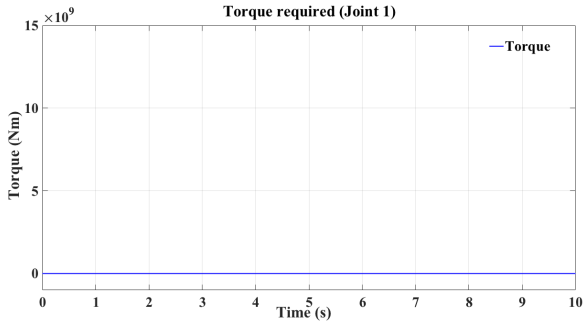

(b)

Figure 4.23: The torque required by Joint 1: (a) PID (b) Fuzzy-based PD controller.

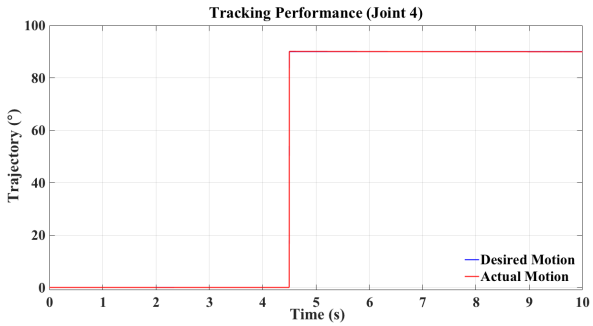

(a)

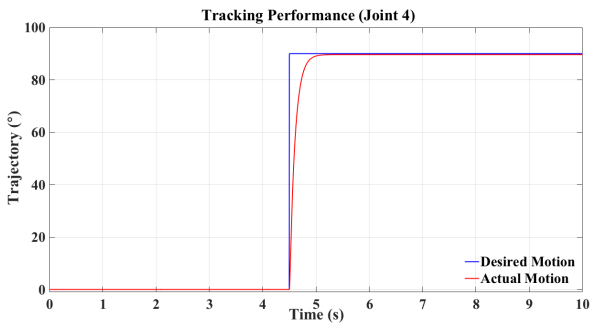

(b)

Figure 4.24: Trajectory tracking performance at Joint 4: (a) PID (b) Fuzzy-based PD controller

trajectory. However, from Figure 4.22 (a) PID shows a better tracking performance compared to fuzzy-based PD controller. The MAE and RMSE for Joint 1 of PID were 2.191°

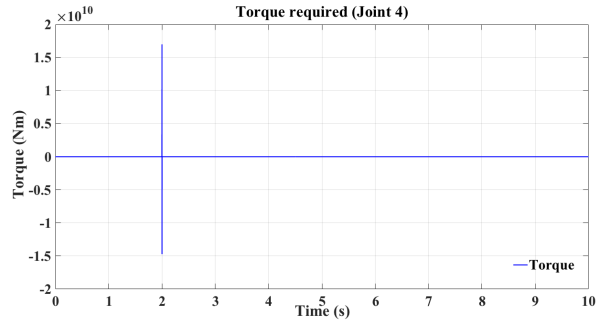

(a)

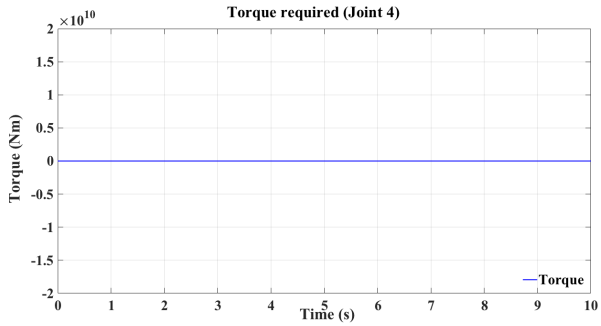

(b)

Figure 4.25: The torque required for Joint 4: (a) PID (b) Fuzzy-based PD controller.

and 0.07040°, and for fuzzy-based PD controller were 90.55° and 22.62°. The MAE and RMSE for PID were lower than fuzzy-based PD controller. Although the tracking performance from deviation point of view for Joint 1, shows that PID was better than fuzzy-based PD, but in terms of torque required for the joints to move in abrupt movements, it is noted that fuzzy-based PD controller needed the least torque compared to PID controller (Figure 4.23). Whereas, the PID generate unrealistic torque to achieve the desired trajectory (Figure 4.23). In addition, the torque required to move Joint 1 for fuzzy-based PD controller, which represent the abduction movement was close to the maximum torque for shoulder abduction. Although it was high, around 157.25 Nm (the maximum torque of shoulder abduction is 134 Nm), but it was still lower compared to that with PID controller.

Figure 4.24 shows results of trajectory tracking, error and torque needed for Joint 4. Similar to Joint 1, the PID controller was able to track the desired trajectory almost exactly to the desired trajectory compared to fuzzy-based PD controller. The RMSE and MAE for Joint 4 with PID and fuzzy-based PD are shown in Table 4.8.

The RMSE for Joint 4 with PID and fuzzy-based PD controller were 0.02302 and

7.087, whereas, the MAE for Joint 4 with PID and fuzzy-based PD were 0.4074 and 90. The value of RMSE and MAE with fuzzy-based PD was greater compared to those with PID controller. Similar to Joint 1, the torque required to move Joint 4 with fuzzy-based PD was lower compared to that with PID controller as shown in Figure 4.25. However, the torque required for Joint 4 with fuzzy-based PD controller, was greater than maximum torque for human elbow flexion movement. This could be enhanced by optimizing the gain parameters or include saturation in the system.

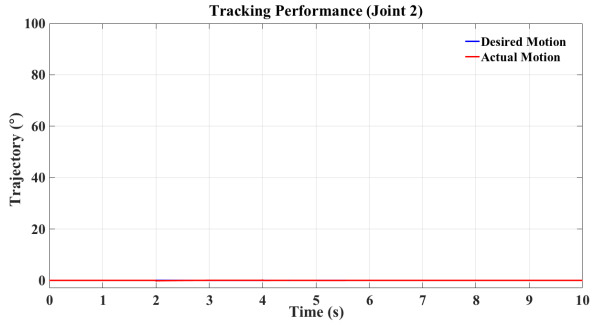

(a)

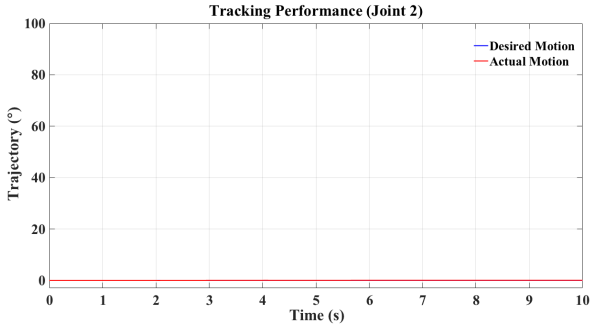

(b)

Figure 4.26: Trajectory tracking performance at Joint 2: (a) PID (b) Fuzzy-based PD controller

Figure 4.26 shows the tracking performance at Joint 2 with PID and fuzzy-based PD controller. In general, both controllers were able to follow the desired movement with small errors. It is noted that the response with PID controller approached 0° due to the I-term. Although the response with fuzzy-based PD controller did not approach to 0°, the error was small (less than 0.1°), and could be neglected. The I-term, which eliminate the steady-state error was not included in the fuzzy-based PD controller. Statistically, as shown in Table 4.8, both RMSE and MAE with fuzzy-based PD were smaller than those with PID. Similar to Joint 1 and 4, the torque required with fuzzy-based PD controller as

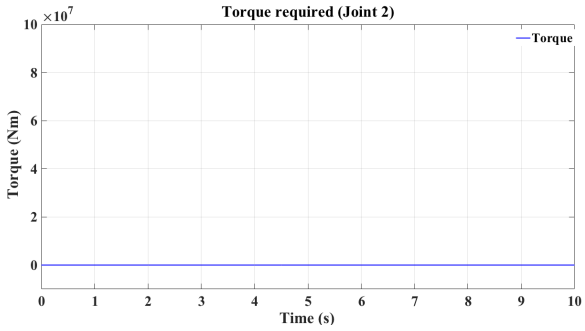

(a)

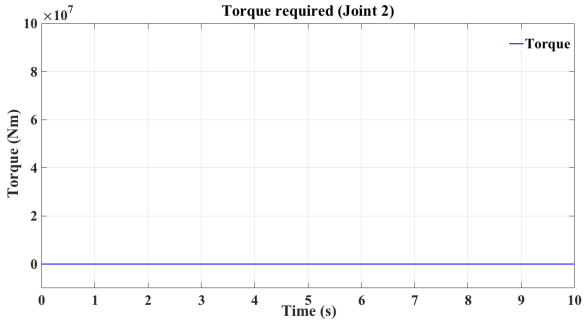

(b)

Figure 4.27: The torque required by Joint 2: (a) PID (b) PD-Fuzzy Controller.

shown in Figure 4.27 was less than that with PID controller, by almost 10000 times.

Figure 4.28 shows the tracking performance at Joint 3 with the controllers. Both controllers were able to track the desired trajectory. The response with PID controller approached to the desired position, whereas with the fuzzy-based PD there was steady-state error, although this was less than 0.12°, and could be considered as small. As noted in Table 4.8, the RMSE and MAE with PID were higher than those with fuzzy-based PD controller. In addition, the torque required by fuzzy-based PD was also less, by almost 10000 times than that with PID controller, although still in the range of the maximum torque of human shoulder flexion (Figure 4.29).

In conclusion, both PID and fuzzy-based PD controller are able to control the movement of an exoskeleton for an abrupt-type motion. The advantage of PID controller is due to the presence of I-element, which could eliminate the steady-state error. However, due to D-term, the spikes with high value will appear at abrupt changes in demand. The tracking performance with fuzzy-based PD is good and the torques required to move the joints are less compared to those with conventional PID controller.

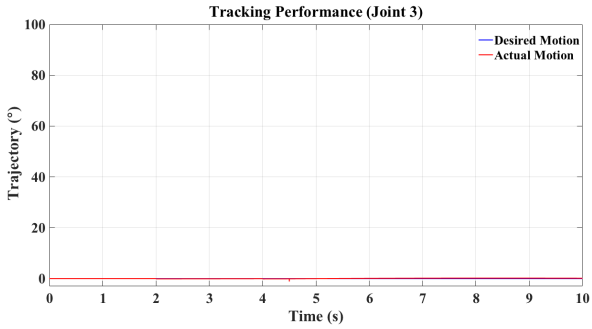

(a)

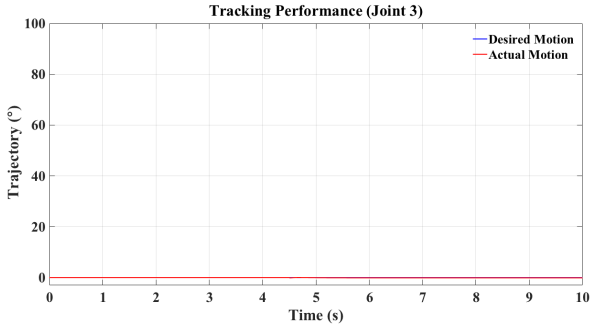

(b)

Figure 4.28: Trajectory tracking performance at Joint 3: (a)PID (b)Fuzzy-based PD controller.

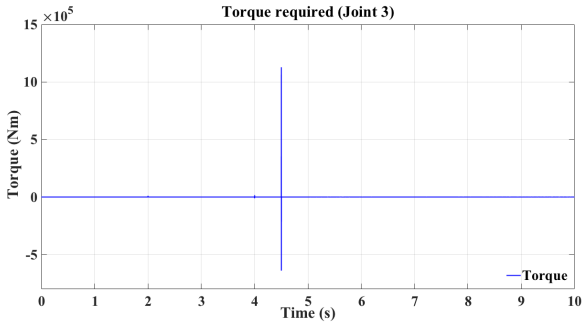

(a)

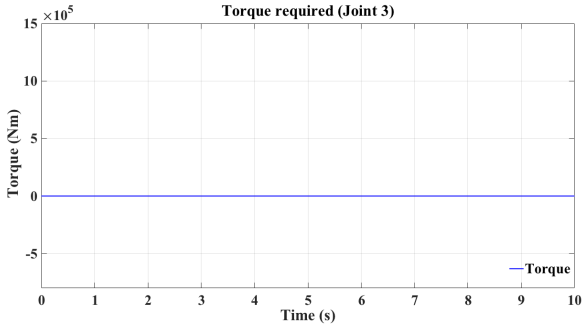

(b)

Figure 4.29: The torque required by Joint 3: (a) PID (b) Fuzzy-PD controller.

4.4.2.2 Non-abrupt Movement

In this section, the performance of fuzzy-based PD controller with non-abrupt movement is presented. Similar non-abrupt movement as presented in Section 4.4.1.2, is applied. The parameter gains were tuned using heuristic approach and these are shown in Table 4.9.

Table 4.9: Parameter gains for non-abrupt movements (Fuzzy-based PD Control)

Gains	Joint 1	Joint 2	Joint 3	Joint 4
K_e	1	0.5	0.5	0.5
$K_{\dot{e}}$	0.002	0.05	20E-04	2E-04
K	250	100	100	100

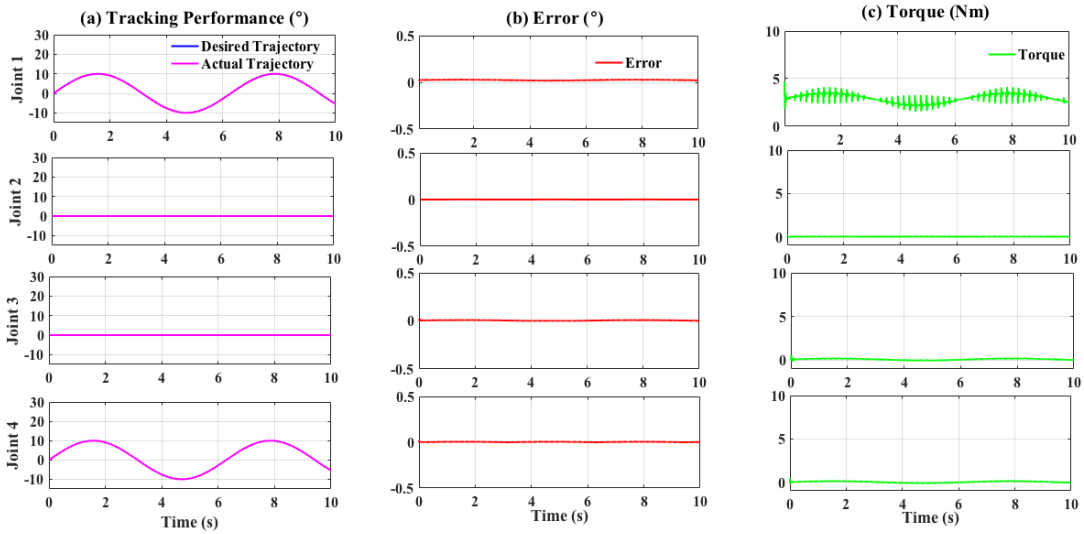

Figure 4.30: Performance of fuzzy-based PD controller for non-abrupt movement: (a) Trajectory tracking (b) Error (c) Torque.

Figure 4.30 shows the tracking performance, deviation of the movement and the torque required to move the exoskeleton to the desired trajectory by fuzzy-based PD controller with non-abrupt movement. As illustrated in Figure 4.30, the exoskeleton was able to follow the desired trajectory with very small error (less than 0.1°). Compared with performance in case of abrupt movement, better results in tracking desired trajectory as well as the torque required were achieved in case of non-abrupt movement. Spikes occurred at each joint at $t = 0$ were due to, the D-term as mentioned in Section 4.4.1.1. However, in

Table 4.10: RMSE, MAE and MAT for PID and fuzzy-based PD controller (Non-abrupt movement)

Joint/Movement	RMSE		MAE	
	PID	PD-Fuzzy	PID	PD-Fuzzy
Joint 1	0.0814	0.02528	0.2455	0.03348
Joint 2	0.0056	0.00005090	0.01174	0.0009336
Joint 3	0.0695	0.005941	0.1036	0.0114
Joint 4	0.0680	0.003584	0.111	0.01883

Joint/Movement	MAT	
	PID	PD-Fuzzy
Joint 1	3.154	4.122
Joint 2	0.1169	0.04840
Joint 3	0.8769	0.1322
Joint 4	0.944	0.1484

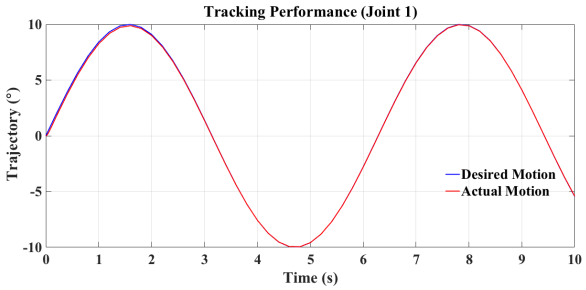

(a)

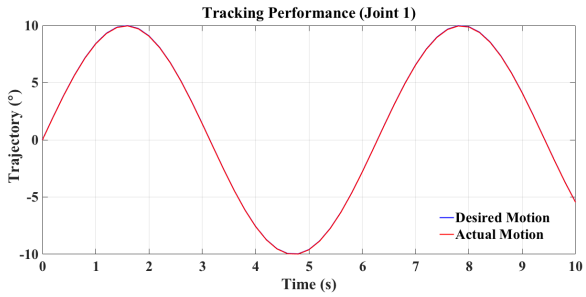

(b)

Figure 4.31: Trajectory tracking performance of (Joint 1): (a) PID (b) Fuzzy-based PD controller.

this case the spikes were small and could be neglected. In addition, usually, any jerk that occurred in the beginning of the movement could be ignored because the system needed some time at start to stabilise.

Table 4.10 presents the RMSE, MAE and MAT for PID and fuzzy-based PD controller for non-abrupt movement. In terms of deviation analysis, it shows that the RMSE and MAE of the fuzzy-based PD controller is less compared to PID. However, the MAT of

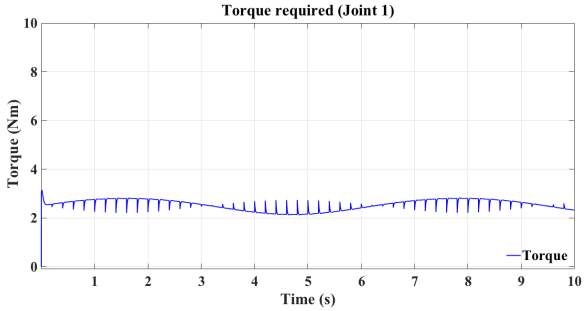

(a)

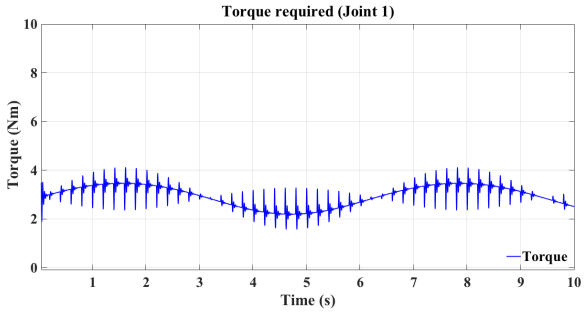

(b)

Figure 4.32: The torque required by (Joint 1): (a) PID (b) Fuzzy-based PD controller.

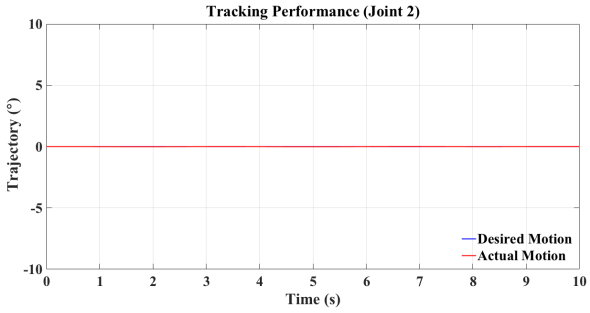

(a)

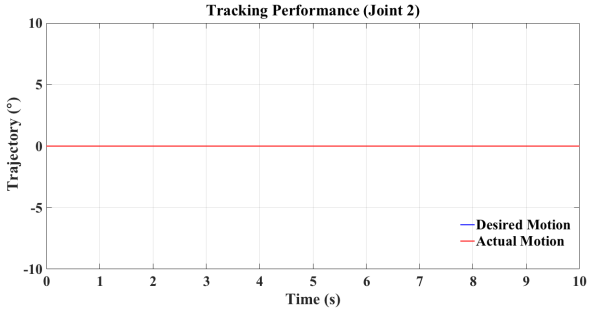

(b)

Figure 4.33: Trajectory tracking performance at Joint 2: (a) PID (b) Fuzzy-based PD controller.

Joint 1 for fuzzy-based PD is higher about 30% than PID. However, the MAT value for fuzzy-based PD is in an acceptable range. Figure 4.31, Figure 4.33, Figure 4.35 and Figure 4.37 show tracking performances of system with PID and fuzzy-based PD controller.

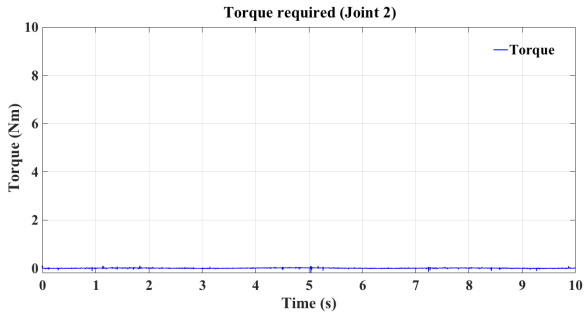

(a)

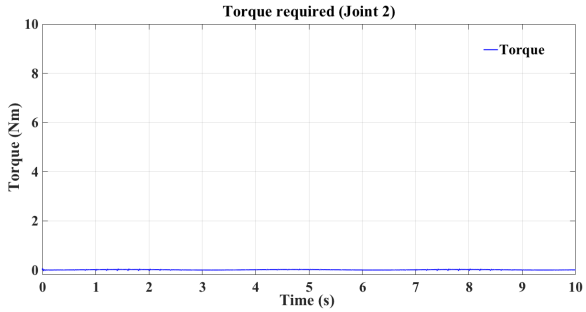

(b)

Figure 4.34: The torque required by Joint 2: (a) PID (b) Fuzzy-based PD controller.

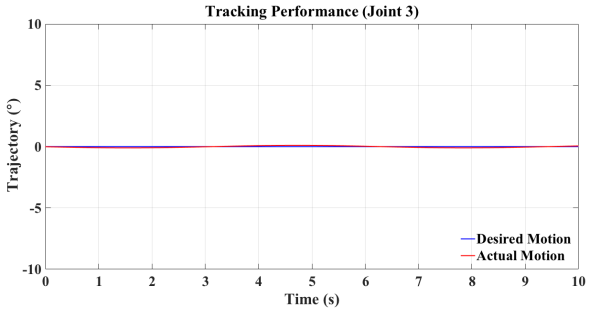

(a)

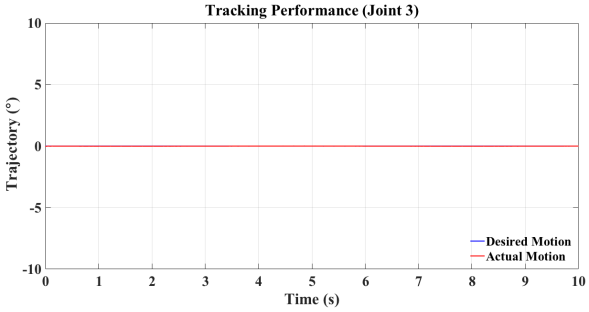

(b)

Figure 4.35: Trajectory tracking performance at Joint 3: (a) PID (b) Fuzzy-based PD controller.

Figure 4.32, Figure 4.34, Figure 4.36 and Figure 4.38 show comparative results in terms of torque required by the controllers for each joint. Generally, from these figures, the torques required were small. Thus, it can be concluded that both controllers performed better in

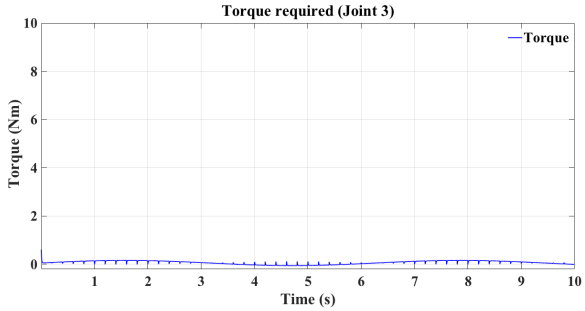

(a)

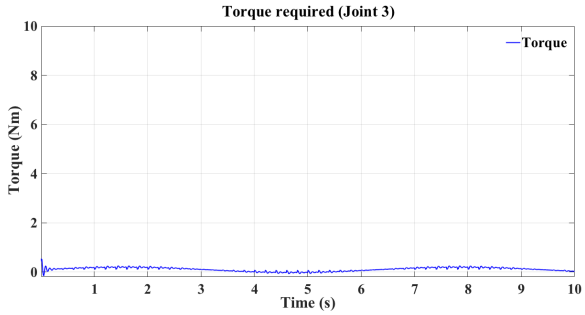

(b)

Figure 4.36: The torque required by (Joint 3): (a) PID (b) Fuzzy-based PD controller.

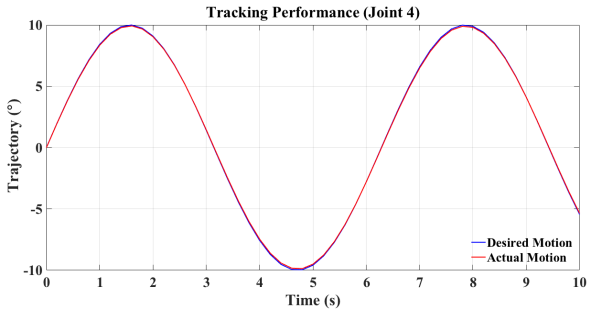

(a)

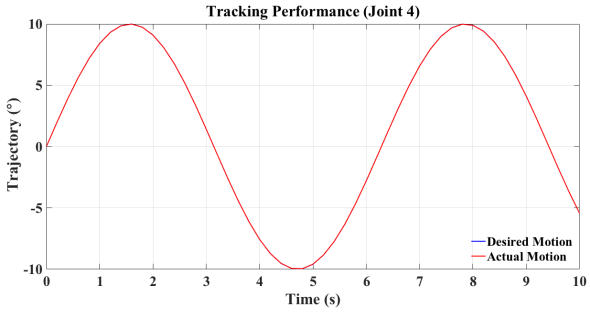

(b)

Figure 4.37: Trajectory trajectory performance at Joint 4: (a) PID (b) Fuzzy-based PD controller.

case of non-abrupt movement.

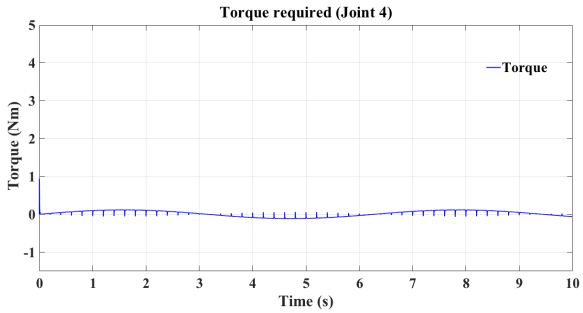

(a)

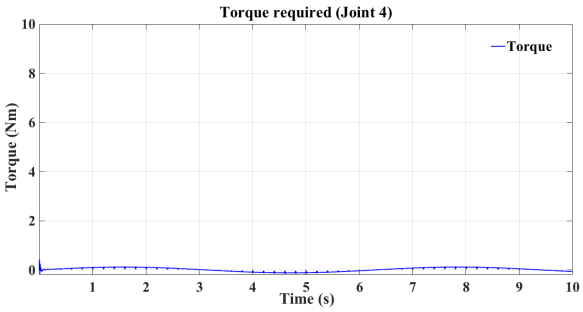

(b)

Figure 4.38: The torque required by (Joint 4): (a) PID (b) PD-Fuzzy Controller.

4.4.3 PID and Fuzzy-Based PD Control with Disturbances

External disturbances were applied to the exoskeleton, and the performances of both controllers were evaluated. The external forces were applied to validate the stability and robustness of the system. The external forces or disturbances were applied at the position shown in Figure 4.39.

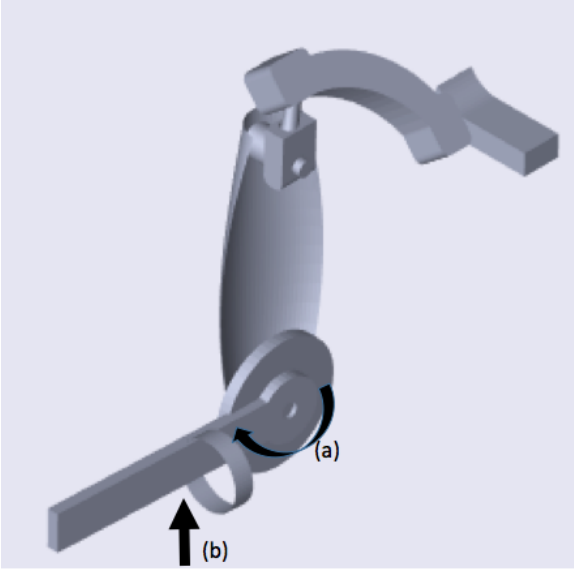

Figure 4.39: Exoskeleton: (a) Exoskeleton movement (b) External disturbance.

Table 4.11: Controller gains for PID and fuzzy-based PD control (first condition)

Gains	Joint 1	Joint 2	Joint 3	Joint 4
K_P	10	1.0	10	100
K_I	5	1.0	5	70
K_D	0.1	0.1	0.0	4.0
K_e	0.02	1.00E-4	1E-2	0.5
$K_{\dot{e}}$	2.5E-5	1E-5	1E-5	0
K	1000	1000	500	1000

Table 4.12: Controller gains for PID and fuzzy-based PD control (second condition)

Gains	Joint 1	Joint 2	Joint 3	Joint 4
K_P	10	1.0	10	100
K_I	5	1.0	5	70
K_D	0.1	0.1	0.1	40
K_e	2	1E-2	5	2
$K_{\dot{e}}$	2.5E-3	1E-3	0.05	0.001
K	100	500	10	500

A disturbance force of 1000 Nm was applied in two conditions. The first condition was 1000 Nm applied from 2.5 s until 10 s. The control parameters used for the first condition were obtained by heuristic tuning (Table 4.11). In the second condition 1000 Nm was applied from 4.0 s until 6.0 s. The control parameters used for the second condition were obtained by heuristic tuning (Table 4.12).

Figure 4.40 and Figure 4.41 show the performance of PID and fuzzy-based PD systems with in the presence of external force. The external force was applied at the forearm, and it was expected to affect the movement of elbow joint. These two figures show that the elbow joint controlled by the PID controller deviation about 1.8° and the deviation with fuzzy-based PD was less than 1.0°. Moreover, the torque required by the elbow joint in dealing with 1000 Nm external force with PID controller was double that with fuzzy-based PD controller. These observations show that the fuzzy-based PD controller is more stable

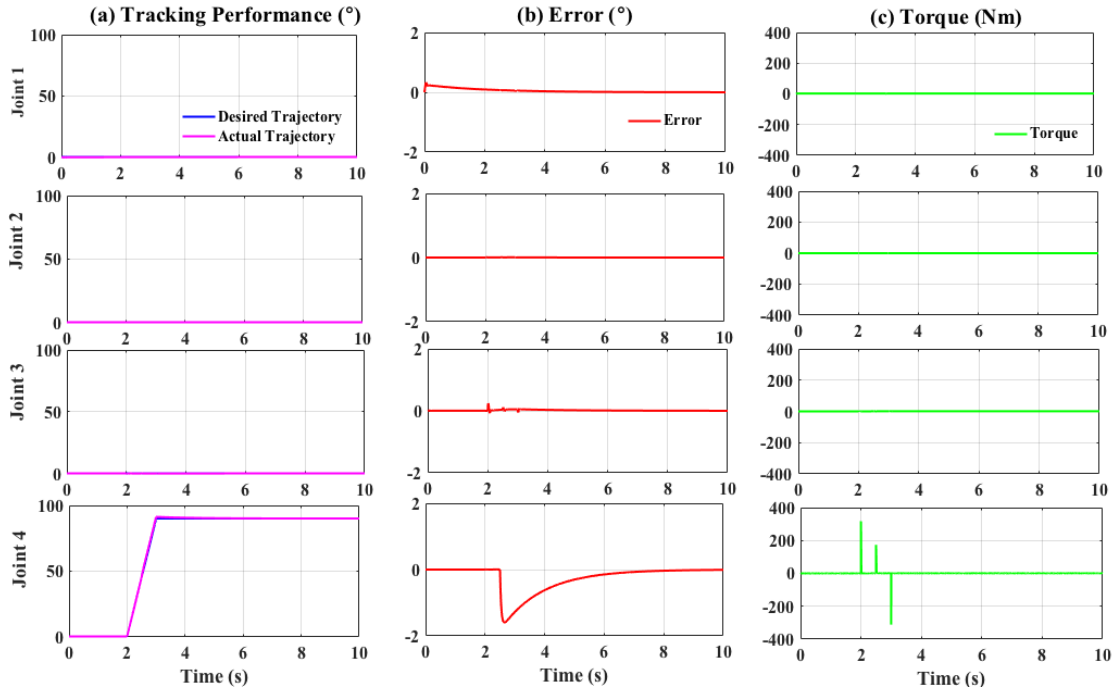

Figure 4.40: Performance of PID controller with external forces (1000 Nm) in first condition.

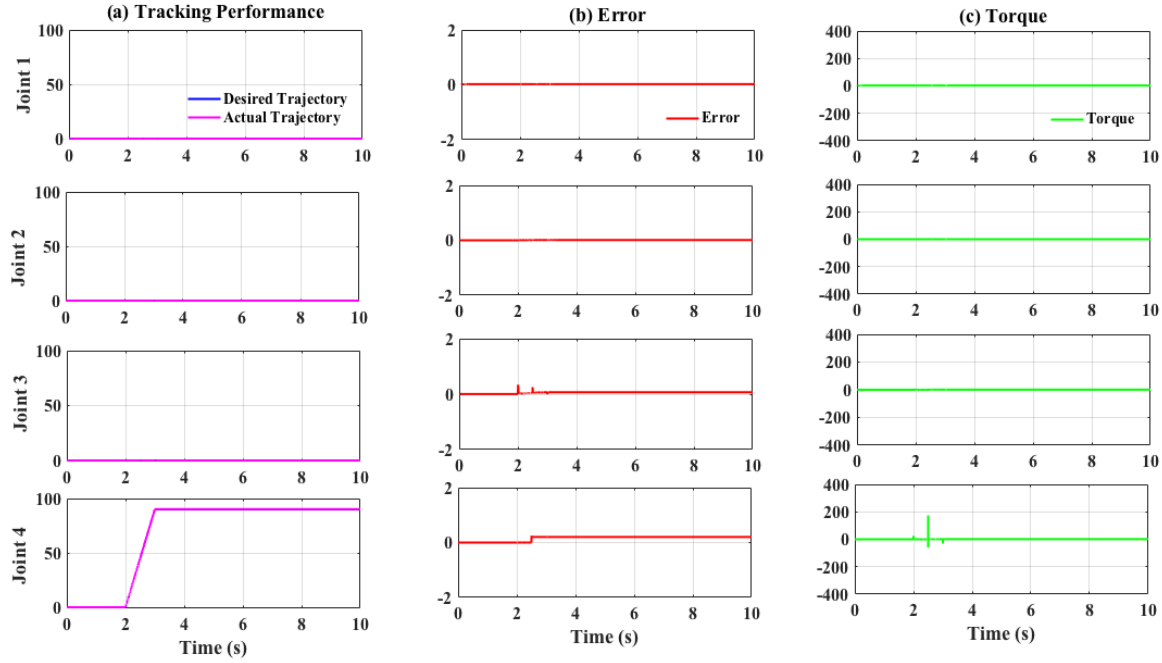

Figure 4.41: Performance of fuzzy-based PD controller with external forces (1000 Nm) in first condition.

in dealing with an external force.

The performances of PID and fuzzy-based PD contoller for the second condition are presented in Figure 4.42 and Figure 4.43. In this case, the external force was also applied

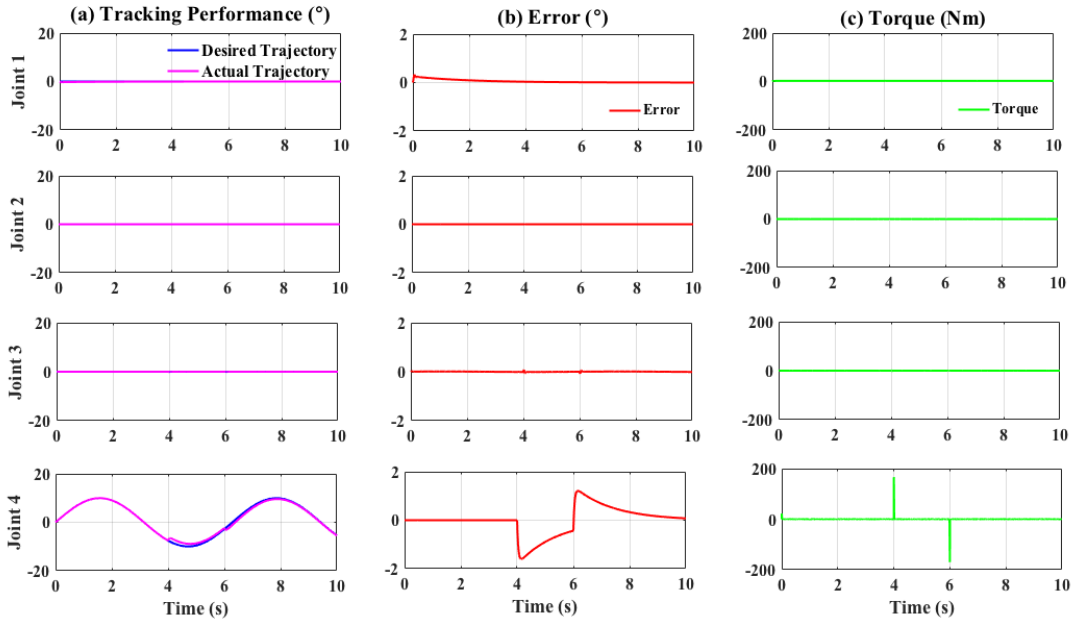

Figure 4.42: Performance of PID controller with external forces (1000 Nm) in second condition.

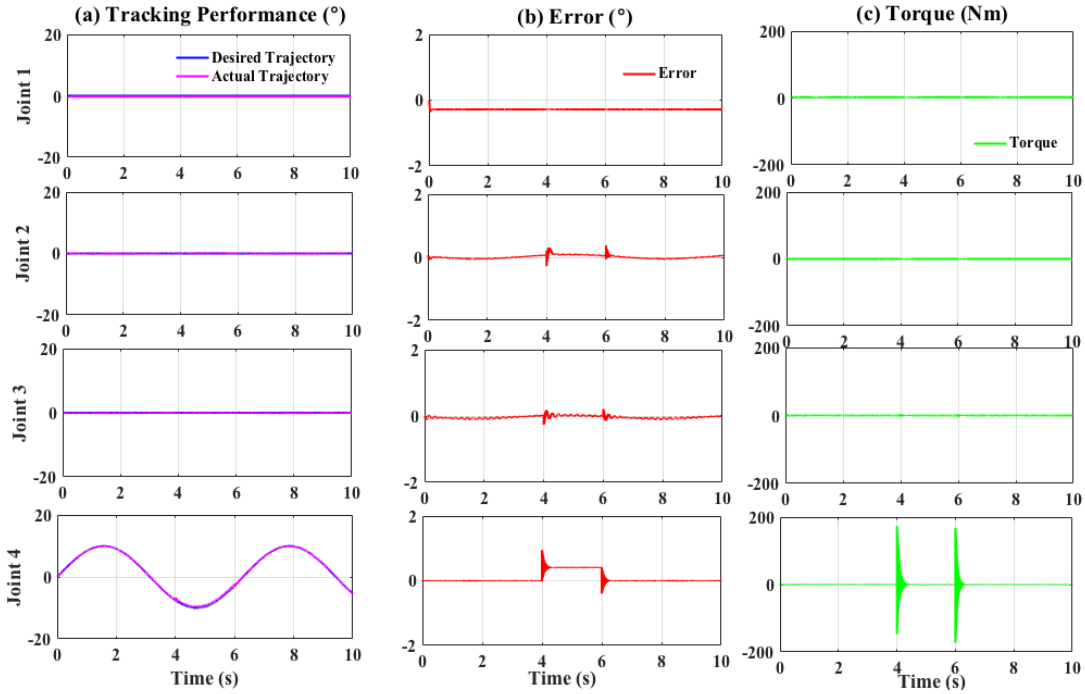

Figure 4.43: Performance of fuzzy-based PD controller with external forces (1000 Nm) in second condition.

on the forearm. Hence, the affected joint was the elbow joint. The movement of the elbow joint was sinusoidal. As noted the fuzzy-based PD controller was able to achieve a continously smooth response with deviation of less than 1.0° and the system was able to

stabilise after approximately 0.05 s.

These validation tests were useful to ensure the system and controller were robust enough to withstand external disturbance. As noted, fuzzy-based PD controller has performed better than PID controller.

4.4.4 Extended Fuzzy Control Without and With Disturbances

In this section, implementation of the extended-fuzzy controller is presented. A single joint i.e elbow joint is considered. The parameters for the extended-fuzzy controller were obtained by heuristic tuning, these are shown in Table 4.13. PID control is used as a baseline for comparison study. This controller is chosen as a baseline because it is a well-known controller and is capable of predicting the gravitational load or force as mentioned in Section 2.5. The gains K_p, K_i and K_d were obtained heuristically and these are presented in Table 4.13.

Table 4.13: Controller gains for extended-fuzzy and PID controller

Gains Hybrid Controller	Joint 1	Joint 2	Joint 3	Joint 4
K_e	0.02	1E-4	1E-2	1
$K_{\dot{e}}$	2.5E-5	1E-6	0.5E-5	0
K_{gain1}	1000	500	500	10
K_e	10	1	5	20
K_α	1E-4	1E-4	1E-3	1E-3
K_{gain2}	5	50	3	500
PID Controller	**Joint 1**	**Joint 2**	**Joint 3**	**Joint 4**
K_P	10	1	10	100
K_I	5	1	5	70
K_D	0.1	0.1	0.1	4

Figure 4.44 and Figure 4.45 show the results of tracking performance, error and torque required for each joint of a single joint for the extended-fuzzy and PID controllers for the case of without the existense of the external disturbance. In general, both controllers showed that they were able to track the desired trajectory within an acceptable range of

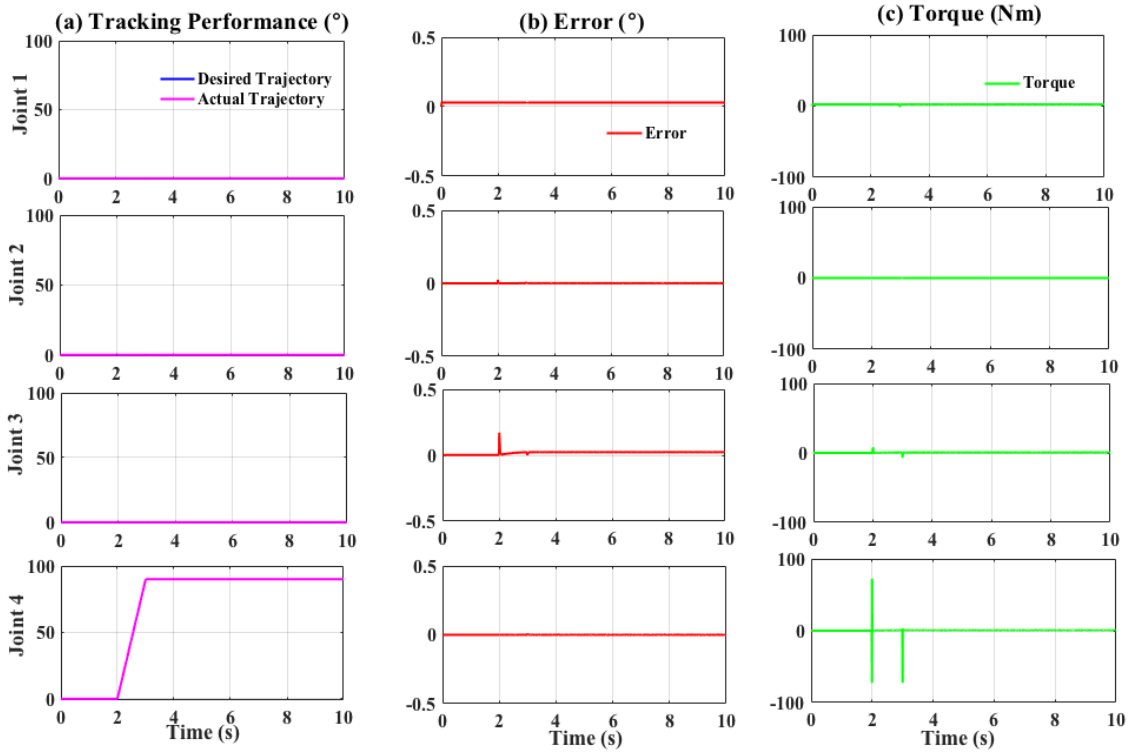

Figure 4.44: Performance for extended-fuzzy controller (Without disturbance).

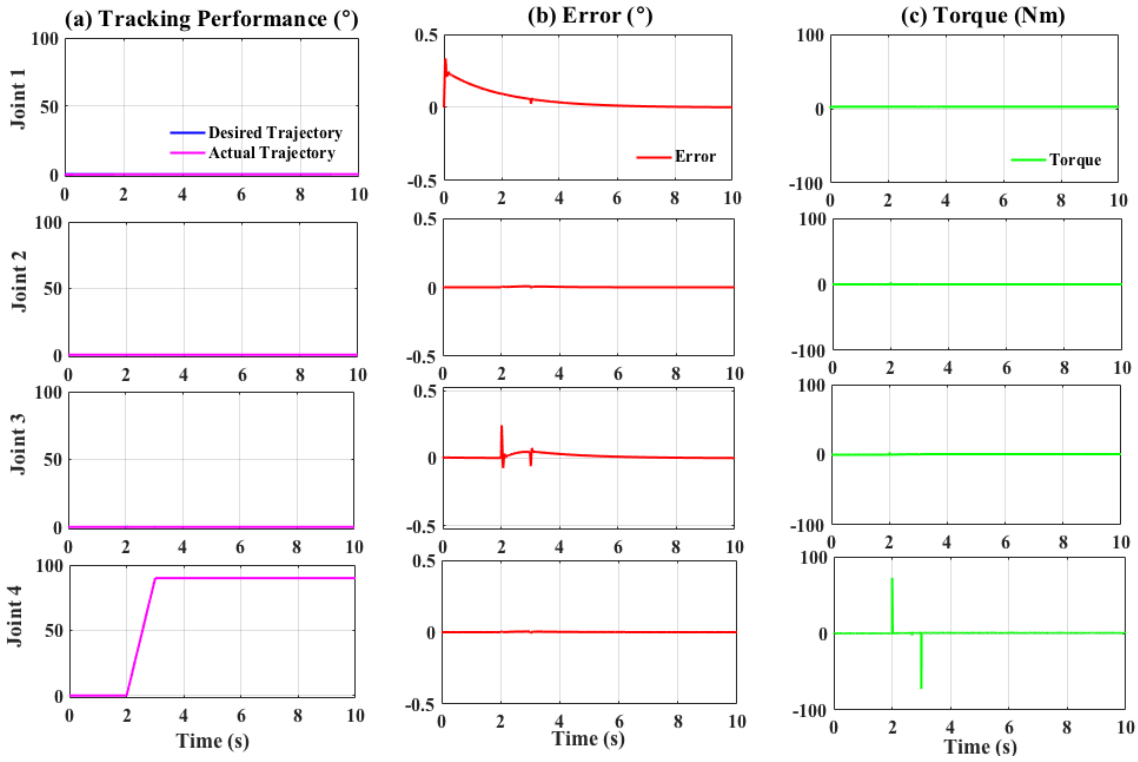

Figure 4.45: Performance for PID controller (Without disturbance).

torque needed as shown in Table 4.3.

The external force (1000 Nm) was applied at the forearm from 2.5 s until 10 s to

Table 4.14: RMS Error of Joints with an existense of external force

Controller / Joint	Joint 1	Joint 2	Joint 3	Joint 4
Hybrid	0.08779	0.0002902	0.06766	0.01915
PID	0.1163	0.002303	0.02572	0.3817

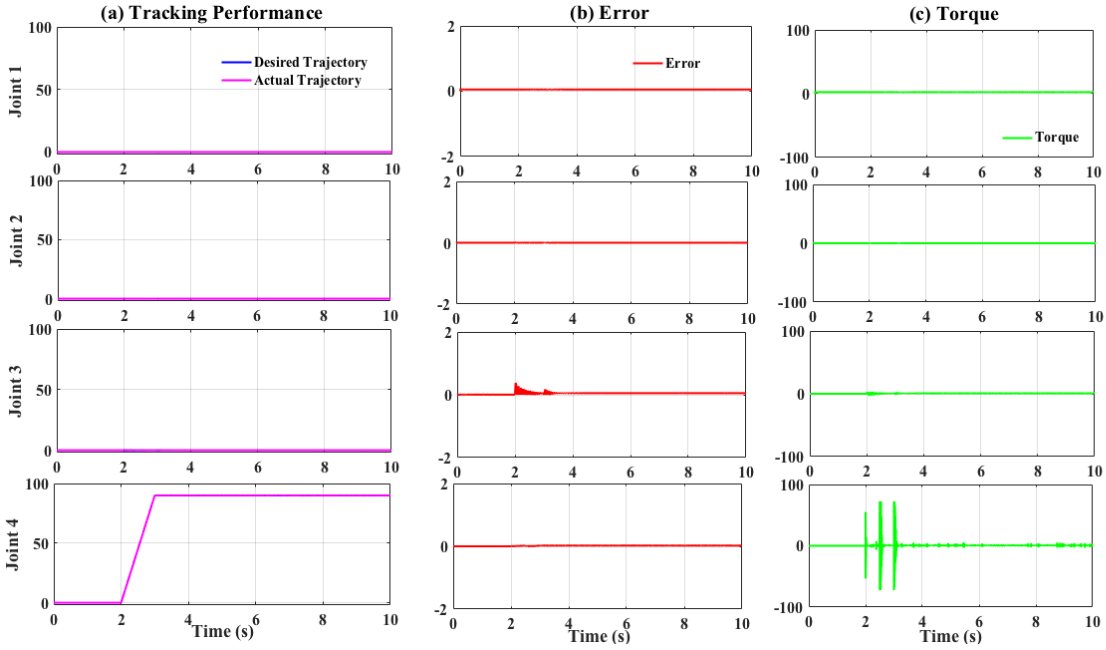

Figure 4.46: Performance for extended-fuzzy controller with external force (1000 Nm).

assess the robustness of each control approach. Figure 4.46 and Figure 4.47 show the tracking performance, error and torque required to move the elbow joint to follow the desired position with an external force applied to the forearm of the exoskeleton with extended-fuzzy and PID controller. In general, both controllers were able to track the desired trajectory. However, Figure 4.48 shows that the MAE by PID controller was about 1.5°, while the error produced with extended-fuzzy controller was about 0.04°. This shows that the proposed controller was able to track the desired trajectory with small error. Table 4.14 shows the comparison of RMS error with extended-fuzzy and PID controller for each joint. It is shown that the RMS errors with the extended-fuzzy controller generally, was less compared to that with PID controller, specifically for the Joint 4. However, the RMSE of extended-fuzzy controller for the third joint is higher, probably due to the de-coupling issue, since a high disturbance is applied onto Joint 4.

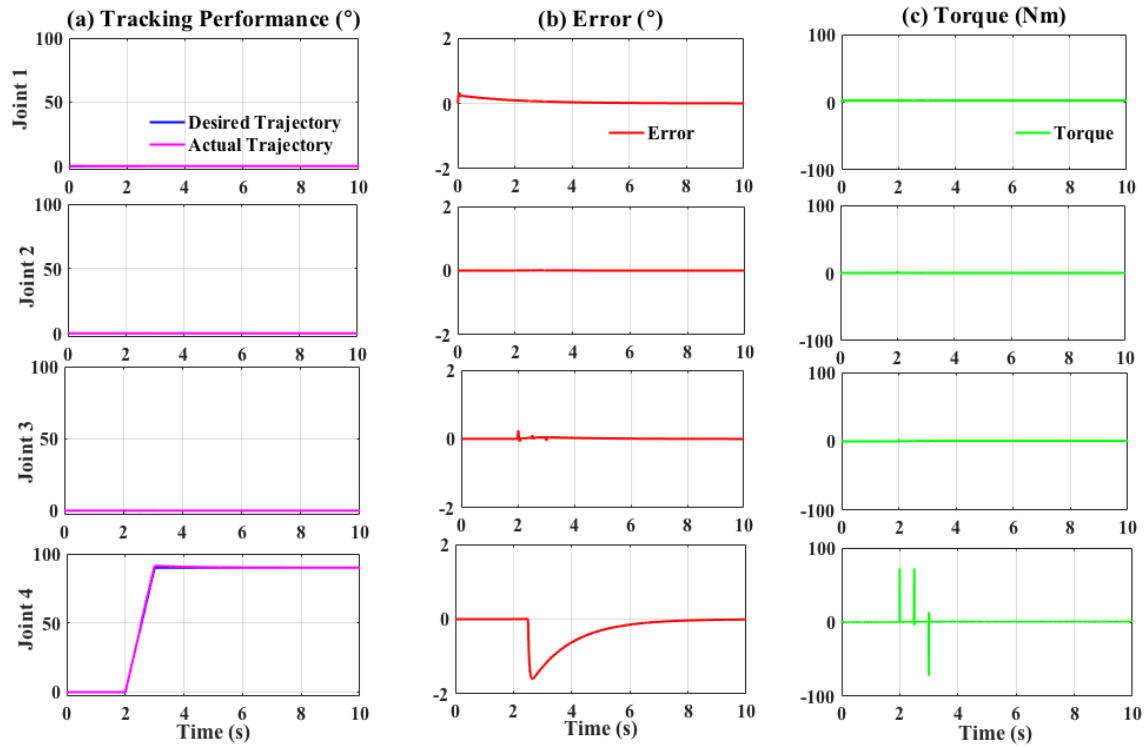

Figure 4.47: Performance for PID controller with external force (1000 Nm).

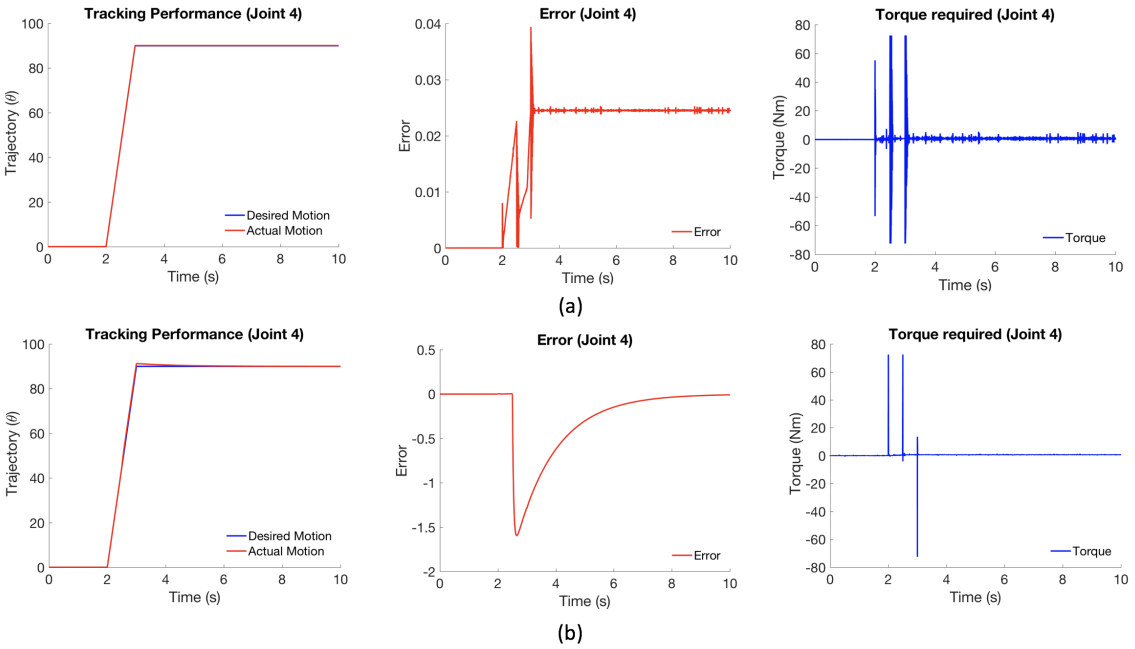

Figure 4.48: Comparison in tracking performance, error and torque required of Joint 4 with external force: (a) Extended-fuzzy (b) PID controller

Table 4.15 presents the maximum torque for each joint in the presence of external force. For Joint 1 and Joint 4, the maximum torque with both controllers were nearly equal. The results (Figure 4.46 and Figure 4.47) show that the torque needed and the error generated

Table 4.15: Maximum torque of joints with an existense of external force

Controller / Joint	Joint 1	Joint 2	Joint 3	Joint 4
Hybrid	3.841	0.8134	3.098	72.50
PID	3.601	3.14	3.21	72.50

with the extended-fuzzy controller for each joint were smaller compared to those with PID controller.

4.5 Summary

A extended-fuzzy controller has been proposed. The extended-fuzzy controller consists of fuzzy-based PD for movement and fuzzy-based compensator for compensating the gravity effect of the exoskeleton. The investigations carried out included observation of performance of the PID and fuzzy-based PD controller. Comparative assessment of the performance of system with PID and extended-fuzzy controller have been carried out. The results have shown that combination of fuzzy-based PD and fuzzy-compensatorhave achieved good performances with minimal torque. Thus, the extended-fuzzy controller is used subsequently in this work for implementation on the exoskeleton. In the next chapter, human is included in the investigation of the proposed controller.

Chapter 5

Control of Upper-limb Exoskeleton with Human

5.1 Introduction

In this chapter, the proposed control technique presented in Chapter 4 is evaluated with real human. The evaluation is done in a virtual environment. Three different human conditions are considered in the evaluations. The first condition is that the human has full strength and the exoskeleton is unactuated. The second condition is that the human strength is at 70% of full strength and the exoskeleton is unactuated. The third condition is that the human strength is at 70% of full strength and the exoskeleton is actuated. PID control is also implemented for comparison purpose.

5.2 Control of Human-Exoskeleton System

In this section, the combined human and exoskeleton system is considered for control investigations in a virtual software platform. Two assumptions are made. The first assumption is, an exoskeleton is moving parallel with human. This is done by applying the parallel constraint between human and the exoskeleton as described in Chapter 3. The second assumption is that the desired trajectory is obtained from human. This is different from Chapter 4, where the desired trajectory is a predefined trajectory.

Figure 5.1 shows the general structure of the human-exoskeleton system in this work. The figure shows that two pieces of information are sent to the exoskeleton. These are

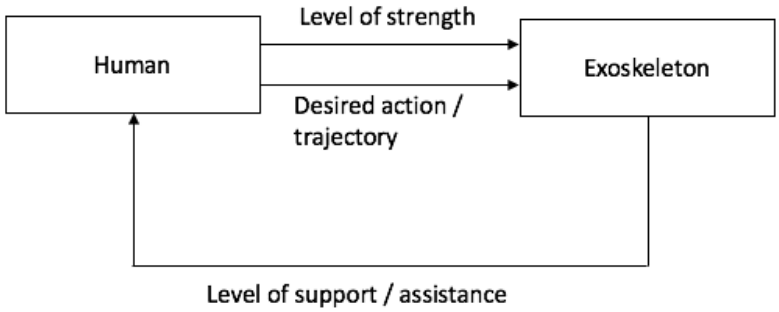

Figure 5.1: Structure of human-exoskeleton system.

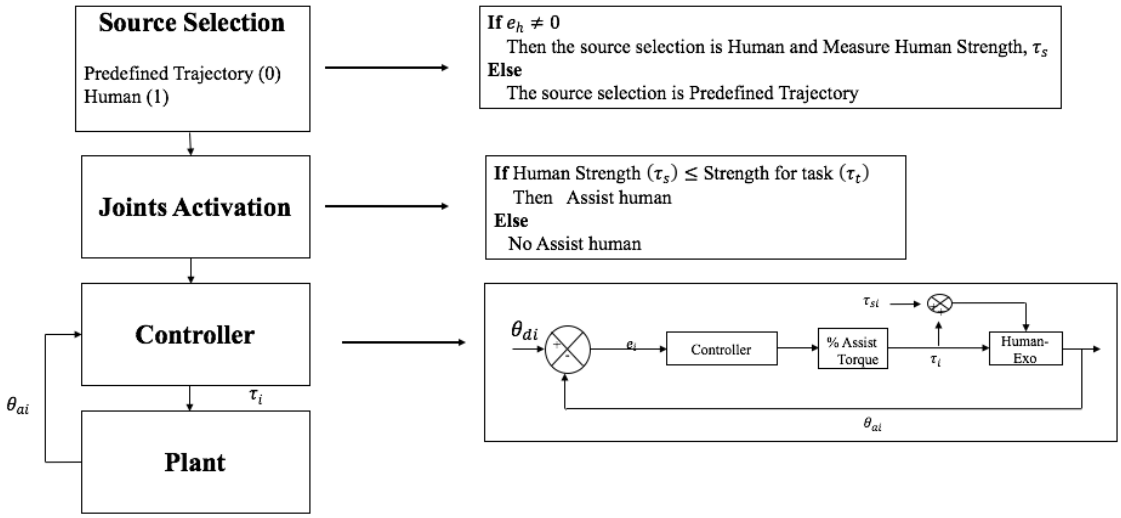

Figure 5.2: Control structure.

desired action or trajectory and level of human strength. In this chapter, it is important for the exoskeleton to have information of human strength because this information will be used to activate the exoskeleton. Besides, this information is needed for the exoskeleton to send the assistive torque to prolong human capability to continue to perform a physical task.

Figure 5.2 shows the user control of an exoskeleton. The steps involved are similar to those in Figure 4.1. The differences are in joint activation and controller block. As shown in Figure 5.2, to determine the source of the reference, signal which is detected by the embedded force sensor in the exoskeleton is used. The signal (e_h) is the difference between the currect and the desired position. If the signal, $e_h \neq 0$, then the source of the reference is obtained from human and is identified as $Ref = 1$ and the human strength is calculated. Else, the source of the reference is obtained from predefined trajectory and is

identified as $Ref = 0$.

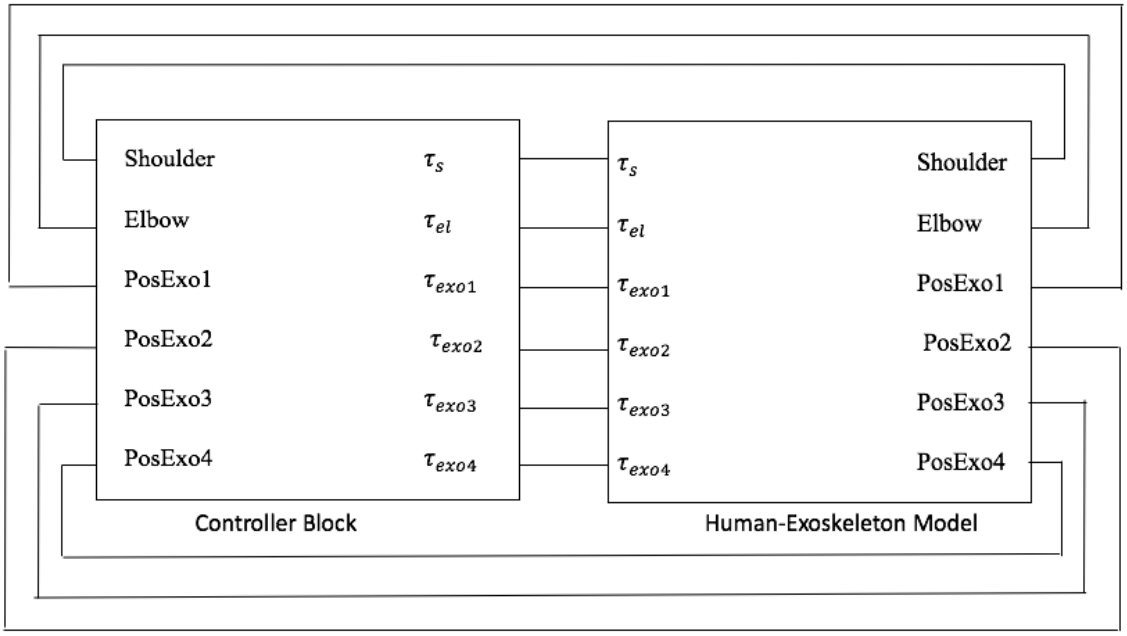

Figure 5.3: Human exoskeleton model.

The joints activation block shown in Figure 5.2 is applied based on the current condition of human strength. When the current condition of human strength (τ_s) is less than the required torque for a particular task (τ_t), then the exoskeleton is needed to assist human to keep moving or maintaining the position. Then, the current human strength (τ_s) and the desired trajectory information are sent to the controller block. In the controller block, if human needs asistance, then the required torque to assist human is calculated, else, no support torque is required.

Figure 5.3 shows Simulink implementation of the user control of an exoskeleton. The 'Human-Exoskeleton' block in Figure 5.3 represents the human and exoskeleton model in Simmechanics. The 'Controller' block consists of the reference selection, joint activation and controller system blocks. The details are presented in Figure 5.4.

Since this work is done in a virtual environment, the human and exoskeleton are designed using Solidwork as presented in Chapter 3. Revolute joints are used in the shoulder and elbow joints. The outputs of the controller for the shoulder and elbow joints are the shoulder torque (τ_h) and elbow torque (τ_e). The shoulder and elbow torques are used as input to the revolute joints. In real life, human strength or human capability to do a task

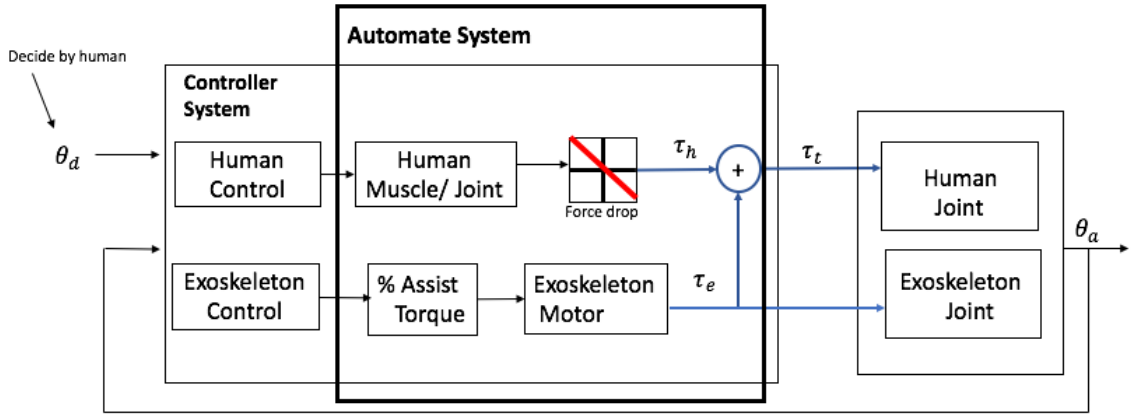

Figure 5.4: User control system.

will be reducing. Hence, to present this scenario, the 'force drop' block is used. As mentioned earlier, the exoskeleton is designed using Solidworks and revolute joints are used to represent each joint of the exoskeleton. The exoskeleton joints are controlled by the controller and the control outputs are the torques of Joint 1, Joint 2, Joint 3 and Joint 4 of the exoskeleton (τ_e). The torques of Joint 1, Joint 2, Joint 3 and Joint 4 of the exoskeleton are initially, the inputs to the revolute joints. However, since the exoskeleton is used for human to assist-as-needed, the '% Assist Torque' block is used to present the needed torque to be supplied by the exoskeleton to human.

Control investigations are performed in two ways. First, the human strength is grouped into three conditions. Secondly, the fatigue model is included to show the strength progression of the human shoulder and elbow joint. The second case will be presented in Chapter 6.

In the first case, the human strength is categorised into three conditions, namely human has 100% strength and the exoskeleton is unactuated, the human strength is reduced to 70% and the exoskeleton is unactuated and then the human strength is 70% and the exoskeleton assists the human for the required 30%.

Figure 5.5 shows description of the approach mentioned above in a Simulink block. In a real world, the orientation or the desired action of the shoulder and elbow are known to human. The gains a1 and b1 represent the strength progression of the shoulder and elbow joints ('force drop' block). Meanwhile, gain blocks a2 and b2, represent the percentage

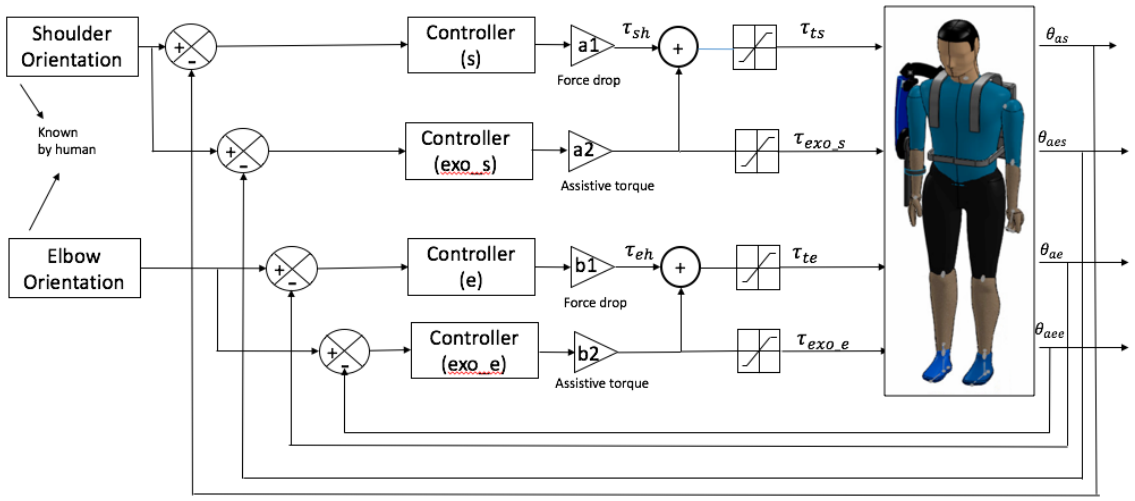

Figure 5.5: Simulink control diagram of shoulder and elbow joints of human and exoskeleton.

needed to assist the human ('% Assist Torque' block).

In this work, PID and extended-fuzzy controllers are investigated. The performance of the tracking action, deviation and torque required are observed for both controllers. PID is used for comparative study.

5.2.1 PID Control of the Human-Exoskeleton System

In this section, implementation of the PID controller is presented. Figure 5.6 shows the Simulink block diagram of the implementation.

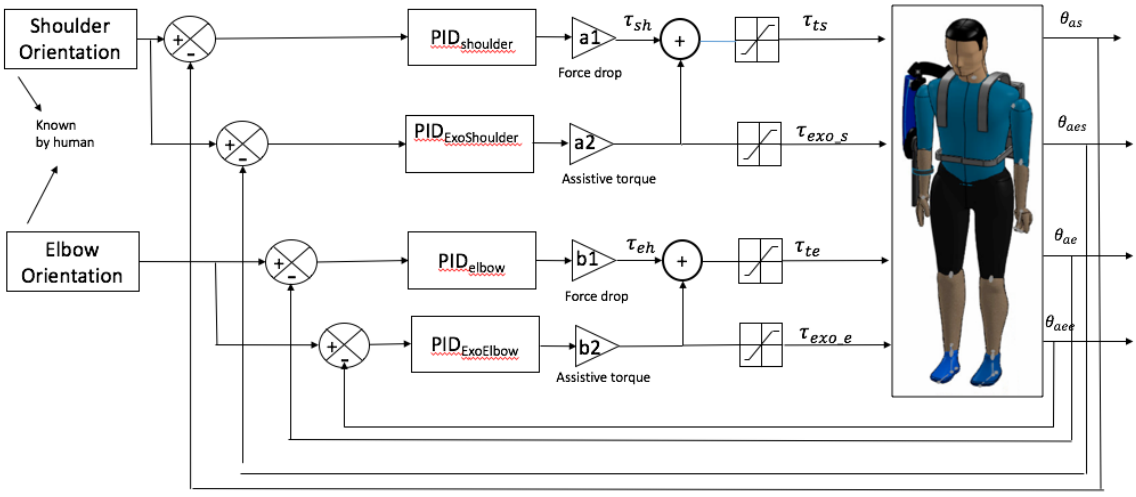

Figure 5.6: Implementation of PID control system.

The three conditions mentioned in Section 5.2 are summarised in Table 5.1. In the next section, the implementation of the extended-fuzzy controller is presented.

Table 5.1: Three conditions: Single Joints

Human strength	a1	a2
Condition 1	100%	0
Condition 2	70%	0
Condition 3	70%	30%

5.2.2 Extended-Fuzzy Control of the Human-Exoskeleton system

In this section, the implementation of the extended-fuzzy controller is presented. The extended-fuzzy controller consists of the fuzzy-based motion with fuzzy-based de-weighting controller (Figure 5.7). The efficiency of the extended-fuzzy controller was presented in Chapter 4. Hence, in this chapter, the efficiency of the controller in providing the assistive torque, to the human with reduced strength is assessed.

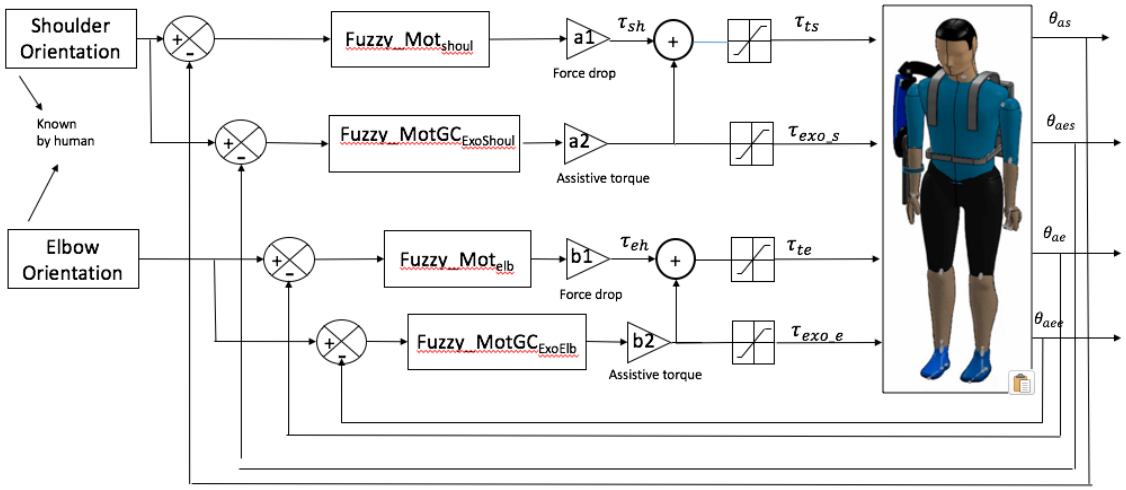

Figure 5.7: Implementation of extended-fuzzy controller.

Similar to that in section 5.2.1, three conditions (Table 5.1) of human joints are considered. This is to observe the capability of the controller in controlling the exoskeleton with reduced strength of human.

5.3 Results and Discussion

In this section, the results and discussion from the implementation of the PID and extended-fuzzy controller are presented. The performances of the controllers are evaluated in terms of: tracking desired trajectory, the deviation (error) and the torque required by human. Two movements are involved in the evaluation: single joint movement and the multi-joint movements. The single joint movement involves shoulder flexion, while the multi-joint movements involve shoulder abduction and elbow flexion.

5.3.1 PID Control of Single Joint Movement

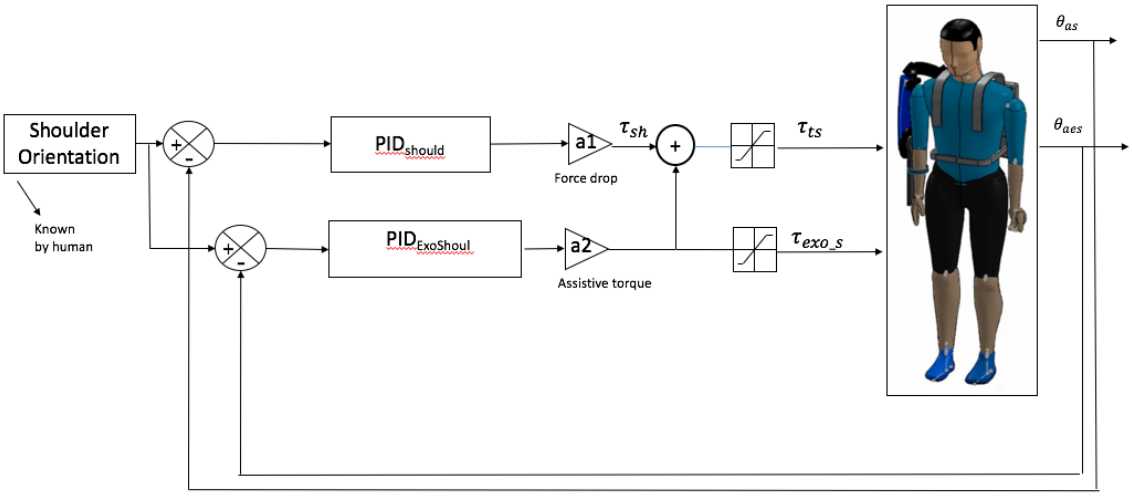

Figure 5.8: PID controller for a single joint (shoulder).

For a single joint movement, only the shoulder joint is considered. The elbow and wrist joints are fixed. The shoulder joint is flexion to 90° at 10 s and remains static at this position until 20 s. Figure 5.8 shows the Simulink block diagram of PID controller for shoulder joint. Figure 5.9 shows the desired trajectory for each joint of human and exoskeleton.

Table 5.2 shows the control parameters used in this experiment. These parameters were obtained using a trial and error approach. Figure 5.11 shows the results of the single joint movement. The first row of Figure 5.11 presents the results for human with full (100%) strength. The second row shows the results for human with 70% strength. The third row

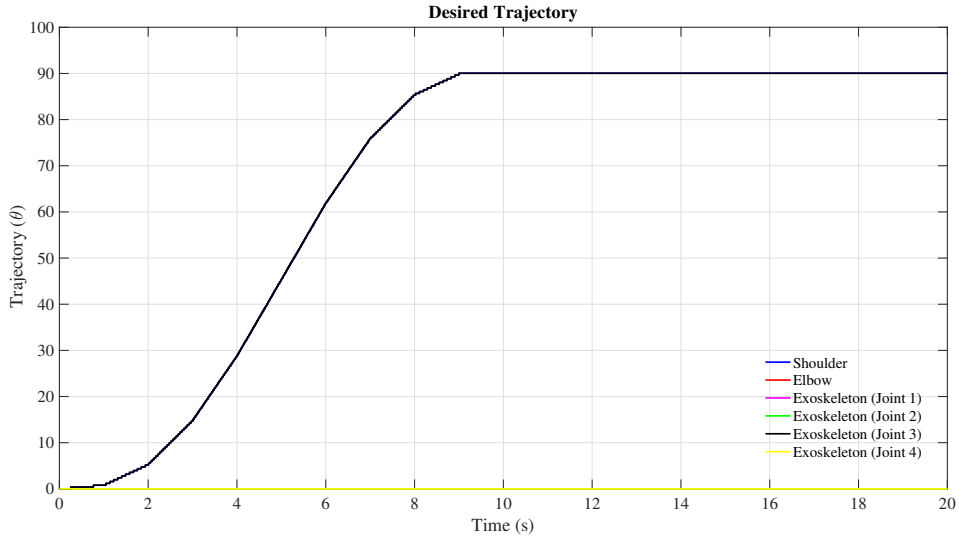

Figure 5.9: Desired trajectory: Single joint.

shows the results for human with strength of 70% and an assistive torque amounted 30% from actuated exoskeleton.

Generally, as noted, in all conditions human was able to achieve the desired trajectory. However, Figure 5.11 (a) and Figure 5.11 (b) show an active fluctuation. This occur due to the graphical issue of the signal builder and could not be avoided (Figure 5.10) but, the range is about 1°.

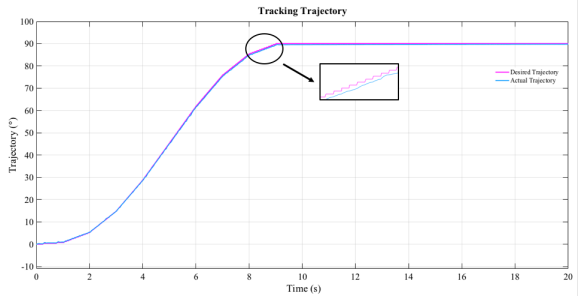

Figure 5.10: Graphical issue of signal builder.

The highest MAE was 2.236° , which was in case of human with strength of 70% with an unactuated exoskeleton. The lowest MAE was 1.80°, and this was case of human with strength of 70% assisted with the actuated exoskeleton. The results in terms of RMSE show similar trends as the MAE. The RMSE of the second condition shows the highest (1.061°), while the third condition shows the smallest RMSE value (0.6229°).

It is noted from torques in Figure 5.11 that, for the first two rows, the movement of

Table 5.2: Controller gains for single joint movement: PID controller

Gains	Shoulder Joint	Exoskeleton Joint 3
K_p	10	10
K_i	1	1
K_d	0.1	0.1

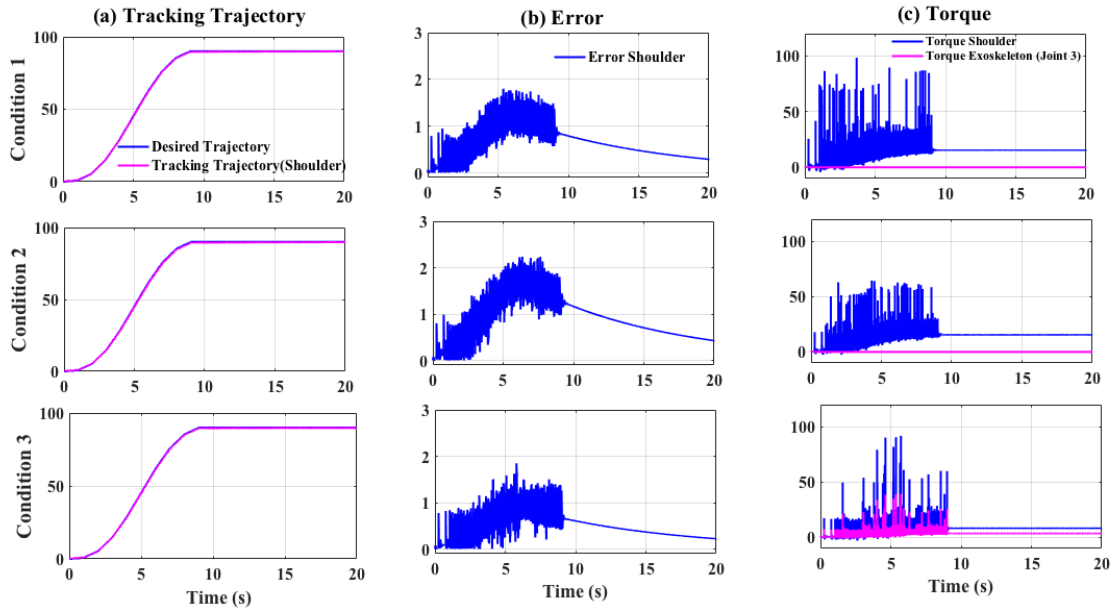

Figure 5.11: Results of PID controller of single joint movements for: (a) Trajectory tracking (b) Error (c) Torque.

the upper-limb and the exoskeleton are dependent on human. In the third row, the human and exoskeleton strengths are combined to support the movement and ensure the desired position is achieved. For purpose of comparison, it is easier to observe the torque required when the upper-limb is at static position since during at this position, human is easily to get fatigue. Hence, for torque analysis, the torque required to maintain the upper-limb and exoskeleton during the static position was observed. During the static position, MAT required by first and second conditions are nearly to 15.4 Nm. The torque required by human with strength at only 70% with an actuated exoskeleton was 11.9 Nm and the torque supplied by the exoskeleton was 3.55 Nm. The error and torque analysis thus shows that the torque needed by human to move the upper-limb and an exoskeleton is less with the

assisted torque from an exoskeleton. This observation shows that, the exoskeleton is potentially capable of reducing the chances of human muscles or joints from fatigue.

5.3.2 Extended-Fuzzy Control of a Single Joint Movement

Similar to previous section shoulder flexion movement is used to assess the system performance. The controller gains were obtained by using a heuristic approach and these are presented in Table 5.3.

Table 5.3: Controller gains for single joint movement: Hybrid-based fuzzy controller

Gains	Shoulder Joint	Exoskeleton Joint 3
K_e	1	1
$K_{\dot{e}}$	0.001	0.001
K_{gain1}	50	50
K_e	-	1
K_α	-	0.001
K_{gain2}	-	10

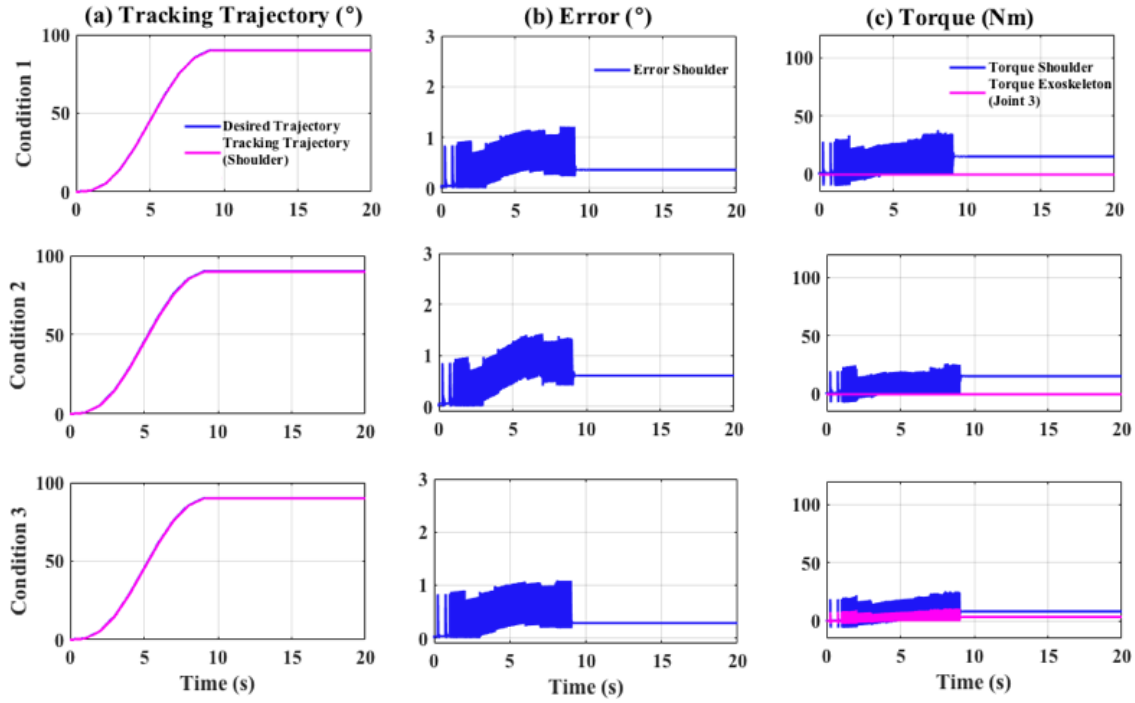

Figure 5.12: Results of extended fuzzy controller of single-joint movements for: (a) Trajectory tracking (b) Error (c) Torque.

Figure 5.12 shows the results with extended-fuzzy controller for all conditions. The first row shows the results for human with full strength. The second row shows the results for human with 70% strength with unactuated exoskeleton. The third row, shows the resuts for human with 70% strength with an actuated exoskeleton. It is noted that, in general, the exoskeleton with extended-fuzzy controller was able to control the movements of the upper-limb in all conditions. Similar as in Section 5.3.1, an active fluctation could be observed occurs in Figure 5.12(b) and Figure 5.12(c). As mentioned in previous section, this occurs due to graphical issue of the signal builder. As shown in Table 5.4, the highest MAE was noted in the second condition. Meanwhile, the lowest MAE (1.052°) was achieved in the third condition. A similar trend was also noted with RMSE.

Table 5.4: RMSE and MAE for PID and extended-based fuzzy controllers

Conditions	RMSE		MAE	
	PID	Extended-Fuzzy	PID	Extended-Fuzzy
Condition 1	0.7829	0.4911	1.848	1.208
Condition 2	1.061	0.5809	2.236	1.423
Condition 3	0.6229	0.4294	1.80	1.052

Figure 5.12 (c) shows the torque required by human and the exoskeleton to achieve the desired movement. To evaluate the torque performance, MAT is used. It is noted in Figure 5.12 (c) that for the first and second conditions, the movement of the human shoulder and the exoskeleton were fully dependent on human shoulder joint, because in these conditions, the exoskeleton was not actuated. The MAT for the extended-fuzzy controller is shown in Table 5.5. As noted the highest MAT value occured in second condition, and the smallest MAT value occured in the third condition. Thus, the results demonstrate that it is possible with an exoskeleton to assists human in carrying out physical tasks, especially when human strength is reducing.

To compare the error or deviation performance between PID and extended-fuzzy controllers, the differences in RMSE and MAE are observed. These are presented in Table 5.4. As noted the RMSE values with PID control for all conditions were higher to nearly 50% than the extended-fuzzy controller. The MAE values were similarly 50% higher with PID control in comparison to those with extended-fuzzy controller. Hence, in deviation or

error observation, extended-fuzzy controller showed better performance compared to PID controller.

Table 5.5: MAT for PID and extended-based fuzzy controllers

Conditions	Shoulder		Exoskeleton (Joint 3)	
	PID	Hybrid-Fuzzy	PID	Extended-Fuzzy
Condition 1	15.4	15.45	0	0
Condition 2	15.4	15.45	0	0
Condition 3	11.9	7.612	3.55	3.915

The values of the MAT for the controllers are shown in Table 5.5. It is noted that the torque required by the exoskeleton, with extended-fuzzy controller assisting the human was about 29% higher than that with the PID controller. However, in terms of trajectory tracking error performace, extended-fuzzy controller performed nearly 50% better compared to PID controller. Moreover, as in addition, Figure 5.12 (c) shows, the torque fluctuated in an acceptable range for human shoulder and the exoskeleton joint. These show that by implementing an intelligent control approach such as fuzzy logic control, the required output can be obtained to an acceptable range, and hence could limit the potential of damage or harm to the whole system.

5.3.3 PID Control of Multi-Joint Movement

The desired movements involved in this section are shoulder and elbow joints, and these are shown in Figure 5.13. The shoulder joint was abducted to reach 39° at 10 s and was kept at this current position until 20 s. The elbow joint was flexed and reached 30° at 16 s and was fix at this position until 20 s. The three conditions mentioned in Section 5.3.1 and Section 5.3.2, were realised here and these are presented in Table 5.6. These three conditions are applied for the PID and extended-fuzzy controllers.

The parameters for K_p, K_i and K_d were obtained by using heuristic approach and these are presented in Table 5.7. Figure 5.14 shows the results of the shoulder abduction. The first row of Figure 5.14 shows the first condition of Table 5.6, the second row shows the second condition of Table 5.6 and the third row shows the third condition of Table 5.6.

Table 5.6: Three conditions: Multi-joints movements

Conditions	Shoulder Joint		Elbow Joint	
	a1	a2	b1	b2
Condition 1	100%	0	100%	0
Condition 2	70%	0	70%	0
Condition 3	70%	30%	70%	30%

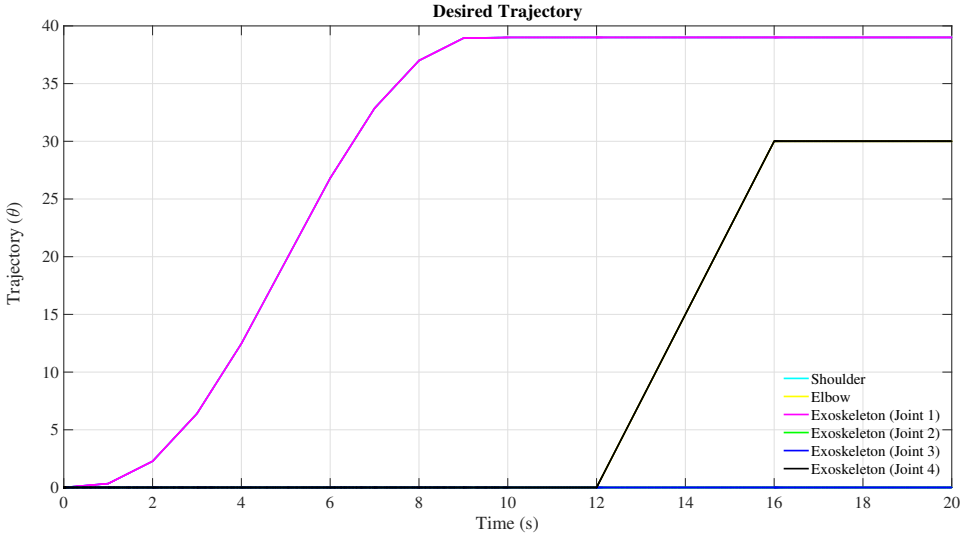

Figure 5.13: Desired trajectory: Multi joint.

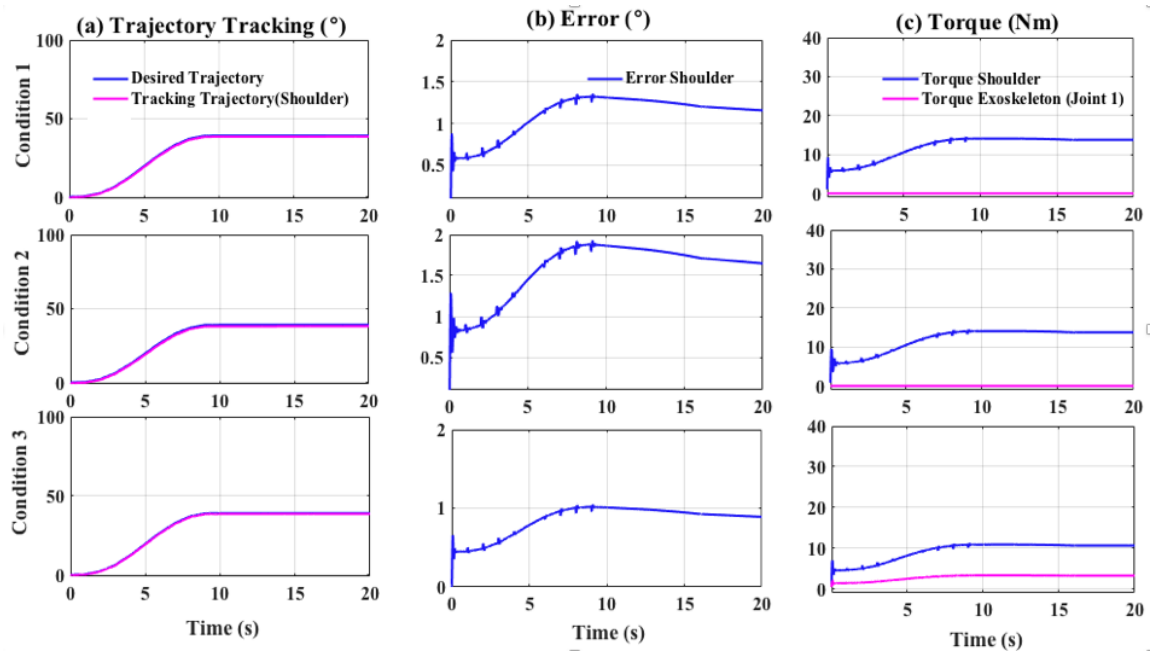

Figure 5.14: Results of PID controller of multi joint movement for shoulder abduction: (a) Trajectory tracking (b) Error (c) Torque.

Generally, in all conditions, the PID controller was able to move the human shoulder and exoskeleton joint to the desired position. Similar as in Section 5.3.1, an active fluc-

Table 5.7: Controller gains for multi-joint movement: PID controller

Gains	Shoulder Joint	Elbow Joint	Exoskeleton Joint 1	Exoskeleton Joint 4
K_p	10	5	10	5
K_i	0.1	0.1	0.1	0.1
K_d	0.1	0.1	0.1	0.1

tation could be observed occurs in Figure 5.14(b) and Figure 5.14(c). As mentioned in Section 5.3.1, this occurs due to graphical issue of the signal builder. Although the PID was capable in following the trajectory, however, in terms of the accuracy, some differences were noted. Figure 5.14 shows that the second condition had the highest deviation amongst the three conditions. This observation is similar to that noted in Section 5.3.1 and Section 5.3.2. In this case, it occurred because, the human strength was limited to only 70% and with this strength, human shoulder needed to lift the whole arm with the unactuated exoskeleton. This could lead the shoulder joint to feel more fatigue, and thus, unable to achieve the desired position accurately. Meanwhile, in the third condition, although the human strength was similar to the second condition, the exoskeleton was actuated to assist the human for the remaining 30%. Hence, as shown in Figure 5.14, the deviation of the third condition was about 50% lower compared to the second condition. Similar evaluation measurements are used in this section: the RMSE and the MAE. Both measurements are shown in Table 5.8. The RMSE for the third condition shows that it was about 39% less than the second condition, and the MAE for the third condition was 45% lower than the second condition.

Figure 5.14 (c) shows the torque required by human to move the upper-extremity and the upper-limb exoskeleton. Similar to observations in Section 5.3.1 and Section 5.3.2, the movements for the upper-limb and the exoskeleton for the first and second conditions are fully dependent on human. Hence, in these two conditions, human torques are higher compared to the third condition. As reported in Table 5.8, the MAT for the first and second conditions are about to 14.50 Nm and 14.45 Nm. Although, the MAT shows that the maximum torque for the first and second conditions are more likely similar,from the error

Table 5.8: Error and torque analysis (PID controller): Shoulder

Error Analysis	RMSE	MAE
Condition 1	0.5486	1.353
Condition 2	0.7189	1.931
Condition 3	0.4363	1.045
Torque Analysis	**MAT (Shoulder)**	**MAT (Exoskeleton)**
Condition 1	14.50	0
Condition 2	14.45	0
Condition 3	11.17	3.18

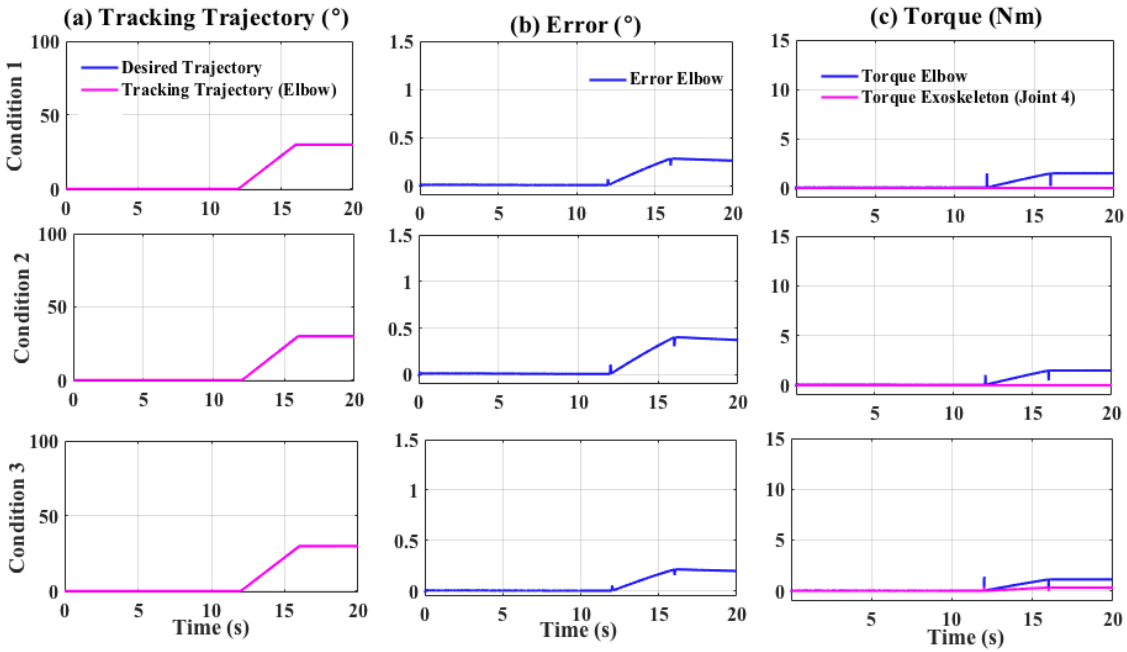

Figure 5.15: Results of PID controller of multi joint movement for elbow flexion: (a) Trajectory tracking (b) Error (c) Torque.

analysis, the second condition, has higher error compared to the first condition. This occurs because, in the second condition, human strength is only 70%, and shoulder joint needs to lift the arm with the unactuated exoskeleton. While, in the first condition, the human strength is 100%. The MAT for the third condition was about 11.17 Nm. In the third condition, the exoskeleton is actuated and it supports the movement of the human shoulder and the exoskeleton. Hence, in this case, the torque required for the shoulder joint is less compared to the first and second condition.

Figure 5.15 shows the trajectory tracking, error and torque performances at the elbow flexion. Comparing Figure 5.14 and Figure 5.15, elbow joint shows the least deviation in all conditions than the shoulder. This occurs because, the shoulder joint, which is at the proximal joint has a major control towards the elbow joint, which is at the distal joint movements. Hence, the movements of the elbow joint would affect the shoulder joint.

Table 5.9: Error and torque analysis (PID controller): Elbow joint

Error Analysis	RMSE	MAE
Condition 1	0.06248	0.2829
Condition 2	0.08696	0.4061
Condition 3	0.04454	0.2181
Torque Analysis	**MAT (Shoulder)**	**MAT (Exoskeleton)**
Condition 1	1.479	0
Condition 2	1.4815	0
Condition 3	1.1350	0.34

Figure 5.15 shows that in general, the PID controller was able to track the elbow flexion trajectory. From this figure, it is noted that the second condition has the highest error amongst all conditions. Meanwhile, the third condition has less approximately near to 50% compared to the second condition. The RMSE and MAE for the elbow flexion are presented in Table 5.9. Both measurements show that the third condition has less error than the first and second conditions, approximately near to 30% and 49%. Figure 5.15 (c) shows the torque required by elbow joint to flex to 30°. Table 5.9 presents the MAT values for all conditions. The least MAT value is noted in third condition (1.135 Nm), and the highest MAT value in second condition (1.4815 Nm).

From the observation in this section, it follows that the exoskeleton, which is controlled by the PID, is able in assisting human for a multi-joint movement, while human strength is reducing. In addition, it is shown that the proximal joint of the body has more control than the distal joint. Hence, more torque is required for the proximal joint for making

movements. By implementing the exoskeleton for assisting human, the required torque for the proximal joint could be reduced, and thus, the tendency for the fatigue is reduced.

5.3.4 Extended-Fuzzy Control of Multi-Joint Movement

This section presents results or realisation of multi-joint movements with extended-fuzzy controller. The desired movement for the shoulder and elbow joints are similar as those in Figure 5.13. The three conditions shown in Table 5.6 are applied in this section. The parameters for the extended fuzzy controller were obtained by using heuristic technique and these are presented in Table 5.10.

Table 5.10: Controller gains for multi-joints movements: Extended fuzzy controller

Gains	Shoulder Joint	Elbow Joint	Exoskeleton Joint 1	Exoskeleton Joint 4
K_e	10	5	10	10
$K_{\dot{e}}$	0.05	0.01	0.05	0.01
K_{gain1}	30	10	30	30
K_e	-	-	10	10
K_α	-	-	0.01	0.001
K_{gain2}	-	-	30	30

Figure 5.16 shows trajectory tracking, deviation and the torque performance of the extended-fuzzy controller for shoulder abduction. As noted, the extended-fuzzy controller was in general able to track the desired trajectory in all conditions. Similar to previous sections, the observations are made on the errors and the torque required by human.

In terms of the error evaluation, as shown in Table 5.11 the highest RMSE and MAE were in the second conditions. This is not in contradiction with the fact that, at this condition, human with less strength, could not achieve the desired action precisely. The third condition, shows the least values of RMSE and MAE. Hence, this shows that the capability of the combination of human with limited strength and the actuated exoskeleton is more likely 90% similar as the first condition.

Table 5.11 presents the required torque of human shoulder in making an abduction movement. The MAT shows that the least shoulder torque was in a third condition (9.058

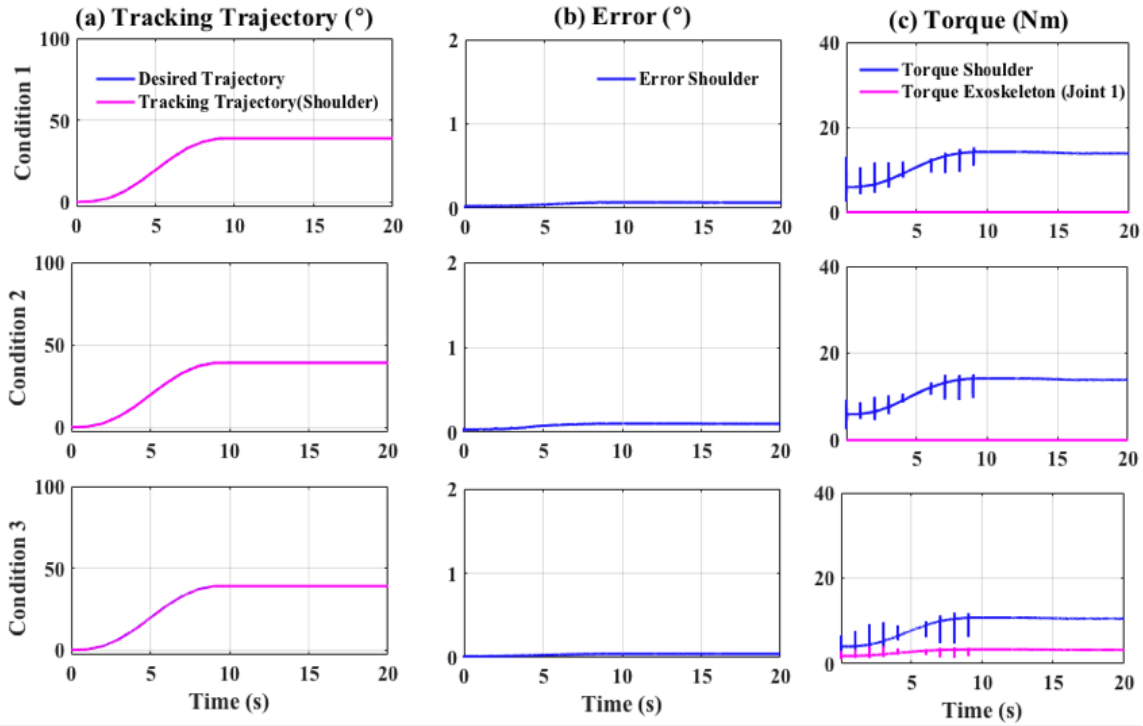

Figure 5.16: Results of extended fuzzy controller of multi joint movement for shoulder abduction: (a) Trajectory tracking (b) Error (c) Torque.

Nm). The assisted torque performed by the actuated exoskeleton for the third condition was about 3 Nm. Hence, the total torque required by the whole system for the third condition was 12 Nm. Thus, the total torque in the third condition is more likely similar to condition 1. This shows that, a combination of the human shoulder joint and the exoskeleton is able to perform similar as human shoulder joint with full strength, even when human strength is limited.

Figure 5.17 shows the tracking, error and torque performance at the elbow flexion. The figure shows that in general, the elbow joint was able to follow the desired action. However, similar to that in Section 5.3.3, the deviation of the elbow joint was less than shoulder joint. This occurs due to the location of the shoulder joint, which is proximal to human body than elbow joint, and any movement of the elbow joint, would affect the shoulder joint. As shown in Table 5.12, the second condition shows greater RMSE and MAE, than first and third condition.

From the MAT of the elbow joint shown in Table 5.12, it is noted that the third condition had the least torque of elbow joint (0.8240 Nm), amongst all conditions. The MAT of the

Table 5.11: Error and torque analysis (Extended Fuzzy): Shoulder

Error Analysis	RMSE	MAE
Condition 1	0.04072	0.07338
Condition 2	0.08658	0.1040
Condition 3	0.03098	0.04472
Torque Analysis	**MAT (Shoulder)**	**MAT (Exoskeleton)**
Condition 1	13.84	0
Condition 2	13.84	0
Condition 3	10.57	3.27

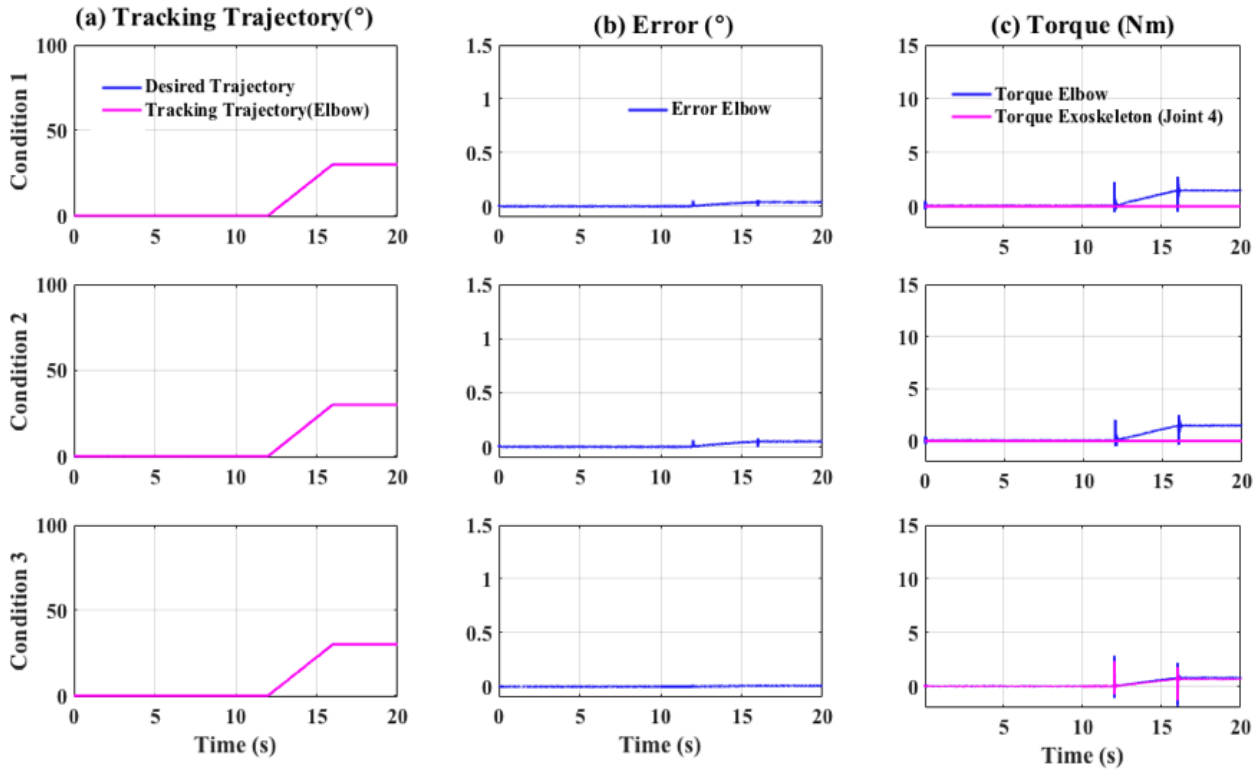

Figure 5.17: Results of extended-fuzzy controller of multi-joint movements for elbow flexion:(a) Trajectory tracking (b) Error (c) Torque.

exoskeleton for the third condition was 0.6820 Nm. The total for the whole system for the third condition was 1.5060 Nm. Similar to the shoulder joint, the exoskeleton is also able to assist elbow joint then its strength is limited.

For the multi-joint movements, it shows that in general, the PID and extended-fuzzy controllers are able to assist human joints to move to the desired position. However, in

Table 5.12: Error and torque analysis (Extended Fuzzy): Elbow

Error Analysis	RMSE	MAE
Condition 1	0.01485	0.05876
Condition 2	0.002843	0.07868
Condition 3	0.002132	0.01714
Torque Analysis	**MAT (Shoulder)**	**MAT (Exoskeleton)**
Condition 1	1.494	0
Condition 2	1.491	0
Condition 3	0.8240	0.6820

terms of accuracy to achieve the desired position and torques needed by human are different.

Table 5.13: RMSE, MAE and MAT for PID and Extended-fuzzy controllers: Shoulder

Error	RMSE		MAE	
	PID	Extended-Fuzzy	PID	Extended-Fuzzy
Condition 1	0.5486	0.04072	1.353	0.07338
Condition 2	0.7189	0.08658	1.931	0.1040
Condition 3	0.4363	0.03098	1.045	0.04472
Torque	**MAT**			
	PID	Extended-Fuzzy		
Condition 1	14.50	13.84		
Condition 2	14.45	13.84		
Condition 3	11.17	10.57		

Table 5.13 and Table 5.14 show the comparison between the PID and extended-fuzzy controllers in terms of RMSE, MAE and MAT. The comparison and discussion will begin for shoulder joint and followed with elbow joint.

The MAT of the third condition for the shoulder joint in the case of the extended-fuzzy controller is lower about 5% than the PID controller (Table 5.13). Moreover, the RMSE and the MAE of the third condition for the extended-fuzzy controller shows that it is able to achieve the desired trajectory more accurately than the PID , where the RMSE and the

Table 5.14: RMSE, MAE and MAT for PID and Extended-fuzzy controllers: Elbow

Error	RMSE		MAE	
	PID	Extended-Fuzzy	PID	Extended-Fuzzy
Condition 1	0.06248	0.01485	0.2829	0.05876
Condition 2	0.08696	0.02843	0.4061	0.07868
Condition 3	0.04454	0.002132	0.2181	0.01714

Torque	MAT	
	PID	Extended-Fuzzy
Condition 1	1.506	1.494
Condition 2	1.532	1.491
Condition 3	1.402	0.8240

MAE of the third condition is almost 91% less than PID (Table 5.13). A similar observation could be seen for the elbow joint.

The RMSE and MAE in Table 5.14 show that the extended-fuzzy controller performs better than the PID controller, where both measurements show that they are almost 50% less than the measurement for the PID. The third condition of the elbow flexion shows that the exoskeleton was able to assist elbow joint by providing the assistive torque to lessen the torque required by human.

5.4 Summary

This chapter has presented the implementation and evaluation of the proposed control technique (extended-fuzzy controller) with the inclusion of human. The PID controller is used for a comparison purpose. The results show that the exoskeleton with both controllers is able to assist human joint to the desired position, although the human strength is reducing. The deviation or error and torque analysis were used to shows the performance of the controllers. In terms of the deviation analysis, the proposed controller is able to perform accurately than the PID controller. In terms of torque analysis, it shows that human joints required less torque in extended-fuzzy controller than the PID controller. In addition, the deviation of the PID controller is higher about 10 times than the proposed controller. Due to this reason, in the next chapter, the extended-fuzzy controller is implemented on

the exoskeleton. The joint fatigue model is implemented in the human model, and the exoskeleton is used to assist the human in making movements.

Chapter 6

Control of Upper-Extremity Exoskeleton including Fatigue Human

6.1 Introduction

In this chapter, investigation into the control mechanism for human with fatigue model with an assisting exoskeleton is presented. In Chapter 5, the human was assumed to have full strength and 70 % strength while moving the shoulder and elbow joints. Based on the results in Chapter 5, an exoskeleton shows its ability and potential in assisting human with less strength. Hence, in this chapter, the fatigue model is included in the human and the exoskeleton is used to assist human performing physical tasks.

6.2 Joint Fatigue Model

The joint fatigue model adopted in this work is based on that proposed by Ma et al. (2008). Ma et al. (2010) extended their muscle-level to the joint-level fatigue model. The extended work model is to allow determining the effort required by muscles during movement. Although, several optimization approaches are proposed, it is difficult to obtain accurate results for each muscle. By implying the inverse dynamics in joint-level fatigue model, the torque required at a joint could be obtained. Moreover, the joint-level fatigue model has been validated for static and quasi-static movements. Hence, due to these advantages, the joint-level fatigue model by Ma et al. (2010) is implemented in this work to identify the occurence of fatigue in the joints.

In the development of the muscle fatigue model Ma et al. (2008), have included the fatigue index and the reduction of the human muscle strength (muscle fatigue). The fatigue index presents the evaluation of human perception of fatigue or in other words, it tells about 'how human feels of fatigue?'. According to Ma et al. (2008), there are three elements in evaluating the fatigue index: the force applied, the duration of an activity and the capacity of human muscle. In terms of the force applied, the muscles are becoming more fatigued when the force applied is large. In terms of duration, the muscles are becoming more fatigued when activities take longer duration. In terms of capacity of muscles, the muscles are becoming more fatigued, when the muscles capacity is smaller. The explanation of the three elements is translated into the differential equation and its integration as

$$\frac{dU}{dt} = \frac{MVC}{F_{cem}(t)} \frac{F_{load}(t)}{F_{cem}(t)} \tag{6.1}$$

$$\begin{aligned} U &= \frac{1}{2k} e^{2kF(t)} - \frac{1}{2k} e^{2kF(0)} \\ F(t) &= \int_0^t \frac{F_{load(u)}}{MVC} du \end{aligned} \tag{6.2}$$

The terms present in these equations are defined in Table 6.1.

Table 6.1: Parameters in muscle fatigue model

Muscle-fatigue model	Unit	Definition
MVC	Newton (N)	Muscle Maximum voluntary contraction
$F_{cem}(t)$	Newton (N)	Muscle force capacity at time instant t
$F_{load}(t)$	Newton (N)	Muscle load at time instant t
k	min^{-1}	Fatigue rate (constant value = 1)
U	min	Fatigue index

The term F_{cem} in equation (6.1) represents the current capacity of human muscle. This term reduces in value during the movement or sustain due to contraction process. The reduction shows that the muscles are getting weaker and fatigue. The term $(\frac{MVC}{F_{cem}(t)})$ represents the relationship between maximum voluntary contraction or the full strength of human with the current capacity of human strength. As the term F_{cem} reduces, this term $(\frac{MVC}{F_{cem}(t)})$ increases. The term $\frac{F_{load}(t)}{F_{cem}(t)}$ shows the relation between the load with the current capacity

of human strength. As the term F_{cem} is reduces, this term ($\frac{F_{load}(t)}{F_{cem}(t)}$) is increases. Hence, the fatigue index ($\frac{dU}{dt}$), shows the inverse relation with the current capacity of human muscle. As the human strength reduces, the value of $\frac{dU}{dt}$ increases, and in this condition, human is at the fatigue state (condition).

As mentioned earlier, the term F_{cem} represents the current capacity of human muscle, and this term reduces due to the contraction process. The contraction process is influenced by the external muscle load, which means that F_{cem} is also influenced by the external muscle load. As the external muscle load gets larger, the contraction process occurs rapidly, thus, the current capacity of human muscle with respect to time ($F_{cem}(t)$) decreases faster.

The motor unit activation pattern muscle is used to explain the development of the basic muscle fatigue model (equation (6.3)). The motor unit consists of a motoneuron and muscle fibres. Motoneurons receive control signals from the Central Nervous-System (CNS), and send these to the muscle fibres. As mentioned in Chapter 2, one of the factors that contribute to muscle twitch or the contraction phenomenon is the composition of muscle fibres. There are three types of the composition of muscle fibres: Type-I, Type-IIa and Type-IIb. The properties of these compositions are presented in Table 2.1. Specifically, the properties of the muscle fibres composition show the motor unit activation pattern for muscle. Large external muscle loads ($F_{load}(u)$) cause more involvement of the Type-II muscle fibres in force generation, which lead to muscles to fatigue rapidly (equation (6.3)). As mentioned earlier, F_{cem} represents the current capacity of human muscle, which, actually shows the number of non-fatigue muscle fibres. Although the Type-II muscle fibres cause the muscle to fatigue at a higher speed due to a reduction in number of Type-II muscle fibres, the Type-I muscle fibres, which have high resistance to fatigue could slow down the decreasing process of the human muscle capacity ($\frac{F_{cem}(t)}{MVC}$). Hence, the muscle fatigue model in equation (6.3) shows the involvement of motor unit activation pattern muscle during the force generation for upper-extremity movement or static position.

$$\frac{dF_{cem}}{dt} = -k\frac{F_{cem}}{MVC}F_{load} \tag{6.3}$$

$$F_{cem}(t) = MVCe^{\int_0^t -k\frac{F_{load}(u)}{MVC}du} \tag{6.4}$$

Equations (6.1) - (6.4) show the development of human fatigue index and the fatigue model in the muscle-level. Ma et al. (2010) extended the work by replacing the parameters used in equation (6.1 - 6.4) to the joint-level parameters. The fatigue index and fatigue model in joint-level for a constant external load ($\tau_{load}(u)$) or a constant posture are shown in equations (6.5) and (6.6).

$$\begin{aligned} U &= \frac{1}{2k}e^{2k\tau(t)} - \frac{1}{2k}e^{2k\tau(0)} \\ \tau(t) &= \int_0^t \frac{\tau_{load(u)}}{\tau_{mvc}}du \end{aligned} \tag{6.5}$$

$$\tau_{cem}(t) = \tau_{mvc}e^{-\frac{k}{\tau_{mvc}}}\int_0^t \tau_{load}(u)du \tag{6.6}$$

Table 6.2 shows the definition of each parameter featured in equations (6.5) and (6.6). Ma et al. (2012) have extended the constant (static) fatigue model to a dynamic joint-level fatigue model. The dynamic joint-level fatigue model, could be determined from the joint condition based on varies quantities depending on the angle, velocity and acceleration;

$$\tau_{cem}(t) = \tau_{mvc}e^{-\frac{k}{\tau_{mvc}}}\int_0^t \tau(u,\theta,\dot{\theta},\ddot{\theta})du \tag{6.7}$$

Table 6.2: Replacement parameters in joint fatigue model

Muscle-fatigue model	Joint-fatigue model	Unit	Definition
MVC	τ_{mvc}	Newton-meter (Nm)	Maximum voluntary contraction of joint torque
F_{cem}	τ_{cem}	Newton-meter (Nm)	Current capacity of the muscle
F_{load}	τ_{load}	Newton-meter (Nm)	Torque from external load
k		min^{-1}	Fatigue rate (constant value = 1)
U		min	Fatigue index

The maximum voluntary contraction of human joint (τ_{mvc}) is one key element in the dynamic joint-level fatigue model (equation (6.7)). This term is a contant value and it varies amongst from person to person during a certain period of time. Due to limitation in gathering a comprehensive dynamic value for t_{mvc}, Sakka et al. (2015); Ma et al. (2012,

2010) chose a static predictive function (Table 6.3), proposed by Chaffin et. al (1999) and implemented this function in equation (6.6) and (6.7). However, to ensure that the joint-level fatigue model is 100 % dynamic, equation (6.7) needs to be full dynamic as well, including τ_{mvc}. But, due to the limitation mentioned earlier, and due to the implementation of Chaffin's function, equation (6.7) becomes a quasi-static fatigue model (Sakka et al., 2015). Therefore, the quasi-static joint-level fatigue model presented in equation (6.7) is deployed in this work to measure the current capacity of human joint and activate the exoskeleton when it is needed.

Table 6.3: Maximum joint capacity (τ_{mvc}) for static movement proposed by Chaffin et. al (1999)

Joint/Movement	Maximum Joint Capacity (τ_{mvc})	G	
		Male	Female
Elbow Flexion	(336.29 + 1.544θ_{elbow} - 0.0085θ^2_{elbow} - 0.5$\theta_{shoulder}$)G	0.1913	0.1005
Elbow Extension	(264.153 + 0.575θ_{elbow} - 0.425$\theta_{shoulder}$)G	0.2126	0.1153
Shoulder Flexion	(227.338 + 0.525θ_{elbow} - 0.296$\theta_{shoulder}$)G	0.2854	0.1495
Shoulder Extension	(204.562 + 0.099$\theta_{shoulder}$)G	0.4957	0.2485

6.2.1 Implementation of Joint-Level Fatigue Model

The implementation of quasi-static joint-level fatigue model (equation (6.7)) to the human upper-extremity is presented in this section. The human upper-extremity is modelled as six DOF system (Figure 6.1 (a)). The shoulder joint has three DOF, while elbow joint has two DOF and wrist joint has one DOF. These are described in Table 6.4. The homogenous joints transformation matrix was presented in Chapter 3.

Table 6.4: The joints and the description

Joint/Movement	Descriptions
θ_1	Flexion and extension of shoulder joint
θ_2	Abduction and adduction of shoulder joint
θ_3	Internal and external of shoulder joint
θ_4	Flexion and Extension of elbow joint
θ_5	Internal and external of shoulder joint
θ_6	Flexion and Extension of wrist joint

The Denavit-Hartenberg (DH) notations (Figure 6.1 (b)) is used to present the geomet-

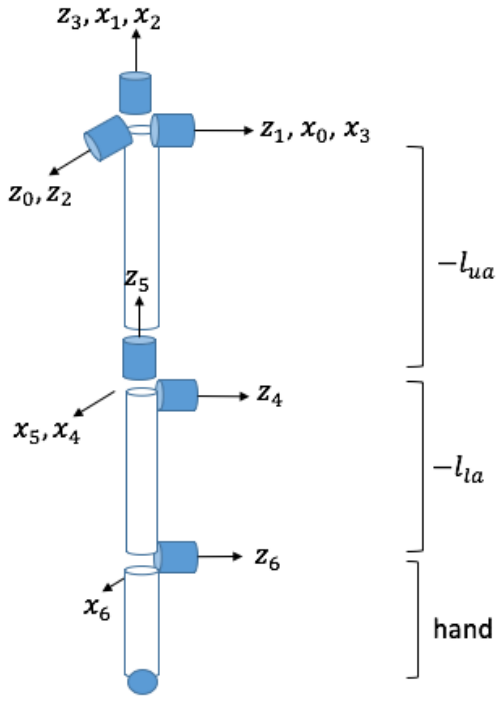

(a)

Joint	θ	d	a	α
1	θ_1	0	0	$\frac{\pi}{2}$
2	θ_2	0	0	$-\frac{\pi}{2}$
3	θ_3	0	0	$-\frac{\pi}{2}$
4	θ_4	$-l_{ua}$	0	$-\frac{\pi}{2}$
5	θ_5	0	0	$\frac{\pi}{2}$
6	θ_6	$-l_{la}$	0	$-\frac{\pi}{2}$

(b)

Figure 6.1: (a)Schematic diagram of human upper-limb (b) Denavit-Hartenberg (DH) table.

rical model of the human upper-extremity (Figure 6.1 (a)). The four parameters in Figure 6.1 (b) are shown in Chapter 3. The information obtained from the homogenous transformation matrix is used to derive the dynamic equation of the human upper-extremity. In this case, the inverse dynamic equation

$$\tau = \frac{d}{dt}\left(\frac{\partial L}{\partial \dot{\theta}}\right) - \left(\frac{\partial L}{\partial \theta}\right) \tag{6.8}$$

is used to represent the dynamic system of the human-upper extremity. The dynmic system of the human upper-extremity would represent the human joint load torque (τ_{task}) or the torque ($\tau(\theta, \dot{\theta}, \ddot{\theta})$). It is essential to measure the joint load torque because this measurement is required in equation (6.7).

The k parameter in equation (6.7) varies according to individual, DOF for each joint and general groups of muscles. According to Chang et al. (2017), this parameter varies from 0.87 min^{-1} to 2.15 min^{-1}. However, in a general condition the value of k is assigned

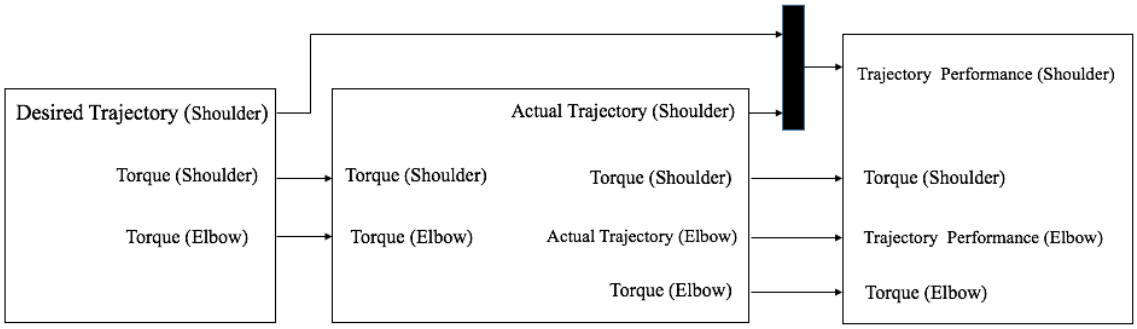

Figure 6.2: Integration of joint-level model to a human.

as 1 min^{-1} (Zhang et al., 2014). Hence, $k = 1$ is used in equation (6.7) in the implementation of the quasi-static joint-level fatigue model to human upper-extremity. Another important issue in the development of the fatigue model is to determine the fatigue occurence. Equation (6.7) only shows the reduction of the human joint strength. Ma et al. (2013b) proposed a term called fatigue risk. Fatigue risk is a time when fatigue is occurs. Fatigue risk occurs when the τ_{cem} is equal to the human joint load torque

$$\tau_{fatigue_risk} = \tau_{cem} = \tau_{task} \tag{6.9}$$

The Simulink platform is used to implement the quasi-static joint-level fatigue model (Figure 6.2). The calculation for each term in equation (6.7) is grouped in fatigue model block. The output of the fatigue model block is the torque for shoulder and elbow joint. The human block consists of the human model designed in Solidwork. The performance block consists of the results of the observation.

To observe the implementation of the quasi-static joint-level fatigue model, only the movement of the shoulder joint is evaluated. The initial position of the shoulder joint is shown in Figure 6.3. The shoulder joint moves upward (flexion) in the sagittal plane. The polynomial function (Ma et al. (2012)) is used to represent the movement of the shoulder joint. The elbow and wrist joints are fixed.

A boundary condition is determined to ensure that the movement only occurs in this

Figure 6.3: Initial position of human upper-extremity.

region (equation (6.10))

$$\begin{aligned} \theta(0) &= \theta^{initial} \qquad \dot{\theta}(0) = 0 \qquad \ddot{\theta}(0) = 0 \\ \theta(t_f) &= \theta^{end} \qquad \dot{\theta}(t_f) = 0 \qquad \ddot{\theta}(t_f) = 0 \end{aligned} \tag{6.10}$$

The trajectory generation used in this chapter is similar to that reported by Ma et al. (2012) to which differentiation is applied to obtain the velocity and the acceleration of the generated trajectory

$$\begin{aligned} &\theta(t) = \theta^{initial} + r(t) \times (\theta^{end} - \theta^{initial}) \qquad 0 <= t <= t_f = 10 \\ &r(t) = 10 \times (t/t_f)^3 - 15 \times (t/t_f)^4 + 6 \times (t/t_f)^5 \end{aligned} \tag{6.11}$$

$$\begin{aligned} \dot{\theta}(t) &= (\frac{30}{10^3}t^2 - \frac{60}{10^4}t^3 + \frac{30}{10^5}t^4) \times (\theta^{end} - \theta^{initial}) \\ \ddot{\theta}(t) &= (\frac{60}{10^3}t - \frac{180}{10^4}t^2 + \frac{120}{10^5}t^3) \times (\theta^{end} - \theta^{initial}) \end{aligned} \tag{6.12}$$

The result and discussion for the implementation of quasi-static joint-level fatigue model will be presented in Section 6.4.1.

6.3 Integration of Human with Fatigue Model with Upper-Extremity Exoskeleton

In this section, the human with quasi-static joint-level fatigue model (equation (6.7)) is integrated with an exoskeleton. The exoskeleton is adopted with the extended-based fuzzy controller. The performance of the exoskeleton with the controller observed by implementing several conditions.

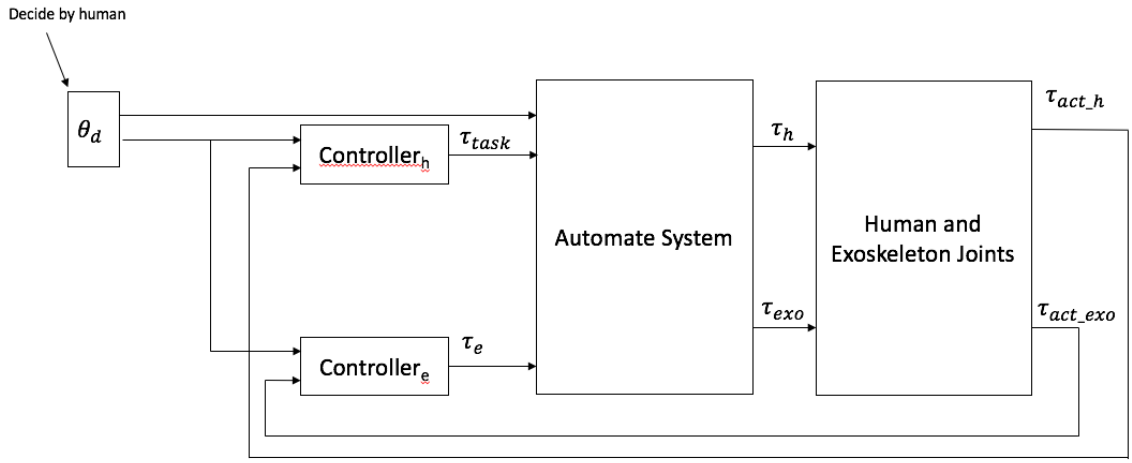

Figure 6.4: Control scheme with human and fatigue model, and the exoskeleton.

The fatigue risk information (equation (6.9)) is important because this information is used to activate the exoskeleton. Figure 6.4 shows the integration of the human with fatigue model and the exoskeleton. In this model, the human joint is controlled by a controller. The controller input for the human, is the desired position (which is, actually known to human), and the controller output is the human joint load torque (τ_{task}). Each joint of the exoskeleton is also controlled by a controller. Similar to human joint, the input to the controller is the desired position, and the output of the controller is the exoskeleton joint torque (τ_e). Both torques (tau_{task} and τ_e) are sent to the 'Automate System' block. Three processes occur in 'Automate System' block. These are, the evaluation of the fatigue occurence, the recovery model and the evaluation of the assistive torque of the exoskeleton. The algorithm showing these three important processes is shown in Figure 6.5.

The algorithm starts by identifying the range of duration to complete the activity. The maximum joint voluntary contraction (τ_{mvc}) is measured (using Table 6.3). Then, the cur-

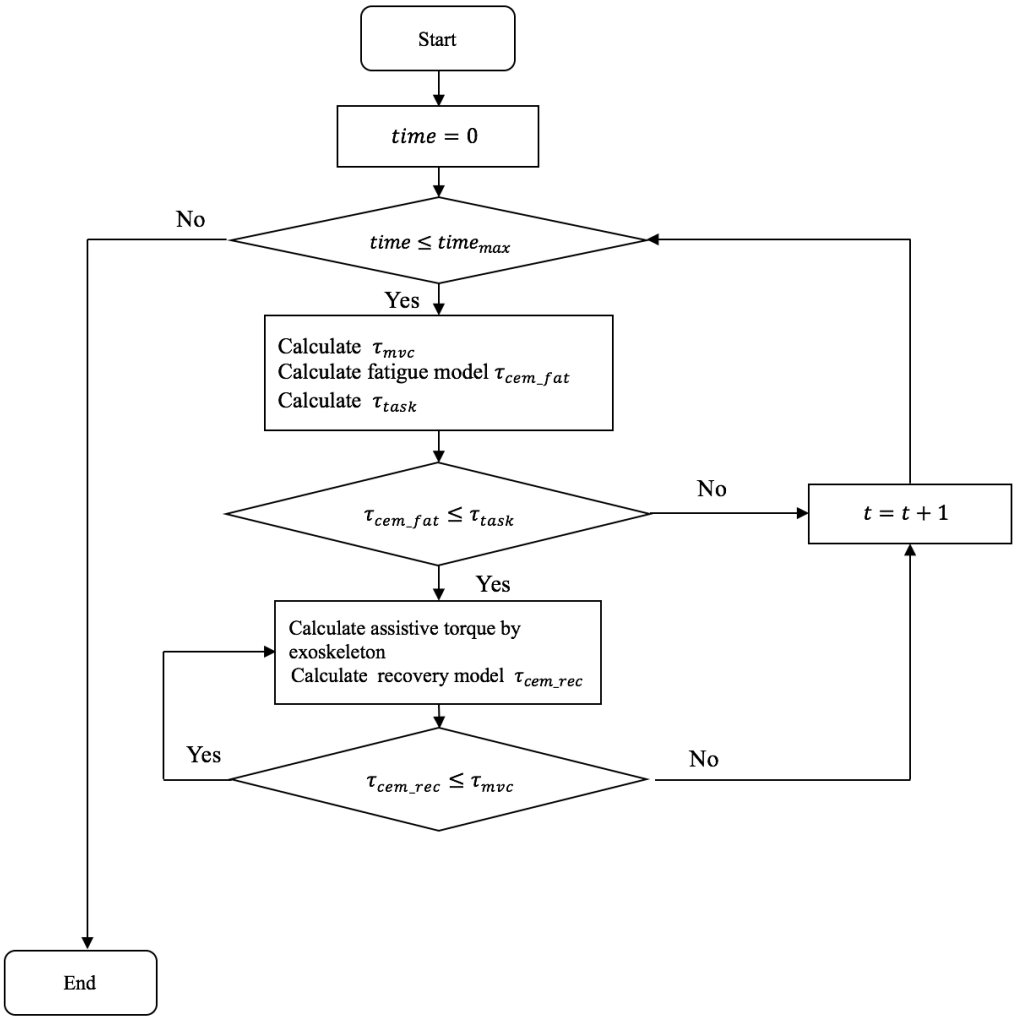

Figure 6.5: The integration of an exoskeleton and fatigue and recovery model.

rent capacity of human joint strength (τ_{cem}) is measured to observe the reduction of the human joint strength, while human is performing the activity. The torque required by joint to perform the activity (τ_{task}) is recorded. Next, the τ_{cem} and τ_{task} are compared. By following equation (6.9), a condition is performed. In this work, the human joint is considered as a fatigue risk, when the $\tau_{cem} <= \tau_{task}$. If this condition is satisfied, an assistive torque from the exoskeleton is required to augment human in continuing the activity. The percentage of the fatigue risk (assis(%)) from τ_{mvc}, and the assistive torque sent by the exoskeleton to assist human performing the activity (τ_{exo}) are given as

$$\begin{aligned} assis(\%) &= (t_{mvc} - t_{cem})/t_{mvc} \\ \tau_{exo} &= assis(\%) * (\tau_e) \end{aligned} \tag{6.13}$$

While exoskeleton assists human, the strength of human joint is measured. During this period, human joint strength is recovered (τ_{cemrec}). The human joint condition during the recovery process is examined to ensure that the strength is achieved to the maximum voluntary contraction torque. The condition $\tau_{cemrec} <= \tau_{mvc}$ is applied. If human joint strength is achieve to maximum voluntary contraction, the activity will be performed by human, and no assistive torque is required. The algortihm is repeated until the activity is completed.

The joint-level recovery model used in this work, is adopted from Ma et al. (2015, 2010). During the recovery process, there is no active motor unit and no information received by motorneurons from CNS. Hence, the joint-level recovery model developed by Ma et al. (2015, 2010) explain the development of this model according to the motor unit activation pattern muscle. The differential equation of the joint-level recovery model is given as:

$$\frac{\tau_{cem}}{dt} = R(\tau_{mvc} - \tau_{cem}) \tag{6.14}$$

The term $\tau_{mvc} - \tau_{cem}$ represents the reduction of the maximum voluntary contraction (τ_{mvc}) to the fatigue risk point. The parameter R, which presents recovery rate, in equation (6.14) is assumed to be a constant ($R = 2.4\ min^{-1}$) (Ma et al., 2015, 2010). The integration of equation (6.14) is given as:

$$\begin{aligned} \tau_{cem} &= \tau_{mvc} + (\tau_{cemini} - \tau_{mvc})e^{-Rt} \\ &= \tau_{cemini} + (\tau_{mvc} - \tau cemini)(1 - e^{-Rt}) \end{aligned} \tag{6.15}$$

Thus, the above equation shows the joint current joint capacity during the recovery process

The Simulink platform is used to implement the human joint with fatigue model and the exoskeleton (Figure 6.6). The control scheme shown in Figure 6.4 is adopted in the 'Controller' block. The 'Human-Exoskeleton Model' blok contains the human and exoskeleton designed in Solidworks. The exoskeleton is controlled by extended-based fuzzy control system. The extended controller is chosen based on the performances shown in

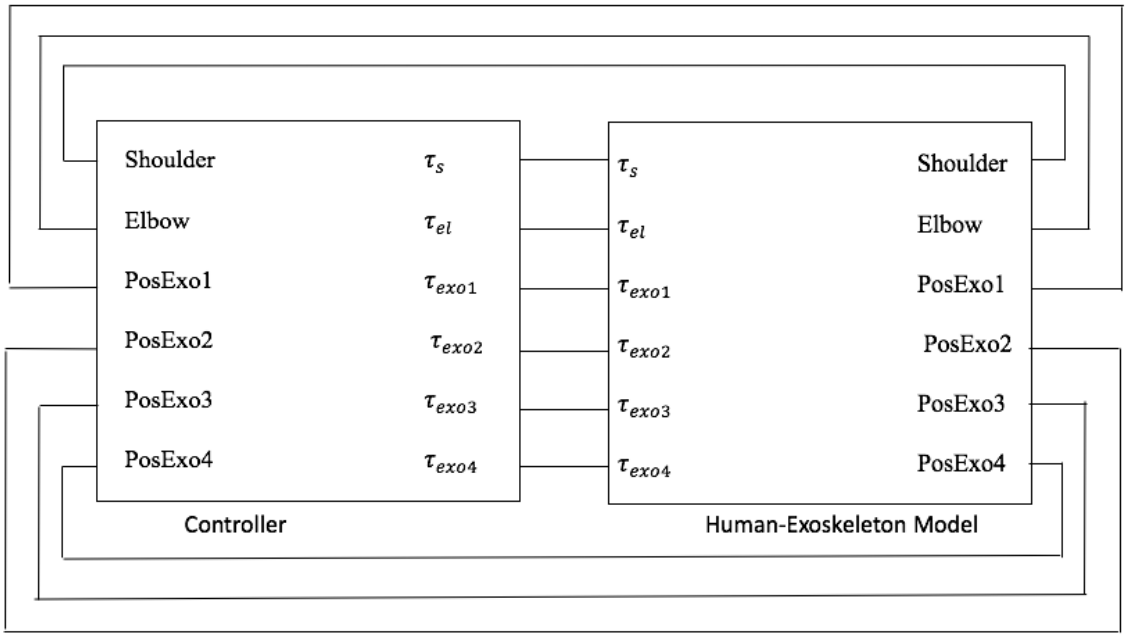

Figure 6.6: Block diagram of human joint with fatigue model and the exoskeleton.

Chapter 4 and Chapter 5.

To observe the performance of the exoskeleton with extended-based fuzzy controller in augmenting and assisting human when fatigue occurs, two conditions are considered. The situations are: the fatigue that occurs to a single joint, and the fatigue that occurs to multi-joint. For both cases, the flexion movement is chosen because this movement is involved in most human daily-life activities (Sakka et al., 2015).The shoulder joint is moved 15° in flexion movement, and the duration of the movement is extended to 200 s. The flexion movement is chosen because this is a major movement in human daily-life activity as well as in industrial tasks (Sakka et al., 2015).

The result and discussion for the implementation of the integration between exoskeleton and human with fatigue model are presented in Section 6.4.2 for single joint and 6.4.3 for multi joint. The next section will present the performance of the whole system.

6.4 Results and Discussions

In this section, the results and performance of Section 6.2.1 and Section 6.3 are presented. This section begins with the result of the implementation of quasi-static joint-level fatigue

model followed with the implementation of the integration between exoskeleton and human with fatigue model.

6.4.1 Implementation of Fatigue Model

Figure 6.7 shows the desired trajectory, velocity and the acceleration which presenting equation (6.11) and equation (6.12).

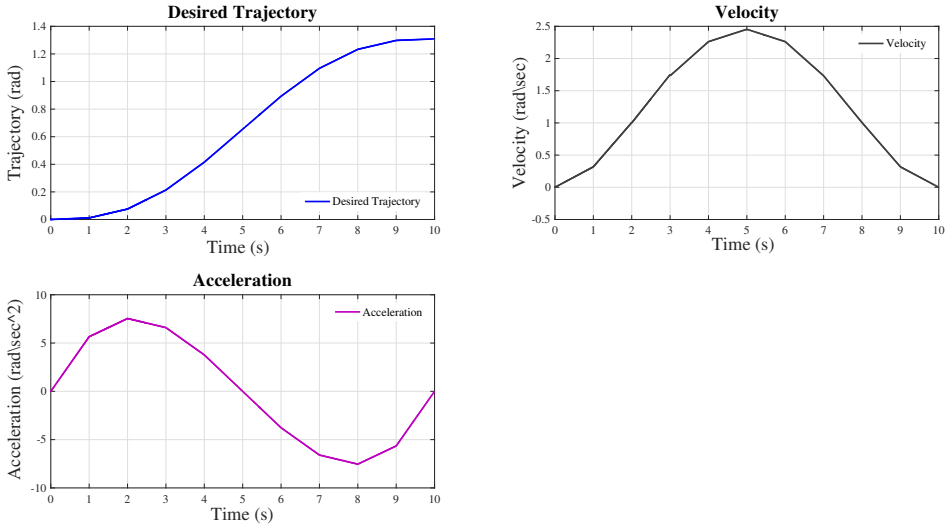

Figure 6.7: Desired displacement, velocity and acceleration of a shoulder joint.

Figure 6.8 shows the two important measurements that are used to identify the fatigue risk condition. The measurements are the human joint load torque (τ_{task}) (Figure 6.8 (a)) and, the current joint strength (τ_{cem})(Figure 6.8 (b)). The maximum shoulder joint voluntary contraction (τ_{mvc}) of the shoulder joint flexion is observed to be approximately 60 Nm to 65 Nm. Due to a flexion movement, which means that, the trajectory of shoulder joint is increasing, this value (τ_{mvc}) is increasing (Figure 6.8(c)). This happens because Chaffin's predictive static formula relies only on the joint motion. Hence, Figure 6.8(b) shows the maximum capacity of shoulder joint for the flexion movement (Sakka et al., 2015). The blue graph of Figure 6.8(b) shows the evolution of the quasi-static joint-level fatigue model (equation (6.7)). During this period, the number of Type-II muscle fibres reduce due to rapid contraction of the muscle fibres. However, with time, the reduction of human strength is slow. This occurs due to the characteristic of Type-I muscle fibres.

In this period, the number of Type-I muscle fibres remain due to their high resistance to fatigue.

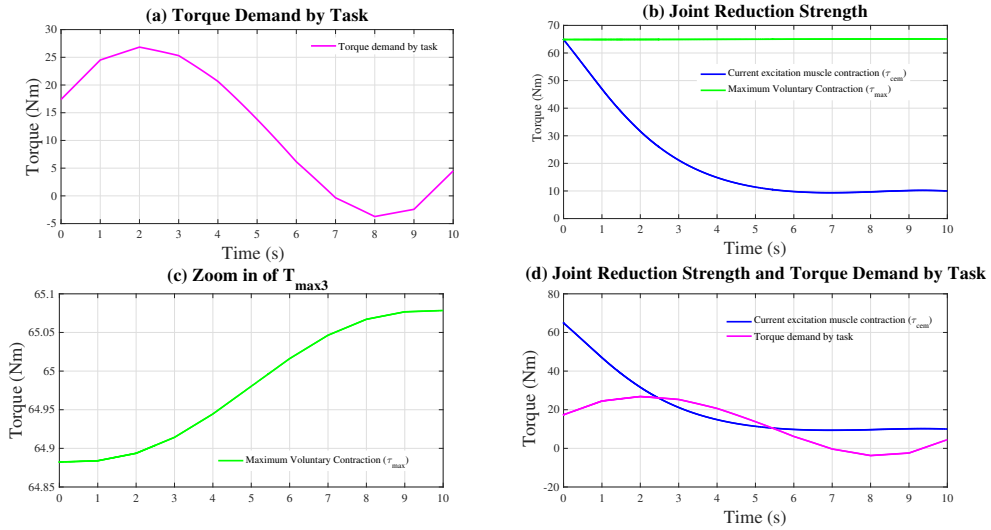

Figure 6.8: Identification of fatigue risk: (a) Torque demand by task (τ_{task}) (b) Human reduction strength (τ_{cem}) (c) Zoom in of τ_{max} (d) Fatigue risk.

Figure 6.8 (b) only shows the reduction of human strength. However, it does not show any possibility of fatigue occurence. Hence, as mentioned earlier, Ma et al. (2013b) identified the fatigue risk occurence by identifying the point where the joint strength reduction is equal to or less than the torque demand by task (Figure 6.8(d)). In this work, this point is known as trigger point. The trigger point or fatigue risk point will be used to inform the exoskeleton that human is at a weak situation. Then, the exoskeleton is to assist or augment human to ensure the task could be completed. Therefore, it is shown that, it is possible to implement the quasi-static joint-level fatigue model to identify the fatigue risk point of human strength. Then, the fatigue risk point is used to trigger the exoskeleton to send the assistive torque.

In the next section, the performances of the exoskeleton in augmenting the human with limited strength of upper-extremity are presented.

6.4.2 Single-Joint Movement

Figure 6.9 shows the desired trajectory for the joints. Table 6.5 presents the parameters used in this experiment. The control parameters were obtained by using a heuristic ap-

proach.

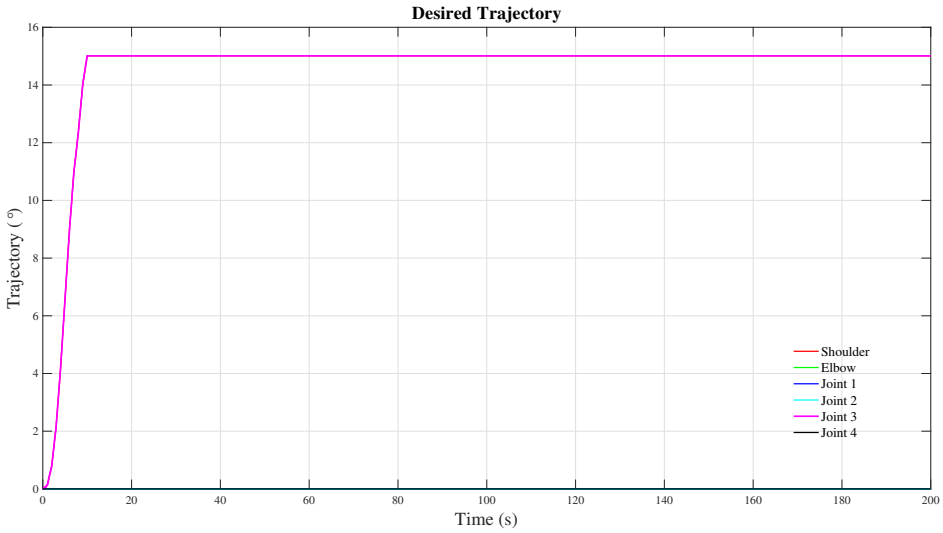

Figure 6.9: Desired trajectory for the shoulder joint.

Table 6.5: Controller gains for single joint movement: Hybrid-based fuzzy controller

Gains	Shoulder Joint	Elbow Joint	Exoskeleton Joint 1	Exoskeleton Joint 2	Exoskeleton Joint 3	Exoskeleton Joint 4
K_e	1	1	0.1	1	0.1	0.1
$K_{\dot{e}}$	0.001	0.001	0.001	0.001	0.001	0.001
K_{gain1}	50	50	50	50	50	10
K_e	-	-	1	1	1	1
K_α	-	-	0.001	0.001	0.001	0.001
K_{gain2}	-	-	50	50	50	50

The maximum joint voluntary contraction (τ_{mvc}) at the beginning of the movement was about 64.883 Nm. As the shoulder joint moved to flex to 15°, the τ_{mvc} reached about 64.923 Nm, then it remained at this maximum strength (Figure 6.10(c)). This is expected so because the Chaffin's predictive maximum voluntary contraction formula depends only on the joint motion. Meanwhile, the torque required by shoulder joint to flex (τ_{task}) was about 4.6352 Nm. In this part of the experiment, this value was obtained from the fuzzy-based PD controller. As presented in Section 6.4.1, the τ_{cem} (equation (6.7)), reduced from the maximum voluntary contraction to 0. However, as mentioned in Section 6.3, a condition known as trigger point or fatigue risk point (equation (6.9) was used to trigger

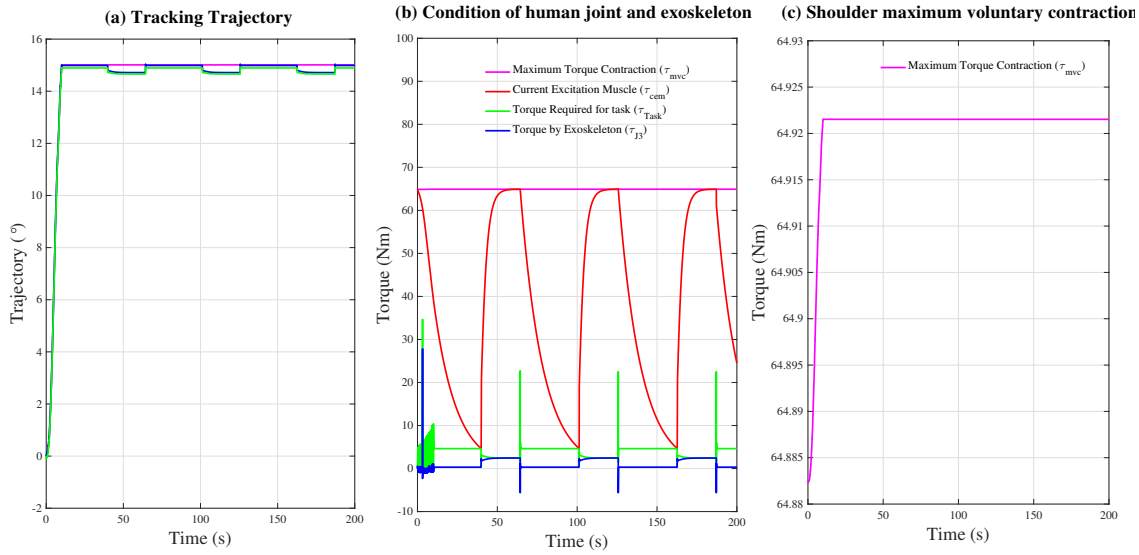

Figure 6.10: Results of extended-based controller of an exoskeleton for a single-joint movement: (a) Trajectory tracking (b) Conditions of human and exoskeleton joint (c) Maximum Voluntary Contraction of shoulder joint (τ_{mvc}).

the exoskeleton to take action. As shown in Figure 6.10 (b), the trigger point or fatigue risk occurred near 40 s. As the τ_{cem} was achieved at this point, human was considered as fatigued, and a deviation from the desired trajectory occurred (Figure 6.10(a)). Due to small deviation at shoulder joint from 40 s to 64.35 s, the τ_{task} reduced. Meanwhile, the torque of the exoskeleton increased (Figure 6.10(b)). This shows that, during this period, the exoskeleton assisted the shoulder joint to ensure it could stay at the desired position. During this period as well, the shoulder joint strength (τ_{cem}) is recovered to the maximum voluntary contraction (Figure 6.10(b)). When the shoulder joint achieved the maximum strength (τ_{mvc}), then switching occurred. At this point, the shoulder joint continued the task, and the exoskeleton was relaxed. This process continues until the task is ended.

Fatigue rate (k), is one factor that could influence the occurence of fatigue. Other factors include height,weight and relative load (Ma et al., 2013a, 2010). As mentioned earlier, the fatigue rate is varies from 0.87 min^{-1} to 2.15 min^{-1} for general groups of muscles and varies across individuals and joints (Ma et al., 2015; Chang et al., 2017), and in this work, fatigue rate is determined as equal to 1 min^{-1}. For the case of $k = 0.17 min^{-1}$, the occurence of fatigue is shown in Figure 6.11. As the fatigue rate decreases, the time for the fatigue occurence increases almost five times than in Figure 6.10 (b). There are

several factors that could influence the fatigue rate. The factors are muscle strength, muscle composition and neuromuscular activation pattern (Ma et al., 2013a). In addition, Ma et al. (2013a) presents a methodology to determine the fatigue rate. However, the method proposed in their work is validated only at the shoulder joint.

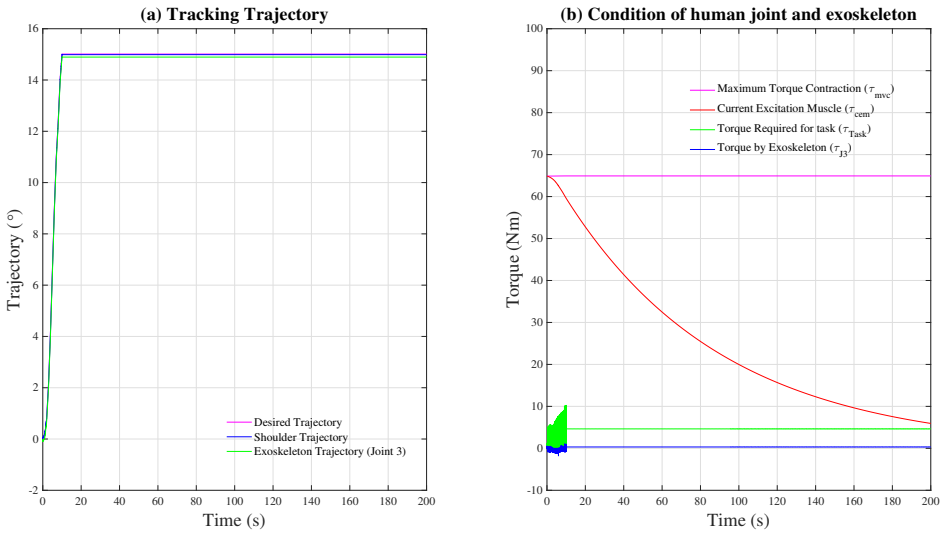

Figure 6.11: Results of extended-based controller of an exoskeleton for a single-joint movement ($k = 0.17 min^{-1}$): (a) Trajectory tracking (b) Conditions of human and exoskeleton joint.

The observation in this section, shows that, the exoskeleton is able to assist human to prolong task peformance, and during the assistance procedure, human joint is recovered. With this result, it shows that, there is a potential for an exoskeleton to enhance human performance while avoiding fatigue, hence, reduce the tendency for MSD.

6.4.3 Multi-Joint Movement

In this section, the shoulder and elbow joints move in parallel. Both joints are move in flexion movement from 0° to 15°. The duration of the movement is 10 s. Then, from 10 s to 1020 s, both joints remain static at 15° (Figure 6.12). Table 6.6 presents the parameters used in this experiment. The control parameters were obtained by using a heuristic approach.

Generally, both joints were able to track the desired trajectory (Figures 6.13 (a) and 6.14 (a)). The τ_{mvc} of shoulder and elbow joints are shown in Figures 6.13 and 6.14.

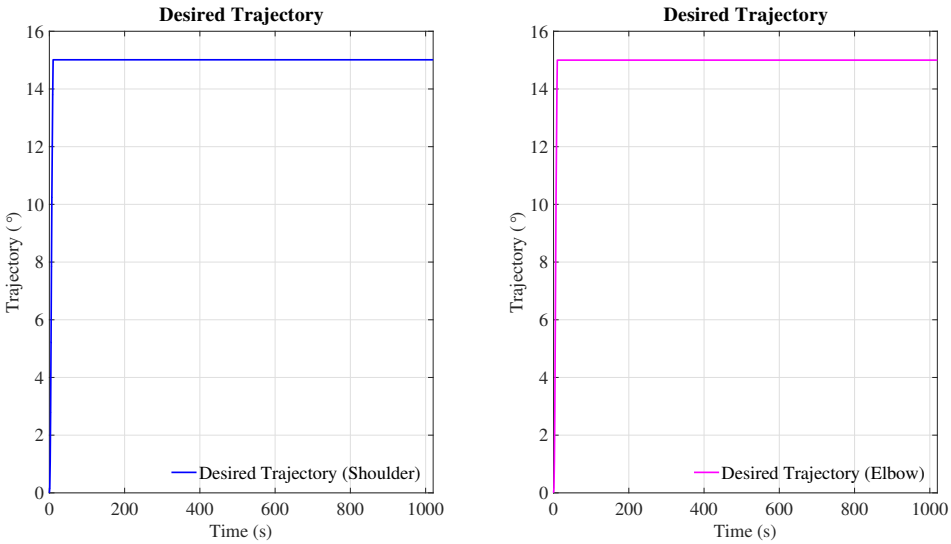

Figure 6.12: Desired trajectory: (a) Shoulder joint (b) Elbow joint.

Table 6.6: Controller gains for multi-joint movements: Hybrid-based fuzzy controller

Gains	Shoulder Joint	Elbow Joint	Exoskeleton Joint 1	Exoskeleton Joint 2	Exoskeleton Joint 3	Exoskeleton Joint 4
K_e	2	1.3	0.1	1	1.5	0.5
$K_{\dot{e}}$	0.005	0.005	0.001	0.001	0.001	0.001
K_{gain1}	10	10	50	50	10	10
K_e	-	-	1	1	0.1	1
K_α	-	-	0.001	0.001	0.001	0.001
K_{gain2}	-	-	50	50	10	10

Similar to that in Section 6.4.2, the maximum voluntary contraction (τ_{mvc}) of both joints depends on the joint motion and gender. Due to this reason, the τ_{mvc} increased from 64.883 Nm to 64.9 Nm (Figure 6.13 (c)) for shoulder joint and 64.331 Nm to 64.382 Nm (Figure 6.14 (c)) for elbow joint. The τ_{mvc} for shoulder and elbow joints show that they remained at joint endurance of 64.9 Nm and 64.382 Nm from 10 s to 1020 s, because both joints were static at 15° during this period.

Meanwhile, the torque required by shoulder and elbow joints to do the movements were about 3.4 Nm and 1.5 Nm. Both values were obtained from fuzzy-based PD controller. The τ_{cem} of equation (6.7) reduced, from the maximum voluntary contraction (τ_{mvc}) to 0 Nm. However, by applying equation (6.9), a fatigue risk for shoulder and elbow joints, as

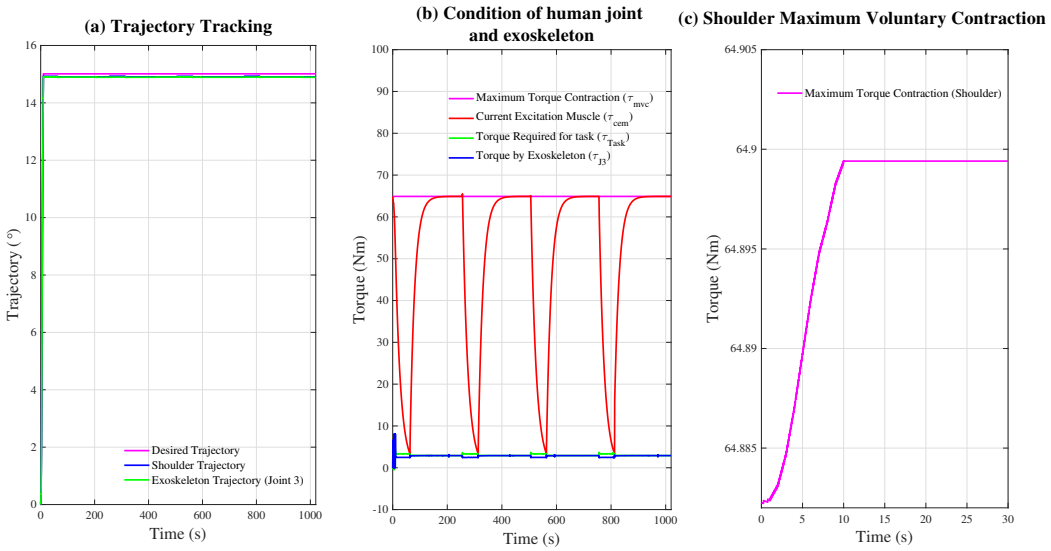

Figure 6.13: Result of extended-based controller of an exoskeleton for a multi-joint movement: (a) Trajectory tracking (b) Conditions of human and exoskeleton joint (c) Maximum voluntary contraction of shoulder joint.

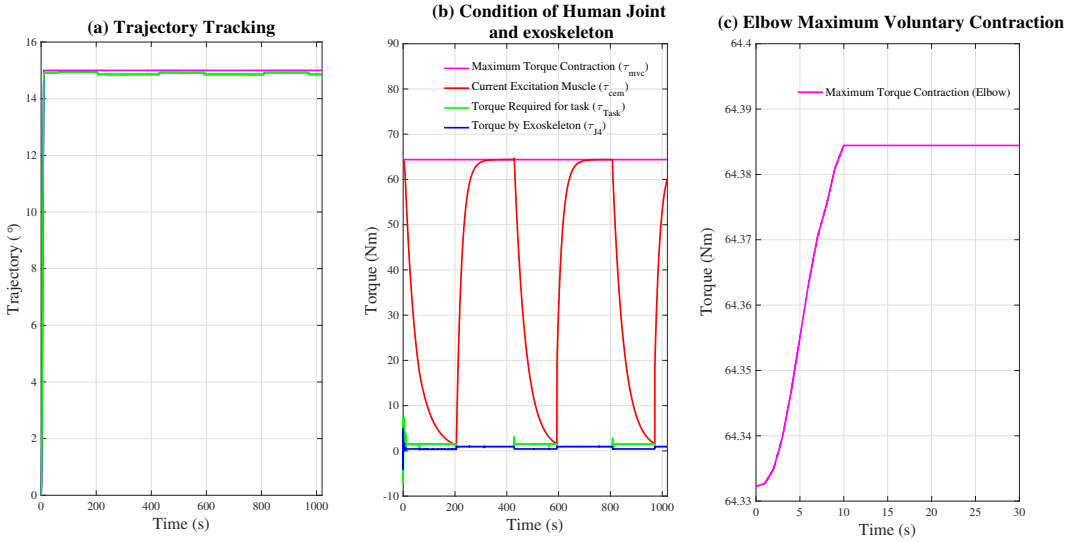

Figure 6.14: Result of extended-based controller of an exoskeleton for a multi-joint movement: (a) Trajectory tracking (b) Conditions of human and exoskeleton joint (c) Maximum voluntary contraction of elbow joint.

explained in Section 6.2.1 was identified. The fatigue risk of shoulder joint occurred in less than 100 s, and in about 200 s for elbow joint. This shows that the fatigue occurence for shoulder joint was faster than elbow joint. One of the factors in calculating the τ_{cem} of equation (6.7), is the torque required for the joints to perform the task. It is known that the shoulder joint is located proximal to elbow and wrist joint. The dynamics of the shoulder joint are more complicated as they require consideration of length and weight

of upper-arm, forearm and hand. Thus, as mentioned earlier that the torque required by shoulder joint (3.4 Nm) was higher than elbow joint (1.5 Nm). In this condition, the number of Type-II muscle fibres of shoulder joint reduce due to rapid contraction of the muscle fibres. Hence, this causes the shoulder joint to fatigue earlier than elbow joint. Another factor that could influence the shoulder joint to fatigue earlier, is the parameter of fatigue rate (k) of equation (6.7). As mentioned earlier, $k = 1\ min^{-1}$ is chosen to be used in this work, which is similar to Ma et al. (2013b). The result reported by Ma et al. (2013b), shows that the occurence of fatigue for shoulder joint is earlier than elbow joint, which is similar as Figure 6.13(b1) and Figure 6.14 (b1). However, Sakka et al. (2015) chose $k = 0.17\ min^{-1}$ for shoulder joint, and $k = 0.24\ min^{-1}$ for elbow joint. The result of fatigue occurence reported by Sakka et al. (2015) shows that the elbow joint fatigue earlier than shoulder joint. This is so because, the fatigue rate chosen for the shoulder joint by Sakka et al. (2015) is lower than the elbow.

Figures 6.13 (b) and 6.14 (b) show the repetitive τ_{cem} during the reduction and the recovery process. These figures show that shoulder joint was potentially for cumulative local joint fatigue, because the frequency of the current joint strength (τ_{cem}) to be at the fatigue risk was more compared to elbow joint. However, these observations could be enhanced by optimizing the extended-based fuzzy controller. Hence, Modified Invasive Weed Optimization (MIWO) algorithm was implemented (Al Rezage et al., 2016). The parameters obtained from the implementation of MIWO are shown in Table 6.7. Although, the time to fatigue risk occurence was delayed about 5 s and 200 s (Figure 6.15 (b) and 6.16 (b)) for shoulder and elbow joint, this probably could help in reducing tendency of the cumulative local joint fatigue, and reducing the chances of MSD. These observations show that, by improving the parameters, there is a chance for the exoskeleton to perform better in reducing the chances of cumulative local joint fatigue.

The third observation is that, there are three important points in Figure 6.13 (b) and 6.14 (b). The points are, the torque of the maximum voluntary contraction of shoulder and elbow joints (τ_{mvc}), the point of the fatigue occurence and the point of recovering from fatigue. The τ_{mvc} is obtained from Table (6.3). The strength of the shoulder and elbow

Table 6.7: Controller gains for multi-joint movements (MIWO): Hybrid-based fuzzy controller

Gains	Shoulder Joint	Elbow Joint	Exoskeleton Joint 1	Exoskeleton Joint 2	Exoskeleton Joint 3	Exoskeleton Joint 4
K_e	1.3534	0.4789	0.0057	0.3117	1.0175	0.4019
$K_{\dot{e}}$	0.00	0.004	0.00	0.0008	0.000	0.0008
K_{gain1}	7.9943	8.7913	4.0259	43.6952	8.7432	9.83
K_e	-	-	0.7061	0.6446	0.0788	0.0195
K_α	-	-	0.0008	0.0008	0.00	0.000
K_{gain2}	-	-	7.4339	13.4827	5.7470	9.1405

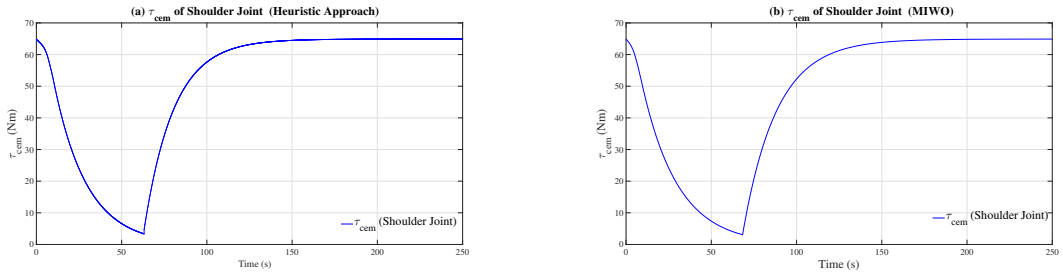

Figure 6.15: Result of extended-based controller of an exoskeleton for a multi-joint movement (shoulder joint): (a) τ_{cem} for heuristic approach (b) τ_{cem} for IWO algorithm.

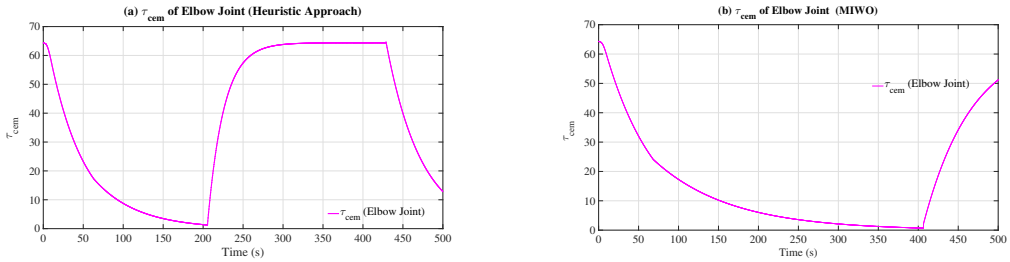

Figure 6.16: Result of extended-based controller of an exoskeleton for a multi-joint movement (elbow joint): (a) τ_{cem} for heuristic approach (b) τ_{cem} for IWO algorithm.

joint at the beginning of the movement was about 64.8822° and 64.33°. This point is noted as the first important point because it predicts the maximum strength of each joint at the beginning of the movement. As shown in Figures 6.13 (c) and 6.14 (c), this initial value increases and then, it is sustained at fixed value, as explained above.

The second important point is known as the fatigue point. As shown in Section 6.2.1, the fatigue point is determined when the current joint strength (τ_{cem}) is less than or equal to the strength required to do the task ($\tau_{cem} = \tau_{reqfortask}$). This point is essential to determine because it is used to predict the occurence of fatigue. Hence, this point is used to activate

the exoskeleton to send the assistive torque. During the period from the maximum strength to the fatigue point, the shoulder and elbow joints were able to perform the movement or stay at the required position whilst the exoskeleton torque is at the lowest value (Figures 6.13 (b) and 6.14 (b)).

The third important point is known as the recovery point. This point shows that the joint is at a fully strength. The increasing graph from the fatigue point to the recovery point shows that the joint is in a process of gaining the strength (Figures 6.15 and 6.16). During this period, the exoskeleton torque increased as shown in Figures 6.13 (b) and 6.14 (b). Hence, when the joint achieved this point, the exoskeleton was deactivated.

From the observations, it is noted that, there is a possibility to implement the joint-level fatigue model to predict the fatigue occurence. In addition, the exoskeleton is able to assist human upper-extremity joints when fatigue occurs.

6.5 Summary

This chapter has presented the the extended work of previous chapter. A quasi-static joint-level fatigue model has been implemented and exoskeleton with the extended-based fuzzy controller has been integrated parallel to the human. The results for single- and multi-joints movements show that the exoskeleton is capable in augmenting and thus, assisting human in continously performing physical tasks. The technique chosen to identify the condition of upper-extremity joint is capable to send out the information to the exoskeleton. With this information, the exoskeleton is activated. In addition to assist human for prolonged activity, the integration of fatigue with the exoskeleton could also decrease the potential of local cumulative fatigue occurence. Hence, this could avoid human from MSD.

Chapter 7

Conclusions and Future Works

7.1 Summary and Conclusion

To gain some knowledge of what has been done and investigated in the developement of an upper-extremity, a detailed literature review has been conducted. However, not all developed or existing exoskeleton system have considered the occurence of muscle fatigue. In addition, most of the existing exoskeleton system are considered for rehabilitation and industrial applications. In this work, an exoskeleton for an upper-extremity has been designed in SolidWorks to represent the real system. The system has been tested with approximated human weight and integrated with Matlab/Simulink for control design and performance evaluation purposes.

In the early development of the control approach, the PID and fuzzy-based PD control have been used to evaluate the trajectory tracking performance of the exoskeleton with a condition of no human. The abrupt and non-abrupt movements of exoskeleton have been used to assess the system performance. Then, the fuzzy-based PD controller has been enhanced by including the fuzzy gravity compensator,referred to as hybrid-based fuzzy controller. Based on the torque analysis in Chapter 4, the hybrid-based fuzzy controller have achieved good performances with minimal torque. The observation in terms of deviation analysis shows that the hybrid-based fuzzy controller, performs better in terms of tracking the desired trajectory. It is almost 80 % accurate compared to PID.

The hybrid-based fuzzy controller has been assessed with inclusion of human. Three conditions of human have been considered: full strength, 70 % strength and 70 % strength

with 30 % strength from an actuated exoskeleton. The analysis shown in Chapter 5 demonstrate that, in terms of the deviation and torque analysis, the performance of the human with 70 % with an actuated exoskeleton has been better with PID and hybrid-based fuzzy controller. The results have shown the capability of the exoskeleton in assisting and augmenting human with less strength. The hybrid-based fuzzy controller has performed better than PID controller. In terms of the deviation analysis, the proposed controller is able to perform accurately than the PID controller. In terms of torque analysis, it shows that human joints required less torque in extended-fuzzy controller than the PID controller. In addition, the deviation of the PID controller is higher about 10 times than the proposed controller.

A further assesssment has constituted inclusion of the quasi-static joint-level fatigue model in the human. The exokeleton has been used to assist human. It has been demonstrated that the assistive torque is provided upon identification of fatigue risk. The assistive torque will stop from providing the torque, when human gains its strength back. The observation show that, the exoskeleton is successful, in deweighting the fatigue, therefore, human could carry prolonged tasks. Moreover, implementation of the invasive weed optimisation algorithm could prolong the occurence of fatigue, hence reduce the tendency of cumulative local joint fatigue.

This work has carried out a first phase of the project in simulations on modelling and control of an upper-limb exoskeleton for deweigting purpose. Several experiments have been done to validate the proposed control approach. The results demonstrates the effectiveness of the proposed control approach and thus suitable for the real hardware implementation.

7.2 Recommendation for Future Work

This research has developed a deweighting upper-extremity exoskeleton mechanism. Although the desired exoskeleton functions have been achieved, further improvement could be made and new capabilities could be developed in future.

(i) It is beneficial to increase the DOF of an exoskeleton. Different humanoid heights and weights may be investigated to find suitable range of human and limitations of the designed controller.

(ii) The implementation of the surface electromyography (s-EMG) could be done in future, to compare the performance of both, the quasi-static joint-level controller and the s-EMG.

(iii) To improve the system performance and hence achieve optimum results, in future, more fuzzy control parameters such as rule base and membership function may be further optimized.

(iv) It is recomended to investigate more optimization techniques so that, the control parameters obtained could enhance the extended-fuzzy controller in dealing with human fatigue.

(v) It is recomended to investigate more unforeseen circumstances such as user's comfort and the tasks.

(vi) To observe the real behaviour of the deweighting upper-extremity exoskeleton, an experimental validation of the system in a controlled condition should be performed.

References

Abane, A., Guiatni, M., Alouane, M. A., Benyahia, I., Tair, M., and Ababou, N. (2017). Auto-tuning fuzzy force/position control of a 5 dof exoskeleton for upper limb rehabilitation. In *Advanced Intelligent Mechatronics (AIM), 2017 IEEE International Conference on*, pages 1731–1736. IEEE.

Al Rezage, G., Kasdirin, H. A., Ali, S. K., and Tokhi, M. O. (2016). Invasive weed optimization algorithm optimized fuzzy logic scaling parameters in controlling a lower limb exoskeleton. In *Methods and Models in Automation and Robotics (MMAR), 2016 21st International Conference on*, pages 1116–1121. IEEE.

Altenburger, R., Scherly, D., and Stadler, K. S. (2016). Design of a passive, iso-elastic upper limb exoskeleton for gravity compensation. *Robomech Journal*, 3(1):12.

Ambrosini, E., Ferrante, S., Rossini, M., Molteni, F., Gföhler, M., Reichenfelser, W., Duschau-Wicke, A., Ferrigno, G., and Pedrocchi, A. (2014). Functional and usability assessment of a robotic exoskeleton arm to support activities of daily life. *Robotica*, 32(8):1213–1224.

Anam, K. and Al-Jumaily, A. A. (2012). Active exoskeleton control systems: State of the art. *Procedia Engineering*, 41:988–994.

Beattie, E., McGill, N., Parrotta, N., and Vladimirov, N. (2012). Titan: A powered, upper-body exoskeleton. *Retrieved November*, 22:2014.

Biesiacki, P., Mrozowski, J., and Awrejcewicz, J. (2015). Study of dynamic forces in human upper limb in forward fall.

Carignan, C., Tang, J., Roderick, S., and Naylor, M. (2007). A Configuration-Space Approach to Controlling a Rehabilitation Arm Exoskeleton. In *10th International Conference on Rehabilitation Robotics*, Noordwijk.

Carlos, C. (2012). Articulated human body.

Carmichael, M. G., Liu, D., and Waldron, K. J. (2010). Investigation of reducing fatigue and musculoskeletal disorder with passive actuators. In *Intelligent Robots and Systems (IROS), 2010 IEEE/RSJ International Conference on*, pages 2481–2486. IEEE.

Carmichael, M. G. and Liu, D. K. (2015). Human biomechanical model based optimal design of assistive shoulder exoskeleton. In *Field and Service Robotics*, pages 245–258. Springer.

Chaffin, D. B. (1984). *Occupational Biomechanics*. WIley.

Chang, J., Chablat, D., Bennis, F., and Ma, L. (2017). Muscle fatigue analysis using opensim. *arXiv preprint arXiv:1705.05570*.

Chang, M.-K. (2010). An adaptive self-organizing fuzzy sliding mode controller for a 2-dof rehabilitation robot actuated by pneumatic muscle actuators. *Control Engineering Practice*, 18(1):13–22.

Chen, C.-J., Cheng, M.-Y., and Su, K.-H. (2013). Observer-based impedance control and passive velocity control of power assisting devices for exercise and rehabilitation. In *Industrial Electronics Society, IECON 2013-39th Annual Conference of the IEEE*, pages 6502–6507. IEEE.

Coffin, C. T. (2012). The use of a vertical arm support device to reduce upper extremity muscle firing in sonographers. *Work*, 42(3):367–371.

de Gea, J. and Kirchner, F. (2008). Modelling and simulation of robot arm interaction forces using impedance control. *IFAC Proceedings Volumes*, 41(2):15589–15594.

De Looze, M. P., Bosch, T., Krause, F., Stadler, K. S., and O'Sullivan, L. W. (2015). Exoskeletons for industrial application and their potential effects on physical work load. *Ergonomics*, 0139(December):1–11.

De Luca, A. and Panzieri, S. (1994). An iterative scheme for learning gravity compensation in flexible robot arms. *Automatica*, 30(6):993–1002.

Dubey, V. N. and Agrawal, S. K. (2011). Study of an upper arm exoskeleton for gravity balancing and minimization of transmitted forces. *Proceedings of the Institution of Mechanical Engineers, Part H: Journal of Engineering in Medicine*, 225(11):1025–1035.

Enoka, R. M. and Duchateau, J. (2008). Muscle fatigue: what, why and how it influences muscle function. *The Journal of physiology*, 586(1):11–23.

Frey-Law, L. A., Looft, J. M., and Heitsman, J. (2012). A three-compartment muscle fatigue model accurately predicts joint-specific maximum endurance times for sustained isometric tasks. *Journal of biomechanics*, 45(10):1803–1808.

Giat, Y., Mizrahi, J., and Levy, M. (1993). A musculotendon model of the fatigue profiles of paralyzed quadriceps muscle under fes. *IEEE transactions on biomedical engineering*, 40(7):664–674.

Głowiński, S., Krzyżyński, T., Pecolt, S., and Maciejewski, I. (2015). Design of motion trajectory of an arm exoskeleton. *Archive of Applied Mechanics*, 85(1).

Gopura, R., Kiguchi, K., and Bandara, D. (2011). A brief review on upper extremity robotic exoskeleton systems. In *Industrial and Information Systems (ICIIS), 2011 6th IEEE International Conference on*, pages 346–351. IEEE.

Gopura, R. A., Bandara, D. S., Kiguchi, K., and Mann, G. K. (2016). Developments in hardware systems of active upper-limb exoskeleton robots: A review. *Robotics and Autonomous Systems*, 75:203–220.

Gopura, R. A. R. C., Kiguchi, K., and Horikawa, E. (2010). A Study on Human Upper-Limb Muscles Activities during Daily Upper-Limb Motions. *International Journal of Bioelectromagnetism*, 12(2):54–61.

Gopura, R. A. R. C., Kiguchi, K., and Li, Y. (2009). Sueful-7: A 7dof upper-limb exoskeleton robot with muscle-model-oriented emg-based control. In *Intelligent Robots and Systems, 2009. IROS 2009. IEEE/RSJ International Conference on*, pages 1126–1131. IEEE.

Gopura, R. A. R. C. and Kiguhi, K. (2009). Mechanical Designs of Active Upper-Limb Exoskeleton Robots. In *11th International Conference on Rehabilitation Robotics*, pages 178–187.

Gupta, A. and Malley, M. K. O. (2006). Robotic Exoskeletons for Upper Extremity Rehabilitation. *Rehabilitation Robotics*, 1(August):648–674.

Herder, J. L., Vrijlandt, N., Antonides, T., Cloosterman, M., and Mastenbroek, P. L. (2006). Principle and design of a mobile arm support for people with muscular weakness. *Journal of rehabilitation research and development*, 43(5):591–604.

Hsu, L.-C., Wang, W.-W., Lee, G.-D., Liao, Y.-W., Fu, L.-C., and Lai, J.-S. (2012). A gravity compensation-based upper limb rehabilitation robot. In *American Control Conference (ACC), 2012*, pages 4819–4824. IEEE.

Huang, J., Huo, W., Xu, W., Mohammed, S., and Amirat, Y. (2015a). Control of Upper-Limb Power-Assist Exoskeleton Using a Human-Robot Interface Based on Motion Intention Recognition. *IEEE Transactions on Automation Science and Engineering*, 12(4):1257–1270.

Huang, J., Huo, W., Xu, W., Mohammed, S., and Amirat, Y. (2015b). Control of upper-limb power-assist exoskeleton using a human-robot interface based on motion intention recognition. *IEEE Transactions on Automation Science and Engineering*, 12(4):1257–1270.

Huang, J. B., Hong, J. C., Young, K. Y., and Ko, C. H. (2014). Development of upper-limb exoskeleton simulator for passive rehabilitation. *CACS 2014 - 2014 International Automatic Control Conference, Conference Digest*, 2(Cacs):335–339.

Huang, Y., Yang, Q., Chen, Y., and Song, R. (2017). Assessment of motor control during three-dimensional movements tracking with position-varying gravity compensation. *Frontiers in neuroscience*, 11.

Jung, C.-Y., Choi, J., Park, S., Lee, J. M., Kim, C., and Kim, S.-J. (2014). Design and control of an exoskeleton system for gait rehabilitation capable of natural pelvic movement. In *Intelligent Robots and Systems (IROS 2014), 2014 IEEE/RSJ International Conference on*, pages 2095–2100. IEEE.

Khan, A. M., Yun, D.-w., Han, J.-s., Shin, K., and Han, C.-s. (2014). Upper Extremity Assist Exoskeleton Robot. In *IEEE International Symposium on Robot and Human Interactive Communication*.

Kiguchi, K. (2007). Active exoskeletons for upper-limb motion assist. *International Journal of Humanoid Robotics*, 4(03):607–624.

Kiguchi, K. and Hayashi, Y. (2012a). An EMG-based control for an upper-limb power-assist exoskeleton robot. *IEEE Transactions on Systems, Man, and Cybernetics, Part B: Cybernetics*, 42(4):1064–1071.

Kiguchi, K. and Hayashi, Y. (2012b). An EMG-based control for an upper-limb power-assist exoskeleton robot. *IEEE Transactions on Systems, Man, and Cybernetics, Part B: Cybernetics*, 42(4):1064–1071.

Kim, W. S., Lee, H. D., Lim, D. H., Han, J. S., Shin, K. S., and Han, C. S. (2014). Development of a muscle circumference sensor to estimate torque of the human elbow joint. *Sensors and Actuators, A: Physical*, 208:95–103.

Laliratne, S. W. H. M. T. D. (2014). *A Study of Controlling Upper-Limb Exoskeletons Using EMG and EEG signals*. PhD thesis, Saga University.

Lalitharatne, T. D., Hayashi, Y., Teramoto, K., and Kiguchi, K. (2012). A study on effects of muscle fatigue on emg-based control for human upper-limb power-assist. In *Information and Automation for Sustainability (ICIAfS), 2012 IEEE 6th International Conference on*, pages 124–128. IEEE.

Li, Z., Su, C. Y., Li, G., and Su, H. (2015). Fuzzy approximation-based adaptive backstepping control of an exoskeleton for human upper limbs. *IEEE Transactions on Fuzzy Systems*, 23(3):555–566.

Liu, J. Z., Brown, R. W., and Yue, G. H. (2002). A dynamical model of muscle activation, fatigue, and recovery. *Biophysical journal*, 82(5):2344–2359.

Lo, H. S. (2014). *Exoskeleton Robot for Upper Limb Rehabilitation : Design Analysis and Control*. PhD thesis, University of Auckland.

Lo, H. S. and Xie, S. Q. (2012). Exoskeleton robots for upper-limb rehabilitation: State of the art and future prospects. *Medical Engineering and Physics*, 34(3):261–268.

Looze, M. P. D., Bosch, T., Krause, F., Stadler, K. S., Sullivan, W. O., Looze, M. P. D., Bosch, T., Krause, F., and Stadler, K. S. (2017). Exoskeletons for industrial application and their potential effects on physical work load. *Ergonomics*, 0139(August).

Lu, R., Li, Z., Su, C.-Y., and Xue, A. (2014). Development and Learning Control of a Human Limb With a Rehabilitation Exoskeleton. *IEEE Transactions on Industrial Electronics*, 61(7):3776–3785.

Luca, A. D. and Panzieri, S. (1993). Learning gravity compensation in robots: Rigid arms, elastic joints, flexible links. *International journal of adaptive control and signal processing*, 7(5):417–433.

Luo, R. C., Yi, C. Y., and Perng, Y. W. (2011). Gravity compensation and compliance based force control for auxiliarily easiness in manipulating robot arm. In *8th Asian Control Conference (ASCC)*, pages 1193–1198, Kaohsiung.

Ma, L., Bennis, F., Chablat, D., and Zhang, W. (2008). Framework for dynamic evaluation of muscle fatigue in manual handling work. In *Industrial Technology, 2008. ICIT 2008. IEEE International Conference on*, pages 1–6. IEEE.

Ma, L., Chablat, D., Bennis, F., and Zhang, W. (2009). A new simple dynamic muscle fatigue model and its validation. *International Journal of Industrial Ergonomics*, 39(1):211–220.

Ma, L., Chablat, D., Bennis, F., Zhang, W., and Guillaume, F. (2010). A new muscle fatigue and recovery model and its ergonomics application in human simulation. *Virtual and Physical Prototyping*, 5(3):123–137.

Ma, L., Chablat, D., Bennis, F., Zhang, W., Hu, B., and Guillaume, F. (2011). A novel approach for determining fatigue resistances of different muscle groups in static cases. *International Journal of Industrial Ergonomics*, 41(1):10–18.

Ma, L., Zhang, W., Hu, B., Chablat, D., Bennis, F., and Guillaume, F. (2013a). Determination of subject-specific muscle fatigue rates under static fatiguing operations. *Ergonomics*, 56(12):1889–1900.

Ma, L., Zhang, W., Wu, S., and Zhang, Z. (2015). A new simple local muscle recovery model and its theoretical and experimental validation. *International Journal of Occupational Safety and Ergonomics*, 21(1):86–93.

Ma, R., Chablat, D., and Bennis, F. (2013b). A new approach to muscle fatigue evaluation for push/pull task. In *Romansy 19–Robot Design, Dynamics and Control*, pages 309–316. Springer.

Ma, R., Chablat, D., Bennis, F., and Ma, L. (2012). Human muscle fatigue model in dynamic motions. In *Latest Advances in Robot Kinematics*, pages 349–356. Springer.

Machorro-Fernández, F. A., Parra-Vega, V., and Olguin-Diaz, E. (2009). Active mechanical compensation to obtain gravity-free robots: Modeling, control, design and preliminary experimental results. In *Robotics and Automation, 2009. ICRA'09. IEEE International Conference on*, pages 1061–1066. IEEE.

Maciejasz, P., Eschweiler, J., Gerlach-Hahn, K., Jansen-Troy, A., and Leonhardt, S. (2014). A survey on robotic devices for upper limb rehabilitation. *Journal of neuroengineering and rehabilitation*, 11(1):3.

Martinez, F., Retolaza, I., Pujana-Arrese, A., Cenitagoya, A., Basurko, J., and Landaluze, J. (2008). Design of a five actuated dof upper limb exoskeleton oriented to workplace help. In *Biomedical Robotics and Biomechatronics, 2008. BioRob 2008. 2nd IEEE RAS & EMBS International Conference on*, pages 169–174. IEEE.

Miller, L. M. (2006). *Gravity Compensation for a 7 Degree of Freedom Powered Upper Limb Exoskeleton*. PhD thesis, University of Washington.

Moubarak, S., Pham, M. T., Moreau, R., and Redarce, T. (2010). Gravity compensation of an upper extremity exoskeleton. In *Engineering in Medicine and Biology Society (EMBC), 2010 Annual International Conference of the IEEE*, pages 4489–4493. IEEE.

Nef, T., Guidali, M., and Riener, R. (2009). ARMin III – arm therapy exoskeleton with an ergonomic shoulder actuation. *Applied Bionics and Biomechanics*, 6(2):127–142.

Nunes, I. L. and Bush, P. M. (2011). Work-Related Musculoskeletal Disorders Assessment and Prevention. *Ergonomics-A system Approach*, pages 1–31.

Ochoa Luna, C., Habibur Rahman, M., Saad, M., Archambault, P. S., and Bruce Ferrer, S. (2015). Admittance-Based Upper Limb Robotic Active and Active-Assistive Movements. *International Journal of Advanced Robotic Systems*, 12(9).

Otten, A., Voort, C., Stienen, A., Aarts, R., van Asseldonk, E., and van der Kooij, H. (2015). Limpact: A hydraulically powered self-aligning upper limb exoskeleton. *IEEE/ASME transactions on mechatronics*, 20(5):2285–2298.

Ozkul, F. and Barkana, D. (2011). Design and control of an upper limb exoskeleton robot rehabroby. *Towards autonomous robotic systems*, pages 125–136.

Park, D. and Cho, K. J. (2017). Development and evaluation of a soft wearable weight support device for reducing muscle fatigue on shoulder. *PLoS ONE*, 12(3):1–24.

Perry, J. C., Powell, J. M., and Rosen, J. (2009). Isotropy of an upper limb exoskeleton and the kinematics and dynamics of the human arm. *Applied Bionics and Biomechanics*, 6(2):175–191.

Proietti, T., Crocher, V., Roby-Brami, A., and Jarrassé, N. (2016). Upper-limb robotic exoskeletons for neurorehabilitation: a review on control strategies. *IEEE reviews in biomedical engineering*, 9:4–14.

Rahman, M. H., Rahman, M. J., Cristobal, O., Saad, M., Kenné, J.-P., and Archambault, P. S. (2015). Development of a whole arm wearable robotic exoskeleton for rehabilitation and to assist upper limb movements. *Robotica*, 33(1):19–39.

Rashedi, E., Kim, S., Nussbaum, M. a., and Agnew, M. J. (2014). Ergonomic evaluation of a wearable assistive device for overhead work. *Ergonomics*, 57(12):1864–74.

Rodriguez, I., Boulic, R., and Meziat, D. (2002). A joint-level model of fatigue for the postural control of virtual humans. In *Proc. of the 5th Int. Conference" Human and Computer" HC02*, number VRLAB-CONF-2007-040.

Sakka, S., Chablat, D., Ma, R., and Bennis, F. (2015). Predictive model of the human muscle fatigue: application to repetitive push–pull tasks with light external load. *International Journal of Human Factors Modelling and Simulation*, 5(1):81–97.

Santiago, I. R. (2003). *Joint-level Fatigue Simulation for Its Exploitation in Human Posture Characterization and Optimization*. PhD thesis, thesis, Universidad de Alcala.

Seth, D., Chablat, D., Bennis, F., Sakka, S., Jubeau, M., and Nordez, A. (2016). Validation of a new dynamic muscle fatigue model and dmet analysis. *The International Journal of Virtual Reality*, 2016(16).

Song, A., Pan, L., Xu, G., and Li, H. (2015). Adaptive motion control of arm rehabilitation robot based on impedance identification. *Robotica*, 33(9):1795–1812.

Spagnuolo, G., Malosio, M., Scano, A., Caimmi, M., Legnani, G., and Tosatti, L. M. (2015). Passive and active gravity-compensation of LIGHTarm, an exoskeleton for the upper-limb rehabilitation. *IEEE International Conference on Rehabilitation Robotics*, 2015-Septe:440–445.

Stienen, A. H., Hekman, E. E., van der Kooij, H., Ellis, M. D., and Dewald, J. P. (2009). Aspects of weight-support mechanisms in rehabilitation robotics. In *World Congress on Medical Physics and Biomedical Engineering, September 7-12, 2009, Munich, Germany*, pages 392–394. Springer.

Sutton, R. P., Halikias, G. D., Plummer, A. R., Wilson, D. A., and Kingdom, U. (1997). Robust control of a lightweight flexible manipulator under the influence of gravity. In *IEEE International Conference on Control Applications*, pages 300–305.

Sylla, N., Bonnet, V., Colledani, F., and Fraisse, P. (2014). Ergonomic contribution of ABLE exoskeleton in automotive industry. *International Journal of Industrial Ergonomics*, 44(4):475–481.

Tsai, B.-C., Wang, W.-W., Hsu, L.-C., Fu, L.-C., and Lai, J.-S. (2010). An articulated rehabilitation robot for upper limb physiotherapy and training. In *Intelligent Robots and Systems (IROS), 2010 IEEE/RSJ International Conference on*, pages 1470–1475. IEEE.

van Diemen, T., van Lankveld, W., van Leeuwen, C., Post, M., and van Nes, I. (2016). Multidimensional fatigue during rehabilitation in persons with recently acquired spinal cord injury. *Journal of rehabilitation medicine*, 48(1):27–32.

Van Ninhuijs, B., van der Heide, L., Jansen, J., Gysen, B., van der Pijl, D., and Lomonova, E. (2013). Overview of actuated arm support systems and their applications. In *Actuators*, volume 2, pages 86–110. Multidisciplinary Digital Publishing Institute.

Wang, L.-X. (1993). Stable adaptive fuzzy control of nonlinear systems. *IEEE Transactions on Fuzzy Systems*, 1(2):146–155.

Xia, T. and Law, L. A. F. (2008). A theoretical approach for modeling peripheral muscle fatigue and recovery. *Journal of biomechanics*, 41(14):3046–3052.

Xiao, J., Song, X., Qin, B., and Wang, H. (2010). Fuzzy gravity compensation for wall-climbing microrobots. *2010 Chinese Control and Decision Conference, CCDC 2010*, pages 4435–4440.

Xiao, J., Xiao, J. Z., Xi, N., Tummala, R. L., and Mukherjee, R. (2004). Fuzzy controller for wall-climbing microrobots. *IEEE Transactions on Fuzzy Systems*, 12(4):466–480.

Xu, G., Song, A., and Li, H. (2011). Control System Design for an Upper-Limb Rehabilitation Robot. *Advanced Robotics*, 25(1-2):229–251.

Xu, W., Chu, B., and Rogers, E. (2014). Iterative learning control for robotic-assisted upper limb stroke rehabilitation in the presence of muscle fatigue. *Control Engineering Practice*, 31:63–72.

Yang, C.-J., Zhang, J.-F., Chen, Y., Dong, Y.-M., and Zhang, Y. (2008). A Review of exoskeleton-type systems and their key technologies. *Journal of Mechanical Engineering Science*, 222(8):1599–1612.

Yu, W. and Rosen, J. (2010). A novel linear PID controller for an upper limb exoskeleton. *Proceedings of the IEEE Conference on Decision and Control*, pages 3548–3553.

Zadeh, L. A. (1973). Outline of a new approach to the analysis of complex systems and decision processes. *IEEE Transactions on Systems, Man and Cybernetics*, 1100:38–45.

Zhang, Z., Li, K. W., Zhang, W., Ma, L., and Chen, Z. (2014). Muscular fatigue and maximum endurance time assessment for male and female industrial workers. *International Journal of Industrial Ergonomics*, 44(2):292–297.

Appendix A

Parts and functions of muscles for upper-extremity

Table A.1: Superficial anterior muscles of the body

Types of muscles	Origin	Insertion	Function(s)
Biceps Brachii	Scapula of shoulder girdle	Proximal radius	Flexes elbow and supinate forerm
Brachialis	Distal humerus	Proximal ulna	Flexes forearm and flexes elbow
Deltoid	Scapular spine and clavicle	Humerus (deltoid tuberosity)	Abducts arm
Pectoralis major	Sternum, clavicle and first to sixth ribs	Proximal humerus	Adducts and flexes humerus
Brachioradialis	Proximal two-thirds of lateral supracondylar ridge of humerus	Lateral side of base of styloid process of radius	Flexes forearm and flexes elbow

Table A.2: Superficial posterior muscles of the body

Types of muscles	Origin	Insertion	Function(s)
Deltoid	Scapular spine and clavicle	Humerus (deltoid tuberosity)	Abducts arm and humerus
Triceps brachii	Shoulder girdle and proximal humerus	Olecranon process of ulna	Extends forearm and extend elbow
Flexor carpi radialis	Distal humerus	Base of metacarpals II and III	Flexes hand and Assists in abduction hand
Flexor carpi ulnaris	Distal humerus and posterior ulna	Carpals of wrist and fifth metacarpal	Flexes wrist and fingers
Flexor carpi ulnaris	Distal humerus and posterior ulna	Carpals of wrist and fifth metacarpal	Flexes wrist and adducts hand
Flexor digitorum superficials	Humeruss	Base of second and third metacarpals	Extends wrist Abducts hands
Extensor carpi radialis	Distal humerus and posterior ulna	Carpals of wrist and fifth metacarpal	Flexes wrist and adducts hand
Extensor digitorum	Distal humerus	Distal phalanges of second to fifth fingers	Extends fingers and wrist
Trapezius	Occipital bone and all cervical and thoracic vertebrae	Scapula spine and clavicle	Extend neck and adducts scapula

Appendix B

Dynamic representation of human upper-extremity

$$\tau_1 = I_1*\ddot{\theta}_1 + I_2*\ddot{\theta}_1 + I_2*\ddot{\theta}_2 + I_3*\ddot{\theta}_1 + I_3*\ddot{\theta}_2 + I_4*\ddot{\theta}_1 + I_3*\ddot{\theta}_3 + I_4*\ddot{\theta}_2 + I_4*\ddot{\theta}_3 + I_4*\ddot{\theta}_4 + L_2^2*\ddot{\theta}_1*m1 + L_2^2*\ddot{\theta}_1*m2 + L_2^2*\ddot{\theta}_1*m3 + L_2^2*\ddot{\theta}_1*m4 + L_3^2*\ddot{\theta}_1*m3 + L_3^2*\ddot{\theta}_1*m4 + L_4^2*\ddot{\theta}_1*m4 - L_3^2*\ddot{\theta}_1*m3*cos(\theta_2)^2 - L_3^2*\ddot{\theta}_1*m4*cos(\theta_2)^2 + L_2*g*m1*cos(\theta_1) + L_2*g*m2*cos(\theta_1) + L_2*g*m3*cos(\theta_1) + L_2*g*m4*cos(\theta_1) - L_3^2*\ddot{\theta}_3*m3*sin(\theta_2) - L_3^2*\ddot{\theta}_3*m4*sin(\theta_2) - L_4^2*\ddot{\theta}_3*m4*sin(\theta_2) - L_4^2*\ddot{\theta}_4*m4*sin(\theta_2) + L_2*L_3*\dot{\theta_3}^2*m3*cos(\theta_3) + L_2*L_3*\dot{\theta_3}^2*m4*cos(\theta_3) - L_3^2*\dot{\theta}_2*\dot{\theta}_3*m3*cos(\theta_2) - L_3^2*\dot{\theta}_2*\dot{\theta}_3*m4*cos(\theta_2) - L_4^2*\dot{\theta}_2*\dot{\theta}_3*m4*cos(\theta_2) - L_4^2*\dot{\theta}_2*\dot{\theta}_4*m4*cos(\theta_2) + L_3*g*m3*cos(\theta_3)*sin(\theta_1) + L_3*g*m4*cos(\theta_3)*sin(\theta_1) + L_3^2*\ddot{\theta}_1*m3*cos(\theta_2)^2*cos(\theta_3)^2 + L_3^2*\ddot{\theta}_1*m4*cos(\theta_2)^2*cos(\theta_3)^2 - L_4^2*\ddot{\theta}_1*m4*cos(\theta_2)^2*cos(\theta_3)^2 - L_4^2*\ddot{\theta}_1*m4*cos(\theta_2)^2*cos(\theta_4)^2 + 2*L_3*L_4*\ddot{\theta}_1*m4*cos(\theta_4) + L_2*L_3*\ddot{\theta}_3*m3*sin(\theta_3) + L_2*L_3*\ddot{\theta}_3*m4*sin(\theta_3) + 2*L_3^2*\dot{\theta}_1*\dot{\theta}_2*m3*cos(\theta_2)*sin(\theta_2) + 2*L_3^2*\dot{\theta}_1*\dot{\theta}_2*m4*cos(\theta_2)*sin(\theta_2) - 2*L_3*L_4*\dot{\theta}_1*\dot{\theta}_4*m4*sin(\theta_4) + L_4*g*m4*cos(\theta_3)*cos(\theta_4)*sin(\theta_1) - L_3*g*m3*cos(\theta_1)*sin(\theta_2)*sin(\theta_3) - L_3*g*m4*cos(\theta_1)*sin(\theta_2)*sin(\theta_3) - L_4*g*m4*sin(\theta_1)*sin(\theta_3)*sin(\theta_4) - L_3^2*\dot{\theta}_2*\dot{\theta}_3*m3*cos(\theta_2)*cos(\theta_3)^2 - L_3^2*\dot{\theta}_2*\dot{\theta}_3*m4*cos(\theta_2)*cos(\theta_3)^2 + L_4^2*\dot{\theta}_2*\dot{\theta}_3*m4*cos(\theta_2)*cos(\theta_3)^2 + L_4^2*\dot{\theta}_2*\dot{\theta}_4*m4*cos(\theta_2)*cos(\theta_4)^2 + L_3^2*\dot{\theta}_2*\dot{\theta}_3*m3*cos(\theta_2)*sin(\theta_3)^2 + L_3^2*\dot{\theta}_2*\dot{\theta}_3*m4*cos(\theta_2)*sin(\theta_3)^2 - L_4^2*\dot{\theta}_2*\dot{\theta}_3*m4*cos(\theta_2)*sin(\theta_3)^2 - L_4^2*\dot{\theta}_2*\dot{\theta}_4*m4*cos(\theta_2)*sin(\theta_4)^2 - L_3^2*\ddot{\theta}_2*m3*cos(\theta_2)*cos(\theta_3)*sin(\theta_3) - L_3^2*\ddot{\theta}_2*m4*cos(\theta_2)*cos(\theta_3)*sin(\theta_3) + L_4^2*\ddot{\theta}_2*m4*cos(\theta_2)*cos(\theta_3)*sin(\theta_3) + L_4^2*\ddot{\theta}_2*m4*cos(\theta_2)*cos(\theta_4)*sin(\theta_4) + 2*L_4^2*\ddot{\theta}_1*m4*cos(\theta_2)^2*cos(\theta_3)^2*cos(\theta_4)^2 + L_3*L_4*\ddot{\theta}_2*m4*cos(\theta_2)*sin(\theta_4) + L_2*L_4*\ddot{\theta}_3*m4*cos(\theta_3)*sin(\theta_4) + L_2*L_4*\ddot{\theta}_3*m4*cos(\theta_4)*sin(\theta_3) - 2*L_3*L_4*\ddot{\theta}_3*m4*cos(\theta_4)*sin(\theta_2) + L_2*L_4*\ddot{\theta}_4*m4*cos(\theta_3)*sin(\theta_4) + L_2*L_4*\ddot{\theta}_4*m4*cos(\theta_4)*sin(\theta_3) - L_3*L_4*\ddot{\theta}_4*m4*cos(\theta_4)*sin(\theta_2) - 2*L_2*L_3*\ddot{\theta}_1*m3*sin(\theta_2)*sin(\theta_3) - 2*L_2*L_3*\ddot{\theta}_1*m4*sin(\theta_2)*sin(\theta_3) - 2*L_3*L_4*\ddot{\theta}_1*m4*cos(\theta_2)^2*cos(\theta_4) + L_2*L_4*\dot{\theta_3}^2*m4*cos(\theta_3)*cos(\theta_4) + L_2*L_4*\dot{\theta_4}^2*m4*cos(\theta_3)*cos(\theta_4) + L_3^2*\dot{\theta_2}^2*m3*cos(\theta_3)*sin(\theta_2)*sin(\theta_3) + L_3^2*\dot{\theta_2}^2*m4*cos(\theta_3)*sin(\theta_2)*sin(\theta_3) - L_4^2*\dot{\theta_2}^2*m4*cos(\theta_3)*sin(\theta_2)*sin(\theta_3) - L_4^2*\dot{\theta_2}^2*m4*cos(\theta_4)*sin(\theta_2)*sin(\theta_4) - L_3*L_4*\dot{\theta_2}^2*m4*sin(\theta_2)*sin(\theta_4) - L_2*L_4*\dot{\theta_3}^2*m4*sin(\theta_3)*sin(\theta_4) - L_2*L_4*\dot{\theta_4}^2*m4*sin(\theta_3)*sin(\theta_4) + L_3*L_4*\dot{\theta_4}^2*m4*sin(\theta_2)*sin(\theta_4) + 2*L_3*L_4*\ddot{\theta}_1*m4*cos(\theta_2)^2*cos(\theta_3)^2*cos(\theta_4) + 2*L_4^2*\dot{\theta_2}^2*m4*cos(\theta_3)*cos(\theta_4)^2*sin(\theta_2)*sin(\theta_3) + 2*L_4^2*\dot{\theta_2}^2*m4*cos(\theta_3)^2*cos(\theta_4)*sin(\theta_2)*sin(\theta_4) + 2*L_3*L_4*\dot{\theta_2}^2*m4*cos(\theta_3)^2*sin(\theta_2)*sin(\theta_4) - 2*L_3^2*\dot{\theta}_1*\dot{\theta}_2*m3*cos(\theta_2)*cos(\theta_3)^2*sin(\theta_2) - 2*L_3^2*\dot{\theta}_1*\dot{\theta}_2*m4*cos(\theta_2)*$$

$$cos(\theta_3)^2 * sin(\theta_2) - 2 * L_3^2 * \dot{\theta}_1 * \dot{\theta}_3 * m3 * cos(\theta_2)^2 * cos(\theta_3) * sin(\theta_3) + 2 * L_4^2 * \dot{\theta}_1 * \dot{\theta}_2 * m4 * cos(\theta_2) * cos(\theta_3)^2 * sin(\theta_2) - 2 * L_3^2 * \dot{\theta}_1 * \dot{\theta}_3 * m4 * cos(\theta_2)^2 * cos(\theta_3) * sin(\theta_3) + 2 * L_4^2 * \dot{\theta}_1 * \dot{\theta}_2 * m4 * cos(\theta_2) * cos(\theta_4)^2 * sin(\theta_2) + 2 * L_4^2 * \dot{\theta}_1 * \dot{\theta}_3 * m4 * cos(\theta_2)^2 * cos(\theta_3) * sin(\theta_3) + 2 * L_4^2 * \dot{\theta}_1 * \dot{\theta}_4 * m4 * cos(\theta_2)^2 * cos(\theta_4) * sin(\theta_4) + 2 * L_3 * L_4 * \dot{\theta}_1 * \dot{\theta}_4 * m4 * cos(\theta_2)^2 * sin(\theta_4) - 2 * L_2 * L_4 * \ddot{\theta}_1 * m4 * cos(\theta_3) * sin(\theta_2) * sin(\theta_4) - 2 * L_2 * L_4 * \ddot{\theta}_1 * m4 * cos(\theta_4) * sin(\theta_2) * sin(\theta_3) - 2 * L_4^2 * \dot{\theta}_2 * \dot{\theta}_3 * m4 * cos(\theta_2) * cos(\theta_3)^2 * cos(\theta_4)^2 - 2 * L_4^2 * \dot{\theta}_2 * \dot{\theta}_4 * m4 * cos(\theta_2) * cos(\theta_3)^2 * cos(\theta_4)^2 + 2 * L_4^2 * \dot{\theta}_2 * \dot{\theta}_3 * m4 * cos(\theta_2) * cos(\theta_4)^2 * sin(\theta_3)^2 + 2 * L_4^2 * \dot{\theta}_2 * \dot{\theta}_4 * m4 * cos(\theta_2) * cos(\theta_3)^2 * sin(\theta_4)^2 - 2 * L_4^2 * \ddot{\theta}_2 * m4 * cos(\theta_2) * cos(\theta_3) * cos(\theta_4)^2 * sin(\theta_3) - 2 * L_4^2 * \ddot{\theta}_2 * m4 * cos(\theta_2) * cos(\theta_3)^2 * cos(\theta_4) * sin(\theta_4) - 2 * L_3 * L_4 * \ddot{\theta}_2 * m4 * cos(\theta_2) * cos(\theta_3)^2 * sin(\theta_4) - 2 * L_3 * L_4 * \dot{\theta}_2 * \dot{\theta}_3 * m4 * cos(\theta_2) * cos(\theta_4) + 2 * L_2 * L_4 * \dot{\theta}_3 * \dot{\theta}_4 * m4 * cos(\theta_3) * cos(\theta_4) - 2 * L_2 * L_3 * \dot{\theta}_1 * \dot{\theta}_2 * m3 * cos(\theta_2) * sin(\theta_3) - 2 * L_2 * L_3 * \dot{\theta}_1 * \dot{\theta}_2 * m4 * cos(\theta_2) * sin(\theta_3) - 2 * L_2 * L_3 * \dot{\theta}_1 * \dot{\theta}_3 * m3 * cos(\theta_3) * sin(\theta_2) - 2 * L_2 * L_3 * \dot{\theta}_1 * \dot{\theta}_3 * m4 * cos(\theta_3) * sin(\theta_2) - 2 * L_2 * L_4 * \dot{\theta}_3 * \dot{\theta}_4 * m4 * sin(\theta_3) * sin(\theta_4) + 2 * L_3 * L_4 * \dot{\theta}_3 * \dot{\theta}_4 * m4 * sin(\theta_2) * sin(\theta_4) - L_4 * g * m4 * cos(\theta_1) * cos(\theta_3) * sin(\theta_2) * sin(\theta_4) - L_4 * g * m4 * cos(\theta_1) * cos(\theta_4) * sin(\theta_2) * sin(\theta_3) - 2 * L_3 * L_4 * \dot{\theta}_2 * \dot{\theta}_3 * m4 * cos(\theta_2) * cos(\theta_3)^2 * cos(\theta_4) - 2 * L_3 * L_4 * \dot{\theta}_2 * \dot{\theta}_4 * m4 * cos(\theta_2) * cos(\theta_3)^2 * cos(\theta_4) + 2 * L_3 * L_4 * \dot{\theta}_2 * \dot{\theta}_3 * m4 * cos(\theta_2) * cos(\theta_4) * sin(\theta_3)^2 - 2 * L_3 * L_4 * \ddot{\theta}_2 * m4 * cos(\theta_2) * cos(\theta_3) * cos(\theta_4) * sin(\theta_3) - 4 * L_4^2 * \dot{\theta}_1 * \dot{\theta}_2 * m4 * cos(\theta_2) * cos(\theta_3)^2 * cos(\theta_4)^2 * sin(\theta_2) - 4 * L_4^2 * \dot{\theta}_1 * \dot{\theta}_3 * m4 * cos(\theta_2)^2 * cos(\theta_3) * cos(\theta_4)^2 * sin(\theta_3) - 2 * L_4^2 * \dot{\theta}_1 * \dot{\theta}_3 * m4 * cos(\theta_2)^2 * cos(\theta_3)^2 * cos(\theta_4) * sin(\theta_4) - 2 * L_4^2 * \dot{\theta}_1 * \dot{\theta}_4 * m4 * cos(\theta_2)^2 * cos(\theta_3) * cos(\theta_4)^2 * sin(\theta_3) - 4 * L_4^2 * \dot{\theta}_1 * \dot{\theta}_4 * m4 * cos(\theta_2)^2 * cos(\theta_3)^2 * cos(\theta_4) * sin(\theta_4) + 2 * L_4^2 * \dot{\theta}_1 * \dot{\theta}_3 * m4 * cos(\theta_2)^2 * cos(\theta_4) * sin(\theta_3)^2 * sin(\theta_4) + 2 * L_4^2 * \dot{\theta}_1 * \dot{\theta}_4 * m4 * cos(\theta_2)^2 * cos(\theta_3) * sin(\theta_3) * sin(\theta_4)^2 - 2 * L_3 * L_4 * \dot{\theta}_1 * \dot{\theta}_3 * m4 * cos(\theta_2)^2 * cos(\theta_3)^2 * sin(\theta_4) - 2 * L_3 * L_4 * \dot{\theta}_1 * \dot{\theta}_4 * m4 * cos(\theta_2)^2 * cos(\theta_3)^2 * sin(\theta_4) - 2 * L_4^2 * \ddot{\theta}_1 * m4 * cos(\theta_2)^2 * cos(\theta_3) * cos(\theta_4) * sin(\theta_3) * sin(\theta_4) + 2 * L_3 * L_4 * \dot{\theta}_1 * \dot{\theta}_3 * m4 * cos(\theta_2)^2 * sin(\theta_3)^2 * sin(\theta_4) - 2 * L_3 * L_4 * \ddot{\theta}_1 * m4 * cos(\theta_2)^2 * cos(\theta_3) * sin(\theta_3) * sin(\theta_4) + 2 * L_3 * L_4 * \dot{\theta}_2^2 * m4 * cos(\theta_3) * cos(\theta_4) * sin(\theta_2) * sin(\theta_3) - 2 * L_2 * L_4 * \dot{\theta}_1 * \dot{\theta}_2 * m4 * cos(\theta_2) * cos(\theta_3) * sin(\theta_4) - 2 * L_2 * L_4 * \dot{\theta}_1 * \dot{\theta}_2 * m4 * cos(\theta_2) * cos(\theta_4) * sin(\theta_3) + 4 * L_3 * L_4 * \dot{\theta}_1 * \dot{\theta}_2 * m4 * cos(\theta_2) * cos(\theta_4) * sin(\theta_2) - 2 * L_2 * L_4 * \dot{\theta}_1 * \dot{\theta}_3 * m4 * cos(\theta_3) * cos(\theta_4) * sin(\theta_2) - 2 * L_2 * L_4 * \dot{\theta}_1 * \dot{\theta}_4 * m4 * cos(\theta_3) * cos(\theta_4) * sin(\theta_2) + 2 * L_2 * L_4 * \dot{\theta}_1 * \dot{\theta}_3 * m4 * sin(\theta_2) * sin(\theta_3) * sin(\theta_4) + 2 * L_2 * L_4 * \dot{\theta}_1 * \dot{\theta}_4 * m4 * sin(\theta_2) * sin(\theta_3) * sin(\theta_4) + 4 * L_4^2 * \dot{\theta}_2 * \dot{\theta}_3 * m4 * cos(\theta_2) * cos(\theta_3) * cos(\theta_4) * sin(\theta_3) * sin(\theta_4) + 4 * L_4^2 * \dot{\theta}_2 * \dot{\theta}_4 * m4 * cos(\theta_2) * cos(\theta_3) * cos(\theta_4) * sin(\theta_3) * sin(\theta_4) + 4 * L_3 * L_4 * \dot{\theta}_2 * \dot{\theta}_3 * m4 * cos(\theta_2) * cos(\theta_3) * sin(\theta_3) * sin(\theta_4) + 2 * L_3 * L_4 * \dot{\theta}_2 * \dot{\theta}_4 * m4 * cos(\theta_2) * cos(\theta_3) * sin(\theta_3) * sin(\theta_4) - 4 * L_3 * L_4 * \dot{\theta}_1 * \dot{\theta}_2 * m4 * cos(\theta_2) * cos(\theta_3)^2 * cos(\theta_4) * sin(\theta_2) - 4 * L_3 * L_4 * \dot{\theta}_1 * \dot{\theta}_3 * m4 * cos(\theta_2)^2 * cos(\theta_3) * cos(\theta_4) * sin(\theta_3) - 2 * L_3 * L_4 * \dot{\theta}_1 * \dot{\theta}_4 * m4 * cos(\theta_2)^2 * cos(\theta_3) * cos(\theta_4) * sin(\theta_3) + 4 * L_4^2 * \dot{\theta}_1 * \dot{\theta}_2 * m4 * cos(\theta_2) * cos(\theta_3) * cos(\theta_4) * sin(\theta_2) * sin(\theta_3) * sin(\theta_4) + 4 * L_3 * L_4 * \dot{\theta}_1 * \dot{\theta}_2 * m4 * cos(\theta_2) * cos(\theta_3) * sin(\theta_2) * sin(\theta_3) * sin(\theta_4)$$

$$\tau_2 = I_2 * \ddot{\theta}_1 + I_2 * \ddot{\theta}_2 + I_3 * \ddot{\theta}_1 + I_3 * \ddot{\theta}_2 + I_4 * \ddot{\theta}_1 + I_3 * \ddot{\theta}_3 + I_4 * \ddot{\theta}_2 + I_4 * \ddot{\theta}_3 + I_4 * \ddot{\theta}_4 + L_3^2 * \ddot{\theta}_2 * m3 * cos(\theta_2)^2 + L_3^2 * \dot{\theta}_1 * \dot{\theta}_3 * m3 * cos(\theta_2) + L_3^2 * \dot{\theta}_1 * \dot{\theta}_3 * m4 * cos(\theta_2) + L_4^2 * \dot{\theta}_1 * \dot{\theta}_3 * m4 * cos(\theta_2) + L_4^2 * \dot{\theta}_1 * \dot{\theta}_4 * m4 * cos(\theta_2) - L_3^2 * \ddot{\theta}_2 * m3 * cos(\theta_2)^2 * cos(\theta_3)^2 + L_3^2 * \ddot{\theta}_2 * m4 * cos(\theta_2)^2 * sin(\theta_3)^2 - L_3^2 * \dot{\theta_1}^2 * m3 * cos(\theta_2) * sin(\theta_2) - L_3^2 * \dot{\theta_1}^2 * m4 * cos(\theta_2) * sin(\theta_2) - L_3^2 * \dot{\theta_2}^2 * m3 * cos(\theta_2) * sin(\theta_2) + L_3^2 * \dot{\theta_2}^2 * m4 * cos(\theta_2) * sin(\theta_2) - L_4^2 * \dot{\theta_3}^2 * m4 * cos(\theta_2) * sin(\theta_2) - L_4^2 * \dot{\theta_4}^2 * m4 * cos(\theta_2) * sin(\theta_2) + L_3^2 * \dot{\theta}_2 * \dot{\theta}_3 * m3 * cos(\theta_3) * sin(\theta_3) + L_3^2 * \dot{\theta}_2 * \dot{\theta}_3 * m4 * cos(\theta_3) * sin(\theta_3) - L_4^2 * \dot{\theta}_2 * \dot{\theta}_3 * m4 * cos(\theta_3) * sin(\theta_3) - 2 * L_4^2 * \dot{\theta}_3 * \dot{\theta}_4 * m4 * cos(\theta_2) * sin(\theta_2) - L_4^2 * \dot{\theta}_2 * \dot{\theta}_4 * m4 * cos(\theta_3) * sin(\theta_3) - L_4^2 * \dot{\theta}_2 * \dot{\theta}_3 * m4 * cos(\theta_4) * sin(\theta_4) - L_4^2 * \dot{\theta}_2 * \dot{\theta}_4 * m4 * cos(\theta_4) * sin(\theta_4) - L_3 * L_4 * \dot{\theta}_2 * \dot{\theta}_3 * m4 * sin(\theta_4) - L_3 * L_4 * \dot{\theta}_2 * \dot{\theta}_4 * m4 * sin(\theta_4) - L_3 * g * m3 * cos(\theta_2) * sin(\theta_1) * sin(\theta_3) - L_3 * g * m4 * cos(\theta_2) * sin(\theta_1) * sin(\theta_3) + L_3^2 * \dot{\theta_1}^2 * m3 * cos(\theta_2) * cos(\theta_3)^2 * sin(\theta_2) + L_3^2 * \dot{\theta_1}^2 * m4 * cos(\theta_2) * cos(\theta_3)^2 * sin(\theta_2) + L_3^2 * \dot{\theta_2}^2 * m3 * cos(\theta_2) * cos(\theta_3)^2 * sin(\theta_2) - L_3^2 * \dot{\theta_2}^2 * m4 * cos(\theta_2) * cos(\theta_3)^2 * sin(\theta_2) - L_4^2 * \dot{\theta_1}^2 * m4 * cos(\theta_2) * cos(\theta_3)^2 * sin(\theta_2) - L_4^2 * \dot{\theta_1}^2 * m4 * cos(\theta_2) * cos(\theta_4)^2 * sin(\theta_2) + L_4^2 * \dot{\theta_2}^2 * m4 * cos(\theta_2) * cos(\theta_3)^2 * sin(\theta_2) + L_4^2 * \dot{\theta_2}^2 * m4 * cos(\theta_2) * cos(\theta_4)^2 * sin(\theta_2) + L_4^2 * \dot{\theta_3}^2 * m4 * cos(\theta_2) * cos(\theta_3)^2 * sin(\theta_2) + L_4^2 * \dot{\theta_3}^2 * m4 * cos(\theta_2) * cos(\theta_4)^2 * sin(\theta_2) + L_4^2 * \dot{\theta_4}^2 * m4 * cos(\theta_2) * cos(\theta_3)^2 * sin(\theta_2) + L_4^2 * \dot{\theta_4}^2 * m4 * cos(\theta_2) * cos(\theta_4)^2 * sin(\theta_2) - 2 * L_3^2 * \dot{\theta_2}^2 * m4 * cos(\theta_2) * sin(\theta_2) * sin(\theta_3)^2 - L_3^2 * \dot{\theta_3}^2 * m3 * cos(\theta_2) * sin(\theta_2) * sin(\theta_3)^2 - L_3^2 * \dot{\theta_3}^2 * m4 * cos(\theta_2) * sin(\theta_2) * sin(\theta_3)^2 - L_3^2 * \dot{\theta}_1 * \dot{\theta}_3 * m3 * cos(\theta_2) * cos(\theta_3)^2 - L_3^2 * \dot{\theta}_1 * \dot{\theta}_3 * m4 * cos(\theta_2) * cos(\theta_3)^2 + L_3^2 * \dot{\theta}_1 * \dot{\theta}_3 * m3 * cos(\theta_2) * sin(\theta_3)^2 + L_3^2 * \dot{\theta}_1 * \dot{\theta}_3 * m4 * cos(\theta_2) * sin(\theta_3)^2 - L_3^2 * \ddot{\theta}_1 * m3 * cos(\theta_2) * cos(\theta_3) * sin(\theta_3) - L_3^2 * \ddot{\theta}_1 * m4 * cos(\theta_2) * cos(\theta_3) * sin(\theta_3) + L_4^2 * \ddot{\theta}_2 * m4 * cos(\theta_2)^2 * cos(\theta_3)^2 * sin(\theta_4)^2 + L_4^2 * \ddot{\theta}_2 * m4 * cos(\theta_2)^2 * cos(\theta_4)^2 * sin(\theta_3)^2 + L_2 * L_3 * \dot{\theta_1}^2 * m3 * cos(\theta_2) * sin(\theta_3) + L_2 * L_3 * \dot{\theta_1}^2 * m4 * cos(\theta_2) * sin(\theta_3) + 2 * L_3 * L_4 * \ddot{\theta}_2 * m4 * cos(\theta_2)^2 * cos(\theta_4) * sin(\theta_3)^2 + L_3^2 * \dot{\theta}_2 * \dot{\theta}_3 * m3 * cos(\theta_2)^2 * cos(\theta_3) * sin(\theta_3) + L_3^2 * \dot{\theta}_2 * \dot{\theta}_3 * m4 * cos(\theta_2)^2 * cos(\theta_3) * sin(\theta_3) + 2 * L_4^2 * \dot{\theta}_2 * \dot{\theta}_3 * m4 * cos(\theta_2)^2 * cos(\theta_3) * sin(\theta_3) + 2 * L_4^2 * \dot{\theta}_2 * \dot{\theta}_4 * m4 * cos(\theta_2)^2 * cos(\theta_3) * sin(\theta_3) + 2 * L_4^2 * \dot{\theta}_3 * \dot{\theta}_4 * m4 * cos(\theta_2) * cos(\theta_3)^2 * sin(\theta_2) + 2 * L_4^2 * \dot{\theta}_2 * \dot{\theta}_3 * m4 * cos(\theta_3) * cos(\theta_4)^2 * sin(\theta_3) + 2 * L_4^2 * \dot{\theta}_2 * \dot{\theta}_3 * m4 * cos(\theta_2)^2 * cos(\theta_4) * sin(\theta_4) + 2 * L_4^2 * \dot{\theta}_3 * \dot{\theta}_4 * m4 * cos(\theta_2) * cos(\theta_4)^2 * sin(\theta_2) + 2 * L_4^2 * \dot{\theta}_2 * \dot{\theta}_3 * m4 * cos(\theta_3)^2 * cos(\theta_4) * sin(\theta_4) + 2 * L_4^2 * \dot{\theta}_2 * \dot{\theta}_4 * m4 * cos(\theta_3) * cos(\theta_4)^2 * sin(\theta_3) + 2 * L_4^2 * \dot{\theta}_2 * \dot{\theta}_4 * m4 * cos(\theta_2)^2 * cos(\theta_4) * sin(\theta_4) + 2 * L_4^2 * \dot{\theta}_2 * \dot{\theta}_4 * m4 * cos(\theta_3)^2 * cos(\theta_4) * sin(\theta_4) - L_3^2 * \dot{\theta}_2 * \dot{\theta}_3 * m3 * cos(\theta_3) * sin(\theta_2)^2 * sin(\theta_3) - L_3^2 * \dot{\theta}_2 * \dot{\theta}_3 * m4 * cos(\theta_3) * sin(\theta_2)^2 * sin(\theta_3) + 2 * L_3 * L_4 * \dot{\theta}_2 * \dot{\theta}_3 * m4 * cos(\theta_2)^2 * sin(\theta_4) + 2 * L_3 * L_4 * \dot{\theta}_2 * \dot{\theta}_3 * m4 * cos(\theta_3)^2 * sin(\theta_4) + 2 * L_3 * L_4 * \dot{\theta}_2 * \dot{\theta}_4 * m4 * cos(\theta_2)^2 * sin(\theta_4) + L_3 * L_4 * \dot{\theta}_2 * \dot{\theta}_4 * m4 * cos(\theta_3)^2 * sin(\theta_4) + L_3^2 * \ddot{\theta}_3 * m3 * cos(\theta_2) * cos(\theta_3) * sin(\theta_2) * sin(\theta_3) + L_3^2 * \ddot{\theta}_3 * m4 * cos(\theta_2) * cos(\theta_3) * sin(\theta_2) * sin(\theta_3) + 2 * L_4^2 * \dot{\theta_1}^2 * m4 * cos(\theta_2) * cos(\theta_3)^2 * cos(\theta_4)^2 * sin(\theta_2) - 2 * L_4^2 * \dot{\theta_2}^2 * m4 * cos(\theta_2) * cos(\theta_3)^2 * cos(\theta_4)^2 * sin(\theta_2) - L_4^2 * \dot{\theta_3}^2 * m4 * cos(\theta_2) * cos(\theta_3)^2 * cos(\theta_4)^2 * sin(\theta_2) - L_4^2 * \dot{\theta_4}^2 * m4 * cos(\theta_2) * cos(\theta_3)^2 * cos(\theta_4)^2 * sin(\theta_2) - 2 * L_4^2 * \dot{\theta_2}^2 * m4 * cos(\theta_2) * cos(\theta_3)^2 * sin(\theta_2) * sin(\theta_4)^2 - 2 * L_4^2 * \dot{\theta_2}^2 * m4 * cos(\theta_2) * cos(\theta_4)^2 * sin(\theta_2) * sin(\theta_3)^2 - L_4^2 * \dot{\theta_3}^2 * m4 * cos(\theta_2) * cos(\theta_3)^2 * sin(\theta_2) * sin(\theta_4)^2 - L_4^2 * \dot{\theta_3}^2 * m4 * cos(\theta_2) * cos(\theta_4)^2 * sin(\theta_2) * sin(\theta_3)^2 - L_4^2 * \dot{\theta_4}^2 * m4 * cos(\theta_2) * cos(\theta_3)^2 * sin(\theta_2) * sin(\theta_4)^2 - L_4^2 * \dot{\theta_4}^2 * m4 * cos(\theta_2) * cos(\theta_4)^2 * sin(\theta_2) * sin(\theta_3)^2 - L_4^2 * \dot{\theta}_1 * \dot{\theta}_3 * m4 * cos(\theta_2) * cos(\theta_3)^2 * cos(\theta_4)^2 - L_4^2 * \dot{\theta}_1 * \dot{\theta}_4 * m4 * cos(\theta_2) * cos(\theta_3)^2 * cos(\theta_4)^2 + L_4^2 * \dot{\theta_3}^2 * m4 * cos(\theta_2) * sin(\theta_2) * sin(\theta_3)^2 * sin(\theta_4)^2 + L_4^2 * \dot{\theta_4}^2 * m4 * cos(\theta_2) * sin(\theta_2) * sin(\theta_3)^2 * sin(\theta_4)^2 + L_4^2 * \dot{\theta}_1 * \dot{\theta}_3 * m4 * cos(\theta_2) * cos(\theta_3)^2 * sin(\theta_4)^2 + L_4^2 * \dot{\theta}_1 * \dot{\theta}_3 * m4 * cos(\theta_2) * cos(\theta_4)^2 * sin(\theta_3)^2 + L_4^2 * \dot{\theta}_1 * \dot{\theta}_4 * m4 * cos(\theta_2) *$$

$$cos(\theta_3)^2 * sin(\theta_4)^2 + L_4^2 * \dot{\theta}_1 * \dot{\theta}_4 * m4 * cos(\theta_2) * cos(\theta_4)^2 * sin(\theta_3)^2 - L_4^2 * \dot{\theta}_1 * \dot{\theta}_3 * m4 * cos(\theta_2) * sin(\theta_3)^2 * sin(\theta_4)^2 - L_4^2 * \dot{\theta}_4 * m4 * cos(\theta_2) * sin(\theta_3)^2 * sin(\theta_4)^2 - L_4^2 * \ddot{\theta}_1 * m4 * cos(\theta_2) * cos(\theta_3) * cos(\theta_4)^2 * sin(\theta_3) - L_4^2 * \ddot{\theta}_1 * m4 * cos(\theta_2) * cos(\theta_3)^2 * cos(\theta_4) * sin(\theta_4) + L_4^2 * \ddot{\theta}_1 * m4 * cos(\theta_2) * cos(\theta_3) * sin(\theta_3) * sin(\theta_4)^2 + L_4^2 * \ddot{\theta}_1 * m4 * cos(\theta_2) * cos(\theta_4) * sin(\theta_3)^2 * sin(\theta_4) - L_3 * L_4 * \ddot{\theta}_1 * m4 * cos(\theta_2) * cos(\theta_3)^2 * sin(\theta_4) + L_2 * L_4 * {\dot{\theta}_1}^2 * m4 * cos(\theta_2) * cos(\theta_3) * sin(\theta_4) + L_2 * L_4 * {\dot{\theta}_1}^2 * m4 * cos(\theta_2) * cos(\theta_4) * sin(\theta_3) - 2 * L_3 * L_4 * {\dot{\theta}_1}^2 * m4 * cos(\theta_2) * cos(\theta_4) * sin(\theta_2) + 2 * L_3 * L_4 * {\dot{\theta}_2}^2 * m4 * cos(\theta_2) * cos(\theta_4) * sin(\theta_2) + L_3 * L_4 * \ddot{\theta}_1 * m4 * cos(\theta_2) * sin(\theta_3)^2 * sin(\theta_4) + 2 * L_3 * L_4 * \dot{\theta}_1 * \dot{\theta}_3 * m4 * cos(\theta_2) * cos(\theta_4) + L_3 * L_4 * \dot{\theta}_1 * \dot{\theta}_4 * m4 * cos(\theta_2) * cos(\theta_4) + L_4^2 * \dot{\theta}_1 * \dot{\theta}_2 * m4 * cos(\theta_3) * sin(\theta_2) * sin(\theta_3) + L_4^2 * \dot{\theta}_1 * \dot{\theta}_2 * m4 * cos(\theta_4) * sin(\theta_2) * sin(\theta_4) + L_3 * L_4 * \dot{\theta}_1 * \dot{\theta}_2 * m4 * sin(\theta_2) * sin(\theta_4) - L_4 * g * m4 * cos(\theta_2) * cos(\theta_3) * sin(\theta_1) * sin(\theta_4) - L_4 * g * m4 * cos(\theta_2) * cos(\theta_4) * sin(\theta_1) * sin(\theta_3) - 4 * L_3 * L_4 * {\dot{\theta}_2}^2 * m4 * cos(\theta_2) * cos(\theta_4) * sin(\theta_2) * sin(\theta_3)^2 - 2 * L_3 * L_4 * {\dot{\theta}_3}^2 * m4 * cos(\theta_2) * cos(\theta_4) * sin(\theta_2) * sin(\theta_3)^2 - L_3 * L_4 * {\dot{\theta}_4}^2 * m4 * cos(\theta_2) * cos(\theta_4) * sin(\theta_2) * sin(\theta_3)^2 - 2 * L_3 * L_4 * \dot{\theta}_1 * \dot{\theta}_3 * m4 * cos(\theta_2) * cos(\theta_3)^2 * cos(\theta_4) - L_3 * L_4 * \dot{\theta}_1 * \dot{\theta}_4 * m4 * cos(\theta_2) * cos(\theta_3)^2 * cos(\theta_4) - L_4^2 * \dot{\theta}_1 * \dot{\theta}_2 * m4 * cos(\theta_3) * cos(\theta_4)^2 * sin(\theta_2) * sin(\theta_3) - L_4^2 * \dot{\theta}_1 * \dot{\theta}_2 * m4 * cos(\theta_3)^2 * cos(\theta_4) * sin(\theta_2) * sin(\theta_4) + 2 * L_3 * L_4 * \dot{\theta}_1 * \dot{\theta}_3 * m4 * cos(\theta_2) * cos(\theta_4) * sin(\theta_3)^2 + L_3 * L_4 * \dot{\theta}_1 * \dot{\theta}_4 * m4 * cos(\theta_2) * cos(\theta_4) * sin(\theta_3)^2 - L_4^2 * \dot{\theta}_1 * \dot{\theta}_2 * m4 * cos(\theta_3) * sin(\theta_2) * sin(\theta_3) * sin(\theta_4)^2 - L_4^2 * \dot{\theta}_1 * \dot{\theta}_2 * m4 * cos(\theta_4) * sin(\theta_2) * sin(\theta_3)^2 * sin(\theta_4) - L_3 * L_4 * \dot{\theta}_1 * \dot{\theta}_2 * m4 * cos(\theta_3)^2 * sin(\theta_2) * sin(\theta_4) - 2 * L_3 * L_4 * \ddot{\theta}_1 * m4 * cos(\theta_2) * cos(\theta_3) * cos(\theta_4) * sin(\theta_3) - L_3 * L_4 * \dot{\theta}_1 * \dot{\theta}_2 * m4 * sin(\theta_2) * sin(\theta_3)^2 * sin(\theta_4) - L_4^2 * \dot{\theta}_2 * \dot{\theta}_3 * m4 * cos(\theta_2)^2 * cos(\theta_3) * cos(\theta_4)^2 * sin(\theta_3) - L_4^2 * \dot{\theta}_2 * \dot{\theta}_3 * m4 * cos(\theta_2)^2 * cos(\theta_3)^2 * cos(\theta_4) * sin(\theta_4) - L_4^2 * \dot{\theta}_2 * \dot{\theta}_4 * m4 * cos(\theta_2)^2 * cos(\theta_3) * cos(\theta_4)^2 * sin(\theta_3) - 2 * L_4^2 * \dot{\theta}_3 * \dot{\theta}_4 * m4 * cos(\theta_2) * cos(\theta_3)^2 * cos(\theta_4)^2 * sin(\theta_2) - L_4^2 * \dot{\theta}_2 * \dot{\theta}_4 * m4 * cos(\theta_2)^2 * cos(\theta_3)^2 * cos(\theta_4) * sin(\theta_4) - L_4^2 * \dot{\theta}_2 * \dot{\theta}_3 * m4 * cos(\theta_3) * cos(\theta_4)^2 * sin(\theta_2)^2 * sin(\theta_3) - 3 * L_4^2 * \dot{\theta}_2 * \dot{\theta}_3 * m4 * cos(\theta_2)^2 * cos(\theta_3) * sin(\theta_3) * sin(\theta_4)^2 - 3 * L_4^2 * \dot{\theta}_2 * \dot{\theta}_3 * m4 * cos(\theta_2)^2 * cos(\theta_4) * sin(\theta_3)^2 * sin(\theta_4) - L_4^2 * \dot{\theta}_2 * \dot{\theta}_3 * m4 * cos(\theta_3)^2 * cos(\theta_4) * sin(\theta_2)^2 * sin(\theta_4) - L_4^2 * \dot{\theta}_2 * \dot{\theta}_4 * m4 * cos(\theta_3) * cos(\theta_4)^2 * sin(\theta_2)^2 * sin(\theta_3) - 3 * L_4^2 * \dot{\theta}_2 * \dot{\theta}_4 * m4 * cos(\theta_2)^2 * cos(\theta_3) * sin(\theta_3) * sin(\theta_4)^2 - 2 * L_4^2 * \dot{\theta}_3 * \dot{\theta}_4 * m4 * cos(\theta_2) * cos(\theta_3)^2 * sin(\theta_2) * sin(\theta_4)^2 - 2 * L_4^2 * \dot{\theta}_3 * \dot{\theta}_4 * m4 * cos(\theta_2) * cos(\theta_4)^2 * sin(\theta_2) * sin(\theta_3)^2 - 3 * L_4^2 * \dot{\theta}_2 * \dot{\theta}_4 * m4 * cos(\theta_2)^2 * cos(\theta_4) * sin(\theta_3)^2 * sin(\theta_4) - L_4^2 * \dot{\theta}_2 * \dot{\theta}_4 * m4 * cos(\theta_3)^2 * cos(\theta_4) * sin(\theta_2)^2 * sin(\theta_4) - L_3 * L_4 * \dot{\theta}_2 * \dot{\theta}_3 * m4 * cos(\theta_2)^2 * cos(\theta_3)^2 * sin(\theta_4) - 2 * L_3 * L_4 * \dot{\theta}_2 * \dot{\theta}_4 * m4 * cos(\theta_2)^2 * cos(\theta_3)^2 * sin(\theta_4) + L_4^2 * \dot{\theta}_2 * \dot{\theta}_3 * m4 * cos(\theta_3) * sin(\theta_2)^2 * sin(\theta_3) * sin(\theta_4)^2 + L_4^2 * \dot{\theta}_2 * \dot{\theta}_3 * m4 * cos(\theta_4) * sin(\theta_2)^2 * sin(\theta_3)^2 * sin(\theta_4) + L_4^2 * \dot{\theta}_2 * \dot{\theta}_4 * m4 * cos(\theta_3) * sin(\theta_2)^2 * sin(\theta_3) * sin(\theta_4)^2 + 2 * L_4^2 * \dot{\theta}_3 * \dot{\theta}_4 * m4 * cos(\theta_2) * sin(\theta_2) * sin(\theta_3)^2 * sin(\theta_4)^2 + L_4^2 * \dot{\theta}_2 * \dot{\theta}_4 * m4 * cos(\theta_4) * sin(\theta_2)^2 * sin(\theta_3)^2 * sin(\theta_4) + L_4^2 * \ddot{\theta}_3 * m4 * cos(\theta_2) * cos(\theta_3) * cos(\theta_4)^2 * sin(\theta_2) * sin(\theta_3) + 2 * L_4^2 * \ddot{\theta}_2 * m4 * cos(\theta_2)^2 * cos(\theta_3) * cos(\theta_4) * sin(\theta_3) * sin(\theta_4) + L_4^2 * \ddot{\theta}_3 * m4 * cos(\theta_2) * cos(\theta_3)^2 * cos(\theta_4) * sin(\theta_2) * sin(\theta_4) + L_4^2 * \ddot{\theta}_4 * m4 * cos(\theta_2) * cos(\theta_3) * cos(\theta_4)^2 * sin(\theta_2) * sin(\theta_3) + L_4^2 * \ddot{\theta}_4 * m4 * cos(\theta_2) * cos(\theta_3)^2 * cos(\theta_4) * sin(\theta_2) * sin(\theta_4) - 3 * L_3 * L_4 * \dot{\theta}_2 * \dot{\theta}_3 * m4 * cos(\theta_2)^2 * sin(\theta_3)^2 * sin(\theta_4) - L_3 * L_4 * \dot{\theta}_2 * \dot{\theta}_3 * m4 * cos(\theta_3)^2 * sin(\theta_2)^2 * sin(\theta_4) - 3 * L_3 * L_4 * \dot{\theta}_2 * \dot{\theta}_4 * m4 * cos(\theta_2)^2 * cos(\theta_3)^2 * sin(\theta_4) - L_4^2 * \ddot{\theta}_3 * m4 * cos(\theta_2) * cos(\theta_3) * sin(\theta_2) * sin(\theta_3) * sin(\theta_4)^2 - L_4^2 * \ddot{\theta}_3 * m4 * cos(\theta_2) * cos(\theta_4) * sin(\theta_2) * sin(\theta_3)^2 * sin(\theta_4) - L_4^2 * \ddot{\theta}_4 * m4 * cos(\theta_2) * cos(\theta_3) * sin(\theta_2) * sin(\theta_3) * sin(\theta_4)^2 - L_4^2 * \ddot{\theta}_4 * m4 * cos(\theta_2) * cos(\theta_4) * sin(\theta_2) * sin(\theta_3)^2 * sin(\theta_4) + L_3 * L_4 * \dot{\theta}_2 * \dot{\theta}_3 * m4 * sin(\theta_2)^2 * sin(\theta_3)^2 * sin(\theta_4) + L_3 * L_4 * \dot{\theta}_2 * \dot{\theta}_4 * m4 * sin(\theta_2)^2 * sin(\theta_3)^2 * sin(\theta_4) + 2 * L_3 * L_4 * \ddot{\theta}_2 * m4 * cos(\theta_2)^2 * cos(\theta_3) * sin(\theta_3) * sin(\theta_4) + L_3 * L_4 * \ddot{\theta}_3 * m4 * cos(\theta_2) * cos(\theta_3)^2 * sin(\theta_2) * sin(\theta_4) - L_3 * L_4 * \ddot{\theta}_3 * m4 * cos(\theta_2) * sin(\theta_2) * sin(\theta_3)^2 * sin(\theta_4) - L_3 * L_4 * \ddot{\theta}_4 * m4 * cos(\theta_2) * sin(\theta_2) * sin(\theta_3)^2 * sin(\theta_4) + 2 * L_3 * L_4 * \dot{\theta}_2 * \dot{\theta}_3 * m4 * cos(\theta_3) * cos(\theta_4) * sin(\theta_3) + L_3 * L_4 * \dot{\theta}_2 * \dot{\theta}_4 * m4 * cos(\theta_3) * cos(\theta_4) * sin(\theta_3) +$$

$$2*L_3*L_4*\dot{\theta_1}^2*m4*cos(\theta_2)*cos(\theta_3)^2*cos(\theta_4)*sin(\theta_2)-2*L_3*L_4*\dot{\theta_2}^2*m4*cos(\theta_2)*cos(\theta_3)^2*cos(\theta_4)*sin(\theta_2)-2*L_3*L_4*\dot{\theta_2}*\dot{\theta_3}*m4*cos(\theta_3)*cos(\theta_4)*sin(\theta_2)^2*sin(\theta_3)-L_3*L_4*\dot{\theta_2}*\dot{\theta_4}*m4*cos(\theta_3)*cos(\theta_4)*sin(\theta_2)^2*sin(\theta_3)-2*L_3*L_4*\dot{\theta_3}*\dot{\theta_4}*m4*cos(\theta_2)*cos(\theta_4)*sin(\theta_2)*sin(\theta_3)^2+2*L_3*L_4*\ddot{\theta_3}*m4*cos(\theta_2)*cos(\theta_3)*cos(\theta_4)*sin(\theta_2)*sin(\theta_3)+L_3*L_4*\ddot{\theta_4}*m4*cos(\theta_2)*cos(\theta_3)*cos(\theta_4)*sin(\theta_2)*sin(\theta_3)-2*L_4^2*\dot{\theta_1}^2*m4*cos(\theta_2)*cos(\theta_3)*cos(\theta_4)*sin(\theta_2)*sin(\theta_3)*sin(\theta_4)-2*L_4^2*\dot{\theta_2}^2*m4*cos(\theta_2)*cos(\theta_3)*cos(\theta_4)*sin(\theta_2)*sin(\theta_3)*sin(\theta_4)-2*L_4^2*\dot{\theta_3}^2*m4*cos(\theta_2)*cos(\theta_3)*cos(\theta_4)*sin(\theta_2)*sin(\theta_3)*sin(\theta_4)-2*L_4^2*\dot{\theta_4}^2*m4*cos(\theta_2)*cos(\theta_3)*cos(\theta_4)*sin(\theta_2)*sin(\theta_3)*sin(\theta_4)-2*L_3*L_4*\dot{\theta_1}^2*m4*cos(\theta_2)*cos(\theta_3)*sin(\theta_2)*sin(\theta_3)*sin(\theta_4)-2*L_4*\dot{\theta_2}^2*m4*cos(\theta_2)*cos(\theta_3)*sin(\theta_2)*sin(\theta_3)*sin(\theta_4)-2*L_3*L_4*\dot{\theta_3}^2*m4*cos(\theta_2)*cos(\theta_3)*sin(\theta_2)*sin(\theta_3)*sin(\theta_4)-L_3*L_4*\dot{\theta_4}^2*m4*cos(\theta_2)*cos(\theta_3)*sin(\theta_2)*sin(\theta_3)*sin(\theta_4)+4*L_4^2*\dot{\theta_1}*\dot{\theta_3}*m4*cos(\theta_2)*cos(\theta_3)*cos(\theta_4)*sin(\theta_3)*sin(\theta_4)+4*L_4^2*\dot{\theta_1}*\dot{\theta_4}*m4*cos(\theta_2)*cos(\theta_3)*cos(\theta_4)*sin(\theta_3)*sin(\theta_4)+4*L_3*L_4*\dot{\theta_1}*\dot{\theta_3}*m4*cos(\theta_2)*cos(\theta_3)*sin(\theta_3)*sin(\theta_4)+2*L_3*L_4*\dot{\theta_1}*\dot{\theta_4}*m4*cos(\theta_2)*cos(\theta_3)*sin(\theta_3)*sin(\theta_4)+2*L_3*L_4*\dot{\theta_2}*\dot{\theta_3}*m4*cos(\theta_2)^2*cos(\theta_3)*cos(\theta_4)*sin(\theta_3)+L_3*L_4*\dot{\theta_2}*\dot{\theta_4}*m4*cos(\theta_2)^2*cos(\theta_3)*cos(\theta_4)*sin(\theta_3)-4*L_4^2*\dot{\theta_3}*\dot{\theta_4}*m4*cos(\theta_2)*cos(\theta_3)*cos(\theta_4)*sin(\theta_2)*sin(\theta_3)*sin(\theta_4)-2*L_3*L_4*\dot{\theta_3}*\dot{\theta_4}*m4*cos(\theta_2)*cos(\theta_3)*sin(\theta_2)*sin(\theta_3)*sin(\theta_4);$$

$$\tau_3 = I_3*\ddot{\theta}_1 + I_3*\ddot{\theta}_2 + I_4*\ddot{\theta}_1 + I_3*\ddot{\theta}_3 + I_4*\ddot{\theta}_2 + I_4*\ddot{\theta}_3 + I_4*\ddot{\theta}_4 + L_3^2*\ddot{\theta}_3*m3 - L_3^2*\ddot{\theta}_1*m3*sin(\theta_2) - 2*L_3^2*\dot{\theta}_1*\dot{\theta}_2*m3*cos(\theta_2) - L_3^2*\dot{\theta}_1*\dot{\theta}_2*m4*cos(\theta_2) + L_4^2*\dot{\theta}_1*\dot{\theta}_2*m4*cos(\theta_2) + L_3*g*m3*cos(\theta_1)*sin(\theta_3) + L_3*g*m4*cos(\theta_1)*sin(\theta_3) - L_3^2*\ddot{\theta}_3*m3*cos(\theta_2)^2*cos(\theta_3)^2 + L_3^2*\ddot{\theta}_3*m4*cos(\theta_1)^2*sin(\theta_3)^2 + L_3^2*\ddot{\theta}_3*m4*sin(\theta_1)^2*sin(\theta_3)^2 + L_2*L_3*\ddot{\theta}_1*m3*sin(\theta_3) + L_3^2*\dot{\theta}_2*\dot{\theta}_3*m3*cos(\theta_2)*sin(\theta_2) + L_3^2*\dot{\theta}_2*\dot{\theta}_3*m4*cos(\theta_2)*sin(\theta_2) - L_4^2*\dot{\theta}_2*\dot{\theta}_3*m4*cos(\theta_2)*sin(\theta_2) - L_4^2*\dot{\theta}_2*\dot{\theta}_4*m4*cos(\theta_2)*sin(\theta_2) - L_2*L_3*\dot{\theta}_1*\dot{\theta}_3*m4*cos(\theta_3) + L_4*g*m4*cos(\theta_1)*cos(\theta_3)*sin(\theta_4) + L_4*g*m4*cos(\theta_1)*cos(\theta_4)*sin(\theta_3) - L_3*g*m3*cos(\theta_3)*sin(\theta_1)*sin(\theta_2) - L_3*g*m4*cos(\theta_3)*sin(\theta_1)*sin(\theta_2) - L_3^2*\ddot{\theta}_1*m4*cos(\theta_1)^2*cos(\theta_3)^2*sin(\theta_2) + L_3^2*\dot{\theta_1}^2*m3*cos(\theta_2)^2*cos(\theta_3)*sin(\theta_3) + L_3^2*\dot{\theta_1}^2*m4*cos(\theta_2)^2*cos(\theta_3)*sin(\theta_3) - L_3^2*\dot{\theta_2}^2*m4*cos(\theta_2)^2*cos(\theta_3)*sin(\theta_3) + L_3^2*\dot{\theta_3}^2*m3*cos(\theta_2)^2*cos(\theta_3)*sin(\theta_3) + 2*L_3^2*\dot{\theta_3}^2*m4*cos(\theta_1)^2*cos(\theta_3)*sin(\theta_3) - L_4^2*\dot{\theta_1}^2*m4*cos(\theta_2)^2*cos(\theta_3)*sin(\theta_3) - L_3^2*\dot{\theta_3}^2*m4*cos(\theta_2)^2*cos(\theta_3)*sin(\theta_3) + L_4^2*\dot{\theta_2}^2*m4*cos(\theta_2)^2*cos(\theta_3)*sin(\theta_3) - L_4^2*\dot{\theta_1}^2*m4*cos(\theta_2)^2*cos(\theta_4)*sin(\theta_4) + L_4^2*\dot{\theta_3}^2*m4*cos(\theta_2)^2*cos(\theta_3)*sin(\theta_3) + L_4^2*\dot{\theta_2}^2*m4*cos(\theta_2)^2*cos(\theta_4)*sin(\theta_4) + L_4^2*\dot{\theta_4}^2*m4*cos(\theta_2)^2*cos(\theta_3)*sin(\theta_3) + L_4^2*\dot{\theta_3}^2*m4*cos(\theta_2)^2*cos(\theta_4)*sin(\theta_4) + L_4^2*\dot{\theta_4}^2*m4*cos(\theta_2)^2*cos(\theta_4)*sin(\theta_4) - L_3^2*\ddot{\theta}_1*m4*cos(\theta_1)^2*sin(\theta_2)*sin(\theta_3)^2 - L_3^2*\ddot{\theta}_1*m4*cos(\theta_3)^2*sin(\theta_1)^2*sin(\theta_2) - L_3^2*\dot{\theta_2}^2*m3*cos(\theta_3)*sin(\theta_2)^2*sin(\theta_3) + 2*L_3^2*\dot{\theta_3}^2*m4*cos(\theta_3)*sin(\theta_1)^2*sin(\theta_3) - L_3*L_4*\dot{\theta_1}^2*m4*cos(\theta_2)^2*sin(\theta_4) + L_3*L_4*\dot{\theta_2}^2*m4*cos(\theta_2)^2*sin(\theta_4) + L_3*L_4*\dot{\theta_3}^2*m4*cos(\theta_2)^2*sin(\theta_4) + 2*L_3^2*\dot{\theta}_1*\dot{\theta}_2*m3*cos(\theta_2)*cos(\theta_3)^2 + 2*L_3^2*\dot{\theta}_1*\dot{\theta}_2*m4*cos(\theta_2)*cos(\theta_3)^2 - 2*L_4^2*\dot{\theta}_1*\dot{\theta}_2*m4*cos(\theta_2)*cos(\theta_3)^2 - 2*L_4^2*\dot{\theta}_1*\dot{\theta}_2*m4*cos(\theta_2)*cos(\theta_4)^2 - L_3^2*\ddot{\theta}_1*m4*sin(\theta_1)^2*sin(\theta_2)*sin(\theta_3)^2 + L_3^2*\ddot{\theta}_3*m4*cos(\theta_1)^2*cos(\theta_3)^2*sin(\theta_2)^2 + L_4^2*\ddot{\theta}_3*m4*cos(\theta_1)^2*cos(\theta_3)^2*sin(\theta_4)^2 + L_4^2*\ddot{\theta}_3*m4*cos(\theta_1)^2*cos(\theta_4)^2*sin(\theta_3)^2 + L_4^2*\ddot{\theta}_4*m4*cos(\theta_1)^2*cos(\theta_3)^2*sin(\theta_4)^2 + L_4^2*\ddot{\theta}_4*m4*cos(\theta_1)^2*cos(\theta_4)^2*sin(\theta_3)^2 + L_3^2*\ddot{\theta}_3*m4*cos(\theta_3)^2*sin(\theta_1)^2*sin(\theta_2)^2 + L_4^2*\ddot{\theta}_3*m4*cos(\theta_3)^2*sin(\theta_1)^2*sin(\theta_4)^2 + L_4^2*\ddot{\theta}_3*m4*cos(\theta_4)^2*sin(\theta_1)^2*sin(\theta_3)^2 + L_4^2*\ddot{\theta}_4*m4*cos(\theta_3)^2*sin(\theta_1)^2*sin(\theta_4)^2 + L_4^2*\ddot{\theta}_4*m4*cos(\theta_4)^2*sin(\theta_1)^2*sin(\theta_3)^2 + L_2*L_3*\ddot{\theta}_1*m4*cos(\theta_1)^2*sin(\theta_3) + L_2*L_3*\dot{\theta_1}^2*m3*cos(\theta_3)*sin(\theta_2) + L_2*L_3*\dot{\theta_1}^2*m4*cos(\theta_3)*sin(\theta_2) + L_2*L_3*\ddot{\theta}_1*m4*sin(\theta_1)^2*sin(\theta_3) + L_4*g*m4*sin(\theta_1)*sin(\theta_2)*sin(\theta_3)*sin(\theta_4) + 2*L_3*L_4*\ddot{\theta}_3*m4*cos(\theta_1)^2*cos(\theta_4)*sin(\theta_3)^2 + L_3*L_4*\ddot{\theta}_4*m4*cos(\theta_1)^2*cos(\theta_4)*sin(\theta_3)^2 + 2*L_3*L_4*\ddot{\theta}_3*m4*cos(\theta_4)*sin(\theta_1)^2*sin(\theta_3)^2 + L_3*L_4*\ddot{\theta}_4*m4*cos(\theta_4)*sin(\theta_1)^2*sin(\theta_3)^2 + L_3^2*\dot{\theta}_2*\dot{\theta}_3*m3*cos(\theta_2)*cos(\theta_3)^2*sin(\theta_2) - 2*L_3^2*\dot{\theta}_2*\dot{\theta}_3*m4*cos(\theta_2)*cos(\theta_3)^2*sin(\theta_2) + 2*L_4^2*\dot{\theta}_2*\dot{\theta}_3*m4*cos(\theta_2)*cos(\theta_3)^2*sin(\theta_2) + 2*L_4^2*\dot{\theta}_2*\dot{\theta}_3*m4*cos(\theta_2)*cos(\theta_4)^2*sin(\theta_2) + 2*L_4^2*\dot{\theta}_2*\dot{\theta}_4*m4*cos(\theta_2)*cos(\theta_3)^2*sin(\theta_2) + 2*L_4^2*\dot{\theta}_2*\dot{\theta}_4*m4*cos(\theta_2)*cos(\theta_4)^2*sin(\theta_2) + 2*L_4^2*\dot{\theta}_3*\dot{\theta}_4*m4*cos(\theta_2)^2*cos(\theta_3)*sin(\theta_3) + 2*L_4^2*\dot{\theta}_3*\dot{\theta}_4*m4*cos(\theta_2)^2*cos(\theta_4)*sin(\theta_4) + L_2*L_3*\dot{\theta}_1*\dot{\theta}_3*m4*cos(\theta_1)^2*cos(\theta_3) - L_3^2*\dot{\theta}_2*\dot{\theta}_3*m3*cos(\theta_2)*sin(\theta_2)*sin(\theta_3)^2 + L_2*L_3*\dot{\theta}_1*\dot{\theta}_3*m4*cos(\theta_3)*sin(\theta_1)^2 + L_3*L_4*\dot{\theta}_3*\dot{\theta}_4*m4*cos(\theta_2)^2*sin(\theta_4) + L_3^2*\ddot{\theta}_2*m3*cos(\theta_2)*cos(\theta_3)*sin(\theta_2)*sin(\theta_3) - L_4^2*\ddot{\theta}_1*m4*cos(\theta_1)^2*cos(\theta_3)^2*cos(\theta_4)^2*sin(\theta_2) + L_3^2*\dot{\theta_2}^2*m4*cos(\theta_1)^2*cos(\theta_2)^2*cos(\theta_3)*sin(\theta_3) + 2*L_4^2*\dot{\theta_1}^2*m4*cos(\theta_2)^2*cos(\theta_3)*cos(\theta_4)^2*sin(\theta_3) + L_4^2*\dot{\theta_1}^2*m4*cos(\theta_2)^2*cos(\theta_3)^2*cos(\theta_4)*sin(\theta_4) - 2*L_4^2*\dot{\theta_2}^2*m4*cos(\theta_2)^2*cos(\theta_3)*cos(\theta_4)^2*sin(\theta_3) + 2*L_4^2*\dot{\theta_3}^2*m4*cos(\theta_1)^2*cos(\theta_3)*cos(\theta_4)^2*sin(\theta_3) - 2*L_4^2*\dot{\theta_2}^2*m4*cos(\theta_2)^2*cos(\theta_3)^2*cos(\theta_4)*sin(\theta_4) + 2*L_4^2*\dot{\theta_3}^2*m4*cos(\theta_1)^2*cos(\theta_3)^2*cos(\theta_4)*sin(\theta_4) - 2*L_4^2*\dot{\theta_3}^2*m4*cos(\theta_2)^2*cos(\theta_3)*cos(\theta_4)^2*sin(\theta_3) + 2*L_4^2*\dot{\theta_4}^2*m4*$$

$$cos(\theta_1)^2 * cos(\theta_3) * cos(\theta_4)^2 * sin(\theta_3) - 2 * L_4^2 * \dot{\theta_3}^2 * m4 * cos(\theta_2)^2 * cos(\theta_3)^2 * cos(\theta_4) * sin(\theta_4) + 2 * L_4^2 * \dot{\theta_4}^2 * m4 * cos(\theta_1)^2 * cos(\theta_3)^2 * cos(\theta_4) * sin(\theta_4) - 2 * L_4^2 * \dot{\theta_4}^2 * m4 * cos(\theta_2)^2 * cos(\theta_3) * cos(\theta_4)^2 * sin(\theta_3) - 2 * L_4^2 * \dot{\theta_4}^2 * m4 * cos(\theta_2)^2 * cos(\theta_3)^2 * cos(\theta_4) * sin(\theta_4) - L_4^2 * \ddot{\theta_1} * m4 * cos(\theta_1)^2 * cos(\theta_3)^2 * sin(\theta_2) * sin(\theta_4)^2 - L_4^2 * \ddot{\theta_1} * m4 * cos(\theta_1)^2 * cos(\theta_4)^2 * sin(\theta_2) * sin(\theta_3)^2 - L_4^2 * \ddot{\theta_1} * m4 * cos(\theta_3)^2 * cos(\theta_4)^2 * sin(\theta_1)^2 * sin(\theta_2) - L_3^2 * \dot{\theta_2}^2 * m4 * cos(\theta_1)^2 * cos(\theta_3) * sin(\theta_2)^2 * sin(\theta_3) + L_3^2 * \dot{\theta_2}^2 * m4 * cos(\theta_2)^2 * cos(\theta_3) * sin(\theta_1)^2 * sin(\theta_3) - 2 * L_3^2 * \dot{\theta_3}^2 * m4 * cos(\theta_1)^2 * cos(\theta_3) * sin(\theta_2)^2 * sin(\theta_3) + 2 * L_4^2 * \dot{\theta_3}^2 * m4 * cos(\theta_3) * cos(\theta_4)^2 * sin(\theta_1)^2 * sin(\theta_3) - 2 * L_4^2 * \dot{\theta_3}^2 * m4 * cos(\theta_1)^2 * cos(\theta_3) * sin(\theta_3) * sin(\theta_4)^2 - 2 * L_4^2 * \dot{\theta_3}^2 * m4 * cos(\theta_1)^2 * cos(\theta_4) * sin(\theta_3)^2 * sin(\theta_4) + 2 * L_4^2 * \dot{\theta_3}^2 * m4 * cos(\theta_3)^2 * cos(\theta_4) * sin(\theta_1)^2 * sin(\theta_4) + 2 * L_4^2 * \dot{\theta_4}^2 * m4 * cos(\theta_3) * cos(\theta_4)^2 * sin(\theta_1)^2 * sin(\theta_3) - 2 * L_4^2 * \dot{\theta_4}^2 * m4 * cos(\theta_1)^2 * cos(\theta_3) * sin(\theta_3) * sin(\theta_4)^2 - 2 * L_4^2 * \dot{\theta_4}^2 * m4 * cos(\theta_1)^2 * cos(\theta_4) * sin(\theta_3)^2 * sin(\theta_4) + 2 * L_4^2 * \dot{\theta_4}^2 * m4 * cos(\theta_3)^2 * cos(\theta_4) * sin(\theta_1)^2 * sin(\theta_4) + 2 * L_3 * L_4 * \dot{\theta_1}^2 * m4 * cos(\theta_2)^2 * cos(\theta_3)^2 * sin(\theta_4) - 2 * L_3 * L_4 * \dot{\theta_2}^2 * m4 * cos(\theta_2)^2 * cos(\theta_3)^2 * sin(\theta_4) + 2 * L_3 * L_4 * \dot{\theta_3}^2 * m4 * cos(\theta_1)^2 * cos(\theta_3)^2 * sin(\theta_4) - 2 * L_3 * L_4 * \dot{\theta_3}^2 * m4 * cos(\theta_2)^2 * cos(\theta_3)^2 * sin(\theta_4) - L_3^2 * \dot{\theta_1} * \dot{\theta_2} * m4 * cos(\theta_1)^2 * cos(\theta_2) * cos(\theta_3)^2 + 4 * L_4^2 * \dot{\theta_1} * \dot{\theta_2} * m4 * cos(\theta_2) * cos(\theta_3)^2 * cos(\theta_4)^2 - L_4^2 * \ddot{\theta_1} * m4 * cos(\theta_1)^2 * sin(\theta_2) * sin(\theta_3)^2 * sin(\theta_4)^2 - L_4^2 * \ddot{\theta_1} * m4 * cos(\theta_3)^2 * sin(\theta_1)^2 * sin(\theta_2) * sin(\theta_4)^2 - L_4^2 * \ddot{\theta_1} * m4 * cos(\theta_4)^2 * sin(\theta_1)^2 * sin(\theta_2) * sin(\theta_3)^2 - L_3^2 * \dot{\theta_2}^2 * m4 * cos(\theta_3) * sin(\theta_1)^2 * sin(\theta_2)^2 * sin(\theta_3) - 2 * L_3^2 * \dot{\theta_3}^2 * m4 * cos(\theta_3) * sin(\theta_1)^2 * sin(\theta_2)^2 * sin(\theta_3) - 2 * L_4^2 * \dot{\theta_3}^2 * m4 * cos(\theta_3) * sin(\theta_1)^2 * sin(\theta_3) * sin(\theta_4)^2 - 2 * L_4^2 * \dot{\theta_3}^2 * m4 * cos(\theta_4) * sin(\theta_1)^2 * sin(\theta_3)^2 * sin(\theta_4) - 2 * L_4^2 * \dot{\theta_4}^2 * m4 * cos(\theta_3) * sin(\theta_1)^2 * sin(\theta_3) * sin(\theta_4)^2 - 2 * L_4^2 * \dot{\theta_4}^2 * m4 * cos(\theta_4) * sin(\theta_1)^2 * sin(\theta_3)^2 * sin(\theta_4) - 2 * L_3 * L_4 * \dot{\theta_3}^2 * m4 * cos(\theta_1)^2 * sin(\theta_3)^2 * sin(\theta_4) + 2 * L_3 * L_4 * \dot{\theta_3}^2 * m4 * cos(\theta_3)^2 * sin(\theta_1)^2 * sin(\theta_4) - L_3 * L_4 * \dot{\theta_4}^2 * m4 * cos(\theta_1)^2 * sin(\theta_3)^2 * sin(\theta_4) - L_3^2 * \dot{\theta_1} * \dot{\theta_2} * m4 * cos(\theta_2) * cos(\theta_3)^2 * sin(\theta_1)^2 - L_3^2 * \dot{\theta_1} * \dot{\theta_2} * m4 * cos(\theta_1)^2 * cos(\theta_2) * sin(\theta_3)^2 - L_4^2 * \ddot{\theta_1} * m4 * sin(\theta_1)^2 * sin(\theta_2) * sin(\theta_3)^2 * sin(\theta_4)^2 - 2 * L_3 * L_4 * \dot{\theta_3}^2 * m4 * sin(\theta_1)^2 * sin(\theta_3)^2 * sin(\theta_4) - L_3 * L_4 * \dot{\theta_4}^2 * m4 * sin(\theta_1)^2 * sin(\theta_3)^2 * sin(\theta_4) - L_3^2 * \dot{\theta_1} * \dot{\theta_2} * m4 * cos(\theta_2) * sin(\theta_1)^2 * sin(\theta_3)^2 + L_2 * L_4 * \ddot{\theta_1} * m4 * cos(\theta_1)^2 * cos(\theta_3) * sin(\theta_4) + L_2 * L_4 * \ddot{\theta_1} * m4 * cos(\theta_1)^2 * cos(\theta_4) * sin(\theta_3) + L_2 * L_4 * \dot{\theta_1}^2 * m4 * cos(\theta_3) * cos(\theta_4) * sin(\theta_2) + L_4^2 * \ddot{\theta_3} * m4 * cos(\theta_1)^2 * cos(\theta_3)^2 * cos(\theta_4)^2 * sin(\theta_2)^2 + L_4^2 * \ddot{\theta_4} * m4 * cos(\theta_1)^2 * cos(\theta_3)^2 * cos(\theta_4)^2 * sin(\theta_2)^2 + L_2 * L_4 * \ddot{\theta_1} * m4 * cos(\theta_3) * sin(\theta_1)^2 * sin(\theta_4) + L_2 * L_4 * \ddot{\theta_1} * m4 * cos(\theta_4) * sin(\theta_1)^2 * sin(\theta_3) + L_4^2 * \ddot{\theta_3} * m4 * cos(\theta_3)^2 * cos(\theta_4)^2 * sin(\theta_1)^2 * sin(\theta_2)^2 + L_4^2 * \ddot{\theta_4} * m4 * cos(\theta_3)^2 * cos(\theta_4)^2 * sin(\theta_1)^2 * sin(\theta_2)^2 - 2 * L_3 * L_4 * \dot{\theta_1} * \dot{\theta_2} * m4 * cos(\theta_2) * cos(\theta_4) - L_2 * L_4 * \dot{\theta_1} * \dot{\theta_3} * m4 * cos(\theta_3) * cos(\theta_4) - L_2 * L_4 * \dot{\theta_1} * \dot{\theta_4} * m4 * cos(\theta_3) * cos(\theta_4) - L_2 * L_4 * \dot{\theta_1}^2 * m4 * sin(\theta_2) * sin(\theta_3) * sin(\theta_4) + L_4^2 * \ddot{\theta_3} * m4 * cos(\theta_1)^2 * sin(\theta_2)^2 * sin(\theta_3)^2 * sin(\theta_4)^2 + L_4^2 * \ddot{\theta_4} * m4 * cos(\theta_1)^2 * sin(\theta_2)^2 * sin(\theta_3)^2 * sin(\theta_4)^2 + L_4^2 * \ddot{\theta_3} * m4 * sin(\theta_1)^2 * sin(\theta_2)^2 * sin(\theta_3)^2 * sin(\theta_4)^2 + L_4^2 * \ddot{\theta_4} * m4 * sin(\theta_1)^2 * sin(\theta_2)^2 * sin(\theta_3)^2 * sin(\theta_4)^2 + L_2 * L_4 * \dot{\theta_1} * \dot{\theta_3} * m4 * sin(\theta_3) * sin(\theta_4) + L_2 * L_4 * \dot{\theta_1} * \dot{\theta_4} * m4 * sin(\theta_3) * sin(\theta_4) - L_4 * g * m4 * cos(\theta_3) * cos(\theta_4) * sin(\theta_1) * sin(\theta_2) - 2 * L_3 * L_4 * \ddot{\theta_1} * m4 * cos(\theta_1)^2 * cos(\theta_4) * sin(\theta_2) * sin(\theta_3)^2 - 2 * L_3 * L_4 * \ddot{\theta_1} * m4 * cos(\theta_3)^2 * cos(\theta_4) * sin(\theta_1)^2 * sin(\theta_2) + 4 * L_3 * L_4 * \dot{\theta_3}^2 * m4 * cos(\theta_3) * cos(\theta_4) * sin(\theta_1)^2 * sin(\theta_3) + L_3 * L_4 * \dot{\theta_4}^2 * m4 * cos(\theta_3) * cos(\theta_4) * sin(\theta_1)^2 * sin(\theta_3) + L_2 * L_4 * \dot{\theta_1} * \dot{\theta_3} * m4 * cos(\theta_1)^2 * cos(\theta_3) * cos(\theta_4) + L_2 * L_4 * \dot{\theta_1} * \dot{\theta_4} * m4 * cos(\theta_1)^2 * cos(\theta_3) * cos(\theta_4) + 4 * L_3 * L_4 * \dot{\theta_1} * \dot{\theta_2} * m4 * cos(\theta_2) * cos(\theta_3)^2 * cos(\theta_4) - 2 * L_3 * L_4 * \ddot{\theta_1} * m4 * cos(\theta_4) * sin(\theta_1)^2 * sin(\theta_2) * sin(\theta_3)^2 + L_2 * L_4 * \dot{\theta_1} * \dot{\theta_3} * m4 * cos(\theta_3) * cos(\theta_4) *$$

$$sin(\theta_1)^2 + L_2 * L_4 * \dot{\theta}_1 * \dot{\theta}_4 * m4 * cos(\theta_3) * cos(\theta_4) * sin(\theta_1)^2 - L_2 * L_4 * \dot{\theta}_1 * \dot{\theta}_3 * m4 * cos(\theta_1)^2 * sin(\theta_3) * sin(\theta_4) - L_2 * L_4 * \dot{\theta}_1 * \dot{\theta}_4 * m4 * cos(\theta_1)^2 * sin(\theta_3) * sin(\theta_4) - L_2 * L_4 * \dot{\theta}_1 * \dot{\theta}_3 * m4 * sin(\theta_1)^2 * sin(\theta_3) * sin(\theta_4) - L_2 * L_4 * \dot{\theta}_1 * \dot{\theta}_4 * m4 * sin(\theta_1)^2 * sin(\theta_3) * sin(\theta_4) + 2 * L_3 * L_4 * \ddot{\theta}_3 * m4 * cos(\theta_1)^2 * cos(\theta_3)^2 * cos(\theta_4) * sin(\theta_2)^2 + L_3 * L_4 * \ddot{\theta}_4 * m4 * cos(\theta_1)^2 * cos(\theta_3)^2 * cos(\theta_4) * sin(\theta_2)^2 + 2 * L_3 * L_4 * \ddot{\theta}_3 * m4 * cos(\theta_3)^2 * cos(\theta_4) * sin(\theta_1)^2 * sin(\theta_2)^2 + L_3 * L_4 * \ddot{\theta}_4 * m4 * cos(\theta_3)^2 * cos(\theta_4) * sin(\theta_1)^2 * sin(\theta_2)^2 + 3 * L_3^2 * \dot{\theta}_2 * \dot{\theta}_3 * m4 * cos(\theta_1)^2 * cos(\theta_2) * cos(\theta_3)^2 * sin(\theta_2) - 4 * L_4^2 * \dot{\theta}_2 * \dot{\theta}_3 * m4 * cos(\theta_2) * cos(\theta_3)^2 * cos(\theta_4)^2 * sin(\theta_2) - 4 * L_4^2 * \dot{\theta}_2 * \dot{\theta}_4 * m4 * cos(\theta_2) * cos(\theta_3)^2 * cos(\theta_4)^2 * sin(\theta_2) + 4 * L_4^2 * \dot{\theta}_3 * \dot{\theta}_4 * m4 * cos(\theta_1)^2 * cos(\theta_3) * cos(\theta_4)^2 * sin(\theta_3) + 4 * L_4^2 * \dot{\theta}_3 * \dot{\theta}_4 * m4 * cos(\theta_1)^2 * cos(\theta_3)^2 * cos(\theta_4) * sin(\theta_4) - 4 * L_4^2 * \dot{\theta}_3 * \dot{\theta}_4 * m4 * cos(\theta_2)^2 * cos(\theta_3) * cos(\theta_4)^2 * sin(\theta_3) - 4 * L_4^2 * \dot{\theta}_3 * \dot{\theta}_4 * m4 * cos(\theta_2)^2 * cos(\theta_3)^2 * cos(\theta_4) * sin(\theta_4) + 3 * L_3^2 * \dot{\theta}_2 * \dot{\theta}_3 * m4 * cos(\theta_2) * cos(\theta_3)^2 * sin(\theta_1)^2 * sin(\theta_2) - L_3^2 * \dot{\theta}_2 * \dot{\theta}_3 * m4 * cos(\theta_1)^2 * cos(\theta_2) * sin(\theta_2) * sin(\theta_3)^2 + 4 * L_4^2 * \dot{\theta}_3 * \dot{\theta}_4 * m4 * cos(\theta_3) * cos(\theta_4)^2 * sin(\theta_1)^2 * sin(\theta_3) - 4 * L_4^2 * \dot{\theta}_3 * \dot{\theta}_4 * m4 * cos(\theta_1)^2 * cos(\theta_3) * sin(\theta_3) * sin(\theta_4)^2 - 4 * L_4^2 * \dot{\theta}_3 * \dot{\theta}_4 * m4 * cos(\theta_1)^2 * cos(\theta_4) * sin(\theta_3)^2 * sin(\theta_4) + 4 * L_4^2 * \dot{\theta}_3 * \dot{\theta}_4 * m4 * cos(\theta_3)^2 * cos(\theta_4) * sin(\theta_1)^2 * sin(\theta_4) + L_3 * L_4 * \dot{\theta}_3 * \dot{\theta}_4 * m4 * cos(\theta_1)^2 * cos(\theta_3)^2 * sin(\theta_4) - 2 * L_3 * L_4 * \dot{\theta}_3 * \dot{\theta}_4 * m4 * cos(\theta_2)^2 * cos(\theta_3)^2 * sin(\theta_4) - L_3^2 * \dot{\theta}_2 * \dot{\theta}_3 * m4 * cos(\theta_2) * sin(\theta_1)^2 * sin(\theta_2) * sin(\theta_3)^2 - 4 * L_4^2 * \dot{\theta}_3 * \dot{\theta}_4 * m4 * cos(\theta_3) * sin(\theta_1)^2 * sin(\theta_3) * sin(\theta_4)^2 - 4 * L_4^2 * \dot{\theta}_3 * \dot{\theta}_4 * m4 * cos(\theta_4) * sin(\theta_1)^2 * sin(\theta_3)^2 * sin(\theta_4) + L_3^2 * \ddot{\theta}_2 * m4 * cos(\theta_1)^2 * cos(\theta_2) * cos(\theta_3) * sin(\theta_2) * sin(\theta_3) + 2 * L_4^2 * \ddot{\theta}_3 * m4 * cos(\theta_1)^2 * cos(\theta_3) * cos(\theta_4) * sin(\theta_3) * sin(\theta_4) + 2 * L_4^2 * \ddot{\theta}_4 * m4 * cos(\theta_1)^2 * cos(\theta_3) * cos(\theta_4) * sin(\theta_3) * sin(\theta_4) - 3 * L_3 * L_4 * \dot{\theta}_3 * \dot{\theta}_4 * m4 * cos(\theta_1)^2 * sin(\theta_3)^2 * sin(\theta_4) + L_3 * L_4 * \dot{\theta}_3 * \dot{\theta}_4 * m4 * cos(\theta_3)^2 * sin(\theta_1)^2 * sin(\theta_4) + L_4^2 * \dot{\theta_2}^2 * m4 * cos(\theta_1)^2 * cos(\theta_2)^2 * cos(\theta_3) * cos(\theta_4)^2 * sin(\theta_3) + L_4^2 * \dot{\theta_2}^2 * m4 * cos(\theta_1)^2 * cos(\theta_2)^2 * cos(\theta_3)^2 * cos(\theta_4) * sin(\theta_4) + L_3^2 * \ddot{\theta}_2 * m4 * cos(\theta_2) * cos(\theta_3) * sin(\theta_1)^2 * sin(\theta_2) * sin(\theta_3) + 2 * L_4^2 * \ddot{\theta}_3 * m4 * cos(\theta_3) * cos(\theta_4) * sin(\theta_1)^2 * sin(\theta_3) * sin(\theta_4) + 2 * L_4^2 * \ddot{\theta}_4 * m4 * cos(\theta_3) * cos(\theta_4) * sin(\theta_1)^2 * sin(\theta_3) * sin(\theta_4) - 3 * L_3 * L_4 * \dot{\theta}_3 * \dot{\theta}_4 * m4 * sin(\theta_1)^2 * sin(\theta_3)^2 * sin(\theta_4) + 2 * L_3 * L_4 * \ddot{\theta}_3 * m4 * cos(\theta_1)^2 * cos(\theta_3) * sin(\theta_3) * sin(\theta_4) + L_3 * L_4 * \ddot{\theta}_4 * m4 * cos(\theta_1)^2 * cos(\theta_3) * sin(\theta_3) * sin(\theta_4) - L_4^2 * \dot{\theta_2}^2 * m4 * cos(\theta_1)^2 * cos(\theta_3) * cos(\theta_4)^2 * sin(\theta_2)^2 * sin(\theta_3) - L_4^2 * \dot{\theta_2}^2 * m4 * cos(\theta_1)^2 * cos(\theta_2)^2 * cos(\theta_3) * sin(\theta_3) * sin(\theta_4)^2 + L_4^2 * \dot{\theta_2}^2 * m4 * cos(\theta_2)^2 * cos(\theta_3) * cos(\theta_4)^2 * sin(\theta_1)^2 * sin(\theta_3) - L_4^2 * \dot{\theta_2}^2 * m4 * cos(\theta_1)^2 * cos(\theta_2)^2 * cos(\theta_4) * sin(\theta_3)^2 * sin(\theta_4) - L_4^2 * \dot{\theta_2}^2 * m4 * cos(\theta_1)^2 * cos(\theta_3)^2 * cos(\theta_4) * sin(\theta_2)^2 * sin(\theta_4) + L_4^2 * \dot{\theta_2}^2 * m4 * cos(\theta_2)^2 * cos(\theta_3)^2 * cos(\theta_4) * sin(\theta_1)^2 * sin(\theta_4) - 2 * L_4^2 * \dot{\theta_3}^2 * m4 * cos(\theta_1)^2 * cos(\theta_3) * cos(\theta_4)^2 * sin(\theta_2)^2 * sin(\theta_3) - 2 * L_4^2 * \dot{\theta_3}^2 * m4 * cos(\theta_1)^2 * cos(\theta_3)^2 * cos(\theta_4) * sin(\theta_2)^2 * sin(\theta_4) - 2 * L_4^2 * \dot{\theta_4}^2 * m4 * cos(\theta_1)^2 * cos(\theta_3) * cos(\theta_4)^2 * sin(\theta_2)^2 * sin(\theta_3) - 2 * L_4^2 * \dot{\theta_4}^2 * m4 * cos(\theta_1)^2 * cos(\theta_3)^2 * cos(\theta_4) * sin(\theta_2)^2 * sin(\theta_4) + L_3 * L_4 * \dot{\theta_2}^2 * m4 * cos(\theta_1)^2 * cos(\theta_2)^2 * cos(\theta_3)^2 * sin(\theta_4) + 2 * L_3 * L_4 * \ddot{\theta}_3 * m4 * cos(\theta_3) * sin(\theta_1)^2 * sin(\theta_3) * sin(\theta_4) + L_3 * L_4 * \ddot{\theta}_4 * m4 * cos(\theta_3) * sin(\theta_1)^2 * sin(\theta_3) * sin(\theta_4) - L_4^2 * \dot{\theta}_1 * \dot{\theta}_2 * m4 * cos(\theta_1)^2 * cos(\theta_2) * cos(\theta_3)^2 * cos(\theta_4)^2 - L_4^2 * \dot{\theta_2}^2 * m4 * cos(\theta_3) * cos(\theta_4)^2 * sin(\theta_1)^2 * sin(\theta_2)^2 * sin(\theta_3) + L_4^2 * \dot{\theta_2}^2 * m4 * cos(\theta_1)^2 * cos(\theta_3) * sin(\theta_2)^2 * sin(\theta_3) * sin(\theta_4)^2 - L_4^2 * \dot{\theta_2}^2 * m4 * cos(\theta_2)^2 * cos(\theta_3) * sin(\theta_1)^2 * sin(\theta_3) * sin(\theta_4)^2 + L_4^2 * \dot{\theta_2}^2 * m4 * cos(\theta_1)^2 * cos(\theta_4) * sin(\theta_2)^2 * sin(\theta_3)^2 * sin(\theta_4) - L_4^2 * \dot{\theta_2}^2 * m4 * cos(\theta_2)^2 * cos(\theta_4) * sin(\theta_1)^2 * sin(\theta_3)^2 * sin(\theta_4) - L_4^2 * \dot{\theta_2}^2 * m4 * cos(\theta_3)^2 * cos(\theta_4) * sin(\theta_1)^2 * sin(\theta_2)^2 * sin(\theta_4) - 2 * L_4^2 * \dot{\theta_3}^2 * m4 * cos(\theta_3) * cos(\theta_4)^2 * sin(\theta_1)^2 * sin(\theta_2)^2 * sin(\theta_3) + 2 * L_4^2 * \dot{\theta_3}^2 * m4 * cos(\theta_1)^2 * cos(\theta_3) * sin(\theta_2)^2 * sin(\theta_3) * sin(\theta_4)^2 + 2 * L_4^2 * \dot{\theta_3}^2 * m4 * cos(\theta_1)^2 * cos(\theta_4) * sin(\theta_2)^2 * sin(\theta_3)^2 * sin(\theta_4) - 2 * L_4^2 * \dot{\theta_3}^2 * m4 * cos(\theta_3)^2 * cos(\theta_4) * sin(\theta_1)^2 * sin(\theta_2)^2 * sin(\theta_4) - 2 * L_4^2 * \dot{\theta_4}^2 * m4 * cos(\theta_3) *$$

$$cos(\theta_4)^2 * sin(\theta_1)^2 * sin(\theta_2)^2 * sin(\theta_3) + 2 * L_4^2 * \dot{\theta_4}^2 * m4 * cos(\theta_1)^2 * cos(\theta_3) * sin(\theta_2)^2 * sin(\theta_3) * sin(\theta_4)^2 + 2 * L_4^2 * \dot{\theta_4}^2 * m4 * cos(\theta_1)^2 * cos(\theta_4) * sin(\theta_2)^2 * sin(\theta_3)^2 * sin(\theta_4) - 2 * L_4^2 * \dot{\theta_4}^2 * m4 * cos(\theta_3)^2 * cos(\theta_4) * sin(\theta_1)^2 * sin(\theta_2)^2 * sin(\theta_4) + 2 * L_3 * L_4 * \dot{\theta_2} * \dot{\theta_3} * m4 * cos(\theta_2) * cos(\theta_4) * sin(\theta_2) + L_3 * L_4 * \dot{\theta_2} * \dot{\theta_4} * m4 * cos(\theta_2) * cos(\theta_4) * sin(\theta_2) - L_3 * L_4 * \dot{\theta_2}^2 * m4 * cos(\theta_1)^2 * cos(\theta_2)^2 * sin(\theta_3)^2 * sin(\theta_4) - L_3 * L_4 * \dot{\theta_2}^2 * m4 * cos(\theta_1)^2 * cos(\theta_3)^2 * sin(\theta_2)^2 * sin(\theta_4) + L_3 * L_4 * \dot{\theta_2}^2 * m4 * cos(\theta_2)^2 * cos(\theta_3)^2 * sin(\theta_1)^2 * sin(\theta_4) - 2 * L_3 * L_4 * \dot{\theta_3}^2 * m4 * cos(\theta_1)^2 * cos(\theta_3)^2 * sin(\theta_2)^2 * sin(\theta_4) - L_3 * L_4 * \dot{\theta_4}^2 * m4 * cos(\theta_1)^2 * cos(\theta_3)^2 * sin(\theta_2)^2 * sin(\theta_4) - L_4^2 * \dot{\theta_1} * \dot{\theta_2} * m4 * cos(\theta_2) * cos(\theta_3)^2 * cos(\theta_4)^2 * sin(\theta_1)^2 - L_4^2 * \dot{\theta_1} * \dot{\theta_2} * m4 * cos(\theta_1)^2 * cos(\theta_2) * cos(\theta_3)^2 * sin(\theta_4)^2 - L_4^2 * \dot{\theta_1} * \dot{\theta_2} * m4 * cos(\theta_1)^2 * cos(\theta_2) * cos(\theta_4)^2 * sin(\theta_3)^2 + L_4^2 * \dot{\theta_2}^2 * m4 * cos(\theta_3) * sin(\theta_1)^2 * sin(\theta_2)^2 * sin(\theta_3) * sin(\theta_4)^2 + L_4^2 * \dot{\theta_2}^2 * m4 * cos(\theta_4) * sin(\theta_1)^2 * sin(\theta_2)^2 * sin(\theta_3)^2 * sin(\theta_4) + 2 * L_4^2 * \dot{\theta_3}^2 * m4 * cos(\theta_3) * sin(\theta_1)^2 * sin(\theta_2)^2 * sin(\theta_3) * sin(\theta_4)^2 + 2 * L_4^2 * \dot{\theta_3}^2 * m4 * cos(\theta_4) * sin(\theta_1)^2 * sin(\theta_2)^2 * sin(\theta_3)^2 * sin(\theta_4) + 2 * L_4^2 * \dot{\theta_4}^2 * m4 * cos(\theta_3) * sin(\theta_1)^2 * sin(\theta_2)^2 * sin(\theta_3) * sin(\theta_4)^2 + 2 * L_4^2 * \dot{\theta_4}^2 * m4 * cos(\theta_4) * sin(\theta_1)^2 * sin(\theta_2)^2 * sin(\theta_3)^2 * sin(\theta_4) + L_3 * L_4 * \dot{\theta_2}^2 * m4 * cos(\theta_1)^2 * sin(\theta_2)^2 * sin(\theta_3)^2 * sin(\theta_4) - L_3 * L_4 * \dot{\theta_2}^2 * m4 * cos(\theta_2)^2 * sin(\theta_1)^2 * sin(\theta_3)^2 * sin(\theta_4) - L_3 * L_4 * \dot{\theta_2}^2 * m4 * cos(\theta_3)^2 * sin(\theta_1)^2 * sin(\theta_2)^2 * sin(\theta_4) + 2 * L_3 * L_4 * \dot{\theta_3}^2 * m4 * cos(\theta_1)^2 * sin(\theta_2)^2 * sin(\theta_3)^2 * sin(\theta_4) - 2 * L_3 * L_4 * \dot{\theta_3}^2 * m4 * cos(\theta_3)^2 * sin(\theta_1)^2 * sin(\theta_2)^2 * sin(\theta_4) - L_3 * L_4 * \dot{\theta_4}^2 * m4 * cos(\theta_3)^2 * sin(\theta_1)^2 * sin(\theta_2)^2 * sin(\theta_4) - L_4^2 * \dot{\theta_1} * \dot{\theta_2} * m4 * cos(\theta_2) * cos(\theta_3)^2 * sin(\theta_1)^2 * sin(\theta_4)^2 - L_4^2 * \dot{\theta_1} * \dot{\theta_2} * m4 * cos(\theta_2) * cos(\theta_4)^2 * sin(\theta_1)^2 * sin(\theta_3)^2 - L_4^2 * \dot{\theta_1} * \dot{\theta_2} * m4 * cos(\theta_1)^2 * cos(\theta_2) * sin(\theta_3)^2 * sin(\theta_4)^2 + L_3 * L_4 * \dot{\theta_2}^2 * m4 * sin(\theta_1)^2 * sin(\theta_2)^2 * sin(\theta_3)^2 * sin(\theta_4) + 2 * L_3 * L_4 * \dot{\theta_3}^2 * m4 * sin(\theta_1)^2 * sin(\theta_2)^2 * sin(\theta_3)^2 * sin(\theta_4) - L_4^2 * \dot{\theta_1} * \dot{\theta_2} * m4 * cos(\theta_2) * sin(\theta_1)^2 * sin(\theta_3)^2 * sin(\theta_4)^2 - 2 * L_3 * L_4 * \ddot{\theta_1} * m4 * cos(\theta_1)^2 * cos(\theta_3)^2 * cos(\theta_4) * sin(\theta_2) + 2 * L_3 * L_4 * \dot{\theta_1}^2 * m4 * cos(\theta_2)^2 * cos(\theta_3) * cos(\theta_4) * sin(\theta_3) - 2 * L_3 * L_4 * \dot{\theta_2}^2 * m4 * cos(\theta_2)^2 * cos(\theta_3) * cos(\theta_4) * sin(\theta_3) + 4 * L_3 * L_4 * \dot{\theta_3}^2 * m4 * cos(\theta_1)^2 * cos(\theta_3) * cos(\theta_4) * sin(\theta_3) - 2 * L_3 * L_4 * \dot{\theta_3}^2 * m4 * cos(\theta_2)^2 * cos(\theta_3) * cos(\theta_4) * sin(\theta_3) + L_3 * L_4 * \dot{\theta_4}^2 * m4 * cos(\theta_1)^2 * cos(\theta_3) * cos(\theta_4) * sin(\theta_3) + 4 * L_3 * L_4 * \dot{\theta_3} * \dot{\theta_4} * m4 * cos(\theta_3) * cos(\theta_4) * sin(\theta_1)^2 * sin(\theta_3) + 2 * L_3 * L_4 * \dot{\theta_2}^2 * m4 * cos(\theta_1)^2 * cos(\theta_2)^2 * cos(\theta_3) * cos(\theta_4) * sin(\theta_3) - 2 * L_3 * L_4 * \dot{\theta_2}^2 * m4 * cos(\theta_1)^2 * cos(\theta_3) * cos(\theta_4) * sin(\theta_2)^2 * sin(\theta_3) + 2 * L_3 * L_4 * \dot{\theta_2}^2 * m4 * cos(\theta_2)^2 * cos(\theta_3) * cos(\theta_4) * sin(\theta_1)^2 * sin(\theta_3) - 4 * L_3 * L_4 * \dot{\theta_3}^2 * m4 * cos(\theta_1)^2 * cos(\theta_3) * cos(\theta_4) * sin(\theta_2)^2 * sin(\theta_3) - L_3 * L_4 * \dot{\theta_4}^2 * m4 * cos(\theta_1)^2 * cos(\theta_3) * cos(\theta_4) * sin(\theta_2)^2 * sin(\theta_3) - 2 * L_3 * L_4 * \dot{\theta_1} * \dot{\theta_2} * m4 * cos(\theta_1)^2 * cos(\theta_2) * cos(\theta_3)^2 * cos(\theta_4) - 2 * L_3 * L_4 * \dot{\theta_2}^2 * m4 * cos(\theta_3) * cos(\theta_4) * sin(\theta_1)^2 * sin(\theta_2)^2 * sin(\theta_3) - 4 * L_3 * L_4 * \dot{\theta_3}^2 * m4 * cos(\theta_3) * cos(\theta_4) * sin(\theta_1)^2 * sin(\theta_2)^2 * sin(\theta_3) - L_3 * L_4 * \dot{\theta_4}^2 * m4 * cos(\theta_3) * cos(\theta_4) * sin(\theta_1)^2 * sin(\theta_2)^2 * sin(\theta_3) - 2 * L_3 * L_4 * \dot{\theta_1} * \dot{\theta_2} * m4 * cos(\theta_2) * cos(\theta_3)^2 * cos(\theta_4) * sin(\theta_1)^2 - 2 * L_3 * L_4 * \dot{\theta_1} * \dot{\theta_2} * m4 * cos(\theta_1)^2 * cos(\theta_2) * cos(\theta_4) * sin(\theta_3)^2 - 2 * L_3 * L_4 * \dot{\theta_1} * \dot{\theta_2} * m4 * cos(\theta_2) * cos(\theta_4) * sin(\theta_1)^2 * sin(\theta_3)^2 + 2 * L_3 * L_4 * \dot{\theta_1} * \dot{\theta_4} * m4 * cos(\theta_1)^2 * cos(\theta_3)^2 * sin(\theta_2) * sin(\theta_4) + 2 * L_3 * L_4 * \dot{\theta_1} * \dot{\theta_4} * m4 * cos(\theta_1)^2 * sin(\theta_2) * sin(\theta_3)^2 * sin(\theta_4) + 2 * L_3 * L_4 * \dot{\theta_1} * \dot{\theta_4} * m4 * cos(\theta_3)^2 * sin(\theta_1)^2 * sin(\theta_2) * sin(\theta_4) + 2 * L_3 * L_4 * \dot{\theta_1} * \dot{\theta_4} * m4 * sin(\theta_1)^2 * sin(\theta_2) * sin(\theta_3)^2 * sin(\theta_4) - 4 * L_4^2 * \dot{\theta_1} * \dot{\theta_2} * m4 * cos(\theta_2) * cos(\theta_3) * cos(\theta_4) * sin(\theta_3) * sin(\theta_4) + 3 * L_4^2 * \dot{\theta_2} * \dot{\theta_3} * m4 * cos(\theta_1)^2 * cos(\theta_2) * cos(\theta_3)^2 * cos(\theta_4)^2 * sin(\theta_2) + 3 * L_4^2 * \dot{\theta_2} * \dot{\theta_4} * m4 * cos(\theta_1)^2 * cos(\theta_2) * cos(\theta_3)^2 * cos(\theta_4)^2 * sin(\theta_2) - 4 * L_3 * L_4 * \dot{\theta_1} * \dot{\theta_2} * m4 * cos(\theta_2) * cos(\theta_3) * sin(\theta_3) * sin(\theta_4) + 3 * L_4^2 * \dot{\theta_2} * \dot{\theta_3} * m4 * cos(\theta_2) * cos(\theta_3)^2 * cos(\theta_4)^2 * sin(\theta_1)^2 * sin(\theta_2) - L_4^2 * \dot{\theta_2} * \dot{\theta_3} * m4 * cos(\theta_1)^2 *$$

$$cos(\theta_2)*cos(\theta_3)^2*sin(\theta_2)*sin(\theta_4)^2-L_4^2*\dot{\theta}_2*\dot{\theta}_3*m4*cos(\theta_1)^2*cos(\theta_2)*cos(\theta_4)^2*sin(\theta_2)*sin(\theta_3)^2+3*L_4^2*\dot{\theta}_2*\dot{\theta}_4*m4*cos(\theta_2)*cos(\theta_3)^2*cos(\theta_4)^2*sin(\theta_1)^2*sin(\theta_2)-L_4^2*\dot{\theta}_2*\dot{\theta}_4*m4*cos(\theta_1)^2*cos(\theta_2)*cos(\theta_3)^2*sin(\theta_2)*sin(\theta_4)^2-L_4^2*\dot{\theta}_2*\dot{\theta}_4*m4*cos(\theta_1)^2*cos(\theta_2)*cos(\theta_4)^2*sin(\theta_2)*sin(\theta_3)^2-4*L_4^2*\dot{\theta}_3*\dot{\theta}_4*m4*cos(\theta_1)^2*cos(\theta_3)*cos(\theta_4)^2*sin(\theta_2)^2*sin(\theta_3)-4*L_4^2*\dot{\theta}_3*\dot{\theta}_4*m4*cos(\theta_1)^2*cos(\theta_3)^2*cos(\theta_4)*sin(\theta_2)^2*sin(\theta_4)-L_4^2*\dot{\theta}_2*\dot{\theta}_3*m4*cos(\theta_2)*cos(\theta_3)^2*sin(\theta_1)^2*sin(\theta_2)*sin(\theta_4)^2-L_4^2*\dot{\theta}_2*\dot{\theta}_3*m4*cos(\theta_2)*cos(\theta_4)^2*sin(\theta_1)^2*sin(\theta_2)*sin(\theta_3)^2+3*L_4^2*\dot{\theta}_2*\dot{\theta}_3*m4*cos(\theta_1)^2*cos(\theta_2)*sin(\theta_2)*sin(\theta_3)^2*sin(\theta_4)^2-L_4^2*\dot{\theta}_2*\dot{\theta}_4*m4*cos(\theta_2)*cos(\theta_3)^2*sin(\theta_1)^2*sin(\theta_2)*sin(\theta_4)^2-L_4^2*\dot{\theta}_2*\dot{\theta}_4*m4*cos(\theta_2)*cos(\theta_4)^2*sin(\theta_1)^2*sin(\theta_2)*sin(\theta_3)^2+3*L_4^2*\dot{\theta}_2*\dot{\theta}_4*m4*cos(\theta_1)^2*cos(\theta_2)*sin(\theta_2)*sin(\theta_3)^2*sin(\theta_4)^2-4*L_4^2*\dot{\theta}_3*\dot{\theta}_4*m4*cos(\theta_3)*cos(\theta_4)^2*sin(\theta_1)^2*sin(\theta_2)^2*sin(\theta_3)+4*L_4^2*\dot{\theta}_3*\dot{\theta}_4*m4*cos(\theta_1)^2*cos(\theta_3)*sin(\theta_2)^2*sin(\theta_3)*sin(\theta_4)^2+4*L_4^2*\dot{\theta}_3*\dot{\theta}_4*m4*cos(\theta_1)^2*cos(\theta_4)*sin(\theta_2)^2*sin(\theta_3)^2*sin(\theta_4)-4*L_4^2*\dot{\theta}_3*\dot{\theta}_4*m4*cos(\theta_3)^2*cos(\theta_4)*sin(\theta_1)^2*sin(\theta_2)^2*sin(\theta_4)+L_4^2*\ddot{\theta}_2*m4*cos(\theta_1)^2*cos(\theta_2)*cos(\theta_3)*cos(\theta_4)^2*sin(\theta_2)*sin(\theta_3)+L_4^2*\ddot{\theta}_2*m4*cos(\theta_1)^2*cos(\theta_2)*cos(\theta_3)^2*cos(\theta_4)*sin(\theta_2)*sin(\theta_4)-3*L_3*L_4*\dot{\theta}_3*\dot{\theta}_4*m4*cos(\theta_1)^2*cos(\theta_3)^2*sin(\theta_2)^2*sin(\theta_4)+3*L_4^2*\dot{\theta}_2*\dot{\theta}_3*m4*cos(\theta_2)*sin(\theta_1)^2*sin(\theta_2)*sin(\theta_3)^2*sin(\theta_4)^2+3*L_4^2*\dot{\theta}_2*\dot{\theta}_4*m4*cos(\theta_2)*sin(\theta_1)^2*sin(\theta_2)*sin(\theta_3)^2*sin(\theta_4)^2+4*L_4^2*\dot{\theta}_3*\dot{\theta}_4*m4*cos(\theta_3)*sin(\theta_1)^2*sin(\theta_2)^2*sin(\theta_3)*sin(\theta_4)^2+4*L_4^2*\dot{\theta}_3*\dot{\theta}_4*m4*cos(\theta_4)*sin(\theta_1)^2*sin(\theta_2)^2*sin(\theta_3)^2*sin(\theta_4)+L_4^2*\ddot{\theta}_2*m4*cos(\theta_2)*cos(\theta_3)*cos(\theta_4)^2*sin(\theta_1)^2*sin(\theta_2)*sin(\theta_3)-L_4^2*\ddot{\theta}_2*m4*cos(\theta_1)^2*cos(\theta_2)*cos(\theta_3)*sin(\theta_2)*sin(\theta_3)*sin(\theta_4)^2+L_4^2*\ddot{\theta}_2*m4*cos(\theta_2)*cos(\theta_3)^2*cos(\theta_4)*sin(\theta_1)^2*sin(\theta_2)*sin(\theta_4)-L_4^2*\ddot{\theta}_2*m4*cos(\theta_1)^2*cos(\theta_2)*cos(\theta_4)*sin(\theta_2)*sin(\theta_3)^2*sin(\theta_4)-2*L_4^2*\ddot{\theta}_3*m4*cos(\theta_1)^2*cos(\theta_3)*cos(\theta_4)*sin(\theta_2)^2*sin(\theta_3)*sin(\theta_4)-2*L_4^2*\ddot{\theta}_4*m4*cos(\theta_1)^2*cos(\theta_4)*sin(\theta_2)^2*sin(\theta_3)*sin(\theta_4)+L_3*L_4*\dot{\theta}_3*\dot{\theta}_4*m4*cos(\theta_1)^2*sin(\theta_2)^2*sin(\theta_3)^2*sin(\theta_4)-3*L_3*L_4*\dot{\theta}_3*\dot{\theta}_4*m4*cos(\theta_3)^2*sin(\theta_1)^2*sin(\theta_2)^2*sin(\theta_4)+L_3*L_4*\ddot{\theta}_2*m4*cos(\theta_1)^2*cos(\theta_2)*cos(\theta_3)^2*sin(\theta_2)*sin(\theta_4)-L_4^2*\ddot{\theta}_2*m4*cos(\theta_2)*cos(\theta_3)*sin(\theta_1)^2*sin(\theta_2)*sin(\theta_3)*sin(\theta_4)^2-L_4^2*\ddot{\theta}_2*m4*cos(\theta_2)*cos(\theta_4)*sin(\theta_1)^2*sin(\theta_2)*sin(\theta_3)^2*sin(\theta_4)-2*L_4^2*\ddot{\theta}_3*m4*cos(\theta_3)*cos(\theta_4)*sin(\theta_1)^2*sin(\theta_2)^2*sin(\theta_3)*sin(\theta_4)-2*L_4^2*\ddot{\theta}_4*m4*cos(\theta_3)*cos(\theta_4)*sin(\theta_1)^2*sin(\theta_2)^2*sin(\theta_3)*sin(\theta_4)+L_3*L_4*\dot{\theta}_3*\dot{\theta}_4*m4*sin(\theta_1)^2*sin(\theta_2)^2*sin(\theta_3)^2*sin(\theta_4)+L_3*L_4*\ddot{\theta}_2*m4*cos(\theta_2)*cos(\theta_3)^2*sin(\theta_1)^2*sin(\theta_2)*sin(\theta_4)-L_3*L_4*\ddot{\theta}_2*m4*cos(\theta_1)^2*cos(\theta_2)*sin(\theta_2)*sin(\theta_3)^2*sin(\theta_4)-2*L_3*L_4*\ddot{\theta}_3*m4*cos(\theta_1)^2*cos(\theta_3)*sin(\theta_2)^2*sin(\theta_3)*sin(\theta_4)-L_3*L_4*\ddot{\theta}_4*m4*cos(\theta_1)^2*cos(\theta_3)*sin(\theta_2)^2*sin(\theta_3)*sin(\theta_4)-4*L_3*L_4*\dot{\theta}_2*\dot{\theta}_3*m4*cos(\theta_2)*cos(\theta_3)^2*cos(\theta_4)*sin(\theta_2)-2*L_3*L_4*\dot{\theta}_2*\dot{\theta}_4*m4*cos(\theta_2)*cos(\theta_3)^2*cos(\theta_4)*sin(\theta_2)+4*L_3*L_4*\dot{\theta}_3*\dot{\theta}_4*m4*cos(\theta_1)^2*cos(\theta_3)*cos(\theta_4)*sin(\theta_3)-2*L_3*L_4*\dot{\theta}_3*\dot{\theta}_4*m4*cos(\theta_2)^2*cos(\theta_3)*cos(\theta_4)*sin(\theta_3)-L_3*L_4*\ddot{\theta}_2*m4*cos(\theta_2)*sin(\theta_1)^2*sin(\theta_2)*sin(\theta_3)^2*sin(\theta_4)-2*L_3*L_4*\ddot{\theta}_3*m4*cos(\theta_3)*sin(\theta_1)^2*sin(\theta_2)^2*sin(\theta_3)*sin(\theta_4)-L_3*L_4*\ddot{\theta}_4*m4*cos(\theta_3)*sin(\theta_1)^2*sin(\theta_2)^2*sin(\theta_3)*sin(\theta_4)+6*L_3*L_4*\dot{\theta}_2*\dot{\theta}_3*m4*cos(\theta_1)^2*cos(\theta_2)*cos(\theta_3)^2*cos(\theta_4)*sin(\theta_2)+3*L_3*L_4*\dot{\theta}_2*\dot{\theta}_4*m4*cos(\theta_1)^2*cos(\theta_2)*cos(\theta_3)^2*cos(\theta_4)*sin(\theta_2)+6*L_3*L_4*\dot{\theta}_2*\dot{\theta}_3*m4*cos(\theta_2)*cos(\theta_3)^2*cos(\theta_4)*sin(\theta_1)^2*sin(\theta_2)-2*L_3*L_4*\dot{\theta}_2*\dot{\theta}_3*m4*cos(\theta_1)^2*cos(\theta_2)*cos(\theta_4)*sin(\theta_2)*sin(\theta_3)^2+3*L_3*L_4*\dot{\theta}_2*\dot{\theta}_4*m4*cos(\theta_2)*cos(\theta_3)^2*cos(\theta_4)*sin(\theta_1)^2*sin(\theta_2)-L_3*L_4*\dot{\theta}_2*\dot{\theta}_4*m4*cos(\theta_1)^2*cos(\theta_2)*cos(\theta_4)*sin(\theta_2)*sin(\theta_3)^2-4*L_3*L_4*\dot{\theta}_3*\dot{\theta}_4*m4*cos(\theta_1)^2*cos(\theta_3)*cos(\theta_4)*sin(\theta_2)^2*sin(\theta_3)-2*L_3*L_4*\dot{\theta}_2*\dot{\theta}_3*m4*cos(\theta_2)*cos(\theta_4)*sin(\theta_1)^2*sin(\theta_2)*sin(\theta_3)^2-L_3*L_4*\dot{\theta}_2*\dot{\theta}_4*m4*cos(\theta_2)*cos(\theta_4)*sin(\theta_1)^2*sin(\theta_2)*sin(\theta_3)^2-4*L_3*L_4*\dot{\theta}_3*\dot{\theta}_4*m4*cos(\theta_3)*cos(\theta_4)*sin(\theta_1)^2*sin(\theta_2)^2*sin(\theta_3)+2*L_3*L_4*\ddot{\theta}_2*m4*cos(\theta_1)^2*cos(\theta_2)*cos(\theta_3)*cos(\theta_4)*sin(\theta_2)*sin(\theta_3)+2*L_3*L_4*\ddot{\theta}_2*m4*cos(\theta_2)*cos(\theta_3)*cos(\theta_4)*sin(\theta_1)^2*sin(\theta_2)*sin(\theta_3)+4*L_4^2*\dot{\theta}_2*\dot{\theta}_3*m4*cos(\theta_2)*cos(\theta_3)*cos(\theta_4)*sin(\theta_2)*$$

$$sin(\theta_3) * sin(\theta_4) + 4 * L_4^2 * \dot{\theta}_2 * \dot{\theta}_4 * m4 * cos(\theta_2) * cos(\theta_3) * cos(\theta_4) * sin(\theta_2) * sin(\theta_3) * sin(\theta_4) + 4 * L_3 * L_4 * \dot{\theta}_2 * \dot{\theta}_3 * m4 * cos(\theta_2) * cos(\theta_3) * sin(\theta_2) * sin(\theta_3) * sin(\theta_4) + 2 * L_3 * L_4 * \dot{\theta}_2 * \dot{\theta}_4 * m4 * cos(\theta_2) * cos(\theta_3) * sin(\theta_2) * sin(\theta_3) * sin(\theta_4) - 8 * L_4^2 * \dot{\theta}_2 * \dot{\theta}_3 * m4 * cos(\theta_1)^2 * cos(\theta_2) * cos(\theta_3) * cos(\theta_4) * sin(\theta_2) * sin(\theta_3) * sin(\theta_4) - 8 * L_4^2 * \dot{\theta}_2 * \dot{\theta}_4 * m4 * cos(\theta_1)^2 * cos(\theta_2) * cos(\theta_3) * cos(\theta_4) * sin(\theta_2) * sin(\theta_3) * sin(\theta_4) - 8 * L_4^2 * \dot{\theta}_2 * \dot{\theta}_3 * m4 * cos(\theta_2) * cos(\theta_3) * cos(\theta_4) * sin(\theta_1)^2 * sin(\theta_2) * sin(\theta_3) * sin(\theta_4) - 8 * L_4^2 * \dot{\theta}_2 * \dot{\theta}_4 * m4 * cos(\theta_2) * cos(\theta_3) * cos(\theta_4) * sin(\theta_1)^2 * sin(\theta_2) * sin(\theta_3) * sin(\theta_4) - 8 * L_3 * L_4 * \dot{\theta}_2 * \dot{\theta}_3 * m4 * cos(\theta_1)^2 * cos(\theta_2) * cos(\theta_3) * sin(\theta_2) * sin(\theta_3) * sin(\theta_4) - 4 * L_3 * L_4 * \dot{\theta}_2 * \dot{\theta}_4 * m4 * cos(\theta_1)^2 * cos(\theta_2) * cos(\theta_3) * sin(\theta_2) * sin(\theta_3) * sin(\theta_4) - 8 * L_3 * L_4 * \dot{\theta}_2 * \dot{\theta}_3 * m4 * cos(\theta_2) * cos(\theta_3) * sin(\theta_1)^2 * sin(\theta_2) * sin(\theta_3) * sin(\theta_4) - 4 * L_3 * L_4 * \dot{\theta}_2 * \dot{\theta}_4 * m4 * cos(\theta_2) * cos(\theta_3) * sin(\theta_1)^2 * sin(\theta_2) * sin(\theta_3) * sin(\theta_4);$$

$$\tau_4 = I_4 * \ddot{\theta}_1 + I_4 * \ddot{\theta}_2 + I_4 * \ddot{\theta}_3 + I_4 * \ddot{\theta}_4 + L_4^2 * \ddot{\theta}_3 * m4 + L_4^2 * \ddot{\theta}_4 * m4 - L_4^2 * \ddot{\theta}_3 * m4 * cos(\theta_2)^2 - L_4^2 * \ddot{\theta}_4 * m4 * cos(\theta_2)^2 - L_4^2 * \ddot{\theta}_1 * m4 * sin(\theta_2) + L_3 * L_4 * \dot{\theta_2}^2 * m4 * sin(\theta_4) - L_4^2 * \dot{\theta}_1 * \dot{\theta}_2 * m4 * cos(\theta_2) + L_4^2 * \ddot{\theta}_3 * m4 * cos(\theta_2)^2 * cos(\theta_3)^2 + L_4^2 * \ddot{\theta}_3 * m4 * cos(\theta_2)^2 * cos(\theta_4)^2 + L_4^2 * \ddot{\theta}_4 * m4 * cos(\theta_2)^2 * cos(\theta_3)^2 + L_4^2 * \ddot{\theta}_4 * m4 * cos(\theta_2)^2 * cos(\theta_4)^2 + L_3 * L_4 * \ddot{\theta}_3 * m4 * cos(\theta_4) + L_4^2 * \dot{\theta_2}^2 * m4 * cos(\theta_3) * sin(\theta_3) + L_4^2 * \dot{\theta_2}^2 * m4 * cos(\theta_4) * sin(\theta_4) + 3 * L_4^2 * \dot{\theta}_2 * \dot{\theta}_3 * m4 * cos(\theta_2) * sin(\theta_2) + 3 * L_4^2 * \dot{\theta}_2 * \dot{\theta}_4 * m4 * cos(\theta_2) * sin(\theta_2) - L_3 * L_4 * \dot{\theta}_3 * \dot{\theta}_4 * m4 * sin(\theta_4) + L_4 * g * m4 * cos(\theta_1) * cos(\theta_3) * sin(\theta_4) + L_4 * g * m4 * cos(\theta_1) * cos(\theta_4) * sin(\theta_3) - 2 * L_4^2 * \dot{\theta_2}^2 * m4 * cos(\theta_2)^2 * cos(\theta_3) * sin(\theta_3) - 2 * L_4^2 * \dot{\theta_3}^2 * m4 * cos(\theta_2)^2 * cos(\theta_3) * sin(\theta_3) - 2 * L_4^2 * \dot{\theta_2}^2 * m4 * cos(\theta_3) * cos(\theta_4)^2 * sin(\theta_3) - 2 * L_4^2 * \dot{\theta_2}^2 * m4 * cos(\theta_2)^2 * cos(\theta_4) * sin(\theta_4) - 2 * L_4^2 * \dot{\theta_4}^2 * m4 * cos(\theta_2)^2 * cos(\theta_3) * sin(\theta_3) - 2 * L_4^2 * \dot{\theta_2}^2 * m4 * cos(\theta_3)^2 * cos(\theta_4) * sin(\theta_4) - 2 * L_4^2 * \dot{\theta_3}^2 * m4 * cos(\theta_2)^2 * cos(\theta_4) * sin(\theta_4) - 2 * L_4^2 * \dot{\theta_4}^2 * m4 * cos(\theta_2)^2 * cos(\theta_4) * sin(\theta_4) - 2 * L_3 * L_4 * \dot{\theta_2}^2 * m4 * cos(\theta_2)^2 * sin(\theta_4) - L_3 * L_4 * \dot{\theta_2}^2 * m4 * cos(\theta_3)^2 * sin(\theta_4) - L_3 * L_4 * \dot{\theta_3}^2 * m4 * cos(\theta_2)^2 * sin(\theta_4) - 2 * L_4^2 * \ddot{\theta}_3 * m4 * cos(\theta_2)^2 * cos(\theta_3)^2 * cos(\theta_4)^2 - 2 * L_4^2 * \ddot{\theta}_4 * m4 * cos(\theta_2)^2 * cos(\theta_3)^2 * cos(\theta_4)^2 + L_2 * L_4 * \ddot{\theta}_1 * m4 * cos(\theta_3) * sin(\theta_4) + L_2 * L_4 * \ddot{\theta}_1 * m4 * cos(\theta_4) * sin(\theta_3) - L_3 * L_4 * \ddot{\theta}_1 * m4 * cos(\theta_4) * sin(\theta_2) - L_3 * L_4 * \ddot{\theta}_3 * m4 * cos(\theta_2)^2 * cos(\theta_3)^2 * cos(\theta_4) + L_4 * g * m4 * sin(\theta_1) * sin(\theta_2) * sin(\theta_3) * sin(\theta_4) - 4 * L_4^2 * \dot{\theta}_2 * \dot{\theta}_3 * m4 * cos(\theta_2) * cos(\theta_3)^2 * sin(\theta_2) - 4 * L_4^2 * \dot{\theta}_2 * \dot{\theta}_3 * m4 * cos(\theta_2) * cos(\theta_4)^2 * sin(\theta_2) - 4 * L_4^2 * \dot{\theta}_2 * \dot{\theta}_4 * m4 * cos(\theta_2) * cos(\theta_3)^2 * sin(\theta_2) - 4 * L_4^2 * \dot{\theta}_2 * \dot{\theta}_4 * m4 * cos(\theta_2) * cos(\theta_4)^2 * sin(\theta_2) - 4 * L_4^2 * \dot{\theta}_3 * \dot{\theta}_4 * m4 * cos(\theta_2)^2 * cos(\theta_3) * sin(\theta_3) - 4 * L_4^2 * \dot{\theta}_3 * \dot{\theta}_4 * m4 * cos(\theta_2)^2 * cos(\theta_4) * sin(\theta_4) - L_4^2 * \ddot{\theta}_2 * m4 * cos(\theta_2) * cos(\theta_3) * sin(\theta_2) * sin(\theta_3) - L_4^2 * \ddot{\theta}_2 * m4 * cos(\theta_2) * cos(\theta_4) * sin(\theta_2) * sin(\theta_4) + L_4^2 * \dot{\theta_1}^2 * m4 * cos(\theta_1)^2 * cos(\theta_3) * cos(\theta_4)^2 * sin(\theta_3) + L_4^2 * \dot{\theta_1}^2 * m4 * cos(\theta_1)^2 * cos(\theta_3)^2 * cos(\theta_4) * sin(\theta_4) + 4 * L_4^2 * \dot{\theta_2}^2 * m4 * cos(\theta_2)^2 * cos(\theta_3) * cos(\theta_4)^2 * sin(\theta_3) - L_4^2 * \dot{\theta_3}^2 * m4 * cos(\theta_1)^2 * cos(\theta_3) * cos(\theta_4)^2 * sin(\theta_3) + 4 * L_4^2 * \dot{\theta_2}^2 * m4 * cos(\theta_2)^2 * cos(\theta_3)^2 * cos(\theta_4) * sin(\theta_4) - L_4^2 * \dot{\theta_3}^2 * m4 * cos(\theta_1)^2 * cos(\theta_3)^2 * cos(\theta_4) * sin(\theta_4) + 4 * L_4^2 * \dot{\theta_3}^2 * m4 * cos(\theta_2)^2 * cos(\theta_3) * cos(\theta_4)^2 * sin(\theta_3) - L_4^2 * \dot{\theta_4}^2 * m4 * cos(\theta_1)^2 * cos(\theta_3) * cos(\theta_4)^2 * sin(\theta_3) + 4 * L_4^2 * \dot{\theta_3}^2 * m4 * cos(\theta_2)^2 * cos(\theta_3)^2 * cos(\theta_4) * sin(\theta_4) - L_4^2 * \dot{\theta_4}^2 * m4 * cos(\theta_1)^2 * cos(\theta_3)^2 * cos(\theta_4) * sin(\theta_4) + 4 * L_4^2 * \dot{\theta_4}^2 * m4 * cos(\theta_2)^2 * cos(\theta_3) * cos(\theta_4)^2 * sin(\theta_3) + 4 * L_4^2 * \dot{\theta_4}^2 * m4 * cos(\theta_2)^2 * cos(\theta_3)^2 * cos(\theta_4) * sin(\theta_4) - L_3 * L_4 * \ddot{\theta}_2 * m4 * cos(\theta_2) * sin(\theta_2) * sin(\theta_4) + L_4^2 * \dot{\theta_1}^2 * m4 * cos(\theta_3) * cos(\theta_4)^2 * sin(\theta_1)^2 * sin(\theta_3) - L_4^2 * \dot{\theta_1}^2 * m4 * cos(\theta_1)^2 * cos(\theta_3) * sin(\theta_3) * sin(\theta_4)^2 - L_4^2 * \dot{\theta_1}^2 * m4 * cos(\theta_1)^2 * cos(\theta_4) * sin(\theta_3)^2 * sin(\theta_4) + L_4^2 * \dot{\theta_1}^2 * m4 * cos(\theta_3)^2 * cos(\theta_4) * sin(\theta_1)^2 * sin(\theta_4) - L_4^2 * \dot{\theta_3}^2 * m4 * cos(\theta_3) * cos(\theta_4)^2 * sin(\theta_1)^2 * sin(\theta_3) + L_4^2 * \dot{\theta_3}^2 * m4 * cos(\theta_1)^2 * cos(\theta_3) * sin(\theta_3) * sin(\theta_4)^2 + L_4^2 * \dot{\theta_3}^2 * m4 * cos(\theta_1)^2 * cos(\theta_4) * sin(\theta_3)^2 * sin(\theta_4) - L_4^2 * \dot{\theta_3}^2 * m4 * cos(\theta_3)^2 * cos(\theta_4) * sin(\theta_1)^2 * sin(\theta_4) - L_4^2 * \dot{\theta_4}^2 * m4 * cos(\theta_3) * cos(\theta_4)^2 * sin(\theta_1)^2 * sin(\theta_3) + L_4^2 * \dot{\theta_4}^2 * m4 * cos(\theta_1)^2 * cos(\theta_3) * sin(\theta_3) * sin(\theta_4)^2 + L_4^2 * \dot{\theta_4}^2 * m4 * cos(\theta_1)^2 * cos(\theta_4) * sin(\theta_3)^2 * sin(\theta_4) - L_4^2 * \dot{\theta_4}^2 * m4 * cos(\theta_3)^2 * cos(\theta_4) * sin(\theta_1)^2 * sin(\theta_4) + L_3 * L_4 * \dot{\theta_1}^2 * m4 * cos(\theta_1)^2 * cos(\theta_3)^2 * sin(\theta_4) + 2 * L_3 * L_4 * \dot{\theta_2}^2 * m4 * cos(\theta_2)^2 * cos(\theta_3)^2 * sin(\theta_4) + 2 * L_3 * L_4 * \dot{\theta_3}^2 * m4 * cos(\theta_2)^2 * cos(\theta_3)^2 * sin(\theta_4) - L_4^2 * \dot{\theta_1}^2 * m4 * cos(\theta_3) * sin(\theta_1)^2 * sin(\theta_3) * sin(\theta_4)^2 - L_4^2 * \dot{\theta_1}^2 * m4 * cos(\theta_4) * sin(\theta_1)^2 * sin(\theta_3)^2 * sin(\theta_4) + L_4^2 * \dot{\theta_3}^2 * m4 * cos(\theta_3) * sin(\theta_1)^2 * sin(\theta_3) * sin(\theta_4)^2 + L_4^2 * \dot{\theta_3}^2 * m4 * cos(\theta_4) * sin(\theta_1)^2 * sin(\theta_3)^2 * sin(\theta_4) + L_4^2 * \dot{\theta_4}^2 * m4 * cos(\theta_3) * sin(\theta_1)^2 * sin(\theta_3) * sin(\theta_4)^2 + L_4^2 * \dot{\theta_4}^2 * m4 * cos(\theta_4) * sin(\theta_1)^2 * sin(\theta_3)^2 * sin(\theta_4) + L_3 * L_4 * \dot{\theta_1}^2 * m4 * cos(\theta_3)^2 * sin(\theta_1)^2 * sin(\theta_4) + L_3 * L_4 * \dot{\theta_3}^2 * m4 * cos(\theta_1)^2 * sin(\theta_3)^2 *$$

$$sin(\theta_4) + L_3 * L_4 * \dot{\theta_3}^2 * m4 * sin(\theta_1)^2 * sin(\theta_3)^2 * sin(\theta_4) - L_3 * L_4 * \dot{\theta_2}^2 * m4 * cos(\theta_3) * cos(\theta_4) * sin(\theta_3) - L_3 * L_4 * \dot{\theta_1} * \dot{\theta_2} * m4 * cos(\theta_2) * cos(\theta_4) + L_2 * L_4 * \dot{\theta_1} * \dot{\theta_3} * m4 * cos(\theta_3) * cos(\theta_4) + L_2 * L_4 * \dot{\theta_1} * \dot{\theta_4} * m4 * cos(\theta_3) * cos(\theta_4) - L_2 * L_4 * \dot{\theta_1} * \dot{\theta_3} * m4 * sin(\theta_3) * sin(\theta_4) - L_2 * L_4 * \dot{\theta_1} * \dot{\theta_4} * m4 * sin(\theta_3) * sin(\theta_4) + L_3 * L_4 * \dot{\theta_1} * \dot{\theta_4} * m4 * sin(\theta_2) * sin(\theta_4) - L_4 * g * m4 * cos(\theta_3) * cos(\theta_4) * sin(\theta_1) * sin(\theta_2) + L_2 * L_4 * \dot{\theta_1}^2 * m4 * cos(\theta_3) * cos(\theta_4) * sin(\theta_1)^2 * sin(\theta_2) + L_3 * L_4 * \dot{\theta_1}^2 * m4 * cos(\theta_3) * cos(\theta_4) * sin(\theta_1)^2 * sin(\theta_3) - L_3 * L_4 * \dot{\theta_3}^2 * m4 * cos(\theta_3) * cos(\theta_4) * sin(\theta_1)^2 * sin(\theta_3) - L_2 * L_4 * \dot{\theta_1} * \dot{\theta_3} * m4 * cos(\theta_1)^2 * cos(\theta_3) * cos(\theta_4) - L_2 * L_4 * \dot{\theta_1} * \dot{\theta_4} * m4 * cos(\theta_1)^2 * cos(\theta_3) * cos(\theta_4) - L_2 * L_4 * \dot{\theta_1}^2 * m4 * cos(\theta_1)^2 * sin(\theta_2) * sin(\theta_3) * sin(\theta_4) - L_2 * L_4 * \dot{\theta_1} * \dot{\theta_3} * m4 * cos(\theta_3) * cos(\theta_4) * sin(\theta_1)^2 - L_2 * L_4 * \dot{\theta_1} * \dot{\theta_4} * m4 * cos(\theta_3) * cos(\theta_4) * sin(\theta_1)^2 - L_2 * L_4 * \dot{\theta_1}^2 * m4 * sin(\theta_1)^2 * sin(\theta_2) * sin(\theta_3) * sin(\theta_4) + L_2 * L_4 * \dot{\theta_1} * \dot{\theta_3} * m4 * cos(\theta_1)^2 * sin(\theta_3) * sin(\theta_4) + L_2 * L_4 * \dot{\theta_1} * \dot{\theta_4} * m4 * cos(\theta_1)^2 * sin(\theta_3) * sin(\theta_4) + L_2 * L_4 * \dot{\theta_1} * \dot{\theta_3} * m4 * sin(\theta_1)^2 * sin(\theta_3) * sin(\theta_4) + L_2 * L_4 * \dot{\theta_1} * \dot{\theta_4} * m4 * sin(\theta_1)^2 * sin(\theta_3) * sin(\theta_4) + 8 * L_4^2 * \dot{\theta_2} * \dot{\theta_3} * m4 * cos(\theta_2) * cos(\theta_3)^2 * cos(\theta_4)^2 * sin(\theta_2) + 8 * L_4^2 * \dot{\theta_2} * \dot{\theta_4} * m4 * cos(\theta_2) * cos(\theta_3)^2 * cos(\theta_4)^2 * sin(\theta_2) - 2 * L_4^2 * \dot{\theta_3} * \dot{\theta_4} * m4 * cos(\theta_1)^2 * cos(\theta_3) * cos(\theta_4)^2 * sin(\theta_3) - 2 * L_4^2 * \dot{\theta_3} * \dot{\theta_4} * m4 * cos(\theta_1)^2 * cos(\theta_3)^2 * cos(\theta_4) * sin(\theta_4) + 8 * L_4^2 * \dot{\theta_3} * \dot{\theta_4} * m4 * cos(\theta_2)^2 * cos(\theta_3) * cos(\theta_4)^2 * sin(\theta_3) + 8 * L_4^2 * \dot{\theta_3} * \dot{\theta_4} * m4 * cos(\theta_2)^2 * cos(\theta_3)^2 * cos(\theta_4) * sin(\theta_4) - 2 * L_4^2 * \dot{\theta_3} * \dot{\theta_4} * m4 * cos(\theta_3) * cos(\theta_4)^2 * sin(\theta_1)^2 * sin(\theta_3) + 2 * L_4^2 * \dot{\theta_3} * \dot{\theta_4} * m4 * cos(\theta_1)^2 * cos(\theta_3) * sin(\theta_3) * sin(\theta_4)^2 + 2 * L_4^2 * \dot{\theta_3} * \dot{\theta_4} * m4 * cos(\theta_1)^2 * cos(\theta_4) * sin(\theta_3)^2 * sin(\theta_4) - 2 * L_4^2 * \dot{\theta_3} * \dot{\theta_4} * m4 * cos(\theta_3)^2 * cos(\theta_4) * sin(\theta_1)^2 * sin(\theta_4) + L_3 * L_4 * \dot{\theta_3} * \dot{\theta_4} * m4 * cos(\theta_2)^2 * cos(\theta_3)^2 * sin(\theta_4) + 2 * L_4^2 * \dot{\theta_3} * \dot{\theta_4} * m4 * cos(\theta_3) * sin(\theta_1)^2 * sin(\theta_3) * sin(\theta_4)^2 + 2 * L_4^2 * \dot{\theta_3} * \dot{\theta_4} * m4 * cos(\theta_4) * sin(\theta_1)^2 * sin(\theta_3)^2 * sin(\theta_4) + 2 * L_4^2 * \ddot{\theta_2} * m4 * cos(\theta_2) * cos(\theta_3) * cos(\theta_4)^2 * sin(\theta_2) * sin(\theta_3) + 2 * L_4^2 * \ddot{\theta_2} * m4 * cos(\theta_2) * cos(\theta_3)^2 * cos(\theta_4) * sin(\theta_2) * sin(\theta_4) + 2 * L_4^2 * \ddot{\theta_3} * m4 * cos(\theta_2)^2 * cos(\theta_3) * cos(\theta_4) * sin(\theta_3) * sin(\theta_4) + 2 * L_4^2 * \ddot{\theta_4} * m4 * cos(\theta_2)^2 * cos(\theta_3) * cos(\theta_4) * sin(\theta_3) * sin(\theta_4) + L_3 * L_4 * \dot{\theta_3} * \dot{\theta_4} * m4 * cos(\theta_1)^2 * sin(\theta_3)^2 * sin(\theta_4) - L_4^2 * \dot{\theta_2}^2 * m4 * cos(\theta_1)^2 * cos(\theta_2)^2 * cos(\theta_3) * cos(\theta_4)^2 * sin(\theta_3) - L_4^2 * \dot{\theta_2}^2 * m4 * cos(\theta_1)^2 * cos(\theta_2)^2 * cos(\theta_3)^2 * cos(\theta_4) * sin(\theta_4) + L_3 * L_4 * \dot{\theta_3} * \dot{\theta_4} * m4 * sin(\theta_1)^2 * sin(\theta_3)^2 * sin(\theta_4) + L_3 * L_4 * \ddot{\theta_2} * m4 * cos(\theta_2) * cos(\theta_3)^2 * sin(\theta_2) * sin(\theta_4) + L_3 * L_4 * \ddot{\theta_3} * m4 * cos(\theta_2)^2 * cos(\theta_3) * sin(\theta_3) * sin(\theta_4) - L_4^2 * \dot{\theta_1}^2 * m4 * cos(\theta_1)^2 * cos(\theta_3) * cos(\theta_4)^2 * sin(\theta_2)^2 * sin(\theta_3) - L_4^2 * \dot{\theta_1}^2 * m4 * cos(\theta_1)^2 * cos(\theta_3)^2 * cos(\theta_4) * sin(\theta_2)^2 * sin(\theta_4) + L_4^2 * \dot{\theta_2}^2 * m4 * cos(\theta_1)^2 * cos(\theta_2)^2 * cos(\theta_3) * sin(\theta_3) * sin(\theta_4)^2 - L_4^2 * \dot{\theta_2}^2 * m4 * cos(\theta_2)^2 * cos(\theta_3) * cos(\theta_4)^2 * sin(\theta_1)^2 * sin(\theta_3) + L_4^2 * \dot{\theta_2}^2 * m4 * cos(\theta_1)^2 * cos(\theta_2)^2 * cos(\theta_4) * sin(\theta_3)^2 * sin(\theta_4) - L_4^2 * \dot{\theta_2}^2 * m4 * cos(\theta_2)^2 * cos(\theta_3)^2 * cos(\theta_4) * sin(\theta_1)^2 * sin(\theta_4) + L_4^2 * \dot{\theta_3}^2 * m4 * cos(\theta_1)^2 * cos(\theta_3) * cos(\theta_4)^2 * sin(\theta_2)^2 * sin(\theta_3) + L_4^2 * \dot{\theta_3}^2 * m4 * cos(\theta_1)^2 * cos(\theta_3)^2 * cos(\theta_4) * sin(\theta_2)^2 * sin(\theta_4) + L_4^2 * \dot{\theta_4}^2 * m4 * cos(\theta_1)^2 * cos(\theta_3) * cos(\theta_4)^2 * sin(\theta_2)^2 * sin(\theta_3) + L_4^2 * \dot{\theta_4}^2 * m4 * cos(\theta_1)^2 * cos(\theta_3)^2 * cos(\theta_4) * sin(\theta_2)^2 * sin(\theta_4) + L_4^2 * \dot{\theta_1} * \dot{\theta_2} * m4 * cos(\theta_1)^2 * cos(\theta_2) * cos(\theta_3)^2 * cos(\theta_4)^2 - L_4^2 * \dot{\theta_1}^2 * m4 * cos(\theta_3) * cos(\theta_4)^2 * sin(\theta_1)^2 * sin(\theta_2)^2 * sin(\theta_3) + L_4^2 * \dot{\theta_1}^2 * m4 * cos(\theta_1)^2 * cos(\theta_3) * sin(\theta_2)^2 * sin(\theta_3) * sin(\theta_4)^2 + L_4^2 * \dot{\theta_1}^2 * m4 * cos(\theta_1)^2 * cos(\theta_4) * sin(\theta_2)^2 * sin(\theta_3)^2 * sin(\theta_4) - L_4^2 * \dot{\theta_1}^2 * m4 * cos(\theta_3)^2 * cos(\theta_4) * sin(\theta_1)^2 * sin(\theta_2)^2 * sin(\theta_4) + L_4^2 * \dot{\theta_2}^2 * m4 * cos(\theta_2)^2 * cos(\theta_3) * sin(\theta_1)^2 * sin(\theta_3) * sin(\theta_4)^2 + L_4^2 * \dot{\theta_2}^2 * m4 * cos(\theta_2)^2 * cos(\theta_4) * sin(\theta_1)^2 * sin(\theta_3)^2 * sin(\theta_4) + L_4^2 * \dot{\theta_3}^2 * m4 * cos(\theta_3) * cos(\theta_4)^2 * sin(\theta_1)^2 * sin(\theta_2)^2 * sin(\theta_3) - L_4^2 * \dot{\theta_3}^2 * m4 * cos(\theta_1)^2 * cos(\theta_3) * sin(\theta_2)^2 * sin(\theta_3) * sin(\theta_4)^2 - L_4^2 * \dot{\theta_3}^2 * m4 * cos(\theta_1)^2 * cos(\theta_4) * sin(\theta_2)^2 * sin(\theta_3)^2 * sin(\theta_4) + L_4^2 * \dot{\theta_3}^2 * m4 * cos(\theta_3)^2 * cos(\theta_4) * sin(\theta_1)^2 * sin(\theta_2)^2 * sin(\theta_4) + L_4^2 * \dot{\theta_4}^2 * m4 * cos(\theta_3) * cos(\theta_4)^2 * sin(\theta_1)^2 * sin(\theta_2)^2 * sin(\theta_3) -$$

$$L_4^2 * \dot{\theta_4}^2 * m4 * cos(\theta_1)^2 * cos(\theta_3) * sin(\theta_2)^2 * sin(\theta_3) * sin(\theta_4)^2 - L_4^2 * \dot{\theta_4}^2 * m4 * cos(\theta_1)^2 * cos(\theta_4) * sin(\theta_2)^2 * sin(\theta_3)^2 * sin(\theta_4) + L_4^2 * \dot{\theta_4}^2 * m4 * cos(\theta_3)^2 * cos(\theta_4) * sin(\theta_1)^2 * sin(\theta_2)^2 * sin(\theta_4) - L_3 * L_4 * \dot{\theta_2} * \dot{\theta_3} * m4 * cos(\theta_2) * cos(\theta_4) * sin(\theta_2) - L_3 * L_4 * \dot{\theta_2} * \dot{\theta_4} * m4 * cos(\theta_2) * cos(\theta_4) * sin(\theta_2) + L_3 * L_4 * \dot{\theta_2}^2 * m4 * cos(\theta_1)^2 * cos(\theta_2)^2 * sin(\theta_3)^2 * sin(\theta_4) + L_3 * L_4 * \dot{\theta_3}^2 * m4 * cos(\theta_1)^2 * cos(\theta_3)^2 * sin(\theta_2)^2 * sin(\theta_4) + L_4^2 * \dot{\theta_1} * \dot{\theta_2} * m4 * cos(\theta_2) * cos(\theta_3)^2 * cos(\theta_4)^2 * sin(\theta_1)^2 - L_4^2 * \dot{\theta_1} * \dot{\theta_2} * m4 * cos(\theta_1)^2 * cos(\theta_2) * cos(\theta_3)^2 * sin(\theta_4)^2 - L_4^2 * \dot{\theta_1} * \dot{\theta_2} * m4 * cos(\theta_1)^2 * cos(\theta_2) * cos(\theta_4)^2 * sin(\theta_3)^2 + L_4^2 * \dot{\theta_1}^2 * m4 * cos(\theta_3) * sin(\theta_1)^2 * sin(\theta_2)^2 * sin(\theta_3) * sin(\theta_4)^2 + L_4^2 * \dot{\theta_1}^2 * m4 * cos(\theta_4) * sin(\theta_1)^2 * sin(\theta_2)^2 * sin(\theta_3)^2 * sin(\theta_4) - L_4^2 * \dot{\theta_3}^2 * m4 * cos(\theta_3) * sin(\theta_1)^2 * sin(\theta_2)^2 * sin(\theta_3) * sin(\theta_4)^2 - L_4^2 * \dot{\theta_3}^2 * m4 * cos(\theta_4) * sin(\theta_1)^2 * sin(\theta_2)^2 * sin(\theta_3)^2 * sin(\theta_4) - L_4^2 * \dot{\theta_4}^2 * m4 * cos(\theta_3) * sin(\theta_1)^2 * sin(\theta_2)^2 * sin(\theta_3) * sin(\theta_4)^2 - L_4^2 * \dot{\theta_4}^2 * m4 * cos(\theta_4) * sin(\theta_1)^2 * sin(\theta_2)^2 * sin(\theta_3)^2 * sin(\theta_4) + L_3 * L_4 * \dot{\theta_1}^2 * m4 * cos(\theta_1)^2 * sin(\theta_2)^2 * sin(\theta_3)^2 * sin(\theta_4) + L_3 * L_4 * \dot{\theta_2}^2 * m4 * cos(\theta_2)^2 * sin(\theta_1)^2 * sin(\theta_3)^2 * sin(\theta_4) + L_3 * L_4 * \dot{\theta_3}^2 * m4 * cos(\theta_3)^2 * sin(\theta_1)^2 * sin(\theta_2)^2 * sin(\theta_4) - L_4^2 * \dot{\theta_1} * \dot{\theta_2} * m4 * cos(\theta_2) * cos(\theta_3)^2 * sin(\theta_1)^2 * sin(\theta_4)^2 - L_4^2 * \dot{\theta_1} * \dot{\theta_2} * m4 * cos(\theta_2) * cos(\theta_4)^2 * sin(\theta_1)^2 * sin(\theta_3)^2 + L_4^2 * \dot{\theta_1} * \dot{\theta_2} * m4 * cos(\theta_1)^2 * cos(\theta_2) * sin(\theta_3)^2 * sin(\theta_4)^2 + L_3 * L_4 * \dot{\theta_1}^2 * m4 * sin(\theta_1)^2 * sin(\theta_2)^2 * sin(\theta_3)^2 * sin(\theta_4) + L_4^2 * \dot{\theta_1} * \dot{\theta_2} * m4 * cos(\theta_2) * sin(\theta_1)^2 * sin(\theta_3)^2 * sin(\theta_4)^2 + L_2 * L_4 * \dot{\theta_1}^2 * m4 * cos(\theta_1)^2 * cos(\theta_3) * cos(\theta_4) * sin(\theta_2) + L_3 * L_4 * \dot{\theta_1}^2 * m4 * cos(\theta_1)^2 * cos(\theta_3) * cos(\theta_4) * sin(\theta_3) + 2 * L_3 * L_4 * \dot{\theta_2}^2 * m4 * cos(\theta_2)^2 * cos(\theta_3) * cos(\theta_4) * sin(\theta_3) - L_3 * L_4 * \dot{\theta_3}^2 * m4 * cos(\theta_1)^2 * cos(\theta_3) * cos(\theta_4) * sin(\theta_3) + 2 * L_3 * L_4 * \dot{\theta_3}^2 * m4 * cos(\theta_2)^2 * cos(\theta_3) * cos(\theta_4) * sin(\theta_3) - L_3 * L_4 * \dot{\theta_3} * \dot{\theta_4} * m4 * cos(\theta_3) * cos(\theta_4) * sin(\theta_1)^2 * sin(\theta_3) + L_3 * L_4 * \ddot{\theta_2} * m4 * cos(\theta_2) * cos(\theta_3) * cos(\theta_4) * sin(\theta_2) * sin(\theta_3) - L_3 * L_4 * \dot{\theta_2}^2 * m4 * cos(\theta_1)^2 * cos(\theta_2)^2 * cos(\theta_3) * cos(\theta_4) * sin(\theta_3) - L_3 * L_4 * \dot{\theta_1}^2 * m4 * cos(\theta_1)^2 * cos(\theta_3) * cos(\theta_4) * sin(\theta_2)^2 * sin(\theta_3) - L_3 * L_4 * \dot{\theta_2}^2 * m4 * cos(\theta_2)^2 * cos(\theta_3) * cos(\theta_4) * sin(\theta_1)^2 * sin(\theta_3) + L_3 * L_4 * \dot{\theta_3}^2 * m4 * cos(\theta_1)^2 * cos(\theta_3) * cos(\theta_4) * sin(\theta_2)^2 * sin(\theta_3) + L_3 * L_4 * \dot{\theta_1} * \dot{\theta_2} * m4 * cos(\theta_1)^2 * cos(\theta_2) * cos(\theta_3)^2 * cos(\theta_4) - L_3 * L_4 * \dot{\theta_1}^2 * m4 * cos(\theta_3) * cos(\theta_4) * sin(\theta_1)^2 * sin(\theta_2)^2 * sin(\theta_3) + L_3 * L_4 * \dot{\theta_3}^2 * m4 * cos(\theta_3) * cos(\theta_4) * sin(\theta_1)^2 * sin(\theta_2)^2 * sin(\theta_3) + L_3 * L_4 * \dot{\theta_1} * \dot{\theta_2} * m4 * cos(\theta_2) * cos(\theta_3)^2 * cos(\theta_4) * sin(\theta_1)^2 - L_3 * L_4 * \dot{\theta_1} * \dot{\theta_2} * m4 * cos(\theta_1)^2 * cos(\theta_2) * cos(\theta_4) * sin(\theta_3)^2 - L_3 * L_4 * \dot{\theta_1} * \dot{\theta_2} * m4 * cos(\theta_2) * cos(\theta_4) * sin(\theta_1)^2 * sin(\theta_3)^2 - 2 * L_3 * L_4 * \dot{\theta_1} * \dot{\theta_3} * m4 * cos(\theta_1)^2 * cos(\theta_3)^2 * sin(\theta_2) * sin(\theta_4) - L_3 * L_4 * \dot{\theta_1} * \dot{\theta_4} * m4 * cos(\theta_1)^2 * cos(\theta_3)^2 * sin(\theta_2) * sin(\theta_4) - 2 * L_3 * L_4 * \dot{\theta_1} * \dot{\theta_3} * m4 * cos(\theta_1)^2 * sin(\theta_2) * sin(\theta_3)^2 * sin(\theta_4) - 2 * L_3 * L_4 * \dot{\theta_1} * \dot{\theta_3} * m4 * cos(\theta_3)^2 * sin(\theta_1)^2 * sin(\theta_2) * sin(\theta_4) - L_3 * L_4 * \dot{\theta_1} * \dot{\theta_4} * m4 * cos(\theta_1)^2 * sin(\theta_2) * sin(\theta_3)^2 * sin(\theta_4) - L_3 * L_4 * \dot{\theta_1} * \dot{\theta_4} * m4 * cos(\theta_3)^2 * sin(\theta_1)^2 * sin(\theta_2) * sin(\theta_4) - 2 * L_3 * L_4 * \dot{\theta_1} * \dot{\theta_3} * m4 * sin(\theta_1)^2 * sin(\theta_2) * sin(\theta_3)^2 * sin(\theta_4) - L_3 * L_4 * \dot{\theta_1} * \dot{\theta_4} * m4 * sin(\theta_1)^2 * sin(\theta_2) * sin(\theta_3)^2 * sin(\theta_4) - L_4^2 * \dot{\theta_2} * \dot{\theta_3} * m4 * cos(\theta_1)^2 * cos(\theta_2) * cos(\theta_3)^2 * cos(\theta_4)^2 * sin(\theta_2) - L_4^2 * \dot{\theta_2} * \dot{\theta_4} * m4 * cos(\theta_1)^2 * cos(\theta_2) * cos(\theta_3)^2 * cos(\theta_4)^2 * sin(\theta_2) - L_4^2 * \dot{\theta_2} * \dot{\theta_3} * m4 * cos(\theta_2) * cos(\theta_3)^2 * cos(\theta_4)^2 * sin(\theta_1)^2 * sin(\theta_2) + L_4^2 * \dot{\theta_2} * \dot{\theta_3} * m4 * cos(\theta_1)^2 * cos(\theta_2) * cos(\theta_3)^2 * sin(\theta_2) * sin(\theta_4)^2 + L_4^2 * \dot{\theta_2} * \dot{\theta_3} * m4 * cos(\theta_1)^2 * cos(\theta_2) * cos(\theta_4)^2 * sin(\theta_2) * sin(\theta_3)^2 - L_4^2 * \dot{\theta_2} * \dot{\theta_4} * m4 * cos(\theta_2) * cos(\theta_3)^2 * cos(\theta_4)^2 * sin(\theta_1)^2 * sin(\theta_2) + L_4^2 * \dot{\theta_2} * \dot{\theta_4} * m4 * cos(\theta_1)^2 * cos(\theta_2) * cos(\theta_3)^2 * sin(\theta_2) * sin(\theta_4)^2 + L_4^2 * \dot{\theta_2} * \dot{\theta_4} * m4 * cos(\theta_1)^2 * cos(\theta_2) * cos(\theta_4)^2 * sin(\theta_2) * sin(\theta_3)^2 + 2 * L_4^2 * \dot{\theta_3} * \dot{\theta_4} * m4 * cos(\theta_1)^2 * cos(\theta_3) * cos(\theta_4)^2 * sin(\theta_2)^2 * sin(\theta_3) + 2 * L_4^2 * \dot{\theta_3} * \dot{\theta_4} * m4 * cos(\theta_1)^2 * cos(\theta_3)^2 * cos(\theta_4) * sin(\theta_2)^2 * sin(\theta_4) + L_4^2 * \dot{\theta_2} * \dot{\theta_3} * m4 * cos(\theta_2) * cos(\theta_3)^2 * sin(\theta_1)^2 * sin(\theta_2) * sin(\theta_4)^2 + L_4^2 * \dot{\theta_2} * \dot{\theta_3} * m4 * cos(\theta_2) * cos(\theta_4)^2 * sin(\theta_1)^2 * sin(\theta_2) * sin(\theta_3)^2 - L_4^2 * \dot{\theta_2} * \dot{\theta_3} * m4 * cos(\theta_1)^2 * cos(\theta_2) * sin(\theta_2) * sin(\theta_3)^2 * sin(\theta_4)^2 + L_4^2 * \dot{\theta_2} * \dot{\theta_4} * m4 * cos(\theta_2) *$$

$$cos(\theta_3)^2 * sin(\theta_1)^2 * sin(\theta_2) * sin(\theta_4)^2 + L_4^2 * \dot{\theta}_2 * \dot{\theta}_4 * m4 * cos(\theta_2) * cos(\theta_4)^2 * sin(\theta_1)^2 * sin(\theta_2) * sin(\theta_3)^2 - L_4^2 * \dot{\theta}_2 * \dot{\theta}_4 * m4 * cos(\theta_1)^2 * cos(\theta_2) * sin(\theta_2) * sin(\theta_3)^2 * sin(\theta_4)^2 + 2 * L_4^2 * \dot{\theta}_3 * \dot{\theta}_4 * m4 * cos(\theta_3) * cos(\theta_4)^2 * sin(\theta_1)^2 * sin(\theta_2)^2 * sin(\theta_3) - 2 * L_4^2 * \dot{\theta}_3 * \dot{\theta}_4 * m4 * cos(\theta_1)^2 * cos(\theta_3) * sin(\theta_2)^2 * sin(\theta_3) * sin(\theta_4)^2 - 2 * L_4^2 * \dot{\theta}_3 * \dot{\theta}_4 * m4 * cos(\theta_1)^2 * cos(\theta_4) * sin(\theta_2)^2 * sin(\theta_3)^2 * sin(\theta_4) + 2 * L_4^2 * \dot{\theta}_3 * \dot{\theta}_4 * m4 * cos(\theta_3)^2 * cos(\theta_4) * sin(\theta_1)^2 * sin(\theta_2)^2 * sin(\theta_4) + L_3 * L_4 * \dot{\theta}_3 * \dot{\theta}_4 * m4 * cos(\theta_1)^2 * cos(\theta_3)^2 * sin(\theta_2)^2 * sin(\theta_4) - L_4^2 * \dot{\theta}_2 * \dot{\theta}_3 * m4 * cos(\theta_2) * sin(\theta_1)^2 * sin(\theta_2) * sin(\theta_3)^2 * sin(\theta_4)^2 - L_4^2 * \dot{\theta}_2 * \dot{\theta}_4 * m4 * cos(\theta_2) * sin(\theta_1)^2 * sin(\theta_2) * sin(\theta_3)^2 * sin(\theta_4)^2 - 2 * L_4^2 * \dot{\theta}_3 * \dot{\theta}_4 * m4 * cos(\theta_3) * sin(\theta_1)^2 * sin(\theta_2)^2 * sin(\theta_3) * sin(\theta_4)^2 - 2 * L_4^2 * \dot{\theta}_3 * \dot{\theta}_4 * m4 * cos(\theta_4) * sin(\theta_1)^2 * sin(\theta_2)^2 * sin(\theta_3)^2 * sin(\theta_4) + L_3 * L_4 * \dot{\theta}_3 * \dot{\theta}_4 * m4 * cos(\theta_3)^2 * sin(\theta_1)^2 * sin(\theta_2)^2 * sin(\theta_4) + 4 * L_3 * L_4 * \dot{\theta}_2 * \dot{\theta}_3 * m4 * cos(\theta_2) * cos(\theta_3)^2 * cos(\theta_4) * sin(\theta_2) + L_3 * L_4 * \dot{\theta}_2 * \dot{\theta}_4 * m4 * cos(\theta_2) * cos(\theta_3)^2 * cos(\theta_4) * sin(\theta_2) - L_3 * L_4 * \dot{\theta}_3 * \dot{\theta}_4 * m4 * cos(\theta_1)^2 * cos(\theta_3) * cos(\theta_4) * sin(\theta_3) + L_3 * L_4 * \dot{\theta}_3 * \dot{\theta}_4 * m4 * cos(\theta_2)^2 * cos(\theta_3) * cos(\theta_4) * sin(\theta_3) - L_3 * L_4 * \dot{\theta}_2 * \dot{\theta}_3 * m4 * cos(\theta_1)^2 * cos(\theta_2) * cos(\theta_3)^2 * cos(\theta_4) * sin(\theta_2) - L_3 * L_4 * \dot{\theta}_2 * \dot{\theta}_3 * m4 * cos(\theta_2) * cos(\theta_3)^2 * cos(\theta_4) * sin(\theta_1)^2 * sin(\theta_2) + L_3 * L_4 * \dot{\theta}_2 * \dot{\theta}_3 * m4 * cos(\theta_1)^2 * cos(\theta_2) * cos(\theta_4) * sin(\theta_2) * sin(\theta_3)^2 + L_3 * L_4 * \dot{\theta}_2 * \dot{\theta}_4 * m4 * cos(\theta_1)^2 * cos(\theta_2) * cos(\theta_4) * sin(\theta_2) * sin(\theta_3)^2 + L_3 * L_4 * \dot{\theta}_3 * \dot{\theta}_4 * m4 * cos(\theta_1)^2 * cos(\theta_3) * cos(\theta_4) * sin(\theta_2)^2 * sin(\theta_3) + L_3 * L_4 * \dot{\theta}_2 * \dot{\theta}_3 * m4 * cos(\theta_2) * cos(\theta_4) * sin(\theta_1)^2 * sin(\theta_2) * sin(\theta_3)^2 + L_3 * L_4 * \dot{\theta}_2 * \dot{\theta}_4 * m4 * cos(\theta_2) * cos(\theta_4) * sin(\theta_1)^2 * sin(\theta_2) * sin(\theta_3)^2 + L_3 * L_4 * \dot{\theta}_3 * \dot{\theta}_4 * m4 * cos(\theta_3) * cos(\theta_4) * sin(\theta_1)^2 * sin(\theta_2)^2 * sin(\theta_3) - 8 * L_4^2 * \dot{\theta}_2 * \dot{\theta}_3 * m4 * cos(\theta_2) * cos(\theta_3) * cos(\theta_4) * sin(\theta_2) * sin(\theta_3) * sin(\theta_4) - 8 * L_4^2 * \dot{\theta}_2 * \dot{\theta}_4 * m4 * cos(\theta_2) * cos(\theta_3) * cos(\theta_4) * sin(\theta_2) * sin(\theta_3) * sin(\theta_4) - 4 * L_3 * L_4 * \dot{\theta}_2 * \dot{\theta}_3 * m4 * cos(\theta_2) * cos(\theta_3) * sin(\theta_2) * sin(\theta_3) * sin(\theta_4) - L_3 * L_4 * \dot{\theta}_2 * \dot{\theta}_4 * m4 * cos(\theta_2) * cos(\theta_3) * sin(\theta_2) * sin(\theta_3) * sin(\theta_4) - 4 * L_4^2 * \dot{\theta}_1 * \dot{\theta}_2 * m4 * cos(\theta_1)^2 * cos(\theta_2) * cos(\theta_3) * cos(\theta_4) * sin(\theta_3) * sin(\theta_4) - 4 * L_4^2 * \dot{\theta}_1 * \dot{\theta}_2 * m4 * cos(\theta_2) * cos(\theta_3) * cos(\theta_4) * sin(\theta_1)^2 * sin(\theta_3) * sin(\theta_4) - 2 * L_3 * L_4 * \dot{\theta}_1 * \dot{\theta}_2 * m4 * cos(\theta_1)^2 * cos(\theta_2) * cos(\theta_3) * sin(\theta_3) * sin(\theta_4) - 2 * L_3 * L_4 * \dot{\theta}_1 * \dot{\theta}_2 * m4 * cos(\theta_2) * cos(\theta_3) * sin(\theta_1)^2 * sin(\theta_3) * sin(\theta_4) + 4 * L_4^2 * \dot{\theta}_2 * \dot{\theta}_3 * m4 * cos(\theta_1)^2 * cos(\theta_2) * cos(\theta_3) * cos(\theta_4) * sin(\theta_2) * sin(\theta_3) * sin(\theta_4) + 4 * L_4^2 * \dot{\theta}_2 * \dot{\theta}_4 * m4 * cos(\theta_1)^2 * cos(\theta_2) * cos(\theta_3) * cos(\theta_4) * sin(\theta_2) * sin(\theta_3) * sin(\theta_4) + 4 * L_4^2 * \dot{\theta}_2 * \dot{\theta}_3 * m4 * cos(\theta_2) * cos(\theta_3) * cos(\theta_4) * sin(\theta_1)^2 * sin(\theta_2) * sin(\theta_3) * sin(\theta_4) + 4 * L_4^2 * \dot{\theta}_2 * \dot{\theta}_4 * m4 * cos(\theta_2) * cos(\theta_3) * cos(\theta_4) * sin(\theta_1)^2 * sin(\theta_2) * sin(\theta_3) * sin(\theta_4) + 2 * L_3 * L_4 * \dot{\theta}_2 * \dot{\theta}_3 * m4 * cos(\theta_1)^2 * cos(\theta_2) * cos(\theta_3) * sin(\theta_2) * sin(\theta_3) * sin(\theta_4) + L_3 * L_4 * \dot{\theta}_2 * \dot{\theta}_4 * m4 * cos(\theta_1)^2 * cos(\theta_2) * cos(\theta_3) * sin(\theta_2) * sin(\theta_3) * sin(\theta_4) + 2 * L_3 * L_4 * \dot{\theta}_2 * \dot{\theta}_3 * m4 * cos(\theta_2) * cos(\theta_3) * sin(\theta_1)^2 * sin(\theta_2) * sin(\theta_3) * sin(\theta_4) + L_3 * L_4 * \dot{\theta}_2 * \dot{\theta}_4 * m4 * cos(\theta_2) * cos(\theta_3) * sin(\theta_1)^2 * sin(\theta_2) * sin(\theta_3) * sin(\theta_4);$$